UNIVERSIDAD COMPLUTENSE DE MADRID
FACULTAD DE VETERINARIA

TESIS DOCTORAL

P2X7 receptor is a new therapeutic target to treat tauopathies

El receptor P2X7 es una nueva diana terapéutica eficaz para el tratamiento de las tauopatías

MEMORIA PARA OPTAR AL GRADO DE DOCTOR

PRESENTADA POR

Caterina di Lauro

Director

Miguel Díaz Hernández

Madrid

Universidad Complutense de Madrid

Facultad de Veterinaria

Departamento de Bioquímica y Biología Molecular IV

P2X7 RECEPTOR IS A NEW TERAPEUTIC TARGET TO TREAT TAUOPATHIES.

EL RECEPTOR P2X7 ES UNA NUEVA DIANA TERAPÉUTICA EFICAZ PARA EL TRATAMIENTO DE LAS TAUOPATÍAS.

PhD thesis by

Dª. Caterina Di Lauro

Supervised by

D. Miguel Díaz Hernández

Madrid, 2021

Universidad Complutense de Madrid

Facultad de Veterinaria

Departamento de Bioquímica y Biología Molecular IV

P2X7 RECEPTOR IS A NEW TERAPEUTIC TARGET TO TREAT TAUOPATHIES.

EL RECEPTOR P2X7 ES UNA NUEVA DIANA TERAPÉUTICA EFICAZ PARA EL TRATAMIENTO DE LAS TAUOPATÍAS.

PhD thesis by

Dª. Caterina Di Lauro

Supervised by

D. Miguel Díaz Hernández

Madrid, 2021

This doctoral thesis was made possible by a pre-doctoral fellowship received from the European Union's Horizon 2020 Research and Innovation Program under the Marie Skodowska-Curie Grant Agreement No. 766124 and No. 739593.

Your living is determined
not so much by what life brings to you
as by the attitude you bring to life;
not so much by what happens to you
as by the way your mind looks at what happens.

-Khalil Gibran

ACKNOWLEDGMENTS

Many people helped me to make it through this PhD; some were already present in my life, others recently joined me on this journey. I would like to express my gratitude to all of them.

En primer lugar, me gustaría dar las gracias al Profesor Miguel Díaz Hernández por haberme seleccionado para este proyecto, confiando en mis capacidades, y haberme dado la posibilidad de crecer como investigadora. También gracias a tus indicaciones que me han llevado hasta este punto.

No puedo olvidarme de mi equipo de trabajo. Muchas gracias a Carolina, a Lucia, al Dr. Álvaro y a la Dra. Beatriz por haberme ayudado siempre en lo posible con gran premura, sobre todo en este último período que ha sido tan intenso.

Gracias también a toda la Facultad de Veterinaria, en particular a los amigos de la segunda planta Lucia, María José, María, Juan Carlos, Nuria y Alberto. Fue un placer conoceros y compartir con vosotros experiencias de "locura" de nuestro doctorado.

A big thank you to the PurinesDx network. Thanks to all the PIs for making it possible and to Isabela for always being such a good programme manager; we would have been lost without you. And of course, many thanks to all my PurinesDx colleagues; meeting you has been the best part of this experience! It has been a pleasure to share time with you all and I hope to have soon the chance to meet you again and finally celebrate all together.

Caro, in principio mia collega, ora grande amica. Se non ci fossi stata tu probabilmente mi sarei data alla fuga dopo pochi mesi. Grazie per tutti i momenti condivisi durante questi tre anni; tutti i pianti, le incazzature, i momenti di follia e le risate, soprattutto quelle, hanno fatto sì che questo dottorato fosse un po' più leggero. Non pensavamo di arrivare fino a questo punto, ma ce l'abbiamo fatta! E anche se non saremo più in lab insieme, so che continueremo ad essere presenti l'una per l'altra. Insieme a Ricki, e ovviamente Arturo, siete ormai come una seconda famiglia qui a Madrid e non potrei essere più grata per avervi incontrato in questa mia esperienza spagnola.

I miei amici italiani qui a Madrid! Giacomo, Mattia, Franci, Arianna, e Miriam, ne è passato di tempo da quella gita ad Aranjuez, e qualcuno nel frattempo è tornato in patria, ma è sempre un piacere quando ci si becca in giro o anche solo per telefono; speriamo in una reunion molto presto!
Amel, compagna di scleri, di giornate in piscina e grandi scorpacciate di sushi; grazie per esserci sempre quando ho bisogno di staccare la spina.

ACKNOWLEDGMENTS

Francesco, il perfetto partner in crime quando si tratta di spettegolare, l'unico che non si lamenta dei miei audio lunghi (sarà perché i tuoi sono altrettanto lunghi?!). Grazie per aver fatto da intermediario durante le Skype call del nostro business group, sai che sarebbe finita male altrimenti. Spero di poter venire presto a trovare te e Dani a Montpellier!

Un grazie di cuore alla Prof.ssa Chiara Gabellini. Se non fosse stato per te probabilmente non avrei intrapreso un dottorato all'estero. Grazie per avermi dato l'opportunità di iniziare il mio percorso fuori dai confini italiani e di esserci sempre quando ho bisogno di un consiglio o di un confronto.

Chiara e Rita, beh che dire. Non potevo avere fortuna più grande di beccare due migliori amiche come voi, e senza volerlo ho creato un duo micidiale. Siete la dimostrazione che non importa quanto si è lontani, se c'è un'amicizia forte alla base si superano anche i km di distanza. Grazie ad entrambe per la vostra costante presenza e per il vostro supporto incondizionato.

Ed infine un grazie immenso va a Mamma, Babbo, Sorella e a tutta la mia famiglia. Se sono quello che sono oggi è grazie voi, che avete sempre creduto in me e continuate ad appoggiarmi in ogni mia scelta, anche se queste scelte mi portano lontano da casa. Non mi fate mai sentire sola e so che sarete sempre lì per me. Questo traguardo è tanto mio quanto vostro. Grazie di tutto.

Thank you all for being a part of this journey.
Gracias a todos por ser parte de este viaje.
Grazie a tutti per aver fatto parte di questo viaggio.

ABBREVIATIONS

ABC	ATP-binding cassette
AD	Alzheimer's Disease
ADO	Adenosine
ADP	Adenosine-5'-diphosphate
Akt	serine/threonine-specific protein kinase B
ALS	Amyotrophic lateral sclerosis
AMP	Adenosine-5'-monophosphate
AP	Alkaline phosphatases
Ap_4A	Diadenosine tetraphosphate
Ap_5A	Diadenosine pentaphosphate
APP	Amyloid Precursor Protein
APS	Ammonium persulfate
ATP	Adenosine-5'-triphosphate
Aβ	β-amyloid peptide
BAC	Bacterial artificial chromosome
BBB	Blood-brain barrier
Bp	base pairs
BSA	Bovine serum albumin
CaMKII	Ca^{2+}-calmodulin dependent protein kinase II
cAMP	Cyclic adenosine monophosphate
CD73	Ecto-5'-nucleotidase
Chr	chromosome
CNS	Central nervous system
CNT	Concentrative nucleoside transporters
CSF	Cerebrospinal fluid
DAMPs	Damage-associated molecular patterns
DAPI	4′,6-diamidino-2-phenylindole
DMSO	Dimethyl sulfoxide
DNA	Deoxyribonucleic acid
dNTP	deoxyribonucleotide triphosphate
DTT	Dithiothreitol
eATP	Extracellular ATP
ECM	Extracellular matrix
EDTA	Ethylenediamine tetraacetic acid

EGFP	Enhanced green fluorescent protein
E-NPP	Pyrophosphatase/phosphodiesterases
ENT	Equilibrative nucleoside transporters
E-NTPDase	Triphosphate diphosphohydrolases
ERKs	Kinases regulated by extracellular signalling
eTau	Extracellular tau
FAK	Focal adhesion kinase
FBS	Fetal bovine serum
FBSi	Inactivated Fetal Bovine Serum
GABA	Gamma-aminobutyric acid
GAPDH	Glyceraldehyde 3-phosphate dehydrogenase
GDP	Guanosine diphosphate
GFAP	Glial fibrillary acid protein
GFP	Green fluorescent protein
GPCRs	G protein-coupled receptors
GPI	Glycophosphatidylinositol
GPRC	G protein-coupled receptors
GSK-3	Glycogen synthase kinase 3
GSK3β	Glycogen synthase kinase 3 beta
GTP	Guanosine-5'-triphosphate
H_2O	Water
H_2O_2	Hydrogen peroxide
HD	Huntington’s disease
HRP	Horseradish peroxidase enzyme
I.C.V.	Intracerebroventricular injection
Iba-1	Ionized calcium binding adaptor molecule 1
IF	Immunofluorescence
IFN-γ	Interferon-γ
IgG	Immunoglobulin G
IL	Interleukin
J20 mouse	Transgenic mouse model of Alzheimer's disease
Kb	Kilobase
LPS	Lipopolysaccharide
MAP	Microtubule-associated protein

MAPK	Protein kinase activated by mitogens
MAPT	Microtubule-associated protein tau
mRNA	Messenger RNA
MS	Multiple sclerosis
N2a	Neuroblastoma cells
Na_3VO_4	Trisodium vanadate salt
NANC	Non-adrenergic, non-cholinergic nerves
Neun	Marker for neurons
NFTs	Neurofibrillary tangles
NLRP2	NLR Family Pyrin Domain Containing 2
NLRP3	NLR Family Pyrin Domain Containing 3
ON	Over night
P1	Purinergic nucleoside receptors
P13K	Phosphoinositide 3-kinase
P2	Purinergic nucleotide receptors
P2X	Purinergic nucleotide ionotropic receptors
P2X7R	Purinergic receptor P2X7
P2Y	Purinergic nucleotide metabotropic receptors
PBS	Phosphate-buffered saline solution
PCR	Polymerase chain reaction
PD	Parkinson’s disease
PFA	Paraformaldehyde
PHF-1	PHD finger protein1 1
PHFs	Paired helical filaments
PI3K	Phosphatidylinositol-3-kinase
PiD	Pick's Disease
PKA	Protein kinase A (cAMP dependent)
PKC	Protein kinase C (Ca^{2+}/phospholipid dependent)
PLP	Pyridoxal-5'-phosphate
PNS	Peripheral nervous system
PPi	Inorganic pyrophosphate
Q-PCR	Quantitative PCR
RNA	Ribonucleic acid
ROS	Reactive oxygen species

Rpm	Revolutions per minute
RT	room temperature
s.e.m.	Standard error of the mean
SDS	Sodium dodecyl sulfate
ShRNA	From English: small hairpin RNA, interference RNA
SNARE	Soluble *N*-ethyl maleimide-sensitive factor attachment protein receptor
TBS	Buffer Tris saline
Temed	Tetramethylethylenediamine
TG	Transgenic
Thr	Threonine
TLR	Toll-like receptors
TNAP	Tissue Nonspecific Alkaline Phosphatase
TNFα	Tumor necrosis factor
TRIS	Tris (hydroxymethyl) -aminomethane
t-SNARE	Target membrane SNARE
UDP	Uridine-5'-diphosphate
UDP	Uridine nucleoside diphosphate
UPS	Ubiquitin proteasome system
UTP	Uridine nucleoside triphosphate
VNUT	Vesicular nucleotide transporter
v-SNARE	Transport vesicles SNARE
WB	Western Blot
WT	Wild Type; wild mouse

ABSTRACT/RESUMEN

II. ABSTRACT

Tau is a highly soluble microtubule-associated protein (MAP) that in brain is mainly expressed in neurons. Its major role in neurons, especially in axons, is to stabilize the microtubules, regulating their assembly, growing, and shortening in a phosphorylation-dependent way (Buée *et al.*, 2000). The accumulation of hyperphosphorylated tau, with the consequent aggregation into paired helical filaments (PHFs) and formation of neurofibrillary tangles (NFTs), has been described as characteristic feature of a family of neurodegenerative disease collectively known as Tauopathies. This disease family comprises several pathological conditions, including Alzheimer's Disease (AD), the most common tauopathy, Pick's disease (PiD), corticobasal degeneration and post-encephalic parkinsonism (Williams, 2006). Tauopathies can show different clinical phenotypes ranging from neuronal loss and reduced synaptic density, with consequent dementia, to behavioural and movement disorders (Lee *et al.*, 2001; Williams, 2006). Although neither the exact causing factors of NFTs aggregation nor the mechanism leading to neuronal and synaptic loss has been elucidated, it has been demonstrated that neuroinflammation is linked to early progression of tauopathies (Metcalfe *et al.*, 2010). Neuroinflammation is an active inflammatory response within the brain characterized by the production of inflammatory mediators and mainly mediated by microglia cells, the innate immune cells of the central nervous system (DiSabato *et al.*, 2016). In addition to inflammatory mediators, other endogenous molecules, known as damage-associated molecular patterns (DAMPs), are secreted from injured cells. These molecules include adenosine triphosphate (ATP), which is released in large amount into the extracellular space during neuroinflammation (Newton and Dixit, 2012).

Extracellular ATP can interact and activate the specific family of ATP-gated ion channels, the P2X receptors, and in particular the P2X7 (P2X7R). This receptor is unique among the P2X family for its specific and distinctive properties: it functions only as a homo-trimer, and it exhibits a low sensitivity to ATP. The activation of P2X7 receptor, and the consequent opening of the channel pore, determines an inward flux of small cations, Na^+, Ca^{2+}, and an efflux of K^+, (Jiang *et al.*, 2013; Sperlágh *et al.*, 2014). In the central nervous system, the receptor is expressed in many cell types (including neurons, microglia, astrocytes, oligodendrocytes, and Schwann cells) and it has been shown to play a leading role in many physiological pathways (Miras-Portugal *et al.*, 2017). High concentrations of extracellular ATP, found only in damaged tissues, are required to activate the receptor, making the P2X7R a favourable therapeutic target for the treatment of neuroinflammatory diseases, such as neurotrauma, epilepsy, amyotrophic lateral sclerosis, Parkinson's disease, Huntington's disease, Alzheimer's disease (AD) (Francistiová *et al.*, 2020; Territo and Zarrinmayeh, 2021).

Previous data obtained in our lab demonstrated that *in vivo* administration of a selective P2X7R antagonist to a mouse model of AD, that mimics the amyloid-toxicity associated to the disease, reduces the number and size of hippocampal amyloid plaques (Díaz-Hernández *et al*., 2012). Furthermore, a recent study has proved that neuroinflammation induced by β-amyloid (Aβ) peptide leads to a change in P2X7R distribution pattern. In particular, it was demonstrated that an increase of the receptor expression occurs in microglial cells at advanced and late stages of the disease, whereas a reduction of P2X7R transcription in neurons occurs at early and advanced stages (Martínez-Frailes *et al.*, 2019).

Despite all evidence that elucidate the role played by P2X7R in Aβ toxicity associated with AD, little is known about its possible role in tau-induced toxicity. The main aim of this project was to evaluate the role of P2X7R on tau-induced toxicity in Alzheimer's disease.

To reach this goal, a mouse model that overexpresses the human tau protein (P301S mice), alongside with human brain samples from patients of two different tauopathies, AD and Pick's Disease (PiD), were analysed. In parallel, the effects of pharmacological blockage and genetic deletion/overexpression of the P2X7 receptor in P301S mice were evaluated. For this purpose, it was performed an intraperitoneal treatment in P301S mice with a P2X7R antagonist, the GSK 1482160A, and two mouse lines were generated, resulting from the crossbreeding of the P301S mice with a P2X7 receptor null mouse line ($P2X7^{-/-}$) and a mouse line overexpressing EGFP-tagged P2X7R ($P2X7^{451P}$-EGFP).

The results obtained in this work showed that P2X7 receptor is upregulated in tauopathy condition. We also observed that *in vivo* pharmacological or genetic blockade of P2X7R is efficient to revert microglial activation in P301S mice, leading to a reduction in microglial migratory, secretory, and proliferative capacities, and promoting phagocytic function. Furthermore, P2X7R blockade determines a reduction in the levels of intraneuronal phosphorylated tau in a GSK3 enzyme dependent way, and an increase in extracellular phosphorylated tau levels by reducing the expression of ectoenzyme TNAP. Accordingly, pharmacological or genetic blockade of P2X7R improves the cellular survival, motor and memory deficits and anxiolytic profile in P301S mice. Contrary, P2X7R overexpression causes a significant worsening of tau-induced toxicity and aggravated the deteriorated motor and memory deficits in P301S mice.

Our results indicate that P2X7 receptor plays a critical role in tau-induced toxicity, and it might be considered a promising treatment for Tauopathies.

Tau es una proteína asociada a microtúbulos (MAP) que se expresa principalmente en neuronas. Su función principal en estas células es estabilizar los microtúbulos, especialmente en los axones, regulando su ensamblaje, crecimiento y acortamiento de forma dependiente de fosforilación (Buée *et al.*, 2000). La acumulación de tau hiperfosforilada favorece la agregación de dicha proteína en filamentos helicoidales emparejados (PHF), cuya acumulación desencadena la formación de ovillos neurofibrilares (NFT). Estas estructuras aberrantes intraneuronales se han descrito como rasgo característico de una familia de enfermedades neurodegenerativas conocidas colectivamente como Tauopatías. Esta familia engloba a varias patologías, incluida la enfermedad de Alzheimer (EA), la Tauopatía más común, la enfermedad de Pick (PiD), la degeneración corticobasal y el parkinsonismo posencefálico (Williams, 2006). Las Tauopatías pueden mostrar diferentes signos patológicos que van desde la pérdida neuronal y la reducción de la densidad sináptica, con la consiguiente demencia, hasta trastornos del comportamiento y del movimiento (Lee *et al.*, 2001; Williams, 2006). Aunque todavía se desconocen los factores exactos que causan la agregación de las NFT ni el mecanismo que conduce a la pérdida neuronal y sináptica, se ha demostrado que la neuroinflamación está relacionada con la progresión temprana de las Tauopatías (Metcalfe *et al.*, 2010). La neuroinflamación es una respuesta inflamatoria activa dentro del cerebro caracterizada por la producción de mediadores inflamatorios y principalmente mediada por células de microglia, las células inmunes innatas del sistema nervioso central (DiSabato *et al.*, 2016). Además de los mediadores inflamatorios, las células lesionadas secretan otras moléculas endógenas, conocidas como patrones moleculares asociados al daño (DAMP, acrónimo del inglés damage-associated molecular patterns). Estas moléculas incluyen el adenosín trifosfato (ATP), el cual se puede liberar en gran cantidad al espacio extracelular durante la neuroinflamación (Newton and Dixit, 2012).

El ATP extracelular puede interactuar y activar la familia específica de canales iónicos activados por ATP, los receptores P2X y, en particular, el P2X7 (P2X7R). Este receptor es único entre la familia P2X por sus propiedades específicas y distintivas: funciona solo como un homotrímero y exhibe una baja sensibilidad al ATP. La activación del receptor P2X7, y la consiguiente apertura del poro del canal, determina un flujo hacia adentro de pequeños cationes, Na^+, Ca^{2+}, y un flujo hacia afuera de K^+, (Sperlágh *et al.*, 2002; Jiang *et al.*, 2013). En el sistema nervioso central, este receptor se expresa en una amplia variedad de tipos células (incluidas neuronas, microglia, astrocitos, oligodendrocitos y células de Schwann) donde desempeña un papel principal en muchas funciones fisiológicas (Miras-Portugal *et al.*, 2017). Dado que se requieren altas concentraciones de ATP extracelular para activar el receptor (como la que se encuentran en tejidos dañados) este receptor se ha convertido en un objetivo terapéutico favorable para el tratamiento de enfermedades neuroinflamatorias, como neurotrauma, epilepsia, esclerosis lateral amiotrófica, enfermedad de

Parkinson, enfermedad de Huntington, enfermedad de Alzheimer (Francistiová *et al.,* 2020; Territo and Zarrinmayeh, 2021).

En un trabajo previo de nuestro grupo de investigación se demostró que la administración *in vivo* de diferentes antagonistas selectivos de P2X7R a un modelo de ratón de EA, que imita la toxicidad amiloide asociada a la enfermedad, reduce el número y tamaño de las placas amiloides del hipocampo (Díaz-Hernández *et al*., 2012). Además, en otro estudio reciente también se demostró que la neuroinflamación inducida por el péptido Aβ conduce a un cambio en el patrón de distribución de P2X7R. En particular, se reportó que se produce un aumento de la expresión del receptor en las células microgliales en etapas avanzadas y tardías de la enfermedad, mientras que una reducción de la transcripción de P2X7R en neuronas ocurre en etapas tempranas y avanzadas (Martínez-Frailes *et al.*, 2019).

A pesar de todas las pruebas obtenidas antes de la realización de la presente tesis doctoral apuntan a que P2X7R desempeña un papel en la toxicidad de Aβ asociada con la EA, poco se sabía sobre el posible papel que este receptor podría desempeñar en la toxicidad inducida por tau. Por lo tanto, el objetivo principal de este proyecto fue evaluar el papel de P2X7R en la toxicidad inducida por tau en la enfermedad de Alzheimer.

Para alcanzar este objetivo, utilizamos un modelo de ratón que sobrexpresa la proteína tau humana (ratones P301S), así con muestras de cerebro humano de pacientes de dos tauopatías diferentes, EA y enfermedad de Pick. En paralelo, se evaluaron los efectos que el bloqueo farmacológico y la deleción/sobrexpresión genética del receptor P2X7 pudieran ejercer sobra la patología desarrollada por los ratones P301S. Para ello, se realizó un tratamiento intraperitoneal de estos ratones con un antagonista del P2X7R, el GSK 1482160A. Además, se generaron dos líneas de ratón, resultado del cruzamiento de los ratones P301S con una línea de ratón nula para el receptor P2X7 ($P2X7^{-/-}$) y una línea de ratón que sobrexpresa P2X7R marcado con EGFP ($P2X7^{451P}$-EGFP).

Los resultados obtenidos mostraron que en las Tauopatías hay un incremento en la expresión del receptor P2X7. También observamos que el bloqueo farmacológico o genético de P2X7R es eficaz para revertir la activación microglial en ratones P301S, lo que conduce a una reducción de las capacidades migratorias, secretoras y proliferativas de la microglía, y promueve la función fagocítica. Además, el bloqueo de P2X7R provoca una reducción en los niveles de tau fosforilada intraneuronal de forma dependiente de la enzima GSK3, mientras que por otro lado induce un aumento de los niveles de tau extracelular fosforilada (eTau), gracias a que reduce la expresión de la ectoenzima TNAP. En consecuencia, el bloqueo farmacológico o genético de P2X7R mejora la supervivencia celular, los déficits motores y de memoria y el perfil ansiolítico en ratones P301S. Por el contrario, la sobrexpresión de P2X7R provoca un empeoramiento significativo de la

toxicidad inducida por tau y agrava los déficits motores y de memoria deteriorados en ratones P301S.

Nuestros resultados indican que el receptor P2X7 desempeña un papel fundamental en la toxicidad inducida por tau y podría considerarse un tratamiento prometedor para las Tauopatías.

INTRODUCTION

1. PURINERGIC SYSTEM

The purinergic system is a form of extracellular paracrine signalling mediated by the purine nucleotides and nucleosides, such as the adenosine and its derivatives adenosine mono-, di-, and triphosphate (AMP/ADP/ATP). This process commonly requires the activation of cell surface receptors, named purinoreceptors, within the proximity of the release of neurotransmitters, thereby transducing signals to regulate intracellular processes (Burnstock, 2007).

Although first evidence of the action of nucleotides as extracellular transmitters were already provided in the late 1920's by Drury and Szent-Györgyi (Drury and Szent-Györgyi, 1929), the hypothesis of a purinergic signalling was not proposed until 1972, when Geoffrey Burnstock described the release of extracellular ATP as a transmitter substance by non-adrenergic, non-cholinergic (NANC) inhibitory nerves in the guina-pig taenia coli (Burnstock, 1972). Initially, the concept of purinergic signalling met with considerable resistance, because of the idea of ATP as intracellular energy source; and it was not well accepted until the early 1990's, when receptor subtypes for purines and pyrimidines were cloned and characterised (Ralevic and Burnstock, 1998).

Few years later, in 1976, Burnstock proposed the existence of specific receptors for nucleoside and nucleotides (Burnstock, 1976), and after two years a basis for distinguishing two types of purinoreceptors, named P1 and P2 for adenosine and ATP/ADP, respectively, was defined (Burnstock, 1978). However, a pharmacological basis for a further classification of P2 receptors into two groups, P2X and P2Y receptors, was only proposed in 1985 (Burnstock and Kennedy, 1985).

Nowadays it is well known that the purinergic signalling is involved in many neuronal and non-neuronal mechanisms, in both exocrine and endocrine secretion, contributing to many events including inflammation, cell proliferation, differentiation, migration and death, in mechanosensory transduction, but also in pathological processes and neurodegenerative diseases (Burnstock, 2006; Burnstock, 2012). Moreover, it is widely recognized the existence of a rich molecular complex responsible for the biological effects of extracellular purine and pyrimidine ligands, named “purinome”, **Figure 1**. The purinome consists of a vast heterogeneity of purinergic ligands, ectonucleotide-metabolizing enzymes hydrolysing nucleoside phosphates, purinergic receptors, nucleoside and nucleotide transporters and channels. All these elements work in synergy in physiological condition (Volonté and D’Ambrosi, 2009; Dos Santos-Rodrigues, 2014).

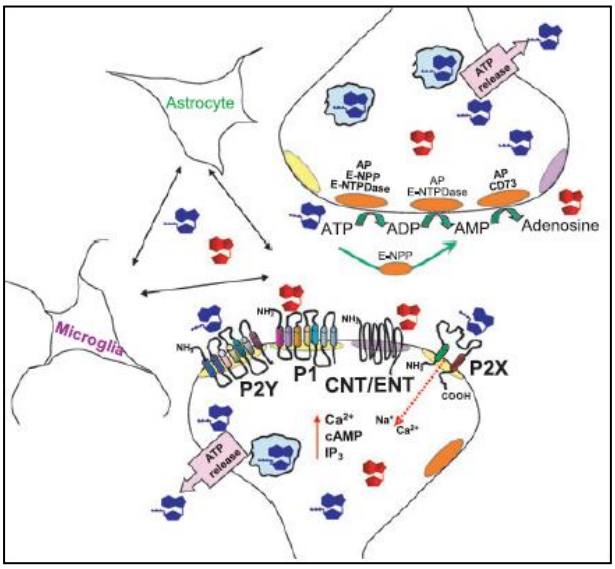

Figure 1. Scheme of the purinome. *The purinome. The protein machinery involved in the biological interplay of extracellular purine and pyrimidine ligands, with: receptors such as P2X and P2Y for nucleotides tri- and diphosphates (exemplified by ATP and ADP), as well as P1 for nucleotides monophosphates and nucleosides (exemplified by AMP and adenosine); ectonucleotide hydrolysing enzymes, such as triphosphate diphosphohydrolases (E-NTPDase), pyrophosphatase/phosphodiesterases (E-NPP), ecto-5'-nucleotidase (CD73) and alkaline phosphatases (AP); and transporters, such as concentrative nucleoside transporters (CNT) and equilibrative nucleoside transporters (ENT). Image adapted from Volonté and D'Ambrosi, 2009.*

1.1. Nucleotides/nucleosides release

Under several physiopathological conditions, ATP, as well as other nucleotides, nucleosides, and cellular mediators, are often released in the extracellular space to operate as transmitters and co-transmitters on pre- and post-junctional membranes and synapses. Although former studies supported the idea that damaged or dead cells were the only extracellular ATP source, it is now widely accepted that ATP and the other nucleotides are packed in specialized granules in neuroendocrine tissues and circulating platelets, and released from cells via regulated exocytosis (Burnstock, 1997; Miras-Portugal *et al.*, 1998; Bodin and Burnstock 2001; Lazarowski *et al.*, 2003; Lazarowski, 2012).

ATP is present in the cytoplasm of most neurons with a concentration of 2-5 mM, but it can be stored at higher concentrations (up to 100 mM) in synaptic vesicles. Synaptic vesicles can also contain other nucleotides such as ADP, AMP, diadenosine tetraphosphate (Ap_4A), diadenosine pentaphosphate (Ap_5A), and guanosine-5'-triphosphate GTP, but at lower concentrations (Burnstock, 1997; Miras-Portugal *et al.*, 1998; Burnstock, 2007a). The presence of nucleotides stored in vesicles requires the existence of an active specific transport system. ATP is accumulated and kept in synaptic vesicles through a vesicular nucleotide transporter (VNUT), an isoform of the

SCL17 phosphate transporter family. VNUT is predominantly expressed in the brain and adrenal gland and plays an essential role in vesicular storage of ATP (Sawada *et al*., 2008).

ATP is released from both peripheral and central neurons, but also from many non-neuronal cell types in response to stimulation by various agents. In neuronal models, stimulation of exocytosis results in granules transport along the filaments of the cytoskeleton network to the subplasma membrane compartment, fusion of the granules with the plasma membrane, and release of the contents into the extracellular space. Considerable evidence links this process to the SNARE (soluble *N*-ethyl maleimide-sensitive factor attachment protein receptor) complex. Accordingly, during membrane fusion, v-SNARE proteins located on vesicles pair with corresponding t-SNARE proteins located on the target membrane and form a trans-SNARE complex, determining the specificity of vesicle targeting, docking, and fusion (Lazarowski *et al*., 2003; Burnstock, 2007; Fizt, 2007).

In non-neuronal cells, ATP and other nucleotides/nucleosides release has been reported to occur in three different contexts: 1) after mechanical stimulation of endothelial, epithelial glial and other cells; 2) pharmacological stimuli; 3) significant release of nucleotides occurs in the absence of an external stimulus (i.e., by resting cells). Various transport mechanisms have been proposed for ATP release in non-neuronal cells, including ATP-binding cassette (ABC) transporters, connexin, or pannexin hemichannels, or possibly plasmalemmal voltage-dependent anion as well as vesicular release (Lazarowski *et al*., 2003; Burnstock, 2007; Fizt, 2007).

During the last twenty years, several studies reported the importance of extracellular ATP (eATP) for several physiological processes (Zimmermann, 2016). Mechanisms controlled by eATP include neurotransmission and neuromodulation (Burnstock, 2013), glial and glial-neurons interactions (Butt, 2011), the development of the nervous system (Zimmermann, 2011; Díaz-Hernández *et al.*, 2008), sensory transmission (Nakatsuka and Gu, 2006) and pain (Tsuda *et al.*, 2010), control of hormone secretion (Burnstock, 2014). Moreover eATP, and other extracellular nucleotides, also regulate the function of a variety of organ systems, such as the cardiovascular system (Gachet, 2008; Burnstock, 2009), the immune system (Burnstock and Boeynaems, 2014; Idzko *et al*., 2014), the musculoskeletal system (Rumney *et al.*, 2012; Burnstock *et al.*, 2013), and many others (Zimmermann, 2016).

To fulfil their role as neurotransmitters, extracellular nucleotides and nucleosides impact specific cell surface located receptors. Specific purinoreceptors, named P1 and P2, for adenosine and ATP/ADP respectively, were described in 1978 by Burnstock, and later, a pharmacological basis for a further classification of P2 receptors into two groups, P2X and P2Y receptors, was proposed in 1985 (Burnstock and Kennedy, 1985).

1.2. Inactivation and degradation of nucleotides/nucleosides

As all the neurotransmitters, ATP and other nucleotides/nucleosides, once released in the extracellular space and bound to specific receptors, need to be inactivated, degraded and removed from the synapsis. To avoid their prolonged action in the synaptic space, nucleotides and nucleosides undergo rapid degradation by a family of extracellular specific enzymes named ecto-nucleotidases. Depending on subtype, ecto-nucleotidases hydrolyse tri-, di-, and monophosphates and dinucleoside polyphosphates and produce nucleoside diphosphates, nucleoside monophosphates, nucleoside phosphate, and inorganic pyrophosphate (Yegutkin, 2008).

Based on their affinity for the substrate, the product they generate, and the optimal pH condition for their activity, ecto-nucleotidases can be divided into four families (Yegutkin, 2014):

- *Ectonucleoside triphosphate diphosphohydrolases (E-NTPDases);* this family (previous names ecto-ATPase, ecto-apyrase, ATP-diphosphohydrolase or CD39) includes eight different members classified in order of their discovery and classification. Four of the NTPDases (1, 2 3 and 8) are expressed as cell surface-located enzymes, are active in physiological to slightly basic pH range of 7-8,5 and require millimolar concentrations of divalent cation Mg^{2+} and Ca^{2+} for maximal activity. NTPDases 5 and 6 exhibit intracellular localization and undergo secretion after heterologous expression, while NTPDases 4 and 7 are intracellularly located, facing the lumen of cytoplasmic organelles. The ecto-nucleotidases of this family hydrolyse nucleotides tri- and diphosphates, generating corresponding monophosphates (Kukulski *et al*., 2005; Zimmermann, 2012).
- *Ecto-nucleotide pyrophosphatase/phosphodiesterases (E-NPPs);* it is a multigene family of five enzymes. E-NPP1-3 are type II transmembrane glycoproteins with a structure composed of a short amino-terminal intracellular domain, a single transmembrane domain, and a large extracellular domain. The extracellular domain contains two somatomedin B-like motifs, a conserved catalytic site, a nuclease-like sequence, and a putative C-terminal “EF-hand” motif. In contrast, E-NPP4-5 are type I transmembrane protein, with a short intracellular carboxy-terminal domain, a small extracellular domain that only contains a phosphodiesterase motif. E-NPP1-3 catalyse the hydrolysis of pyrophosphate and phosphodiester bonds in a two-step mechanism; in this reaction two essential divalent metal ions are required for the formation of a nucleotidylated active-site threonine intermediate and the subsequent release of nucleoside 5'-monophosphate (Goding *et al.*, 2003).

- *Ecto-5'-nucleotidase/CD73;* also known as CD73, is a zinc-binding metalloenzyme and its structure consists of two disulfide linked (glyco)protein subunits with a molecular mass of ~60-80 kilodaltons (kDa) anchored to the plasma membrane at the C-terminal by glycophosphatidylinositol. Ecto-5'-nucleotidase acts on nucleosides monophosphate generating the corresponding nucleosides, namely it hydrolyses AMP to adenosine (Zimmermann, 2012).
- *Alkaline phosphates (AP);* the members of this family are ubiquitous enzymes typically comprising of homodimeric or heterodimeric proteins with subunit sizes of ~80 kDa. Alkaline phosphates are attached to the plasma membrane via a glycophosphatidylinositol (GPI)-anchor and each of their catalytic site contains two Zn^{2+} and one Mg^{2+} metal ions that are necessary for catalytic activity. The enzymes possess broad substrate specificity towards different phosphomonoesters and other phosphate-containing compounds, and hydrolyse nucleosides 5'-tri, -di and monophosphate, generating their corresponding nucleosides. The genome encodes four genes, ALPL, ALPP, ALPP2 and ALPI, corresponding to tissue-nonspecific, placental, germ cell and intestinal alkaline phosphatase isozymes, respectively. Tissue Nonspecific Alkaline Phosphatase (TNAP) is the most extensive characterized member of this family (Millan, 2006; Zimmermann, 2012).

1.2.1. Tissue Nonspecific Alkaline Phosphatase (TNAP)

Tissue nonspecific AP (TNAP) is one of the four alkaline phosphatase isozymes, present in both humans and mice. Among the AP family, TNAP is the only one present both in tissues such as liver, kidney and bone, and in the central nervous system (CNS).

In humans, TNAP is encoded by the *ALPL* (alkaline phosphatase, liver/bone/kidney) gene, which, unlike the other isoforms, is located on the distal short arm of chromosome 1 (1p36.1-p34). The gene is composed of 12 exons and 11 introns, with its initial sequence located in the exon 2 (Smith *et al.*, 1988). In mouse, the gene for TNAP is the *Akp2* (alkaline phosphatase 2) and, as well as the human one, is composed by 12 exons, but its localization is on chromosome 4 (Terao *et al.*, 1988; Terao *et al.*, 1990). In both species, two different transcripts derived from the same coding region, and under the control of two promoters, have been described. In human these promoters are 1B and 1L (Matsuura *et al.*,1990), which correspond to mice promoters E1A and E1B respectively (Studer *et al.*, 1991).

Similar to the rest of the mammalian AP family, TNAP functions physiologically as a homodimer, anchored within the plasma membrane via a GPI-anchor, and oriented towards the extracellular

space. The central core of the protein consists of an extended β-sheet and flaking α-helices, and each dimer contains a flexible surface loop "crown domain", which mediates the interaction with the extracellular matrix (ECM), the GPI-anchor site, and the biochemically active site, **Figure 2A-B**. Typical TNAP substrates are inorganic pyrophosphate (PPi) and pyridoxal-5'-phosphate (PLP) as well as ATP/ADP/AMP, **Figure 2 C**. The presence of the GPI-anchor protein determines the recruitment of the enzyme to subcellular sites and extracellular vesicles, where it can influence microenvironmental concentrations of its substrates and products (Millan, 2006).

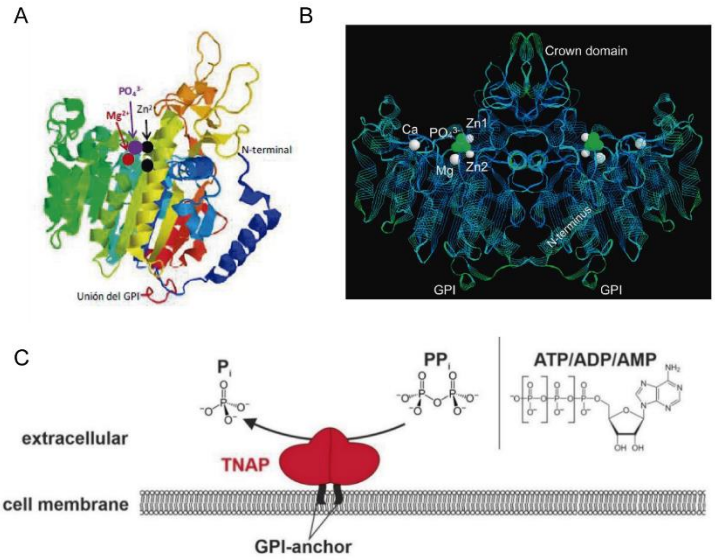

Figure 2. Structural 3D representation and potential enzymatic functions of TNAP. *(A) Monomer. (B) Dimer. The active site phosphate (PO_4^{3-}) bound to Ser residues during catalysis is shown in green. The three metal-binding sites are shown in white as well as the structural Ca^{2+} ion (Ca). Also indicated are the flexible exposed sequence, known as the "crown domain". (C) Depiction of potential TNAP substrates. ATP/ADP/AMP: adenosine tri-/di-/monophosphate; Pi: phosphate; PPi: inorganic pyrophosphate. Image adapted from Liedtke et al., 2020.*

Over the years, several TNAP inhibitors have been used for study; the most common ones consist of small non-competitive molecules, including L-homoarginine, levamisole and theophylline (Kozlenkov *et al.*, 2004). Other inhibitors, with higher efficiency than the previous ones (nanomolar range) have been later developed, including competitive molecules, such as pyrazole derivatives (Sidique *et al.*, 2009) and non-competitive molecules like sulfonamides derivatives (Dahl *et al.*, 2009).

The role of TNAP has been primarily studied in patients affected by hypophosphatasia, a metabolic disease caused by mutations in the *ALPL* gene. This pathology is characterized by an accumulation of pyrophosphate that acts as an inhibitor of mineralization in bones and teeth; another effect is an alteration in the metabolism of the vitamin B6, leading to epileptic seizures in the most serious cases (Whyte, 2016). Transgenic mice lacking TNAP activity display the characteristic skeletal and

dental phenotype of infantile hypophosphatasia, as well as spontaneous epileptic seizures and die around 10 days after birth. Moreover, these mice show abnormal development of the lumbar nerve roots and intestinal physiology, increased apoptosis in the thymus and alterations in the spleen. As a consequence of alterations in PLP metabolism, the brain of these mice also shows reduced levels of gamma-aminobutyric acid, GABA, (Waymire *et al*., 1995; Narisawa *et al*., 1997).

A recent study by Sebastián-Serrano *et al.* (2016) reported that seizures associated with hypophosphatasia were linked to neurodevelopmental alterations caused by partial dysregulation of P2X7R expression. In the early postnatal period, these authors showed that TNAP-knockout mice possess shorter callosal axonal projections than their wild-type littermates. This deficiency was prevented by selective knockdown of P2X7R in cortical neurons after *in utero* electroporation at the embryonic stage (Sebastián-Serrano *et al.*, 2016), thus demonstrating that this is a cellular autonomous process.

Moreover, TNAP was shown to promote axonal growth and branching, by hydrolysing ATP and preventing the activation of the P2X7 receptor (Díez-Zaera *et al.*, 2011). TNAP also regulates the metabolism of several compounds involved in synaptic functionality (Fedde and Whyte, 1990; Martin and Barke, 1998). Furthermore, TNAP regulates the nucleotide-mediated signalling (Sebastián-Serrano *et al.*, 2015) by which the vesicular release of numerous neurotransmitters such as acetylcholine, glutamate may be controlled, or GABA (Gomez-Villafuertes *et al.*, 2001; Díaz-Hernández *et al.*, 2002; Gualix *et al.*, 2003), and favours amyloid processing of the amyloid precursor protein, APP, (Díaz-Hernández *et al.*, 2012). Therefore, TNAP alterations may results in nucleotide signalling alterations that would finally give rise to the synaptopathy detected in the Alzheimer's Disease (Sebastián-Serrano *et al.*, 2019).

1.3. Purinergic receptors

Implicit in the concept of purinergic neurotransmission is the existence of postjunctional purinergic receptors localized at the plasma membrane. Purinergic receptors were first defined by Burnstock in 1976, and 2 years later a basis for distinguishing two types of purinoreceptor, identified as P1 and P2 was proposed (Burnstock, 1976; Burnstock, 1978). Two further P1 (adenosine) receptor subtypes were recognized at about the same time (Van Calker *et al*. 1979; Londos *et al*., 1980), but it was not until 1985 that a proposal suggesting a pharmacological basis for distinguishing two types of P2 receptor (P2X and P2Y) was made (Burnstock and Kennedy, 1985).

Over the next ten years a wide variety of purinergic receptors was discovered (Lustig *et al*., 1993; Webb *et al*., 1993; Brake *et al*., 1994; Valera *et al*., 1994), and in 1994 Abbracchio and Burnstock established the criteria for a common nomenclature, dividing the purinoreceptors into two major

families: a P2X family of ligand-gated ion channel receptors and a P2Y family of G protein-coupled receptors (Abbracchio and Burnstock, 1994). This nomenclature was universally accepted and adopted through the years and currently seven P2X and eight P2Y receptor subtypes are recognized (North, 2002; Burnstock and Knight, 2004).

1.3.1. Nucleosides receptors P1

The P1 are G protein-coupled receptors (GPCRs) activated by adenosine (ADO). Four different subtypes have been cloned so far: A_1, A_{2A}, A_{2B}, A_3 (Yaar *et al.*, 2005). All of them share the same structure, characterized by 7 transmembrane domains, and mainly modulate the activity of the cyclic adenosine monophosphate (cAMP). Adenosine receptors have been deeply studied and there are several specific agonists and antagonists available to target them; a summarize of these compounds is present in **Table 1**. P1 receptors are involved in the modulation of different physiological processes, such as in the cardiovascular system, immune system and nervous system (Burnstock, 2007; Burnstock 2007b).

In our group it was demonstrated that the activation of presynaptic adenosine receptors is able to modulate the dinucleotide response in hippocampal nerve terminals (Díaz-Hernández *et al.*, 2000; Díaz-Hernández *et al.*, 2002b).

Family	Receptor	Endogenous agonist	Main distribution	Main signalling pathway	Agonists	Antagonists
P1 (Adenosine)	A1	Adenosine	Brain, spinal cord, testis, heart, autonomic nerve terminals	Coupled to G_i proteins	CCPA	DPCPX
	A_{2A}		Brain, heart, lungs, spleen	Coupled to G_s proteins	CGS-21680, ATL-146e	SCH58261, KW 6002
	A_{2B}		Large intestine, bladder	Coupled to G_s proteins	BAY 60-6583, NECA	MRE2029-F20, PBS1115
	A_3		Lung, liver, brain, testis, heart	Coupled to G_i proteins	Cl-IB-MECA, MRS3558	MRE2029-F20, MRS-1523

Table 1. *Summary of all the P1 receptors, their endogenous ligands, their main distribution, the main signalling pathways they activate, and the most known, used or potent ligands used for their activation/inhibition. Adapted from Burnstock, 2007 and from Calzaferri et al., 2020.*

1.3.2. Metabotropic receptors P2Y

Metabotropic P2Y receptors are a family of purinergic GPCRs classified in eight subtypes: $P2Y_1$, $P2Y_2$, $P2Y_4$, $P2Y_6$, $P2Y_{11}$, $P2Y_{12}$, $P2Y_{13}$, and $P2Y_{14}$. These receptors are activated by both adenine and uridine nucleoside tri- and diphosphate (ATP, ADP, UTP and UDP), except $P2Y_{14}$, whose endogenous antagonists are UDP, UDP-glucose, UDP-N-acetylglucosamine, UDP-glucuronic acid, and UDP-galactose (Abbracchio *et al*., 2003; Carter *et al*., 2009).

A P2Y typical subunit contains seven helical trans-membrane segments, connected by three extracellular loop (EL-1 to EL-3) and three intracellular loops (IL-1 to IL-3). Each of the transmembrane regions consists of approximately 24 mostly hydrophobic amino acids. The N-terminus of the receptor extends into the extracellular space, whereas the C-terminus resides into the intracellular space, and, between them, the seven domains associate together to form an oblong ring within the plasma membrane. The ligand-binding site resides within a pocket formed in the center of the seven membrane-spanning segments (Waxham, 2004; Burnstock 2017).

When a GPCR is activated, it couples to a G-protein and initiates the exchange of guanosine diphosphate (GDP) for GTP, activating the G-protein. Activated G-proteins then couple to downstream effectors to alter the activity of other intracellular enzymes or ion channels. Many of the G-protein target enzymes produce diffusible second messengers that stimulate further downstream biochemical processes, including the activation of protein kinases (Erb and Weisman, 2012).

P2Y receptors are widely distributed in the whole organism and involved in a myriad of different cellular functions and physiological/pathological processes, including neuroprotection and neuroinflammation. In the CNS, $P2Y_1$, $P2Y_2$, and $P2Y_{13}$ receptors have neuroprotective functions (Fujita *et al*., 2009; Pérez-Sen *et al*., 2015; Beamer *et al*., 2016) and can have a role in anxiety and AD (Moore *et al*., 2000; Kittner *et al*., 2003).

It was recently reported that lipopolysaccharide (LPS)-induced neuroinflammation causes an impairment of the ubiquitin proteasome system (UPS) in glial cells by blocking $P2Y_2R$ (de Diego Garcia *et al*., 2018). Moreover, *in vivo* pharmacological activation of $P2Y_2R$ by its specific agonist diuridine tetraphosphate reversed the astrocytic UPS impairment by promoting the expression of the proteasomal β5 subunit (de Diego Garcia *et al*., 2018). This study provided the first direct evidence that a specific $P2Y_2R$ agonist might have anti-inflammatory properties (de Diego Garcia *et al*., 2018).

The $P2Y_4$, $P2Y_6$, and $P2Y_{12}$ receptors are involved in the modulation of microglia activation (Rafehi *et al*., 2017; Illes *et al*., 2020); in particular $P2Y_{12}$ has been proposed to be a marker of demyelinating lesions in amyotrophic lateral sclerosis (ALS) (Amadio *et al*., 2014). Finally, $P2Y_{11}$

receptors seem to be involved in sleep disorders (Kornum *et al*., 2011), whereas $P2Y_{14}$ receptors are interesting target for the treatment of chronic pain (Mufti *et al*., 2020).

Table 2 summarises the main features, as well as the agonists and antagonists of P2Y receptors.

Family		Receptor	Endogenous agonist	Main distribution	Main signalling pathway	Agonists	Antagonists
P2	P2Y	$P2Y_1$	ADP	Epithelial and endothelial cells, platelets, immune cells, osteoclasts	Coupled to G_q proteins	MRS-2365	MRS-2500
		$P2Y_2$	UTP, ATP	Immune cells, epithelial and endothelial cells, kidney tubules, osteoblasts		UTP, MRS-2698	AR-C-126313
		$P2Y_4$	UTP, ATP	Endothelial cells		2'-azido-dUTP	ATP, RB2, Suramin
		$P2Y_6$	UDP	Some epithelial cells, placenta, T cells, thymus		MRS-2696	MRS-2578
		$P2Y_{11}$	ATP	Spleen, intestine, granulocytes	Coupled to G_q+G_S proteins	ATPγS	NF-157
		$P2Y_{12}$	ADP	Platelets, glial cells	Coupled to G_i proteins	2-MeSADP	ARC-69931MX
		$P2Y_{13}$	ADP	Spleen, brain, lymph nodes, bone marrow		ADP, 2-MeSADP	ARC-69931MX
		$P2Y_{14}$	UDP	Placenta, adipose tissue, stomach, intestine, discrete brain regions		MRS-2690	-

Table 2. *Summary of all the P2Y receptors, their endogenous ligands, their main distribution, the main signalling pathways they activate, and the most known, used or potent ligands used for their activation/inhibition. Adapted from Burnstock, 2007 and from Calzaferri et al., 2020.*

1.3.3. Ionotropic receptors P2X

P2X receptors are extracellular, ATP-gated, calcium-permeable, non-selective cation channels. The family is characterized by seven types of subunits (P2X1-P2X7) that can assemble to form trimeric homomers or trimeric heteromers. Each subunit is composed of two α-helical transmembrane domains (TM1 and TM2), a short intracellular *N*-terminus, a more variable in length *C*-terminus, and a large extracellular domain (the "ectodomain") of 269-288 amino acids, mostly folded as β-sheets and loops (Kopp *et al*., 2019). Each subunit resembles the shape of a dolphin, with the transmembrane helices and the extracellular region akin to the fluxes and the body, respectively, **Figure 3** (Browne, 2012).

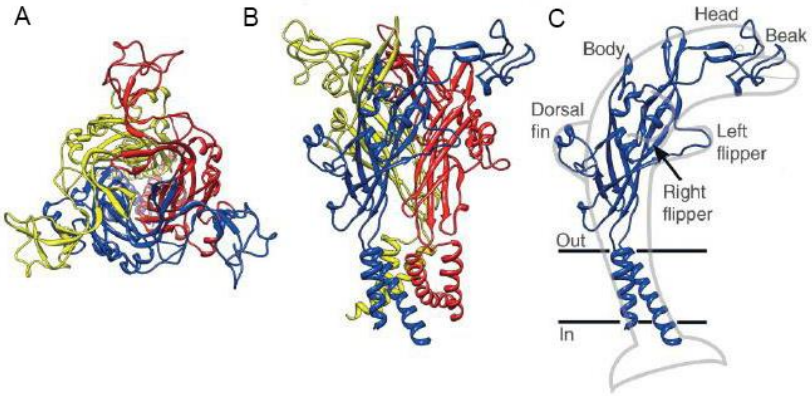

Figure 3. Crystal structure of the P2X2 receptor. *(A) and (B) The P2X2 receptor with each of the three subunits shown in a different colour, viewed along the axis of threefold symmetry from the extracellular side (A), and parallel to the membrane plane (B). (C) A single P2X2 receptor subunit viewed parallel to the membrane normal, with shape of a dolphin. The membrane is represented by black lines. Image adapted from Browne, 2012.*

The determination of X-ray structure of the zebrafish P2X4 receptor in a closed state and in an ATP-bound open-channel state (Díaz-Hernández *et al.*, 2002; Kawate *et al.*, 2009; Hattori and Gouaux, 2012) allowed to resolve the question of whether P2X receptor channel opening involves the occupancy of one, two or three binding sites. Early study based on single-channel recordings suggested that the activation of P2X receptors proceeds through three ATP binding steps before opening (Ding and Sachs, 1999); however, more recent works showed that two ATP molecules are sufficient to activate P2X receptors (Yan *et al.*, 2010; Stelmashenko *et al.*, 2012). Interestingly, there is now evidence of a conformational change in the receptor structure when one ATP binding site is occupied. This structural change is then spread to the second and third binding sites, leading to a transient state that precedes channel activation (Chataigneau *et al.*, 2013). It has been proposed a five steps activation mechanism, during which the binding of extracellular ATP between the subunits causes them to flex together within the ectodomain and separate in the membrane spanning region to open the central channel. This open structure finally provides a pathway through the membrane. Except for P2X5, which is permeable to Cl^-, the other P2X receptors allow Na^+ and $Ca2^+$ influx and K^+ efflux, according to the electrochemical gradient of plasmalemma (Browne, 2012). Although all functional P2X receptors undergo conformational changes that result in the opening of a cationic pore within millisecond of ATP binding, some P2X receptors (notably P2X7) also undergo additional pore dilation within several seconds of ATP activation, allowing the permeation of small molecules (Jacobson, 2010).

The kinetics of activation, inactivation and deactivation vary considerably among the components of this family. Depending on these characteristics, P2X receptors can be classified in three main groups. The first one includes the P2X1 and the P2X3, which are activated in the range of

milliseconds and rapidly desensitise. The other two groups comprise the remaining subtypes, all characterized by a rapid activation in about a second but can undergo a slow or no desensitisation. In fact, P2X2, P2X4 and P2X6 slow desensitise, whereas P2X5 and P2X7 present a persistent current plateau during prolonged ATP stimulation (Coddou *et al*., 2011; Jacobson *et al*., 2002).

The kinetic of activation is also regulated by the affinity of the different P2X receptors for ATP. P2X1 is highly sensitive to ATP, with an EC_{50} (half maximal effective concentration) of 7.3, followed by P2X3 (EC_{50} 6.5), P2X4 (EC_{50} 6.3), P2X5 (EC_{50} 6.0), P2X2 (5.9), and P2X7 (EC_{50} 4.0), (Kasuya *et al*., 2017).

P2X receptors isoforms have been found to be widely but specifically distributed among different tissues in the vertebrate body.

- *P2X1;* the encoding gene for this receptor consists of 12 exons and is located close to the P2X5 on chromosome 17 in human, chromosome 11 in mouse, and chromosome 10 in rat genome (Longhurst *et al.*, 1996; Sun *et al.*, 1998; Liang *et al.*, 2001). P2X1 is highly expressed in smooth muscle cells of various organs, including arteries, urinary bladder, and vas deferens (Chan *et al*., 1998; Vial and Evans, 2001; Turner *et al*., 2003). Although its precise localization in the CNS remains unsettled, it was reported its contribution to functional responses in cortical astrocytes (Lalo *et al*., 2008; Palygin *et al.*, 2010). Moreover, it was demonstrated that P2X1 receptor expression is downregulated in the hippocampus by TNP-ATP (trinitrophenyl-substituted nucleotides) (Cavaliere *et al*., 2007). Knockout mice for this receptor present a severe reduction in male fertility (up to 90%) (Mulryan *et al*.; 2000).
- *P2X2;* is one of the most widely distributed subtypes of the P2X family and its expression is abundant in both central and peripheral nervous systems, in particular in the olfactory bulb, cerebral cortex, basal ganglia and cerebellum (Nörenberg and Illes, 2000; Burnstock and Knight, 2004). In addition, multiple non-neuronal tissues, including skeletal muscle, cardiac muscle, vasculature smooth muscle, have been shown to express significant amounts of this receptor (Kaczmarek-Hájek *et al.*, 2012). P2X2 gene includes 11 exons and is located, together with the P2X4 and P2X7 genes, on chromosome 12 in the human and on chromosome 5 in the mouse genome (Buell *et al.*, 1998; Koshimizu and Tsujimoto, 2006). Despite the wide distribution of the P2X2, knockout mice for this receptor only present small differences in body weight, compared with wild type (wt) animals, and are histopathologically normal for up to 1 year of age.
- *P2X3;* the gene encoding for this receptor was mapped in chromosome 11 in human, and chromosome 2 in mouse, containing 12 exons in both species (Garcia-Guzman *et al.*, 1997;

Souslova *et al.*, 1997). The P2X3 subunit has been detected in sensory neurons within dorsal root ganglion (DRG), as well as in nodose and trigeminal ganglia, and in the spinal cord within the superficial laminae of the dorsal horn (Xiang and Burnstock, 1998; Bradbury *et al.*, 1998; Barden and Bennett, 2000). Deletion of P2X3 gene in mice leads to a significant effect on sensory functions (Cockayne *et al.*, 2005).

- *P2X4;* this receptor was one of the first P2Xs cloned and fully characterized in zebrafish (Díaz-Hernández *et al.*, 2002). It is extensively distributed in several regions of the central and peripheral nervous systems, as well as in all vital and reproductive organs. Its expression overlaps to a large extent with the localization pattern of the P2X6 receptor (Rubio and Soto, 2001; Bo *et al.*, 2003). P2X4 encoding gene comprises 12 exons and it is located in close proximity to P2X7 on chromosome 12. Multiple splicing variants, often resulting in different pattern of expression, have been found for this receptor (Dhulipala *et al.*, 1998). P2X4 receptor has been shown to be involved in the pathogenesis of chronic neuropathic and inflammatory pain. A study conducted in a rat model of neuropathic pain showed that the expression of the receptor is increased in microglia of the dorsal horn after the spinal nerve ligation, and intrathecal administration of P2X4 antisense oligodeoxynucleotides significantly attenuated both spinal cord-induced tactile hypersensitivity as well as the increase in P2X4 receptor levels (Dhulipala *et al.*, 1998). Knockout mice for P2X4 showed the same decrease in tactile allodynia caused by nerve injury and a reduction in peripheral inflammation-induced pain (Tsuda *et al.*, 2010). Moreover, a recent study showed that P2X4 blockage in microglia results in a reduced oligodendrocyte differentiation and remyelination after lysolecithin-induced demyelination (Zabala *et al.*, 2018).
- *P2X5;* the gene encoding for this receptor shares chromosomal localization with the P2X1 gene and consists of 12 exons in human and of 13 exons in mouse (Cox *et al.*, 2001). In mouse, P2X5 receptor is widely expressed in the central and enteric nervous system, and it has also been detected in cardiac and skeletal muscle, kidney, adrenal gland, and testis (Cox *et al.*, 2001; Ruan and Burnstock, 2005; Guo *et al.*, 2008). P2X5 knockout or transgenic animals have not been described so far.
- *P2X6;* this receptor is predominantly expressed in skeletal muscle, both in human and mouse. Its expression overlaps to a large extent with the expression pattern of P2X2 and P2X4 subunits (Nawa *et al.*, 1998; Yu *et al.*, 2010). The gene for P2X6 comprises 12 exons and is located on chromosome 22 in humans and chromosome 16 in mouse (Urano *et al.*, 1997). P2X6 subunits have been shown to translocate to the nucleus in hippocampal

neurons, where they are able to interact with members of the spliceosome leading to altered splicing activity (Díaz-Hernández *et al.*, 2015).

- *P2X7;* is probably the most studied receptor of this family, due to its strong involvement in many neuroinflammatory disorders, and it will be extensively discussed in the following chapters.

The study of P2X receptors has long been slowed down by the scarcity of small-molecule tools that serve as selective agonists and antagonists. In the last 10 years, thanks to cell-based high-throughput screening methods, there has been progress in the identification of some drug-like molecules that selectively target P2X1, P2X3, or P2X7 receptors. One of the first antagonists used was the quinidine, an alkaloid adrenergic receptor antagonist that acts on ATP receptor-mediated effects on smooth muscle contractility (Burnstock, 1972). Other early nonselective ATP antagonists included derivatives of the antiparasitic agent suramin, and various histochemical dyes (for example, the Brilliant Blue G, BBG). Suramin is a large polysulfonated molecule that can act on multiple targets, including G protein-coupled receptors, and multiple P2 receptor subtypes (Jacobson *et al.*, 2002), whereas BBG is a potent antagonist of P2X7 receptors, with an EC_{50} value of approximately 40 nM (Jiang *et al*., 2000). Nucleotide derivates have also served as useful ligands to negatively modulate the effects of ATP. Trinitrophenyl-ATP (TNP-ATP) and the corresponding di- and monophosphate derivatives represent the first nanomolar antagonists for P2X1, P2X3 and P2X2/3 subtypes (Virginio *et al.*, 1998). In the last years particular attention has been given to chemotypes that act as potent and selective antagonists of P2X7 receptor and they will be discussed in the following chapters.

Table 3 summarises the main features, as well as the agonists and antagonists of P2Y receptors.

Family		**Receptor**	**Endogenous agonist**	**Main distribution**	**Main signalling pathway**	**Agonists**	**Antagonists**
P2	P2X	$P2X_1$	ATP	Smooth muscle, platelets, cerebellum, dorsal horn spinal neurons	Permeable to Na^+, Ca^{2+}, K^+	BzATP, ATP, 2-MeSATP	NF-449, IP5I
		$P2X_2$		Smooth muscle, CNS, retina, chromaffin cells, autonomic and sensory ganglia		ATP, 2-MeSATP	RB2, iso PPADS
		$P2X_3$		Sensory neurons, NTS, some sympathetic neurons		ATP, 2-MeSATP	TNP-ATP
		$P2X_4$		CNS, testis, colon		ATP	5-BDBD
		$P2X_5$		Proliferating cells in skin, gut, bladder, thymus, spinal cord	Permeable to Cl^-	ATPγS, ATP	BBG
		$P2X_6$		CNS, motor neurons in spinal cord	Permeable to Na^+, Ca^{2+}, K^+	-	-
		$P2X_7$		Apoptotic cells in, for example, immune cells, pancreas, skin		BzATP	BBG, JNJ-47965567, A-804598, A-740003, KN-62

Table 3. *Summary of all the P2X receptors, their endogenous ligands, their main distribution, the main signalling pathways they activate, and the most known, used or potent ligands used for their activation/inhibition. Adapted from Burnstock, 2007 and from Calzaferri et al., 2020.*

1.3.4. Ionotropic receptor P2X7

Since their discovery in the 1960's by Geoffrey Burnstock, researchers have extensively investigated the receptors activated by ATP; the P2X7 receptor is one of them.

P2X7 belongs to the P2X receptor family, however, it was originally identified as a unique ATP-receptor named "the P2Z receptor", as it exhibits many characteristics distinct from P2X and P2Y receptors. Among the purinergic receptors, P2X7 has become the most widely investigated for its involvement in several pathways and with the largest amount of specific pharmacological tools available.

1.3.4.1. P2X7R structure, activation and distribution

The P2X7 receptor is an ATP-gated, non-selective cation channels, that functions in homo-trimeric form and supports Na^+ and Ca^+ influx into and K^+ out of the cell cytoplasm.

The *P2RX7* gene includes 13 exons encoding for a subunit with 595 amino acids in length; in humans the gene is 53 kB (kilobase) and is located at chromosome position 12q24.31, close to the *P2RX4* gene, whereas in mice is located at chromosome 5. It was initially described as containing 13 exons codifying for a 595 amino acids protein (Buell *et al.*, 1998), but more recent studies indicated the existence of two new exons: the exon N3 in human, localized in the intronic region between exon 2 and 3 (Cheewatrakoolpong *et al.*, 2005), and the exon 1' in rat, localized in the intronic region between exons 1 and 2 (Nicke *et al.*, 2009). Alternative splicing and several single nucleotide polymorphisms (SNPs) have been identified (more than 250) for P2X7, including 10 loss- and 3 gain-of-function (Barden *et al.*, 2006; Lucae *et al.*, 2006). More than 150 SNPs in the extracellular loop and C-terminus, as well as 13 natural splice variants (P2X7A-J) have been discovered in human tissues (Jimenez-Mateos *et al*., 2019). P2X7A is well characterised as the full-length protein, whereas the P2X7B isoform has relevance for being the *C*-terminus-truncated form of the receptor (Cheewatrakoolpong *et al*., 2005; Nicke *et al*., 2009). Together with isoform P2X7B, the other one fully functional in mice is the isoform P2X7K, which has 8-fold higher sensitivity to agonists and slower deactivation (Nicke *et al*., 2009).

P2X7R structure

The P2X7 receptor differs from all other P2X subtypes for its structure and for its pharmacological and functional properties. The typical P2X7R subunit consists of two transmembrane domains (TM1 and TM2), a large, glycosylated, cysteine-rich extracellular loop, a short intracellular N-terminal domain, and in intracellular C-terminal domain, longer than that of other P2X receptor subunits. This long C-terminus comprises 239 amino acid residues (from 356 to 595) and contains several binding domains. One of them is the Ca^{2+}-dependent calmodulin (CaM) binding motif (located between residues 541 and 560); it was demonstrated that CaM binds constitutively to closed P2X7 receptor and dynamically during channel activation to significantly enhance and prolong calcium entry (Roger *et al.*, 2008). Other interesting motifs are two *C*-cys anchor sections present in both C- and N-termini, consisting in two regions rich in palmitoyalated cysteins anchored to the plasmatic membrane. It was shown that palmitoylation of residues in the two *C*-cys anchors uniquely prevent the P2X7 receptor subtype from undergoing desensitization, which is a typical property inherent to all other P2X subtypes (McCarthy *et al.*, 2019). Similar to the shape of zebrafish P2X4 (Díaz-Hernández *et al.*, 2002; Kawate *et al.*, 2009), P2X7R subunit is characterized by a molecular architecture akin to a leaping dolphin, with its extracellular loop forming the body, and the TM domains forming the tail. In its homo-trimeric form the receptor has a chalice-like shape, and, both in the closed and open states, the three subunits are positioned in a threefold symmetry around an axis perpendicular to the plasma membrane and running through the centre of the receptor, **Figure 4** (Kawate *et al.*, 2009; Hattori and Gouaux, 2012; Jiang *et al.*, 2013).

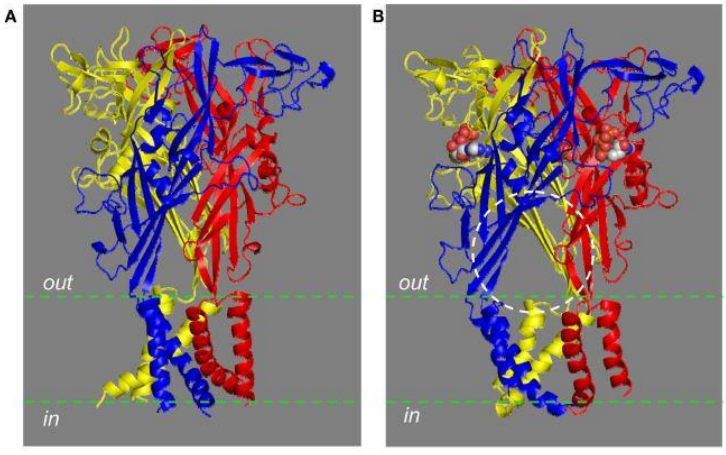

Figure 4. Chalice-like structural models of the human P2X7R. *The structural models of the trimeric human P2X7R in the closed (A) and ATP-bound open state (B), based on the structures of the zebrafish P2X4.1R. The two structures are viewed parallel to the plasma membrane (top) or from the extracellular side of the membrane (bottom). Each subunit is shown in a different color. Three ATP molecules shown in space filling representation bind to the three inter-subunit*

interfaces. The circle [top in (B)] shows one of the three lateral fenestrations for ions to enter or exit from the transmembrane ion-conducting pathway in the open state. Image adapted from Jiang et al., 2013.

P2X7R activation

P2X7R has three ATP binding sites; the activation of the receptor only occurs when at least two of these sites are occupied by ATP. In comparison with the other P2X receptors, P2X7R has 10 to 100-fold reduced ATP sensitivity; thanks to this peculiarity, P2X7R can function as a "danger signal" detector for high ATP concentrations that are released at sites of tissue damage (Linden *et al.*, 2019). The ATP-binding pocket is located at the interface of two subunits, in the upper body (UB), between the head domain (Hdom) and the dorsal fin (DF). Each subunit comprises an UB and a lower body (LB), a Hdom, left and right flippers (LF and RF, respectively), a DF and a fluke (FL), which are the two α-helix transmembrane domains, constituting the channel pore, **Figure 3**, (Karasawa and Kawate, 2016).

Upon its binding, ATP acquires a U-shaped conformation, whereas the upper body of the subunit shrinks toward the central axis of the receptor. This leads the lower body to widen and to form fenestrations, allowing the passage of ions through a lateral pathway, away from central axis. All these conformational changes result in vertical stretch and rotation of the two TMs, finally opening the channel gate (Jiang *et al.*, 2013).

When activated, P2X7R, like other ion channels, opens a non-selective cation channel, mediating the influx of Ca^+ and Na^+, and efflux of K^+. Also, unlike other members of P2X family, during prolonged exposure to ATP, the receptor opens a so-called "macropore" that can reach the diameter of 8.5 Å and allows the passage of large molecules (Di Virgilio *et al.*, 2018b). Two mechanisms have been proposed to explain macropore formation: 1) progressive dilatation of the P2X7R ion channel pore; and 2) recruitment of an accessory pore-forming molecule downstream of P2X7R activation (North, 2002; Pelegrin and Surprenant, 2006). However, convergent evidence from the two most used techniques to investigate this process (electrophysiology and fluorescent dye uptake) showed that no pore dilation or additional proteins are involved in the generation of the P2X7R macropore, but that the pore is intrinsically wide (Di Virgilio *et al.*, 2018b).

P2X7R distribution

The P2X7 receptor has a ubiquitous distribution in nearly all tissues and organs of the body, despite the expression may vary over orders of magnitude (Burnstock and Knight, 2004). Initial studies showed mRNA (messenger RNA) for the P2X7 receptor in many endothelial and epithelial cells, as well as in cells of hematopoietic lineage, including macrophages, microglia, and lymphocytes

(Surprenant *et al*., 1996). P2X7R is present on epithelial cells from the skin, kidney, reproductive and urinary tracts, and various exocrine glands (Burnstock and Knight, 2004).

In the brain, quantitative studies of P2X7R expression and immunohistochemical analysis showed that the receptor is expressed in high amounts on microglia and macrophages, followed by astrocytes, oligodendrocytes, dendritic cells, monocytes, and natural killer cells (Deuchars *et al.*, 2001; Kukley *et al.*, 2001; Gu *et al.*, 2000; Gu *et al.*, 2004; Xiang and Burnstock, 2005).

The presence of the receptor in neurons has been the subject of a long-stating debate; initial studies suggested an absence of P2X7 mRNA in these cells, and the apparent non-specificity of the antibodies used to identify P2X7R raised further doubts. However, later studies using new pharmacological and biomolecular tools provided evidence supporting the presence of functional P2X7Rs in neurons (Miras-Portugal *et al.*, 2017). On one hand early *in situ* hybridization analysis in rat brain suggested that P2X7 mRNA is not present in neurons, but only in ependymal cells (Collo *et al.*, 1997); on the other, later studies based on the most used antibodies to detect P2X7 showed persistent neuronal immunostaining in two putative knock-out mice (Solle *et al.*, 2001; Sim *et al.*, 2004). Several works tried to elucidate these initial findings, providing evidence of functional P2X7R in neurons using microfluorimetry, electrophysiology or immunohistochemistry techniques (Deuchars *et al*., 2001; Armstrong *et al*., 2002; Sperlágh *et al*., 2002; Miras-Portugal *et al*., 2003; Atkinson *et al*., 2004), but only in 2008 Yu et al., through a more sensitive *in situ* hybridization analysis demonstrated the presence of P2X7 mRNA in neurons (Yu *et al.*, 2008). At the same time, a work from our research group, using pure cultures of hippocampal neurons, demonstrated that P2X7 receptor is involved in the regulation of axonal growth and branching (Díaz-Hernández *et al*., 2008). Proof supporting the presence of P2X7R in neurons was further provided by Díaz-Hernández in 2012; in this work it was reported that inhibition of neuronal P2X7R decreases the glycogen synthase kinase 3 (GSK3) activity, increasing the proteolytic processing of the APP through an increase in α-secretase activity (Díaz-Hernández *et al.*, 2012).

During the years new mice models have been generated for the *in vivo* study of P2X7R. One of them is a knock-in mouse that expresses a humanized P2X7R under the control of the endogenous murine regulatory elements and sensitive to Cre recombinase-mediated activation (Metzger *et al.*, 2017); analysis of this model confirmed the presence of the receptor in glutamatergic pyramidal neurons of the CA3 hippocampal areas (Metzger *et al.*, 2017). Another model used for different works is a mouse expressing the enhanced green fluorescent protein (EGFP) immediately downstream of the P2X7R mouse promoter (^{P2X7}EGFP mice); selective agonists and antagonists have been employed to demonstrate the presence of functional P2X7 receptor in EGFP-hippocampal neurons (Engel *et al*., 2012; Sebastián-Serrano *et al*., 2016). In his work, Sebastián-

Serrano showed that granule neurons in the hippocampal dentate gyrus from postnatal P2X7R hypomorphic mice displayed altered synaptogenesis and a dendrite branching, thus suggesting that this receptor plays a key role in the somatodendritic compartment development (Sebastián-Serrano *et al*., 2016).

Another study from our group, using a transgenic line obtained by crossing ^{P2X7}EGFP mice with an Aβ peptide mouse model, demonstrated a significant reduction of P2X7R transcription in neuronal cells at early and advanced stages of the Alzheimer's Disease, and a significant increase of its expression in microglial cells at advanced and late stages of the disease (Martínez-Frailes *et al.*, 2019).

1.3.4.2. P2X7R involvement in physiological events

As receptor for an extracellular ligand, P2X7R activates a series of intracellular signalling pathways, mainly via alterations of the ion permeability, but also through formation of the large unselective pore, direct interaction with other proteins and activation of downstream proteases, kinases, and nuclear factor.

P2X7R role in axonal growth and branching

Axonal growth is essential for establishing neuronal circuits during brain development and for regenerative processes in the adult brain. Early studies performed in neural tube explants from 12-days-old rat embryos suggested that ATP acts as a negative modulator of neurite extension (Cheung *et al*., 2005). Moreover, studies of rat thoracolumbar sympathetic neurons revealed the expression of P2X7 mRNA and protein along the axons of these neurons (Allgaier *et al*., 2004).

Díaz-Hernández *et al.* in 2008 reported that extracellular ATP negatively controls axonal growth and branching in hippocampal neurons. In particular, it was demonstrated that exposure of cultured hippocampal neurons to ATP induced an intracellular Ca^{2+} increase in the axonal growth cone, generating a Ca^{2+} wave mainly at the distal region of the axon, where P2X7R is localized (Díaz-Hernández *et al.*, 2008). The focal Ca^{2+} influx correlates with changes in growth cone morphology, from lamellipodial to filopodial extensions. This morphological change was shown to be mediated by the P2X7 receptor. Activation of the receptor resulted in local actin polymerization and repression of axon growth, through regulation of proteins such as CaMKII (Ca^{2+}-calmodulin dependent protein kinase II) and FAK (focal adhesion kinase), and consequent modulation of the phosphoinositide 3-kinase P13K and its downstream targets, the serine/threonine-specific protein kinase B (Akt) and the glycogen synthase kinase 3 beta (GSK3β), (Díaz-Hernández *et al.*, 2008; Gomez-Villafuertes *et al.*, 2009; Miras-Portugal *et al*, 2017).

P2X7R interaction with Tissue Nonspecific Alkaline Phosphatase

Recently, it has been described a strong relationship between the P2X7 receptor and the TNAP enzyme. The interaction between these two proteins was shown to play a relevant role in the axonal growth.

In vitro studies on cultured hippocampal neurons showed that extracellular ATP levels are notably reduced during the first days of culturing (Díez -Zaera *et al.*, 2011). The reduction in extracellular ATP levels correlated with a significant increase in TNAP activity, especially at the axonal growth. The presence of TNAP at growth cones suggested a colocalization and a close functional interrelation with P2X7 receptor. It was indeed demonstrated that TNAP is able to induce axonal elongation by hydrolysing ATP in the immediate environment of the P2X7 receptors, thus preventing their activation. In addition, it was shown a relationship between the two proteins at the transcriptional level: inhibition of P2X7R reduced TNAP expression while addition of exogenous TNAP enhanced P2X7R expression (Díez-Zaera *et al.*, 2011).

In agreement with these findings, a more recent study demonstrated that seizures associated with hypophosphatasia were linked to neurodevelopmental alterations caused by partial dysregulation of P2X7R (Sebastián-Serrano *et al.*, 2016). Moreover, knock-out mice for TNAP were characterized by shorter callosal axonal projections than their wild-type littermates. This deficiency was prevented by selective knockdown of P2X7R in cortical neurons after *in utero* electroporation at the embryonic state (Sebastián-Serrano *et al.*, 2016). In addition, further proof of the involvement of P2X7R in axonal elongation and branching was obtained following *in vivo* administration of BBG to wild-type mice, which induced a significant increase in the thickness of the densely packed hippocampal CA3 pyramidal layer proximal to the dentate gyrus (Sebastián-Serrano *et al.*, 2016).

Presynaptic P2X7R role in neurotransmitters release

After the axonal growth cone reaches its target and establishes a functional synaptic contact, P2X7R expressed in the growth cone remains present at the presynaptic element (Miras-Portugal *et al*, 2017).

P2X7R was shown to be present in isolated nerve terminals from the cortex (Alloisio *et al*., 2008; Marcoli *et al*., 2008), striatum (Díaz-Hernández *et al*., 2009), midbrain (Miras-Portugal *et al*., 2003), hippocampus (Armstrong *et al*., 2002; Engel *et al*., 2012; Sebastián-Serrano *et al*., 2016), and cerebellum (Sánchez-Nogueiro *et al*., 2005).

Because the vesicular release of neurotransmitters is a direct consequence of increased calcium levels in nerve terminals, subsequent works studied the involvement of P2X7R in this event. Activation of presynaptic P2X7R was found to induce glutamate release in the cortex, cerebellum,

and hippocampus (Sperlágh *et al*., 2002; Sánchez-Nogueiro *et al*., 2005; Alloisio *et al*., 2008; León *et al*., 2008; Marcoli *et al*., 2008; Cervetto *et al*., 2012), GABA release in the hippocampus (Sperlágh *et al*., 2002; Wirkner *et al*., 2005), and arginine-vasopressin release in the hypothalamic-neurohypophysial system (Cuadra *et al*., 2014). Exocytotic release induced by P2X7R has also been confirmed using total internal reflection fluorescence microscopy (Gutiérrez-Martín *et al*., 2011). In those experiments, P2X7R stimulation induced both an increase in near membrane Ca^{2+} concentration and the exocytosis of fluorescence-labeled vesicles. Furthermore, P2X7R activation was shown to affect vesicle motion in all directions, implicating this receptor in the control of the early stages (docking and priming) of the secretory pathway (Gutiérrez-Martín *et al*., 2011). In line with these observations, P2X7R activation was shown to induce phosphorylation of synapsin-I, resulting in its dissociation from synaptic vesicles and promoting vesicle mobilization and fusion with the plasma membrane (León *et al*., 2008).

P2X7R role in neuroinflammation

It is widely accepted that P2X7R acts as a "sensor of danger", as it is the main sensor for the release of ATP at inflammation sites. During this process, inflammatory mediators, as well as other endogenous molecules, known as damage-associated molecular patterns (DAMPs), and including ATP, are secreted in large amount out to the extracellular space, as result of stress or tissue damage. The high levels of ATP can interact and activate the P2X7 receptor on microglia, leading to the maturation and secretion of several proinflammatory mediators (Di Virgilio *et al.*, 2017; Francistiová *et al.*, 2020).

Data collected from studies using animal model of induced neuroinflammation, obtained through administration of LPS, allowed to clarify the role of microglial P2X7R in neuroinflammation (Boche *et al*., 2013). LPS, after binding the LBP (LPS-binding protein), is able to interact with the Toll-like receptor 4 (TLR4), determining the activation of an intracellular signalling pathway. The trigger of this pathway finally leads to the activation of nuclear factor NF-kB by a Myeloid differentiation primary response protein MyD88 (MyD88)-dependent mechanism. In its activated status, NF-kB translocates to the nucleus, where it binds the DNA, and in this way promotes the transcription of proinflammatory mediators, such as proinflammatory cytokines like pro-interleukin-1 beta (pro-IL1β), pro-interleukin-18 (pro-IL18), and NLRP3 inflammasome (Akira and Takeda, 2004; Venigalla *et al*., 2016).

NLRP3 inflammasome is a cytosolic multiprotein oligomer responsible for the activation of inflammatory responses, and for its oligomerization and activation a decrease in K^+ levels in the cytosolic microenvironment is required. Once activated, the inflammasome recruits the apoptosis-

associated speck-like protein (ASC) and the procaspase-1 (another apoptosis-related protein), leading to the secretion of IL1β and IL18 (Petrilli *et al*., 2007; He *et al.*, 2016).

Several studies have shown that ATP, found at high extracellular concentrations following insults (Burnstock, 2008, 2016) or released by Aβ peptide (Kim *et al*., 2007; Sanz *et al*., 2009; Saez-Orellana *et al*., 2018; Goncalves *et al*., 2019), may be one of the signals promoting NLRP-inflammasome assembling and subsequent IL1β processing (Laliberte *et al*., 1999; Perregaux *et al*., 2000; Ye *et al*., 2013). Later works using both *in vitro* and *in vivo* approaches, suggested that Aβ-induced microglial activation requires the activation of P2X7R via an autocrine/paracrine stimulatory loop (Kim *et al*., 2007; Sanz *et al*., 2009). Additional research revealed that Aβ causes via a P2X7R-dependent mechanism NF-kB activation and NLRP3 inflammasome expression in microglial cells (Chiozzi *et al*., 2019). Since pre-treatment of cultured microglial cells with potassium chloride, KCl, avoided microglial NRLP3 activation (Gustin *et al*., 2015), it is reasonable to postulate that efflux of K^+ induced by P2X7R activation is the mechanism by which P2X7R promotes NRLP3 activation in microglial cells.

However, the mechanism by which K^+ concentration drop is translated into intracellular signals is still unclear. Two mechanisms have been proposed to elucidate this question: (i) the kinase NEK7 could sense the decrease of K^+ and bind to NLRP3 inflammasome regulating its function (He *et al.*, 2016; Shi *et al.*, 2016); (ii) K^+ efflux could lead to mitochondrial ROS (Reactive oxygen species) generation, *via* organellar Ca^+ influx, and in this way activate the inflammasome (Yaron *et al.*, 2015).

In addition to the K^+ efflux, other P2X7R-dependent signalling have been demonstrated to determine the activation of the inflammasome. One of them is the P2X7R-dependent ROS production *via* NADPH (Nicotinamide adenine dinucleotide phosphate) activation and MEK (Mitogen-activated protein kinase kinase)-ERK (extracellular signal-regulated kinases) signalling network (Lenertz *et al.*, 2009); the other one proposes a direct interaction between P2X7 receptor and components of the inflammasome, including NLRP2 (NLR Family Pyrin Domain Containing 2), ASC and NLRP3 (Minkiewicz *et al.*, 2013; Franceschini *et al.*, 2015). These studies are suggesting that P2X7R/NLRP3/Caspase1 signaling is a crucial pathway in the inflammasome activation once the microglial cell is primed (Francistiová *et al.*, 2020).

P2X7R-related cell death pathways leading to apoptosis, autophagy and pyroptosis

The involvement of P2X7R in regulating cell death has proven to be complex and varied and governed by the cell type nature of the stimulus, and duration of the stimulus.

In pathological conditions, acute activation of P2X7R by high ATP concentrations induces cell death, promoting the subsequent spread of neuronal death. Consistent with this hypothesis, acute P2X7R activation by high concentrations of ATP induces neuronal death in pure cortical neuron cultures from mouse or rat, an effect prevented by selective P2X7R antagonists (Nishida *et al*., 2012; Ohishi *et al*., 2016). The molecular mechanism underlying this neuronal death involves the activation of caspase-3, caspase-8, and caspase-9, as well as mitochondrial dysfunction and fragmentation followed by cytochrome c release in the cytosol, and stimulation of ROS production (Nishida *et al*., 2012; Bartlett *et al*., 2013; Miras-Portugal *et al*., 2017).

Besides these pathways, P2X7 receptor can also activate canonical pyroptosis pathway mediated by inflammatory caspases (caspase-1 and -11). In this case, ATP can act as a DAMP, leading to cell blebbing, release of cytokines and finally to lytic cell death (Bidula *et al.,* 2019).

Finally, P2X7 receptor can play a role also in autophagy. It was demonstrated that P2X7R-dependent autophagy was not mediated by calcium but subordinated to receptor's interaction with the heat shock protein 90, HSP90, (Young *et al.*, 2015).

P2X7R role in the PI3K/Akt/GSK3β pathway

The PI3K signalling network is an intracellular pathway important for the regulation of the cell cycle, directly related to cellular proliferation, quiescence, and cancer. It comprises the phosphoinositide 3-kinase (PI3K), the serine/threonine-specific protein kinase B (Akt) and the GSK3β. Activation of the PI3K signalling increases GSK3β phosphorylation, that is associated with reduced GSK3β activity. In its activated, non-phosphorylated form GSK3β mediates proteasome degradation of different oncoproteins, including the N-myc proto-oncogene protein (MYCN), thus behaving as anti-oncogene (Kaidanovich-Beilin and Woodgett, 2011; Hogarty and Maris, 2012; Fruman and Rommel, 2014).

Studies from our group demonstrated that the inhibition of P2X7R in neuroblastoma cells (N2a) increased the activity of α-secretase, an enzyme involved in the proteolytic processing of the APP, through inhibition of GSK3β (Díaz-Hernández *et al*., 2012). These results were further confirmed *in vivo*. Pharmacological inhibition of P2X7 receptor, with BBG, in a mouse model for AD determined a decrease in the activity of GSK3β, correlating with a significant decrease in the number of hippocampal amyloid plaques (Díaz-Hernández *et al*., 2012).

Moreover, it was reported that in neuroblastoma Akt itself can up-modulate P2X7R expression via EGFR and the nuclear factor Sp-1, suggesting that oncogenesis will induce an Akt/P2X7R positive loop (Gomez-Villafuertes *et al.*, 2015).

1.3.4.3. Ligands targeting the P2X7 receptor

In light of its role in physiological and pathological conditions, it is no surprise that P2X7R is considered a fascinating therapeutic target and potential biomarker for inflammation, pain disorders and cancers; for this reason, research on the development of P2X7R antagonists has continually increased.

P2X7R ligands, including agonists, antagonists and allosteric modulators are either present in nature or were synthetically developed. Apart from its endogenous agonist ATP, the synthetic 2'(3')-O-(4-Benzoylbenzoyl) adenosine-5'-triphosphate (Bz-ATP) is a more potent full agonist of P2X7 (pEC_{50} = 5.3) (Jacobson *et al*., 2002). Several P2X7R positive allosteric modulators (PAMs) have also been described, mainly from natural sources (e.g. isatin, agelasine, garcilonoic acid, and ginsenosides) or drug repurposing (e.g. clemastine, polymixin B, tenidap, and ivermectin) (Stokes *et al*., 2020). P2X7 receptor antagonists are commonly divide into two main groups: the first one comprising the blockers that bind orthosterically and competitively to the ATP binding pocket, and the other one including molecules that bind allosterically to sites other than the ATP site and reduces ligand binding affinity.

The first generation of P2X7 receptor antagonists was developed in the 1990's and includes compounds such as Reactive Blue 2, Suramin (and its derivates), Coomassie Brilliant Blue G (BBG), pyridoxal phosphate-6-azophenyl-2-4-disulfonic acid (PPADS), 1-N,O-bis(5-isoquinolinesulfonyl)-N-methyl-1-tyrosyls-4-phenylpiperazine (KN-62), and oxidized ATP (oATP), (Bertlett *et al.*, 2014). Among the earlier compounds, BBG remains the most useful and widely used, as it is effective at human, mouse, rat, dog, and guinea pig (Bartlett *et al.*, 2014). For this reason, BBG was initially the main compound used as a proof-of-concept of the P2X7 role in neurodegenerative diseases (Díaz-Hernández *et al*., 2009; Apolloni *et al.*, 2014; Chen *et al*., 2014; Bartlett *et al*., 2017).

During the last two decades, many pharmaceutical companies have endeavoured to develop a clinical candidate targeting this receptor. The second generation antagonists began to emerge in 2006 with the developments by Abbott Labs of disubstituted tetrazoles such as A438079 (Nelson *et al.*, 2006) and cyanoguanidines such as A740009 (Honore *et al.*, 2006). At about same time other companies started disclosing P2X7R antagonists; this led to the identification of Glaxo GSK314181A (Broom *et al.*, 2008) and AstraZeneca AZ11645373 (Stokes *et al.*, 2006), followed by AZD9056, also from AstraZeneca (Keystone *et al.*, 2012) and CE-224,535 from Pfizer (Stock *et al.*, 2012).

Since the development of these new drugs, pharmacological inhibition of P2X7R has proven to be effective and well-tolerated treatment in multiple rodent models of inflammatory diseases (Bartlett

et al., 2014; Zhao *et al*., 2016) as well as in Alzheimer's and psychiatric disorders, such as depression, and also in prion disease (Savio *et al.*, 2018). In the last few years have been registered >70 patents for P2X7 receptor antagonists, developed from several pharmaceutical companies, including AstraZeneca, Roche, Pfizer, Janssen, Abbott, Evotec, Glaxo, and others more (Park and Kim, 2017).

During 2010-2012, Glaxo was the most active in filing patents for novel P2X7R antagonists. The first group of compounds developed from this company included similar chemotypes such as imidazolidine, isothiazolidine and piperidone (US20100075968, WO2011054947, US20110046137), whereas the second group comprises molecules such as piperazine-2-one, and heterocycle-fused piperazine (US20100311749, US20120157436). The antagonistic activity of these compounds against human P2X7 receptor was evaluated in HEK293 (human embryonic kidney) cells expressing human recombinant P2X7R using the fluorescent imaging plate reader (FLIPR) Ca^{2+} assay (Park and Kim, 2017).

In this study we used the GSK 1482160A, N-{[2-chloro-3-(trifluoromethyl) phenyl] methyl}-1-methyl-5-oxo-L-prolinamide, **Figure 5**, an orally available negative allosteric modulator of the P2X7 receptor with good *in vitro* potency (Ali *et al*., 2013; Territo *et al.*, 2017), and an excellent biological activity IC_{50} (half maximal inhibitory concentration) 3 nM for human P2X7R and 2.5 nM for rat P2X7R (Abberley *et al.*, 2010; Ali *et al*., 2013). This compound readily crosses the blood brain barrier (BBB), and has been evaluated as a therapeutic agent in a Phase 1 human study, making it an attractive candidate for possible translation to a PET (Positron emission tomography) diagnostic agent (Gao *et al*., 2015).

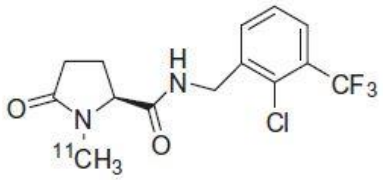

[^{11}C]GSK1482160

Figure 5. Chemical structures of [^{11}C] GSK1482160. *Image adapted from Gao et al., 2015*

1.3.4.4. Role of P2X7 receptor in neurodegenerative diseases

Neurodegenerative diseases (ND) are a cluster of disorders caused by either hereditary or sporadic conditions and characterized by progressive dysfunction of the nervous system that leads to inflammation, gliosis, and degeneration of neurons in the brain and/or spinal cord.

Up-regulated expression of P2X7R has been observed in several neurodegenerative diseases: e.g, in the neocortex and hippocampus of patients with epilepsy (Jimenez-Pacheco *et al*.,2016), in

microglia from spinal cord of multiple sclerosis and amyotrophic lateral sclerosis (ALS) (Yiangou *et al*., 2006), in the soma and terminals of neurons in Huntington's Disease (Díaz-Hernández *et al.*, 2009), and in astrocytes and microglia in Alzheimer's Disease (AD) (Ryu and McLarnon *et al.*, 2006; Martínez-Frailes *et al.*, 2019).

In the brains of patients with drug-resistant epilepsy, as well as in rodents subjected to status epilepticus, the expression of P2X7R has been shown to be elevated in the in the hippocampus and cortex (Engel *et al.*, 2012; Jimenez-Pacheco *et al*., 2013-2016); this upregulation was primarily detected in microglia (Rappold *et al*., 2006), but later studies demonstrated that it also occurs in neurons (Engel *et al.*, 2012; Jimenez-Pacheco *et al*., 2016).

Inflammation and autophagy paly critical roles in the pathogenesis of ALS, for this reason P2X7R has been long investigated in this disease. Increased expression of the receptor was detected in microglia and astrocytes (D'ambrosi *et al*., 2009; Gandelman *et al.*, 2010), and application of the P2X7 receptor BBG improved spinal cord pathology and ameliorated the disease in mice (Apolloni *et al.*, 2014). Additionally, more potent and selective P2X7R antagonists, such as A804598 and JNJ-47965567, have provided some beneficial effects in ALS mouse models (Fabbrizio *et al*., 2017; Ly *et al*., 2020; Ruiz-Ruiz *et al*., 2020).

Increased levels of P2X7R expression were reported also in multiple sclerosis (MS), in microglia (Yiangou *et al.*, 2006), in astrocytes (Narcisse *et al.*, 2005) and oligodendrocytes (Matute *et al.*, 2007) of the post-mortem brain from patients. In the acute phase of the disease, the elevated expression of P2X7R has been related to the release of pro-inflammatory cytokines, contributing to the progression of inflammation, degeneration and cell death (Grygorowicz *et al.*, 2016). Remarkably, a P2X7R down-regulation was observed during the acute phase of the disease on peripheral monocytes of MS patients (Amadio *et al.*, 2017). Moreover, studies have reported that P2X7 receptor antagonist decreased astrogliosis, reduced demyelination, and improved neurological symptoms in rat model of MS (Grygorowicz *et al.*, 2016). However, the difference in expression levels of P2X7R during the early and late phases of the disease has created a gap in understanding of the receptor function in MS and the treatment of the disease.

In Parkinson's Disease (PD) P2X7 receptor has been shown to induce microglia activation (Carmo *et al*., 2014) and to participate in the nigrostriatal degeneration in rat model (Marcellino *et al.*, 2010). In PD motor and memory deficit are related to loss of dopaminergic neurons; regrettably, administration of BBG in a mouse model for the disease (6-OHDA) was reported to not prevent this loss. Moreover, genetic deletion of P2X7R did not induce neuroprotection in mouse models of PD (Hracsko *et al.*, 2011).

Increased levels of P2X7 mRNA and protein, as well as altered P2X7-mediated calcium permeability in the soma and terminals of neurons, were detected in mouse models of Huntington's Disease (HD) (Díaz-Hernández *et al.*, 2009). In addition, *in vivo* P2X7R inhibition with BBG prevented neuronal apoptosis and attenuated body weight loss and motor-coordination deficits (Díaz-Hernández *et al.*, 2009). Interestingly, a recent work showed an up-regulation of the receptors, and in some case also altered splicing, in the brain of HD patients (Olla *et al.*, 2020).
The involvement of P2X7R in Alzheimer's Disease will be discussed in detail in the section 3.
Figure 6 shows a diagram of common neurologic diseases mediated via P2X7 receptors.

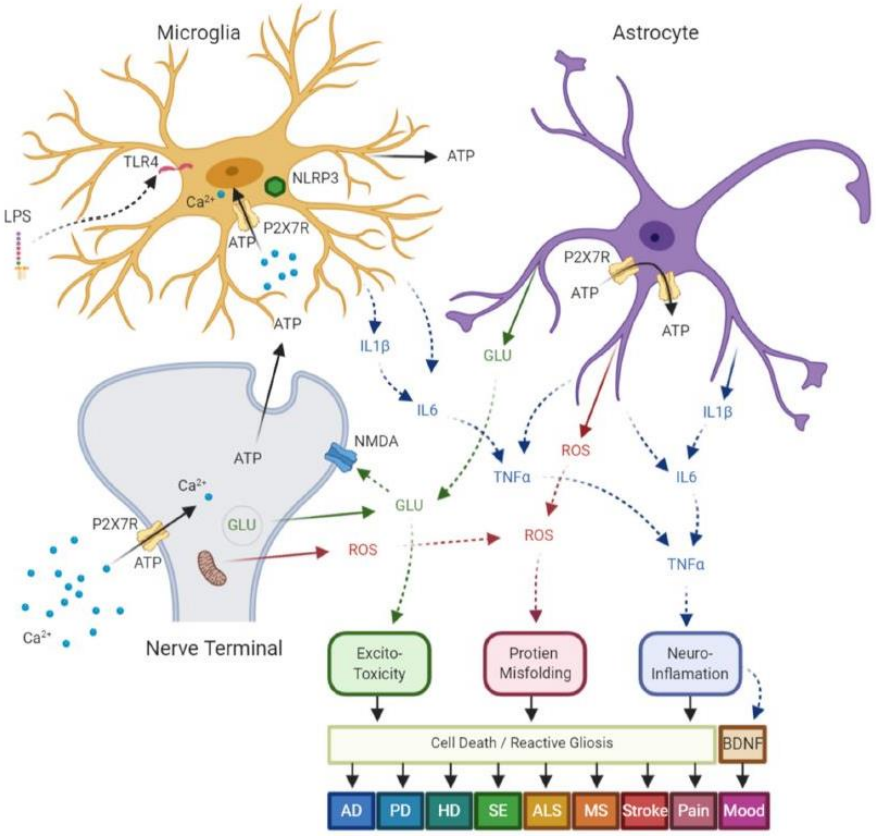

Figure 6. Diagram of common neurologic diseases mediated via P2X7 receptors (P2X7R)- in central nervous system (CNS). *Following ATP dependent Ca2+ influx through the receptor ion channel complex, P2X7R activation results in: (1) releases glutamate from nerve terminals and astrocytes by both exo and endocytotic mechanisms, which results in excite-toxicity; (2) synthesis and post-translational modification of pro-interleukin-1β (pro-IL-1β) which leads to mature IL-1β and ultimate release via the NLRP3 inflammasome. This activation then leads to other cytokine release and activation leading to neuroinflammation; (3) enhance reactive oxygen and nitrogen species which results in neuronal damage and protein misfolding; which in turn (4) leads to cell death and reactive astrogliosis; and (5) the downregulation of brain-derived neurotrophic factor (BDNF) and alterations in neuronal plasticity. The afore mentioned mechanisms have been shown independently, or in concert, to contribute to disease pathology in Alzheimer's disease (AD), Parkinson's disease (PD), Huntington's disease (HD), status epilepticus (SE), amyotrophic lateral sclerosis (ALS), multiple sclerosis (MS), stroke, pain, and mood disorders. ATP, Adenosine Triphosphate; GLU, glutamate; ROS, reactive oxygen species. Figure adapted from Territo and Zarrinmayeh, 2021.*

2. TAUOPATHIES

Tauopathies are a class of neurodegenerative diseases characterized by abnormal hyperphosphorylation of microtubule-associated protein tau that leads to the formation of neurofibrillary tangles (NFTs). Among the several tauopathies, Alzheimer's Disease is the most prevalent one.

2.1. Tau protein: structure, isoforms, and cellular function

Tau protein belongs to the family of microtubule-associated proteins (MAP), involved in the assembly and stabilization of tubulin monomers into microtubules to constitute the neuronal microtubules network (Weingarten *et al.*, 1975).

Based on its interaction with microtubules and its amino acid composition, the primary structure of tau can be divided into an N-terminal projection domain, a proline-rich region, a repeat region, and a C-terminal domain (Avila *et al.*, 2016). Human tau protein is encoded by the microtubule-associated protein tau gene, *MAPT,* located on chromosome 17q21 and containing 16 exons. The key discovery directly involving tau protein in neurodegeneration and dementia came from the finding that highly penetrant, dominant mutations in the *MAPT* gene cause an inherited form of frontotemporal dementia and parkinsonism (Medina and Avila, 2014). This gene can undergo an alternative splicing of the exons 2, 3 and 10, generating six tau isoforms. These isoforms may contain 0, 1, or 2 inserts near the amino-terminal end (0N, 1N, or 2N, respectively) and, depending on the alternative splicing of exon 10, the C-terminal microtubule binding region (MBR) may contain 3 or 4 repeat motifs (3R and 4R tau), ensuring the assembly and stabilization of axonal microtubules through their interaction with heterodimers of α- and β-tubulin, **Figure 7** (Andreadis, 2000; Buée *et al.*, 2000). The six isoforms of tau have been found in the adult brain; however, only shorter tau is found in the fetal brain. In the normal brain there are similar levels of 3R and 4R tau, but in neurodegeneration this ratio is often altered (Williams, 2006).

Tau is mainly found in neurons, but is also present at low levels in glia, and has been detected even outside cells (Wang and Mandelkow, 2015; Sebastián-Serrano *et al.*, 2018).

Although a large portion of tau is located in the axons, a small amount is physiologically distributed in dendrites; besides these two subcellular compartments, the presence of tau has been also reported in nuclei (Loomis *et al.*, 1990; Hirokawa *et al.*, 1996; Ittner *et al.*, 2010). Studies revealed that cytosolic tau protein is involved in physiological functions, including neural polarization (Caceres and Kosik, 1990), axonal transport (Terwel *et al.*, 2002; Rodriguez-Martin *et al.* 2013), axonogenesis (DiTella *et al.*, 1994), regulation of synaptic function (Souter and Lee, 2010), and neural polarization (Reynolds *et al.*, 2008). In the nucleus, it has been proposed that tau protein

might play an important role in DNA protection and in the regulation of the cell cycle (Andorfer *et al.*, 2005; Sultan *et al.*, 2011).

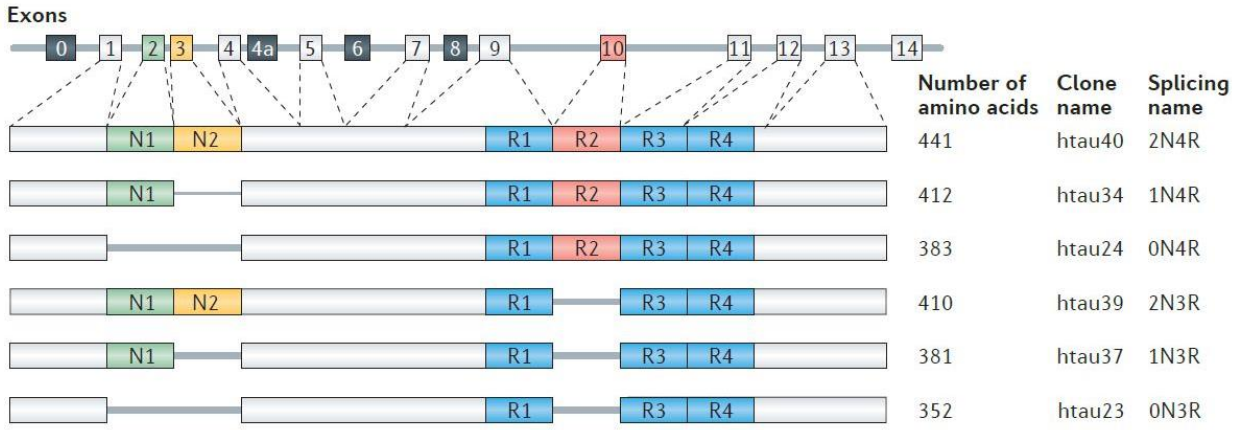

Figure 7. The human MAPT gene and the splice isoforms of tau in the human brain. *MAPT, the gene encoding human tau, contains 16 exons. The six human brain tau isoforms are generated through alternative splicing of E2, E3 and E10. These tau isoforms differ according to the presence of 0, 1 or 2 near-amino-terminal inserts (0N, 1N or 2N, respectively) and the presence of repeat R2, yielding 3 or 4 carboxy-terminal repeat domain (3R or 4R, respectively) tau species. Image adapted from Wang and Mandelkow, 2016.*

2.2. Tau protein post-translational modifications and aggregation

Post-translational modifications (PMTs) on tau have long been recognized as affecting the protein function, by preventing its interaction with microtubules and contributing to neurodegeneration (Bramblett *et al.*, 1993). These modifications are usually catalysed by enzymes and consist in phosphorylation, glycosylation, isomerization, truncation, glycation, deamination, nitration, methylation, ubiquitylation, and sumoylation (Alquezar *et al.*, 2021).

Among all of them, phosphorylation is the most common one and is developmentally regulated, such that fetal tau (which carries an average of approximately seven phosphates per molecule) is more highly modified than adult tau (approximately two phosphates per molecule), (Kanemaru *et al.* 1992; Ercan *et al.*, 2017). As a dynamic and highly regulated process, tau phosphorylation requires a balanced interplay of kinases and phosphatases. There are several putative Ser (serine) or Thr (threonine) sites on brain tau protein, target of different serine/threonine kinases, including GSK3β, cyclin dependent kinase 5 (cdk5), cyclic AMP-dependent protein kinase (PKA), protein kinase C (PKC), calmodulin-dependent protein kinase II (CaMKII), the brain-specific kinases 1 and 2, the tau-tubulin kinases 1 and 2 (Ferrer *et al.*, 2005). Tau can be dephosphorylated by protein phosphatases (PP) 1, 2A, 2B, 2C, and 5 (Hanger *et al.*, 2009). Among these phosphatases, PP2A accounts for around 70 percent of all tau dephosphorylation in the human brain. Interestingly, PP2A

also dephosphorylates and modulates the activity of components along the ERK (extracellular signal-regulated kinases) 1/2 MAPK (mitogen-activated protein kinases) cascade that leads to GSK3β activation, suggesting potential feedback cycles (Gong *et al.*,1993; Braithwaite *et al*., 2012; Alquezar *et al.*, 2021).

In its native unfolded status, tau is present as soluble monomers, capable to interact with microtubules. In this state, the protein shows a limited tendency to aggregate, but the change in tau electrostatics associated with phosphorylation determines an increase in the formation of aggregates. The result of this process is an anomalous accumulation of hyperphosphorylated tau dimers, trimers, and oligomers, that leads to the formation of intracellular aberrant aggregates called neurofibrillary tangles, NFTs (Wang and Mandelkow, 2015; Sebastián-Serrano *et al.*, 2018). These structures are a common histopathological hallmark of a set of neurodegenerative diseases known as tauopathies, including Alzheimer's disease, progressive supranuclear palsy, corticobasal degeneration, argyrophilic grain disease, Pick disease, Huntington's disease, and frontotemporal dementia with parkinsonism (Lee *et al.*, 2001; Williams, 2006).

2.3. Tau release and extracellular tau toxicity

The pathological progression of tauopathies is linked to gradual neuronal loss and cognitive decline. It was initially postulated that the presence of extracellular tau is a consequence of the protein release from dead cells; supporting this hypothesis, elevated tau levels were found in cerebrospinal fluid (CSF) samples from AD patients (Kurz *et al.*, 1998; Medina and Avila, 2014). However, over the last years, several studies showed that extracellular tau is released from cell lines and neurons via multiple pathways, supporting the notion that secretion of tau protein may be an important biological function of this protein, especially in disease (Pooler *et al.*, 2013). The presence of tau has been reported both in the culture media from primary neurons (Karch *et al.*, 2012) or cell lines overexpressing tau (Simon *et al.*, 2012), and in the CSF of mice (Yamada *et al.*, 2011) and humans (Magnoni *et al.*, 2012). Other studies showed, both *in vitro* and *in vivo*, that stimulation of neuronal activity enhances tau release, thus suggesting that tau is physiologically released into the extracellular space by neurons (Pooler *et al.*, 2013; Yamada *et al.*, 2014).

So far, the mechanism underlying tau release remains unclear. The lack of a signal peptide on tau protein sequence, that facilitates its translocation to the endosomal reticulum for the conventional secretory pathway, is the main reason why this process is still unknown. Although the inability to clearly identify this mechanism, it has been hypothesized that tau release mainly occurs in the synapsis (Sokolow *et al.*, 2015) through four different pathways: direct translocation from the cytoplasm across the plasma membrane (Chai, Dage and Citron, 2012; Merezhko *et al.* 2018),

release via secretory lysosomes (Dujardin *et al.* 2014), microvesicle shedding (Pooler *et al.*, 2013) or exosomes release (Saman *et al.*, 2012). Exosomal tau secretion has been proposed to account for the elevated CSF tau levels typically observed in early AD (Saman *et al.*, 2012). Even though strong evidence suggests that tau may be released by presynaptic vesicular secretion (Pooler *et al.*, 2013), tau protein was not found between the protein components of the synaptic vesicles under physiological conditions (Takamori *et al.*, 2006). Thus, the precise relationship between tau release under physiological conditions and the propagation of pathology in AD and other tauopathies remains to be determined.

In vivo approaches showed that, once in the extracellular space, soluble tau has a half-life of around 9,7 days, whereas in its insoluble form the half-life may last around 34,2 days; this low clearance rate may underlie the capacity of extracellular tau protein to reach distant regions from it release (Yamada *et al.*, 2015). Regrettably, the factors involved in extracellular tau clearance are still poorly understood. *In vitro* works suggested that macrophages and microglia cells could play a role in this process, by phagocytizing extracellular oligomerized tau protein, with macrophages being the main player (Majerova *et al.*, 2014). Another work has demonstrated that tau is a substrate of both matrix-metalloproteinases MMP-3 and MMP-9, and that a limited proteolysis by MMP-9 leads to an increase in tau oligomer formation (Nubling *et al.*, 2012).

One of the first works describing the extracellular tau-induced neurotoxic effect was carried out by Gómez-Ramos *et al*. using an in vitro approach; the authors showed that tau can be toxic when applied extracellularly to cultured hippocampal cells (Gómez-Ramos *et al.*, 2006). In a later work from the same group, it was demonstrated that the plasma membrane muscarinic receptors M1 and M3 are involved in the neurotoxic effect induced by tau (Gómez-Ramos *et al.*, 2008). In agreement with these findings, a muscarinic receptor binding region was found in the C-terminal domain of tau protein, including residues 391–407, and it was reported that changes in the level of intracellular calcium occur when extracellular monomeric tau binds and activates M1 and M3 receptors (Gomez-Ramos *et al.*, 2008). Interestingly, it was also showed that repetitive stimulation of neuronal muscarinic receptor by tau might cause a sustained increase of intracellular calcium levels that result in cell death (Gomez-Ramos *et al.*, 2009).

Interestingly, a later work described that only dephosphorylated tau protein behaves as an agonist for M1 and M3 receptors (Díaz-Hernández *et al.*, 2010). In this work, the authors demonstrated that tissue-nonspecific alkaline phosphatase recognizes and dephosphorylates the hyperphosphorylated tau protein, enabling its interaction with the muscarinic receptors (Díaz-Hernández *et al.*, 2010). It was also reported that specific activation of muscarinic receptors by dephosphorylated tau induces TNAP expression and phosphorylation of intracellular tau (Díaz-Hernández *et al.*, 2010). Finally, in

this study it was described that brain samples from Alzheimer's disease patients presented increased protein and messenger levels of TNAP as well as a higher TNAP enzymatic activity than samples from healthy controls (Díaz-Hernández *et al.*, 2010). In agreement with these observations, a preclinical assay with more than 100 AD patients also revealed that TNAP activity was significantly increased both in the hippocampus and in the blood of the AD patients, independently of sporadic or familial AD diagnosis (Vardy *et al.*, 2012).

In the last years, evidence also suggested a role of extracellular tau in the extensive loss of synapses observed in AD. A recent work reported that phosphorylation of tau protein is required for amyloid-beta-induced synapse loss (Mairet-Coello *et al.*, 2013). Moreover, in another study a strong association between the presence of hyperphosphorylated tau tangles and a reduction in presynaptic protein expression was observed in the brain of AD patients (Coleman and Yao, 2003). Furthermore, it was reported that the addition of extracellular tau oligomers impairs memory long-term potentiation in mice (Fa *et al.*, 2016; Puzzo *et al.*, 2017), and another work showed that the application of low-n-oligomers of tau to neurons in culture affects the morphology and density of dendritic spines. Interestingly, this effect was accompanied by increased expression of reactive oxygen species and alterations in intracellular calcium homeostasis (Kaniyappan *et al.*, 2017).

2.4. Spreading of tau pathology

In the brains of AD patients, tau pathology propagates following an anatomically defined pattern described by the neuropathological Braak sequential staging (Braak and Braak, 1991; Braak *et al*., 2006; Braak *et al*., 2011). According to this system, tau pathology is characterized by six stages based on the presence and density of the neurofibrillary tangles in the medial temporal lobe and several brain isocortical regions. Stages I–II (transen- torhinal) correlate with the lengthy preclinical phase of the disease; whereas stages III–IV (limbic) do so with mild cognitive impairment (loss of episodic memory) or mild dementia; and advanced V–VI stages (isocortical) usually correspond to cases with moderate to severe dementia (Braak and Braak, 1991; Braak *et al*., 2006; Braak *et al*., 2011; Medina and Avila, 2014).

Over the last years, evidence has suggested that the spreading of pathological tau occurs predominantly through neuron-to-neuron transmission (Wang and Mandelkow, 2016). This hypothesis is supported by different studies showing that intracranial injection of various forms of tau protein, such as fibrils (Clavaguera *et al.*, 2009; Peeraer *et al.*, 2015), filaments (Ahmed *et al.*, 2014), oligomers (Levarska *et al.*, 2013), or monomers (Michel *et al.*, 2014), have seeding properties, inducing tau pathology spreading from the injection site to anatomically connected brain areas (Sebastián-Serrano *et al.*, 2018).

It was also reported that in vivo injection of synthetic tau fibrils can induce selective neuronal loss in the surrounding area together with tau pathology spreading to connected brain areas (Peeraer *et al.*, 2015), and another study postulated that monomeric tau protein is the minimal initiating element able to induce tau pathology spreading (Michel *et al.*, 2014). Although these finding, the exact mechanism underlying the spreading of tau pathology remains unknown.

However, considering the previous works, Sebastián-Serrano *et al.* postulated a theory that could elucidate the pathological spreading of tau. An initial unknown event would cause an increase in the extracellular levels of tau and its subsequent dephosphorylation by TNAP. As a consequence of this initial event, an unusual activation of muscarinic receptors would occur in the affected area, promoting the phosphorylation of intracellular tau and the increased expression of TNAP. The phosphorylation of intracellular tau would prevent its interaction with microtubules, favouring its localization at the synaptic terminals and leading to an unusual tau release, eventually causing synaptic dysfunction. Besides, it has been reported that muscarinic M1 receptors may undergo agonist-induced receptor internalization (Lameh *et al.*, 1992), so their activation by the extracellular dephosphorylated tau protein could mediate the internalization of extracellular tau. In addition, both pre- and post-synaptic neurons may internalize or take up extracellular tau protein, by a still unknown mechanism, which would also favour intracellular tau nucleation and generation of NFTs. As result of both events, NFTs formation will be exacerbated in the neurons of this region, increasing tau release, and thus favouring the spreading of tau and the related synaptic dysfunction. Further, the increased expression of TNAP induced by extracellular tau would produce a more efficient dephosphorylation of tau itself, closing a positive feedback loop. This scenario will compromise cell viability by disturbing cellular homeostasis, first affecting the cells closest to the focus of initial tau release. Subsequently, the rupture of the plasma membrane would lead to the release of intracellular content into the interstitial space where the NFTs will provide a new source of extracellular tau. Moreover, due to the low disassemble rate of NFTs, the associated tau release will be sustained on time, contributing to the spreading of this aberrant cycle of stimulation, cell death, and tau release to new surrounding regions (Sebastián-Serrano *et al.*, 2018).

2.5. Alzheimer's Disease

Among the several tauopathies, Alzheimer's Disease is the one with the highest prevalence. AD is the most common type of dementia and can be defined as a slowly progressive neurodegenerative disease characterized by a progressive impairment of higher cognitive function, memory loss, and altered behaviour (Alzheimer, 1907; Rathmann and Conner, 1984). Typical AD onset is after 65 years old, although in less than 5% of cases the onset may be earlier (Alzheimer's-Association,

2020). Approximately between 1 and 3% of AD patients present autosomal dominant form of AD, denominated early familiar AD (eFAD) (Price and Sisodia, 1998). This form is characterized by mutations in both amyloid-β (Aβ) precursor protein (APP), and enzymes related in its processing, like presenilin-1 and presenilin-2 (PSEN1 and PSEN2) (Price and Sisodia, 1998; Ling *et al.*, 2003).

There are two types of neuropathological changes in AD which provide evidence about disease progress: (1) positive lesions, due to the accumulation of amyloid plaques, neurofibrillary tangles, and other deposits found in the brains of AD patients; and (2) negative lesions, characterized by large atrophy due to a neural and synaptic loss. Besides, other factors can cause neurodegeneration such as neuroinflammation, oxidative stress, and injury of cholinergic neurons (Serrano-Pozo *et al.*, 2011; Spires-Jones and Hyman, 2014; Singh *et al.*, 2016). Senile plaques are extracellular deposits of beta-amyloid protein (Aβ) peptides, generated by the sequential proteolysis of amyloid precursor protein (APP) by the enzymes β- and γ-secretase (Guo *et al*., 2020). Neurofibrillary tangles are assembled by abnormal accumulation of hyperphosphorylated tau protein (Avila, 2006). Aβ peptide and phosphorylated tau protein, primary criteria for AD diagnosis, are considered the main toxic species involved in AD (Long and Holtzman, 2019).

During the last years, researchers made great effort to identify other factors that may play a critical role in the early stages of AD. Among them, the role of microglia activation and neuroinflammation in the early onset and progression of AD has received tremendous attention (Heneka *et al.*, 2015).

Symptoms associated to AD follow a progressive course, starting with an impairment in learning and memory, proceeding to later detriments in complex attention, executive functions, language, visuospatial compartment, praxis, gnosis, behaviour, and/or social compartment (McKhann *et al.*, 2011). So far, there is no effective treatment available for symptomatic AD patients. There are only four commercial palliative-treatments available: three acetylcholinesterase inhibitors (donepezil, rivastigmine, galantamine) and memantine, a non-competitive NMDA (N-methyl-D-aspartate) receptors modulator (Long and Holtzman, 2019).

Over the last decade, numerous clinical trials have been carried out trying to reduce the amyloid toxicity associated with AD progression. These studies focused on different strategies, such as developing specific monoclonal antibodies against Aβ, both soluble and fibrillary form (Doody *et al.*, 2013; Salloway *et al.*, 2014; Selkoe, 2019); or trying to reduce brain Aβ through potent secretase inhibitors (Egan *et al*., 2018, 2019; Henley *et al*., 2019; Lopez Lopez *et al*., 2019); or avoiding Aβ-induced neuroinflammation using anti-inflammatory drugs (Aisen *et al*., 2000; de Jong *et al*., 2008). Regarding tau-based clinical trials, the strategies followed by researchers have been focused on reducing its intracellular phosphorylation rate (Domínguez *et al*., 2012), avoiding its aggregation (Wischik *et al*., 1996, 2015), or allowing its removal using immunotherapy approaches.

However, despite all the efforts made and the several clinical trials still ongoing, no effective treatment has been identified, and complementary approaches targeting alternative pathways still need to be explored.

2.6. GSK3 enzyme in Alzheimer's Disease

Glycogen synthase kinase 3 (GSK3) is a proline-directed serine/threonine kinase that plays a part in a number of physiological processes ranging from glycogen metabolism to gene transcription (Woodgett, 1990).

There are two GSK3 genes from which derive two isoforms of the enzyme, GSK3α and GSK3β, ubiquitously expressed and constitutively active (Mukai *et al*. 2002; Schaffer *et al*. 2003). A peculiar characteristic of GSK3 is that it does not act like others constitutively active kinases; its substrates usually need to be pre-phosphorylated by another kinase. Moreover, this enzyme is inhibited, rather than activated, in response to stimulation of the two main signalling pathways known to affect GSK3, the insulin and Wnt pathways (Beurel *et al.*, 2015). Insulin signalling leads to the activation of PI3-kinase and subsequently the activation of Akt, which in turn phosphorylates free cytoplasmic GSK3β and GSK3α at serine (Ser) residues 9 and 21, respectively, inhibiting both isoforms (Saltiel and Kahn 2001). In addition to regulatory Ser phosphorylation, GSK3β and GSK3α activity can be regulated by tyrosine (Tyr) phosphorylation at residues 216 or 279, respectively. Under physiological conditions, GSK3 is phosphorylated at these sites and increases in Tyr phosphorylation augment GSK3 activity. However, regulation of GSK3 at Tyr 216/279 is perhaps less common than regulation at Ser9/21 (Bhat *et al*. 2000; Bijur and Jope 2001).

The evidence that GSK3 plays a central role in AD and that its deregulation accounts for many of the pathological hallmarks of the disease in both sporadic and familial AD cases, has led researcher to formulate the "GSK3 hypothesis of AD" (Hooper *et al.*, 2008). In vitro and in vivo studies have shown that GSK3β activation is involved in Aβ formation and accumulation in the AD brain by modulating the cleavage of APP. In vitro studies suggest that GSK3β affects PS1 (presenilin 1) function, which is required for the generation of the toxic Aβ (Uemura *et al*., 2007). Moreover, GSK3β also regulates Aβ production by interfering with APP cleavage at the γ-secretase complex step, since both APP and PS1 are substrates of this kinase (Cai *et al*., 2012; Llorens-Martín *et al.*, 2014). In addition, our group confirmed the involvement of GSK3β in the proteolytic processing of the APP. In this work from 2012, Díaz-Hernández *et al*. showed that the inhibition of P2X7R in neuroblastoma cells (N2a) increased the activity of α-secretase, through inhibition of GSK3β (Díaz-Hernández *et al*., 2012). These results were additionally confirmed *in vivo*. Pharmacological

inhibition of P2X7 receptor, BBG, in a mouse model for AD determined a decrease in the activity of GSK3β, leading to a significant decrease in the number of hippocampal amyloid plaques (Díaz-Hernández *et al*., 2012).

GSK3 was also shown to be involved in tau phosphorylation. Studies *in vitro* and in cell culture models of neurodegeneration, demonstrated that GSK3β and GSK3α induce the hyper-phosphorylation of tau at both primed and non-primed phosphorylation sites, implicating GSK3 as an important tau-kinase possibly involved in the formation of NFTs in vivo (Toral-Rios *et al.*, 2020). Consistent with this, GSK3β transgenic mice display tau hyperphosphorylation and neurodegeneration (Lucas *et al.*, 2001). In addition, chronic lithium (GSK3 inhibitor) treatment prevents tau hyperphosphorylation and NFT formation in double transgenic mice over-expressing GSK3β and tau (harbouring a triple mutation associated with frontotemporal dementia and parkinsonism linked to chromosome 17), although reversal of pre-formed tangles was not observed (Engel *et al*., 2006).

There is then substantial data implicating GSK3 in the pathogenesis of AD, strongly indicating GSK3 inhibitors as a novel treatment strategy for this disease.

3. P2X7R INVOLVMENT IN AD

Over recent years, several studies have suggested the involvement of the purinergic receptor P2X7 in the AD brain pathology.

First evidence suggesting a possible involvement of P2X7R in AD came from analysis of its expression, that was found to be increased in microglial cells surrounding amyloid plaques both in AD patients and different AD mouse models (Parvathenani *et al*., 2003; McLarnon *et al*., 2006). More recent works using two different mouse models of AD based on the transgenic expression of human APP confirmed that P2X7R upregulation in activated microglial was parallel with AD progression (Lee *et al*., 2011; Martínez-Frailes *et al.*, 2019).

Different studies using both *in vitro* and *in vivo* approaches postulated that P2X7R might be one of the factors controlling APP processing (Francistiová *et al.,* 2020). Initial works, using mouse neuroblastoma cells (N2a) expressing human APP, reported that P2X7R activation through BzATP induces the release of soluble APP in a MAPK-dependent manner. This release was inhibited by selective P2X7R knockdown with siRNA and by specific P2X7R antagonists (Delarasse *et al*., 2011). However, as described before, a study from our group, using *in vitro* and *in vivo* approach, showed that the inhibition and not the activation of native P2X7R increases α-secretase activity through GSK3-β inhibition (Díaz-Hernández *et al*., 2012).

To elucidate these contradictory results, a recent study generated P2X7R deficient APP/PS1 mice. APP/PS1 mice express a chimeric mouse/human APP and human PSEN1, with the deletion of exon 9 found in eFAD patients, under the mouse prion protein promoter (APP/PSN1/P2X7$^{-/-}$) (Jankowsky *et al*., 2004). Results obtained in this work confirmed that genetic depletion of P2X7R leads to a significant reduction in the number of senile plaques in 10-months-old APP/PS1 mice. This decrease was accompanied by a drastic decreasing in Aβ peptides levels and rescue of the cognitive deficit developed by APP/PS1 mice (Martin *et al*., 2019).

Over the past decades, neuroinflammation and related microglia response were observed in *post mortem* tissues of AD patients (McGeer *et al.*, 2000). The P2X7R upregulation found in microglia cells surrounding amyloid plaques (Parvathenani *et al.*, 2003; McLarnon *et al.*, 2006) suggests that this receptor could be involved in microglia mediated-neuroinflammatory response in AD. Microglial cells have dual effects on AD progression. On one side, they promote a decrease of Aβ accumulation by stimulating its phagocytosis, clearance, and degradation. On the other side, chronic microglial activation leads to the release of proinflammatory cytokines that can contribute to the neuronal loss (Wang S. *et al.*, 2015; Wang W. Y. *et al.*, 2015). This dual effect may be caused by the activation of microglial cells in two subsets that present different molecular phenotype: the classical (M1) or the selective (M2) activated state. M1 state-activated microglia cells promote the

release of pro-inflammatory cytokines, playing a pivotal role in the defense against pathogens or tumor cells. M2 state-activated microglia cells secrete anti-inflammatory cytokines promoting tissue repairment (Francistiová *et al.*, 2020). As described in section 1.3.4.2., P2X7R has been widely shown to be involved in the NLRP3/Caspase1 signalling, a crucial pathway in the neuroinflammation, since it leads to inflammasome activation once the microglial cell is primed. Preliminary *in vitro* studies using microglial cells isolated from rat brains showed that P2X7R is involved in the $A\beta_{1-42}$ peptide-induced ATP-release (Kim *et al.*, 2007). Later, using both *in vitro* and *in vivo* approaches, it was suggested that Aβ-induced microglial activation requires the activation of P2X7R *via* an autocrine/paracrine stimulatory loop (Sanz *et al.*, 2009). In accordance with this hypothesis, Martinez-Frailes *et al.* (2019) found that upregulation of P2X7R in microglial cells takes place in advanced and late stages of AD, but not in the early stages, when the microglial priming has not yet occurred, and there is a reduced number of senile plaques (Martínez-Frailes *et al.*, 2019). Interestingly, recent studies have reported that NLRP3 activation may also induce tau hyperphosphorylation and aggregation in an IL-1β-dependent manner (Ising *et al.*, 2019).

Besides inflammasome activation, other evidence suggested an involvement of P2X7R in microglia migration and phagocytosis. Using *in vitro* and *in vivo* approaches, Martinez-Frailes *et al.* (2019) have recently confirmed that ATP-induced P2X7R activation promotes microglial migration. These findings might explain why there is an enrichment on P2X7R positive microglial cells around the senile plaques both in AD mouse models and in post-mortem brain samples from AD patients (Parvathenani *et al.*, 2003; McLarnon *et al.*, 2006). In the same work, Martinez-Frailes *et al.* also showed that inhibition, using the selective GSK 1482160A inhibitor, significantly increased the phagocytosis of 2 μm diameter fluorescence microspheres by microglial cells expressing P2X7R (Martínez-Frailes *et al.*, 2019). Accordingly, other *in vitro* studies using cultured primary human microglial cells confirmed that P2X7R activation induced by Bz-ATP decreased the phagocytic capacity of microglial cells. That effect was prevented when they used the selective P2X7R antagonist A438079 (Janks *et al.*, 2018). In agreement with these findings, ATP induced P2X7R activation causes cytoskeleton changes in microglial, reducing their phagocytic capacity (Fang *et al.*, 2009). In line with these works, and considering the important role that microglial phagocytosis plays in the removing of senile plaques, it is worth highlighting that, both in the hippocampus of J20 mice (a transgenic mouse line for human APP) and in *post mortem* cortical samples from human AD patients, the majority of microglial cells in contact with senile plaques did not express P2X7R. Furthermore, the percentage of microglia expressing P2X7R inside extracellular Aβ deposits remains constant along the AD progression, in opposition to the rising of the total number of microglial cells (Martinez-Frailes *et al.*, 2019). Besides its involvement in neuroinflammation,

P2X7R has been shown to play a role also in the oxidative stress, synaptic dysfunction and cellular death associated with AD (Miras-Portugal *et al.*, 2017; Francistiová *et al.*, 2020).

Despite all evidence that elucidate the role played by P2X7R in Aβ toxicity associated with AD, little is known about its possible role in tau-induced toxicity.

PROJECT OBJECTIVES

As described in the introduction, it is widely accepted that P2X7 receptor contributes to the Aβ toxicity associated with AD. However, little is known about its possible involvement in tau-induced toxicity. Our hypothesis is that this receptor could also play an important role in Tauopathies progression and for this reason be an interesting target to treat this kind of disease.

To verify this hypothesis, we proposed to accomplish the following objectives:

1. To evaluate if P2X7R is altered in tauopathies. To do that we analysed expression levels and distribution pattern of the P2X7R in both human Tauopathy patients and in tau mouse model (P301S mice).

2. To evaluate the possible beneficial effects derived from the pharmacological P2X7R blockade.

3. To supplement the pharmacological approach generating double transgenic mice by crossing P301S mice with P2X7 receptor null mice and overexpressing EGFP-tagged P2X7R mice.

MATERIAL AND METHODS

1. MATERIAL

1.1. Equipment

Table 4 lists the different devices used during the performance of the Biochemical, Molecular biology and Behavioural techniques described in this thesis.

Table 4. List of the different equipment used.

Technique	Instrumentation and Model	Commercial provider
Gene Expression	SimpliAmp™ Thermal Cycler, StepOnePlus Real-Time PCR	Applied Biosystem
	Biophotometer Plus Spectrophotometer	Eppendorf
	Wide mini-sub cell GT Horizontal Electrophoresis System	Bio-Rad
	Gel Logic 200 Imagin System Tranluminator	Kodak
	Gel Doc XR^{+} System	Bio-Rad
Immunological Techniques	Cryostat CM1950	Leica
	DTS-2 Digital Thermo Shaker	Elmi
	Stereo Microscope Zoom WF 10x/20	VWR
	Microscope TE-200	Nikon
	DFC310 FX Camera, Magnifier MZ10F, Confocal Microscope TCS SPE, DM 1000 Microscope	Leica
	pE-300^{white} fluorescence LED	CoolLED
Western Blotting	Mini-Protean 3 Electrophoresis System	Bio-Rad
	Mini-Trans-Blot Electrophoretic Transfer Cell Transfer System	Bio-Rad
	CP1000 Autoradiography Developer	AGFA
	LAS500 chemiluminescence detector	GE Healthcare
Stereotaxic injection	Stereotaxic equipment	UNO Anesthesia
	EVERFLO Oxygen Concentrator	Respironics
	Anesthesia equipment	MPB
	Infusion pump	KdsScientific
Behavioural assay	Open Field/Novel object	Instrumental facility of UCM
	Elevated plus maze	Instrumental facility of UCM
	Rotarod	Ugo Basile

1.2. Reagents and chemicals

All the compounds and reagents used for the protocols carried out, as well as the commercial companies that supplied them, are listed in the **Table 5** below.

Table 5. List of reagents and chemicals used.

Experimental Technique	Reagents and chemicals	Commercial provider
DNA and RNA techniques	NaOH, Tris-HCl, Agarose, *SYBR-Safe DNA Stain, RNase-Zap*, Moloney Murine Leukemia Virus Reverse Transcriptase, dNTPs, Kapa2G Fast HotStart Ready mix with dye	Sigma-Aldrich
	DNA ladder mix (100-5000)	PanReac Applichem
	Ultratools polymerase, HotSplit polymerase, MasterMix polymerase, TaqMan Fast Universal PCR Master Mix, LuminoCt Ready Mix, SpeedTools Total RNA Extraction Kit	Biotools
	EconoTaq Plus Green 2x Master Mix	Lucigene
Western Blotting	Hepes, EDTA, NaCl, NaF, Sodium Ortovanadate, NP40, Nitrocellulose Membranes, SDS, Glycine, Tris, *Tween-20*, Ponceau Red, Skimmed Milk Powder, BSA, glycerol	Sigma-Aldrich
	Okadaic acid	Calbiochem
	Bradford Reagent, Bromophenol Blue	Merck-Millipore
	Complete TM Protease Inhibitor Cocktail Tablets	Roche
	Ammonium persulfate, Bis-acrylamide 30%, Temed, β-mercaptoethanol	Bio-Rad
	Methanol, Protein Marker VI (10-245) prestained	PanReac Applichem
	ECL Pro	Perkin Elmer
	Autoradiography films, developer liquid and fixative	AGFA
Immunofluorescence/ Immunohistochemistry	H_2O_2, PBS, BSA, FBS, TritonX-100, Xylene, Ethanol, diaminobenzidine	Sigma-Aldrich
	Microscope slides	Thermo Scientific
	FluorSave™ Reagent	EMD Millipore
	Elite Vectastain kit	Vector Laboratories

1.3. Antibodies

Primary and secondary antibodies used for immunofluorescence (IF), or western blot techniques are listed in **Table 6-7**. For nucleic labelling, the 4'-6-diamidino-2-phenylindole nucleic acid marker (DAPI, Invitrogen) was used.

Table 6. List of the different primary antibodies used.

Primary Antibody	Species	Commercial provider	Dilution Western Blot	Dilution IF
Anti-P2X7R	Rabbit	Alomone Labs	1:1000	1:100
Anti-αTubulin	Mouse	Sigma-Aldrich	1:10.000	
Anti-GFP	Rabbit	Sigma-Aldrich	1:1000	1:500
Anti-GFP	Chicken	AVES Lab		1:400
Anti-GAPDH	Rabbit	Sigma-Aldrich	1:10.000	
Anti-β-Actin	Mouse	Sigma-Aldrich	1:10.000	
Anti-Iba1	Rabbit	Wako		1:100
Anti-NeuN	Mouse	Merck Millipore		1:100
Anti-GFAP	Mouse	Santa Cruz		1:200
Anti-AT8	Mouse	Thermo Fisher Scientific	1:500	1:100
Anti-TAU1	Mouse	Sigma-Aldrich	1:500	
Anti-PHF1	Mouse	Provided by Jesús Avila group	1:1000	
Anti-TAU5	Mouse	Merck Millipore	1:1000	
Anti-cleave caspase-3 (Casp3)	Rabbit	Cell Signaling		1:50
Anti-phospho-GSK-3	Rabbit	Cell Signaling	1:1000	
Anti-GSK3 α/β	Mouse	Invitrogen	1:1000	
Anti-IL-1β	Rat	R&D Systems	1:200	
Anti-IL6	Mouse	Jena Bioscience	1:500	
Anti-IL10	Mouse	Jena Bioscience	1:200	
Anti-TNFα	Rabbit	Jena Bioscience	1:500	
Anti-Ki-67	Rabbit	Santa Cruz		1:600
Anti-Tnap	Rabbit	GeneTex	1:1000	

Table 7. List of the different secondary antibodies used.

Secondary Antibody	Species	Commercial provider	Dilution Western Blot	Dilution IF
Anti-rabbit Alexa 488	Goat	Invitrogen		1:400
Anti-chicken Alexa 488	Goat	Invitrogen		1:400
Anti-rabbit Alexa 555	Goat	Invitrogen		1:400
Anti-rabbit Alexa 594	Goat	Invitrogen		1:400
Anti-mouse Alexa 594	Goat	Invitrogen		1:400
Anti-rabbit IgG conjugated with horseradish peroxidase	Goat	DAKO	From 1:1000 to 1:10.000	
Anti-mouse IgG conjugated with horseradish peroxidase	Goat	DAKO	From 1:1000 to 1:10.000	
Streptavidin Alexa Fluor 488		Abcam		1:400

1.4. Oligonucleotides

Transgenic mice were genotyped using specific primers listed in **Table 8**. The 4 oligonucleotides used to identify the hemizygous P301S mice (A, B, C, D) amplify a wild type sequence of 200 base pairs (bp) as positive control and a transgenic sequence of 450 bp. The transgene (PS19) inserted at chromosome (Chr) 3 (Build GRCm38/mm10) causes a 249 kilobase (Kb) deletion; details of the mutation are described in section 1.5.1.1.

For the genotyping of ^{P2X7}EGFP mice, oligonucleotides E and F were used, where sequences of 300 bp in size were obtained. The transgenic sequence is an insertion mutation in which an EGFP reporter gene, followed by a polyadenylation sequence, was inserted into a bacterial artificial chromosome (BAC); mutation is described in detail in section 1.5.1.2.

In the case of P2X7^{451P}-EGFP mice, oligonucleotides G and H were used, which amplified sequences of 1284 bp in size containing a Strep-His-EGFP cassette directly inserted upstream of the stop codon into exon 13 of the *P2rx7*. A complete description of the BAC-P2X7-EGFP is present in the section 1.5.1.3.

P2X7$^{-/-}$ were genotyped using oligonucleotides I and L, obtaining sequences of 415 bp for the KO, and of 1142 bp for the WT; full detailed description is provided in section 1.5.1.3.

Table 9 shows the oligonucleotides used for the RT-qPCR amplification of human *P2RX7* and mouse *P2rx7* RNA.

Table 8. List of the different oligonucleotides and amplification protocols used for the genotype of P301S mice, ^{P2X7}EGFP mice, P2X7^{451P}-EGFP mice and P2X7$^{-/-}$ mice. *Numbers between brackets indicate the number of amplification cycles. The time of each step is indicated in minutes (min) or seconds (sec).*

Oligonucleotides	Sequence	Amplifying protocol		
P301S	**A:** Fw 5'-GGC ATC TCA GCA ATG TCT CC-3'	(1) 94°C 5 min	(20) 94°C 15 sec 65°C 15 sec 72°C 10 sec	(1)72°C 10min
	B: Rv 5'-GGT ATT AGC CTA TGG GGG ACAC-3'			
	C: 5'-CAA ATG TTG CTT GTC TGG TG-3'			
	D: 5'-GTC AGT CGA GTG CAC AGT TT-3'			
^{P2X7}EGFP	**E:** Fw 5'-CCTACGGCGTGCAGTGCTTCAGC-3'	(1) 94°C 5 min	(40) 94°C 30 sec 60°C 45 sec 72°C 45 sec	(1)72°C 10min
	F: Rv 5'-CGGCGAGCTGCACGCTGCGTCCTC-3'			
P2X7^{451P}-EGFP	**G:** Fw 5'-GGTTCTTAGCAGGCTTAACAGCA-3'	(1) 94°C 5 min	(35) 94°C 30 sec 60°C 60 sec 72°C 60 sec	(1)72°C 10min
	H: Rv 5'-ATGGGGGTGTTCTGCTGG AG T-3'			
P2X7$^{-/-}$	**I:** Fw 5'-CTGGCAACTATCCATTTTCC-3'	(1) 94°C 5 min	(35) 94°C 30 sec 60°C 60 sec 72°C 125 sec	(1)72°C 10min
	L: Rv 5'-GTGTGAGTGAATGAGATCGTG-3'			

Table 9. List of the different oligonucleotides and amplification protocols used for the RT-qPCR amplification. *Numbers between brackets indicate the number of amplification cycles. The time of each step is indicated in minutes (min) or seconds (sec).*

Oligonucleotides	Sequence	Amplifying protocol	
Human P2RX7	**A:** Fw 5'- AAAACAGAAGGCCAAGAGCA -3'	(1) 94°C 20 sec	(40) 95°C 1 sec 60°C 20 sec
	B: Rv 5'- CACCAGGCAGAGACTTCACA -3'		
Mouse P2rx7	Fw 5′- GGTGCCAGTGTGGAAATTG-3′	(1) 94°C 20 sec	(40) 95°C 1 sec 60°C 20 sec
	Rv 5′- TAGGGATACTTGAAGCCACT-3′		
GAPDH	5′-CACCACCAACTGCTTAGCCC-3′	(1) 94°C 20 sec	(40) 95°C 1 sec 60°C 20 sec
	Rv 5′-TGTGGTCATGAGCCCTTCC-3′		

1.5. Biological material

1.5.1. Human brain tissues

Human *post mortem* hippocampal samples were kindly provided by the Banco de Tejidos Fundación CIEN (BT-CIEN, Madrid, Spain). A written informed consent for brain removal after death for diagnostic and research purposes was obtained from the brain donors and/or nexts of kin. Procedures, information, and consent forms were approved by the Bioethics Subcommittee of Fundación Cien Madrid, Spain. **Table 10** summarizes gender and age of the patients with AD or PiD and controls from whom the hippocampal *post mortem* samples were collected.

Table 10. List case information for Control, Alzheimer´s and Pick´s disease and cases. *M, male. F, female*

Diagnosis	Sex	Age (years)	Western Blot analysis	Quantitative Real-Time PCR	Immunofluorescence/ Immunohistochemistry
Alzheimer	M	81	√	√	
Alzheimer	M	76	√	√	
Alzheimer	M	69	√	√	
Alzheimer	M	68	√	√	√
Alzheimer	M	63	√	√	√
Alzheimer	M	57	√	√	
Alzheimer	F	94	√	√	
Alzheimer	F	86	√	√	
Alzheimer	F	65	√		√
Pick	F	89	√	√	
Pick	F	86	√	√	√
Pick	F	79	√	√	√
Pick	M	70	√	√	√
Control	F	83	√	√	√
Control	F	74	√	√	
Control	F	61	√	√	
Control	F	58	√	√	√
Control	M	73	√		√
Control	F	70	√		

1.5.2. Animals

All mice used in this Doctoral thesis were breeded in the animal facility of the Faculty of Medicine (CAI) of the Universidad Complutense de Madrid (UCM). The mice were housed in a light and temperature-controlled humid environment, with a 12h light-dark cycle and a light onset at 08:00 am; grouped 4-6 per cage and allowed free access to water and food (*ad libitum*).

All animal procedures were carried out at the Universidad Complutense de Madrid (UCM), in compliance with National and European regulations (RD1201/2005; 86/609/CEE) and following the guidelines of the International Council for the Laboratory Animal Science. The protocol for animal experiments was approved by the Committee of Animal Experiments at the UCM and the Environmental Counselling of the Comunidad de Madrid, Spain (PROEX 374/15 and PROEX 185/17). All surgeries were performed under isoflurane anaesthesia, and all efforts were made to minimize suffering.

The mouse models used for this work were the following: P301S Tg mice, expressing a mutant form of human microtubule-associated protein tau (*MAPT*); ^{P2X7}EGFP Tg mice, expressing EGFP (green fluorescent protein) immediately downstream of P2X7 receptor promoter; P2X7 null mice and overexpressing EGFP-tagged P2X7R mice. A detailed description of each mouse model line follows below.

1.5.2.1 Mice expressing a mutant form of human microtubule-associated protein tau (*MAPT*).

P301S mice were obtained from Jackson laboratory, line B6; C3-Tg (Prnp-MAPT*P301S)PS19Vle/J, stock number 008169. The original B6C3H/F1 genetic background was changed to C57BL/6J by back-crossing them with C57 animals in our laboratory. In all experimental groups wild type littermates were used as control, keeping a balanced ratio between females and males.

The P301S model is a transgenic line carrying in hemizygous a mutant form of the human microtubule-associated protein tau, MAPT, under the control of the mouse prion protein promoter (Prnp). The transgene encodes the disease-associated P301S mutation (mutation type: point, missense; codon change: CCG to TCG; genomic region: coding, exon 10; genomic position: rs63751438, **Figure 8**) and includes four microtubule-binding domains and one N-terminal insert (4R/1N) (The Jackson Laboratory, 2019). The expression of the hyperphosphorylated, insoluble mutant human MAPT is five-fold higher than the expression of the endogenous mouse MAPT; the protein accumulates with age causing decreased microtubule binding/density (Yoshiyama *et al.*, 2007).

P301S mice have a median lifespan of around nine months with approximately 80% dying by 12 months. Histological analysis of the hippocampus reveals a progressively decrease in synaptophysin immunoreactivity from three to six months of age in the CA3 region, and neuron degeneration, with consequent ventricular dilatation (brain atrophy), by eight months of age. Neuron loss spreads to the amygdala, neocortex and entorhinal cortex by 12 months of age. Increased microgliosis is also observed at three months in the white matter of the brain and spinal cord, spreading to the white and grey matter of the hippocampus, amygdala, entorhinal cortex and spinal cord by six months (Yoshiyama *et al.*, 2007).

P301S mice develop widespread neurofibrillary tangle-like inclusions in neocortex, amygdala, hippocampus, brain stem and spinal cord from five months of age with progressive accumulation, but not amyloid plaques. The ultrastructure of the neurofibrillary tangle-like lesions detected is similar to the one found in brain lesions of human Alzheimer's disease and tauopathy patients. Prior to the appearance of tau pathology, these mice were shown to display tau seeding activity in the brain, first detected at 1.5 months of age, indicating that proteopathic tau seeding is an early phenotype in this model (Holmes *et al*, 2014).

Behaviourally, P301S mice display signs of age-associated cognitive impairment, including selective deficits in spatial learning and memory ability in the Morrir water maze. At three months of age, transgenic mice also exhibit clasping and limb retraction when lifted by the tail, which progresses to limb weakness. By ten months of age the mice exhibit a hunched back and paralysis, followed by inability to feed (Yoshiyama *et al.*, 2007, Takeuchi *et al*, 2011).

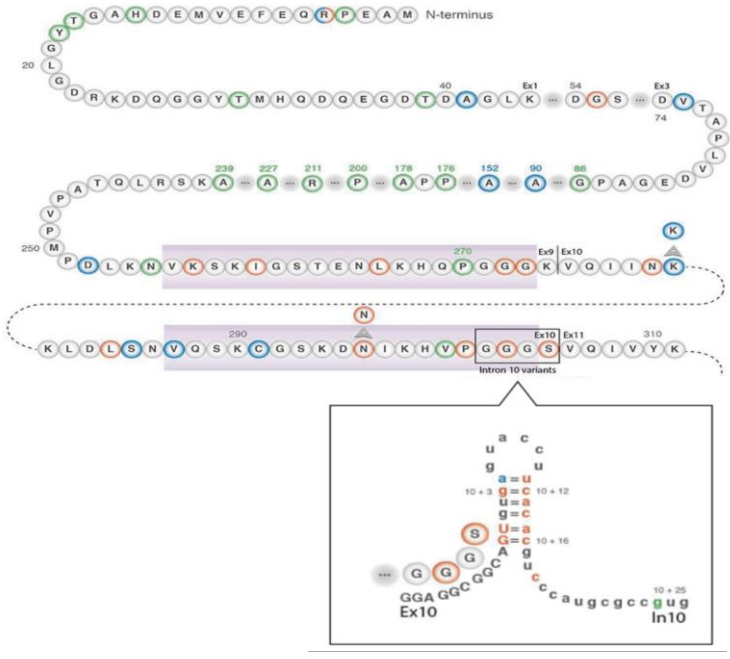

Figure 8. Scheme of P301S mutation. *Image adapted from Alzforum.org*

1.5.2.2. Mice expressing EGFP immediately downstream of P2X7 receptor promoter.

P2X7 receptor reporter mice (Tg [P2rx7-EGFP]FY174Gsat/Mmcd, stock 011959-UCD) were obtained from the U.S. National Institutes of Health Mutant Mouse Regional Resource Centers and granted by Dr. M. Nedergaard (University of Rochester, Rochester, NY, U.S.A.). The genotype of this mice line is mutated with an insertion. The mutation consists of an EGFP reporter gene, followed by a polyadenylation sequence, inserted into a BAC clone (BAC address: RP23-181F3) at the initiating ATG codon of the first coding exon of the P2rx7 gene, so that EGFP expression is driven by the regulatory sequences of the BAC gene (Gong *et al*, 2003).

1.5.2.3. P2X7 receptor null mice and overexpressing EGFP-tagged P2X7R mice.

P2X7 receptor null mice ($P2X7^{-/-}$, B6N-$P2rx7^{tm1d(EUCOMM)Wtsi/Ieg}$) and overexpressing EGFP-tagged P2X7R ($P2X7^{451P}$-EGFP, B6N-Tg(RP24-114E20-P2X7451P/StrepHisEGFP)17Ani) mice were provided by Prof. Annette Nicke.

$P2X7^{-/-}$ mice were purchased from the European Mutant Mouse Archive. The knockout mouse is obtained by insertion of L1L2_Bact_P vector at position 122652263 of Chromosome 5 upstream of the critical exon(s) (Build GRCm38). The cassette is composed of an flippase recognition target (FRT) site followed by lacZ (lac operon Z gene) sequence and a loxP (locus of X-over P1) site. This first loxP site is followed by a neomycin resistance gene (neo) under the control of the human beta-actin promoter, SV40 polyA (simian virus 40 late polyadenylation signal), a second FRT site and a second loxP site, **Figure 9**. A third loxP site is inserted downstream of the targeted exon(s) at position 122653166. The critical exon(s) is(are) thus flanked by loxP sites. A "conditional ready" (floxed) allele can be created by flippase (flp) recombinase expression in mice carrying this allele. Subsequent cre (causes recombination) expression results in a knockout mouse (http://www.informatics.jax.org/mgihome/nomen/IKMC_schmatics.shtml).

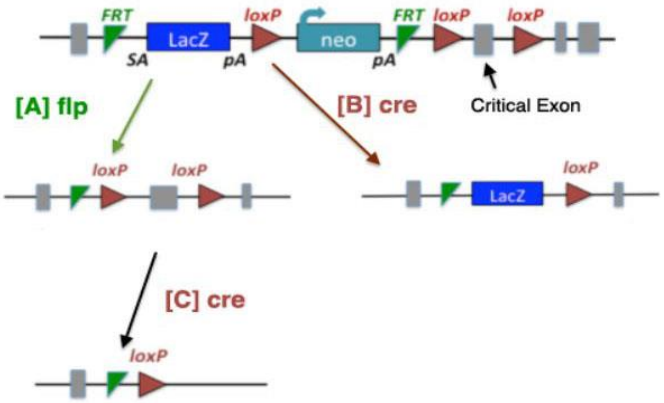

Figure 9. Scheme of the L1L2_Bact_P cassette. *The Bac cassette is inserted at position 122652263 of Chromosome 5 upstream of the critical exon(s) (Build GRCm38).*

P2X7^{451P}-EGFP mice were generated in Prof. Nicke as previously described (Kaczmarek-Hajek *et al.*, 2018). For the generation of P2X7-EGFP BAC transgenic mice, the *P2rx7* cDNA was obtained from C57BL/6 mouse brain and C-terminally fused to the EGFP-sequence via a Strep-tagII-Gly-7xHis-Gly linker sequence to provide additional labelin/purification options and minimize interference with the receptor function. Next, BAC clone RP24-114E20, containing the full lenght *P2rx7* and more than 100 kb of the 5´region was modified accordingly by insertion of the Strep-His-EGFP sequence in exon 13 to preserve the exon-intron structure of the gene, **Figure 10**. Upon verification by Southern and sequencing, the linearized BAC was injected into pronuclei of FVB/N mouse oocytes.

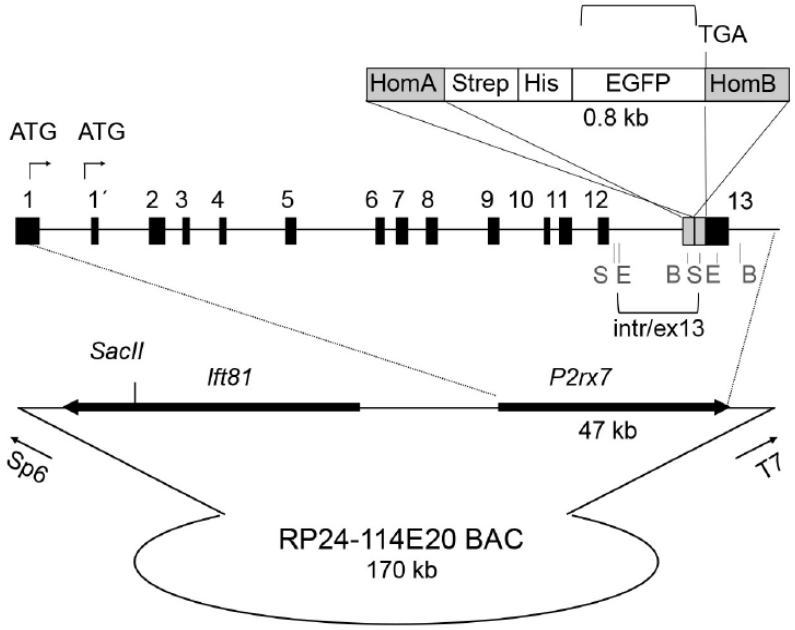

Figure 10. Scheme of the BAC clone containing the full-length P2rx7 plus about 103 kb (5') and 10 kb (3') flanking sequence. *A Strep-His-EGFP cassette (0.8 kb) flanked by two homology arms (grey boxes) was inserted directly upstream of the stop codon into exon 13 of the P2rx7.*

1.5.2.4 Double transgenic mice expressing a mutant form of MAPT and EGFP immediately downstream of P2X7 receptor promoter.

For the analysis of *P2rx7* gene transcription, we generated a double transgenic mice line (^{P2X7}EGFP;P301S) expressing the mutant form of MAPT and the EGFP immediately downstream of P2X7 receptor promoter. This line was obtained by crossing P301S mice and ^{P2X7}EGFP mice, both heterozygous, as shown in **Figure 11**. The production frequency of these double transgenic mice is 25%.

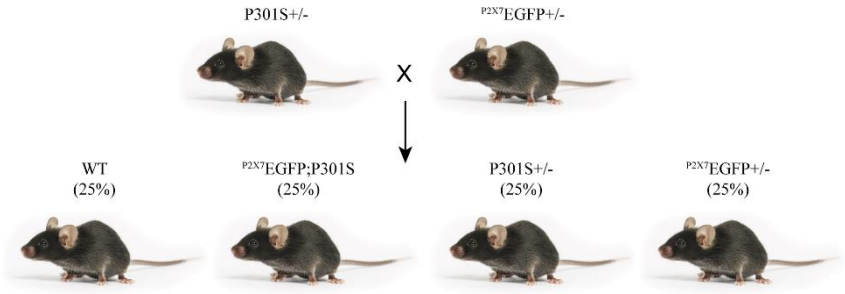

Figure 11. Schematic representation of the crossbreeding designed to obtain double transgenic ^{P2X7}EGFP;P301S mice. *The line was obtained by crossing P301S mice and ^{P2X7}EGFP mice, both heterozygous.*

1.5.2.5 P2X7 receptor null mice expressing a mutant form of MAPT.

In order to evaluate how the total absence of P2X7 receptor could affect the neuroinflammation associated with tau toxicity, we generated P2X7 receptor null mice expressing a mutant form of MAPT (P301S;P2X7$^{-/-}$ mice). Heterozygous P301S mice were crossed with P2X7R null mice; P301S;P2X7+/- mice obtained from this crossbreeding were then backcrossed with P2X7$^{-/-}$ mice to finally generate P301S;P2X7$^{-/-}$ mice (frequency of 25%), as shown in **Figure 12**.

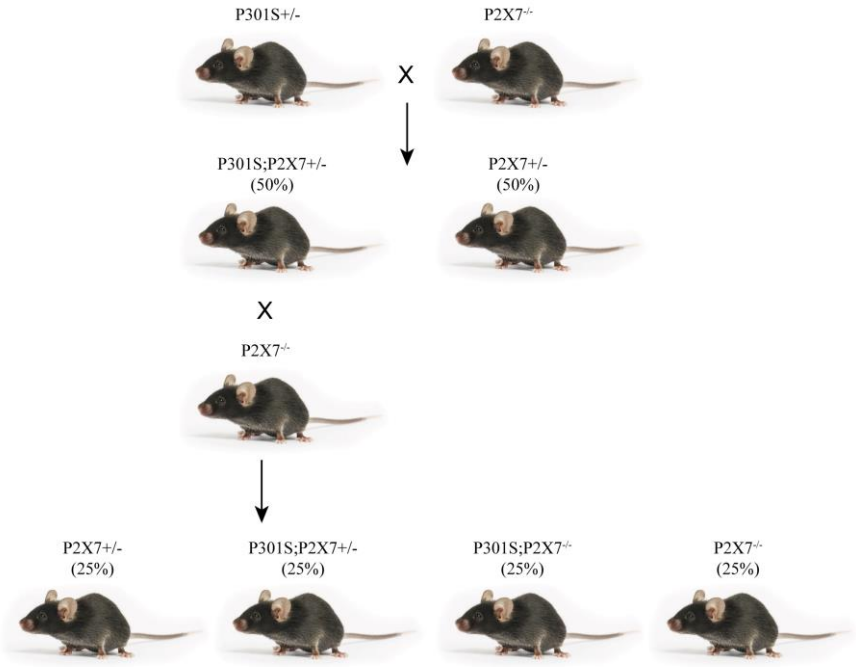

Figure 12. Schematic representation of the crossbreeding designed to obtain P2X7 receptor null mice expressing a mutant form of MAPT. *The line was obtained by crossing heterozygous P301S mice with P2X7R null mice; P301S;P2X7+/- mice were then backcrossed with P2X7-/- to finally obtain P301S;P2X7$^{-/-}$.*

1.5.2.6 Double transgenic mice expressing a mutant form of MAPT and overexpressing EGFP-tagged P2X7R mice.

Finally, a double transgenic mice line expressing a mutant form of MAPT and overexpressing EGFP-tagged P2X7R mice (P301S;P2X7^{451P}-EGFP) was generated to analyse the effect of P2X7R overexpression on tau-induced toxicity. Heterozygous P301S mice were crossed with heterozygous P2X7^{451P}-EGFP mice, as shown in **Figure 13**, with a production frequency of these double transgenic mice of 25%.

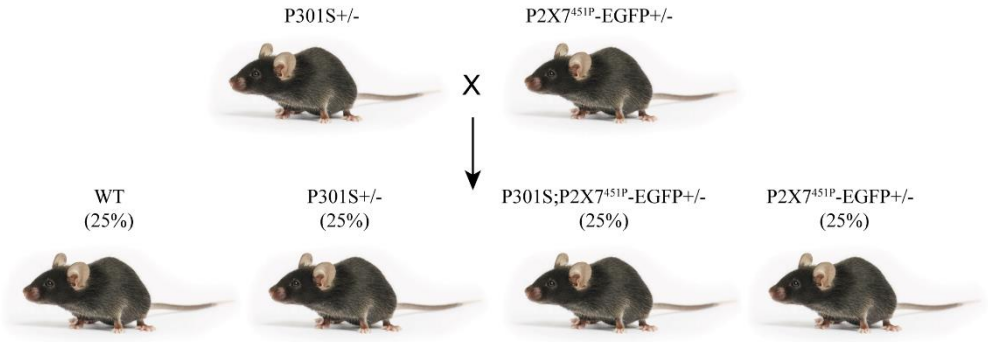

Figure 13. Schematic representation of the crossbreeding designed to obtain double transgenic P301S;P2X7^{451P}-EGFPR mice. *The line was obtained by crossing P301S mice and P2X7^{451P}-EGFP mice, both heterozygous.*

2. METHODS

2.1. PCR Genotyping

Mice genomic DNA was extracted from fragments of tissue. For P301S and ^{P2X7}EGFP tail fragments were digested by incubation with 600 µL of NaOH 50 mM at 99°C for 30 minutes. The reaction was then neutralized by adding 50 µL of Tris-HCl 1M pH 8,0 and the samples were centrifuged for 6 minutes at 13.000 rpm to separate the organic and aqueous phases.

For P2X7^{451P}-EGFP and P2X7$^{-/-}$ mice tail fragments were incubated at 55°C overnight with 200 µL of lysis buffer pH 7,5 (100 mM Tris-HCl, 5 mM EDTA, 200 mM NaCl, 0,2% SDS) and proteinase K. The day after, samples were centrifuged at 13.000 for 10 minutes to separate the organic and aqueous phases. The supernatant was then transferred to new tube with 2-Propanol and the samples were mixed until the DNA became visible. Samples were later centrifuged at 13.000 rpm for 5 min and washed with EtOH 70%. Finally, the pellet was diluted in H2O milliQ.

Simple PCR reactions were carried out using: for P301S mice DNA Kapa2G Fast HS Master Mix from Sigma-Aldrich (Madrid-Spain), specific primers (0.5 µM each) and 2 µL of genomic DNA in a final volume of 12 µL; for P301S;P2X7$^{-/-}$ and P301S;P2X7^{451P}-EGFP mice Econo PLUS Green 2x Master Mix, specific primers (10 µM each) and 1 µL of genomic DNA in a final volume of 25 µL; for ^{P2X7}EGFP mice DNA Amplitools Master Mix (Biotools, Madrid, Spain), specific primers (0.4 µM each) and 5 mL of genomic DNA in a final volume of 25 µL.

DNA amplification was carried out in a SimpliAmp^{TM} Thermal Cycler (Applied Biosystem). Specific oligonucleotides and amplification protocols are showed in the **Table 8**.

PCR amplification products were electrophoresed on a 1.5% (w/v) agarose gel and stained with SYBR® Safe DNA Gel Stain (Life Technologies CA, USA). PCR bands were visualized by gel imaging system Gel Logic 200 Imaging System (Kodak, Rochester, NY, USA) or Gel Doc XR^{+} System (Bio-Rad).

Table 8. List of the different oligonucleotides and amplification protocols used for the genotype of P301S mice, ^{P2X7}EGFP mice, P2X7^{451P}EGFP mice and P2X7$^{-/-}$ mice. *Numbers between brackets indicate the number of amplification cycles. The time of each step is indicated in minutes (min) or seconds (sec).*

Oligonucleotides	Sequence	Amplifying protocol		
P301S	**A:** Fw 5'-GGC ATC TCA GCA ATG TCT CC-3'	(1) 94°C 5 min	(20) 94°C 15 sec 65°C 15 sec 72°C 10 sec	(1)72°C 10min
	B: Rv 5'-GGT ATT AGC CTA TGG GGG ACAC-3'			
	C: 5'-CAA ATG TTG CTT GTC TGG TG-3'			
	D: 5'-GTC AGT CGA GTG CAC AGT TT-3'			

^{P2X7}EGFP	**E:** Fw 5'-CCTACGGCGTGCAGTGCTTCAGC-3'	(1) 94°C 5 min	(40) 94°C 30 sec 60°C 45 sec 72°C 45 sec	(1)72°C 10min
	F: Rv 5'-CGGCGAGCTGCACGCTGCGTCCTC-3'			
P2X7^{451P}EGFP	**G:** Fw 5'-GGTTCTTAGCAGGCTTAACAGCA-3'	(1) 94°C 5 min	(35) 94°C 30 sec 60°C 60 sec 72°C 60 sec	(1)72°C 10min
	H: Rv 5'-ATGGGGGTGTTCTGCTGG AG T-3'			
P2X7$^{-/-}$	**I:** Fw 5'-CTGGCAACTATCCATTTTCC-3'	(1) 94°C 5 min	(35) 94°C 30 sec 60°C 60 sec 72°C 125 sec	(1)72°C 10min
	L: Rv 5'-GTGTGAGTGAATGAGATCGTG-3'			

2.2. Drug preparation and administration

P2X7 specific negative allosteric antagonist GSK 1482160A was diluted at 10 mg/ml in vehicle solution. Vehicle solution was calcium- and magnesium-free sterile phosphate buffered saline (PBS) plus 20% hydroxypropyl-b-cyclodextrin and 0.2% DMSO. 10 µL of GSK solution (corresponding to a dosage of 100 mg per Kg of body weight) or the same volume of vehicle solution were daily intraperitoneally injected to 9-months-old P301S and wild-type (WT) mice for three weeks, **Figure 14**. The treatment protocol followed a single-blind design, by which the experimenter was unaware of the genotype and treatment applied to each mouse (n = 5-7 mice per group and condition). After treatment, mice cognitive status was assessed with a battery of behavioural tests. Mice were later sacrificed, and brain tissue was processed to perform immunoblot and immunohistochemical analyses.

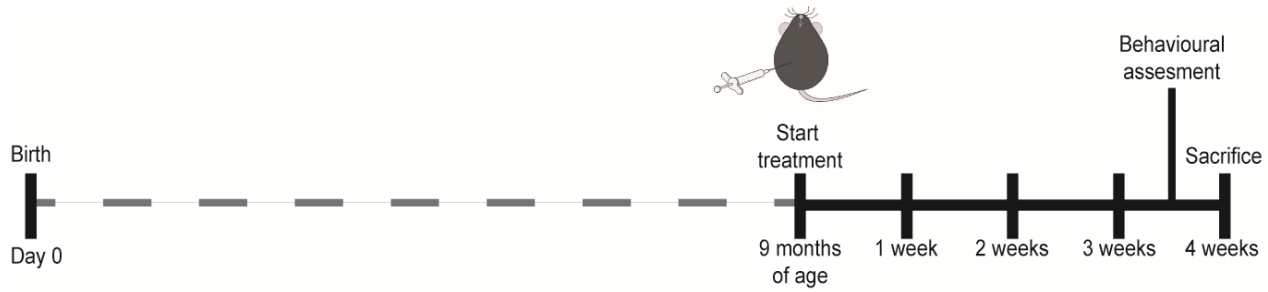

Figure 14. Schematic timeline of the experimental schedule. *WT and P301S mice were daily intraperitoneally treated with either a vehicle solution or with the P2X7 antagonist GSK 1482160A (GSK) for 3 weeks.*

2.3.Behavioral assay

Mice were handled for at least 3–4 consecutive days and tested in random order; the experimenter conducting the tests was unaware of the genotype/group. All behavioural devices were located in a sound-proof room and the experimental area was homogeneously illuminated around 70 lux. All apparatus was carefully cleaned with alcohol (70° proof) after each session. The protocols of behavioural test are described in detail below.

2.3.1.Open field (OF): is an experimental test used to assay general locomotor activity levels, anxiety, and willingness to explore a novel environment. The protocol is based on the fact that animals, such as mice and rats, display a natural aversion to brightly lit open areas. Decreased levels of anxiety lead to increased exploratory behaviour. Increased anxiety will result in less locomotion and a preference to stay close to the walls of the field (thigmotaxis).

The apparatus consists of a large cubic box (42 cm x 42 cm), and the top of the cube is typically left uncovered, **Figure 15**. There is no need to habituate the mouse before the test. A single adult mouse is gently placed in the middle of the bottom surface, and its movements are recorded over the curse of 10 minutes as it moves around and explores the environment.

After the experiment is completed, computer tracking programs analyse the movements of the animal over time. The analysis consists of measuring the amount of time spent by the mouse in the centre (17 x 17 cm) of the tank and in the periphery (the surrounding area of the arena). The tendency to avoid the centre of a novel environment and remain close to the wall of the tank is an index of anxiety. Data acquisition and analysis were performed automatically using Any-Maze software (Stoelting Co, Wood Dale, IL, USA).

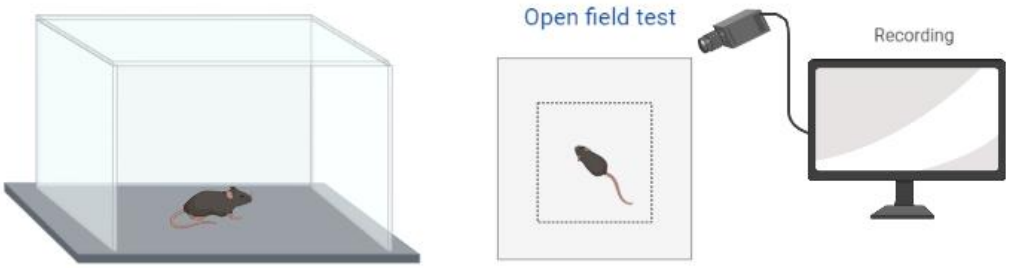

Figure 15. Schematic representation of the Open Field setup. *Draw created with BioRender.com.*

2.3.2. Elevated plus maze (EPM): is a test used to assess anxiety-related behaviour in rodents. The model is based on the animal's aversion to open spaces and tendency to be thigmotaxic. EPM apparatus consists of a plus shaped (+) apparatus elevated above the floor with two oppositely positioned closed arms, two oppositely positioned open arms, and a central area (at the intersection of the open and enclosed arms), **Figure 16**. There is no need to habituate the mouse before the test. A single adult mouse is gently placed into the central area of setup. As subjects freely explore the maze, their

behaviour is recorded for 5 minutes by a video camera mounted above the maze and analysed using a video tracking system. The percentage of being in open arms over closed arms (expressed as either as a percentage of entries and/or a percentage of time spent in the open arms) is calculated using Any-Maze software to measure anxiety-like behaviour.

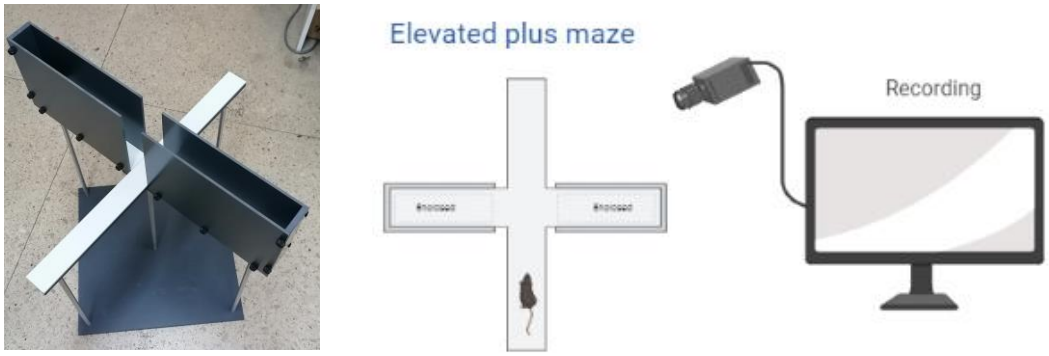

Figure 16. Schematic representation of the Elevated plus maze setup. *Draw created with BioRender.com.*

2.3.3. Rotarod (RT): is a test widely used to evaluate motor coordination and locomotor functions of the mice. The test measures a mice's ability to maintain itself on a rod that turns at accelerating speeds rather than fall onto a platform just below, **Figure 17**.

The apparatus consists of a rotating bar, at constant speed or acceleration between 4 and 40 rpm, on which the mice are placed in individual rails. Mice need to be trained during two days before the test. On the first day of trial the animals are placed on the testing rod at a fixed speed of 4 rotation per minute (rpm) for 1 minute. Mice are trained during 4 sessions and allowed to rest between each session. On the second day of trial, the animals are placed on the rod at an initial speed of 4 rpm for 45 seconds, then the rod speed increase gradually until 8 rpm over 75 seconds. Even in this case the animals are trained during 4 sessions, with a rest between each session.

After the trial, the rotarod is set to accelerate from 4 to 40 rpm over 5 min, and the test is repeated 4 times. The time spent on the rod is recorded automatically for each animal, and the average performance of the 4 sessions is used for within-animal comparisons. Motor coordination and locomotor ability is evaluated by measuring the time that the mouse manages to keep walking on the bar before fall onto the platform below.

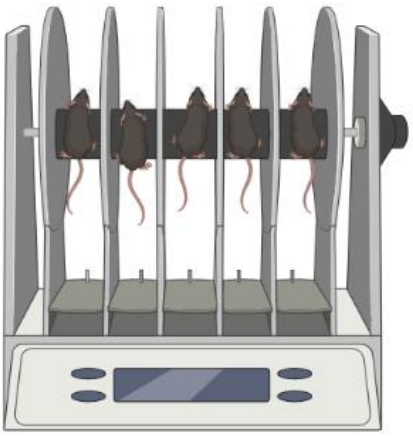

Figure 17. Schematic representation of the Rotarod setup. *Draw created with BioRender.com*

2.3.4. Novel object recognition (NOR): is a commonly used behavioural assay for the investigation of various aspects of learning and memory in mice. This test is based on the spontaneous tendency of rodents to spend more time exploring a novel object than a familiar one. The choice to explore the novel object reflects the use of learning and recognition memory.

The NOR task is conducted in an open field arena with two different kinds of objects, **Figure 18**. Both objects are generally consistent in height and volume, but are different in shape and appearance. The test consists of a training phase, during which the mice are exposed to the familiar arena with two identical objects placed at an equal distance for ten minutes. The next day, the mice are allowed to explore, again for ten minutes, the open field in the presence of the familiar object and a novel object to test long-term recognition memory. The time spent exploring each object is recorded and analysed using Any-Maze software. A normal animal should spend more time investigating the new object instead of the familiar one.

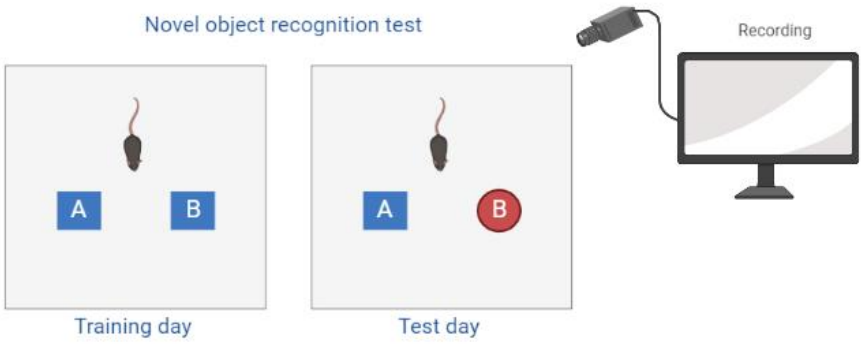

Figure 18. Schematic representation of the Novel object recognition test. *Draw created with BioRender.com*

The behavioural test battery was performed with the following order, **Figure 19**:

- 1st day – Open field test
- 2nd day – Novel object recognition training
- 3rd day – Novel object recogniction test
- 4th day – Elevated plus maze test
- 5th day – Rotarod first trial day
- 6th day – Rotarod second trial day
- 7th day – Rotarod test day

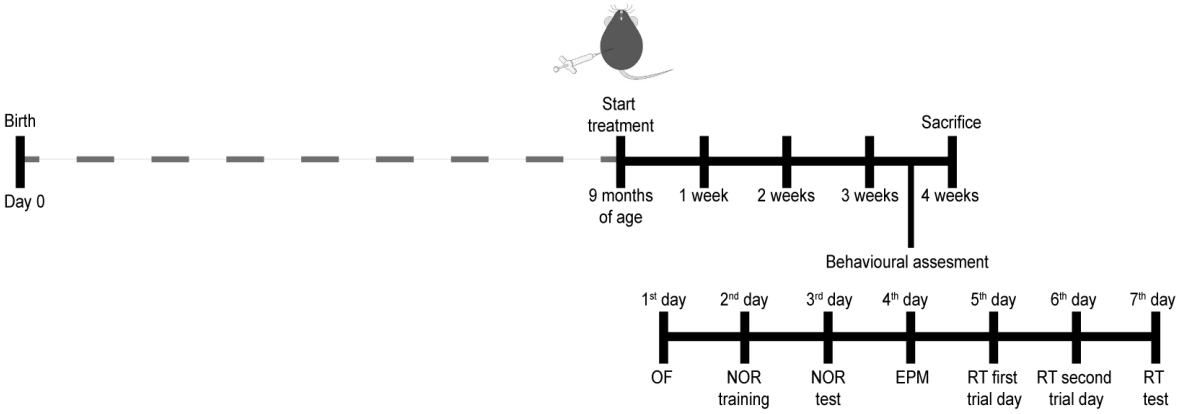

Figure 19. Schematic timeline of the GSK treatment and behavioral assesment. *WT and P301S mice were daily intraperitoneally treated with either a vehicle solution or with the P2X7 antagonist GSK for 3 weeks; after that they underwent the OF, NOR, EPM and RT test.*

2.4. Phagocytosis assay

In vivo phagocytosis assays were done as previously described (Martinez-Frailes *et al.*, 2019). 9-month-old WT (n≥4) and P301S mice (n≥4) treated either with vehicle and GSK solution were randomly anesthetized with isoflurane (1-chloro-2, 2, 2-trifuoroethyl-difluorormethylether; Isovet®, BRAUN, Rubi, Barcelona, Spain) diluted in 50% O_2 and the experimenter was blinded to the genotype of mice. The scalp was incised along the midline, and one hole was made at the appropriate stereotaxic coordinates from Bregma (**Figure 20,** mediolateral, 1 mm; anteroposterior, 2 mm; dorsoventral, 1.8 mm). 2 µL of 0.02% red Fluorescent 2 µm microspheres in PBS was hippocampal administrated (i.c.) at a rate of ≈0.5 µL/min.

Brain sections were stained with a rabbit polyclonal anti-Iba1 (1:200 and revealed with goat anti-rabbit IgG labelled with Alexa 488, 1:400). For each coverslip, 4 random pictures were taken, using the TCS SPE confocal microscope. Images were analysed using ImageJ software. The number of fluorescent beads inside each cell was counted, and the average number of phagocyted microspheres per microglial cell was calculated for each experiment and treatment.

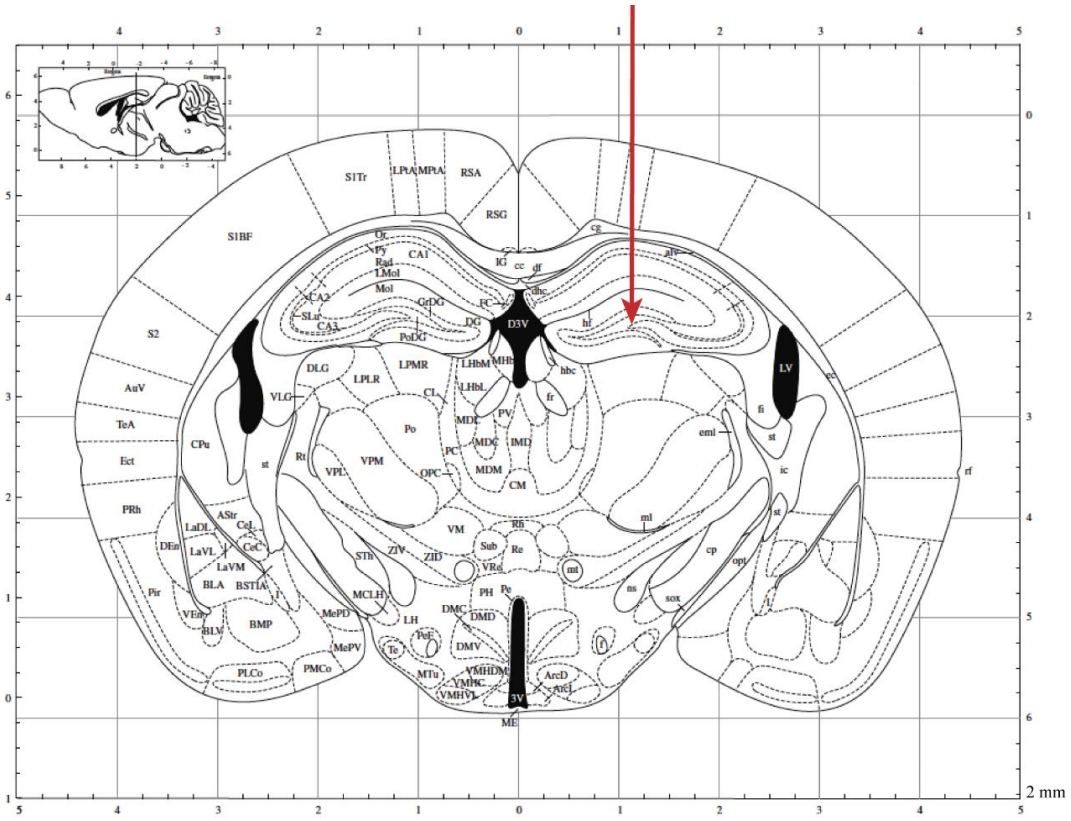

Figure 20. Intracranial beads injection. *Representative scheme of brain coronal section from a 9-month-old mouse. Red arrow indicates the paths of Hamilton needle. Head of the arrow indicates the point in which beads were injected. Image obtained from Paxinos and Franklin 2012.*

2.5.Collection of cerebrospinal fluid (CSF) samples

Mice were anesthetized with isoflurane diluted in 50% O_2 and placed in a stereotaxic frame with the head forming a near 135º angle with the body, **Figure 21**. Mice were kept under anaesthesia during the surgery. The CSF was collected from the cisterna magna with a pulled capillary. Blood vessels were carefully avoided when penetrating the *dura mater* with the capillary tube in order to prevent contamination by plasma proteins. CSF was immediately frozen on dry ice.

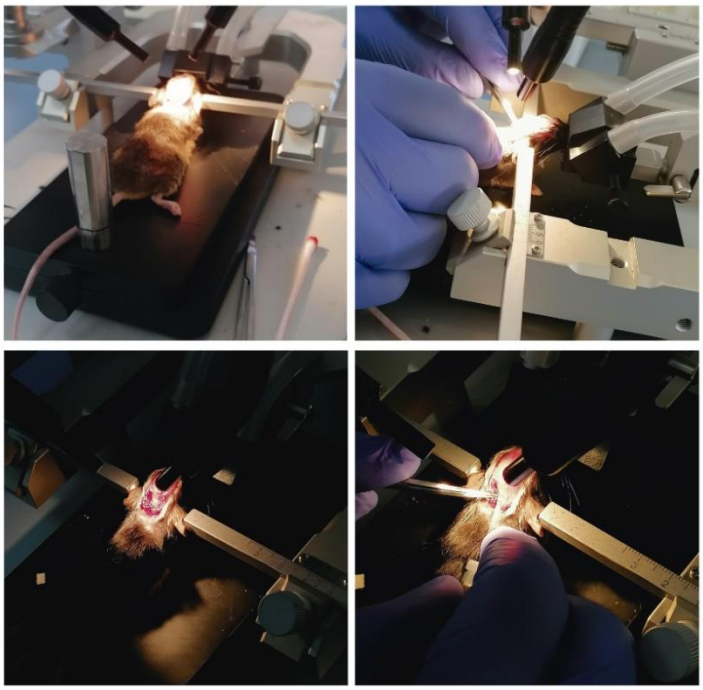

Figure 21. Representative scheme of CSF collection.

2.6. Tissue processing

Mouse brain: mice were sacrificed by cervical dislocation and their forebrain removed. The brain was divided into the two hemispheres; one of them was immediately frozen in dry ice for later protein and RNA extraction. The other hemisphere was fixed in 4% paraformaldehyde and cryoprotected in 30% sucrose solution. The samples were embedded in OCT compound (Sakura) and frozen using dry ice. Finally, 20 µm floating sections were cut in sagittal planes with a cryostat and stored in a solution of 30% ethylene glycol, 30% glycerol and 0.1 M PBS at -20°C until processed.

Human brain: human brain from control, AD, and PiD subjects were processed at the Fundación Centro de Investigación Enfermedades Neurológicas (CIEN) within the Vallecas Project. The whole brain was separate into two hemispheres, through a sagittal interhemispheric incision. One of the hemispheres was dissected and samples of the hippocampus were immediately frozen in dry ice and

stored at -80°C for biochemical studies. The other hemisphere was fixed in 10% buffered formalin for at least 3 weeks. Samples (2 mm thickness) of the hippocampus were then obtained through dissection, embedded in paraffin following standard protocols (Leica, HistoCore Pearl), and later sectioned (5 μm) by using a microtome (Microm HM 355 S) and stored at -80°C until use.

2.7. RNA extraction and quantification, Reverse Transcriptase (RT-PCR), Quantitative Real-Time PCR (qRT-PCR)

Total RNA was extracted from hippocampi of human or adult mouse using the Speedtools total RNA Extraction Kit (Biotools) and following the manufacturer's instructions. Once finished the extraction, samples were digested with TURBO DNase (Ambion) to remove any contamination of DNA. After that, DNase was inactivated, and total purified RNA was recovered. Samples RNA concentration was then quantified by measuring the absorbance at 260 nm in a Biophotometer Plus spectrophotometer. To estimate RNA purity, the ratio of samples absorbance at 260 nm and 280 nm (A_{260}/A_{280}) was calculated; typical requirements for A_{260}/A_{280} ratios are 1.8-2.2.

Process of reverse transcriptase (retrotranscription or RT-PCR) for the synthesis of complementary DNA (cDNA) was performed using 1 μg of total RNA, 6 μg of random primers, 350 μM dNTPs and M-MLV reverse transcriptase. The reaction was carried out at 37°C for 90 minutes, followed by an incubation at 70°C for 15 minutes in order to inactivate the enzyme.

Quantitative Real Time PCR (qRT-PCR) was performed on cDNA using reaction mixtures containing DNA Master SYBR Green I mix. Specific oligonucleotides and amplification protocols are showed in **Table 9**; reactions were carried out in a StepOnePlus Real-Time PCR System. Expression levels of mRNA were represented as $2^{-\Delta\Delta Ct}$, where average cycle threshold (Ct) was obtained from triplicates of each sample. First, ΔCt means were normalized to parallel amplification of GAPDH as endogenous control. Next, ΔΔCt means were normalized to the average of corresponding controls.

Table 9. List of the different oligonucleotides and amplification protocols used for the RT-qPCR amplification. *Numbers between brackets indicate the number of amplification cycles. The time of each step is indicated in minutes (min) or seconds (sec).*

Oligonucleotides	Sequence	Amplifying protocol	
Human P2RX7	**A:** Fw 5'- AAAACAGAAGGCCAAGAGCA -3'	(1) 94°C 20 sec	(40) 95°C 1 sec 60°C 20 sec
	B: Rv 5'- CACCAGGCAGAGACTTCACA -3'		
Mouse P2rx7	Fw 5′- GGTGCCAGTGTGGAAATTG-3′	(1) 94°C 20	(40) 95°C 1 sec

	Rv 5′- TAGGGATACTTGAAGCCACT-3′	sec	60°C 20 sec
GAPDH	5′-CACCACCAACTGCTTAGCCC-3′	(1) 94°C 20 sec	(40) 95°C 1 sec 60°C 20 sec
	Rv 5′-TGTGGTCATGAGCCCTTCC-3′		

2.8. Western blot analysis

The western blot is a technique often used in research to separate and identify proteins. In this technique a mixture of proteins is separated on the basis of the molecular weight through gel electrophoresis. The results are transferred to a nitrocellulose membrane, producing a band for each protein, and the membrane is then incubated with labels antibodies specific for the proteins of interest.

The unbound antibody is washed off leaving only the bound antibody to the protein of interest, then detected by developing the film. As the antibodies only bind to the protein of interest, only one band should be visible. The thickness of the band corresponds to the amount of protein present; thus, doing a standard it should be possible to analyse the amount of protein present.

Protein extracts for Western blot analysis were prepared by homogenizing fresh dissected human or mouse brain hippocampi in ice-cold extraction buffer containing 20 mM Hepes, 100 mM NaCl, 50 mM NaF, 5 mM EDTA, 5 mM Na_3VO_4, 1% Triton X-100, okadaic acid (Calbiochem), and Complete TM Protease Inhibitor Cocktail Tablets, pH 7.4. The samples were homogenized at 4°C, and protein content was determined by Bradford assay. Protein extract was mixed with a 5x loading buffer (composition 57% glycerol, 125 mM Tris-HCl 1M pH 6.8, 10% SDS, 0.5% Bromophenol Blue) and heated at 99°C for 5 minutes.

Samples (protein amount between 10-20 μg) were loaded in a 10% Tris-Glycine-SDS gel and then electrophoresed on a in a Mini-Protean 3 Electrophoresis System, with a constant voltage of 120 V in an electrophoresis buffer (composition 25mM Tris, 200 mM glycine and 0.1% SDS, pH 8.3). One of the wells of the gel was reserved for a mixture of standards of known molecular weight.

After the electrophoresis, proteins were transferred to nitrocellulose membranes, previously equilibrated for 5 minutes in a transfer buffer (composition 192 mM glycine, 25 mM Tris and 20% methanol, pH 8.3), in a Mini-Trans-Blot system with intensity of 240 mA for 70 minutes.

Once this step was completed, transfer was confirmed with Ponceau staining; membranes were incubated with the dye for 10 minutes at RT, then washed with PBS 1x and 0.1% Tween-20 (PBS-Tween or washing solution). Membranes were later incubated with blocking buffer (5% milk powder or 3% BSA in PBS-Tween) for 1 hour at RT on an orbital shaker and finally incubated with

primary antibodies at 4°C ON. Primary antibodies used for the experiments are listed in **Table 6**. On the second day membranes were washed for 10 min with PBS-Tween three times and incubated with secondary antibodies (listed in **Table 7**) for 1 h at room temperature, followed by enhanced chemo luminescence detection. This system contains luminol, which is the specific substrate for peroxidase and when oxidized generated a luminescent signal that can be detected by autoradiographic. For this purpose, Agfa X-ray films were used together with CP1000 Agfa autoradiography developing machine or ImageQuant LAS 500 chemiluminescent detector.

Gel band images were analysed using ImageJ software. Protein expression was normalized respect to the expression of housekeeping proteins, like α-Tubulin, β-actin, or GAPDH from the same experiment. In figures, the representative Western blot images show only the quantified bands.

2.9. Immunohistochemistry and immunofluorescence.

For immunohistochemical analysis, sagittal sections (25 µm of thickness) of mouse brain were pre-treated for 45 min at RT with 1% H_2O_2 in PBS to inactivate endogenous peroxidase. Afterwards, sections were washed three times in PBS 1x for 10 minutes, blocked for 1 h with block solution (1% bovine serum albumin (BSA), 5% fetal bovine serum (FBS), and 0.2% TritonX-100 in PBS) and finally incubated over night at 4°C with primary antibodies diluted in blocking solution (listed in **Table 6**). Later sections were incubated with avidin-biotin complex using the Elite Vectastain kit and staining reactions were performed with diaminobenzidine and 0.003% H_2O_2 for 10 min. Finally, brain sections were washed with PBS and mounted in FluorSave.

For immunofluorescence studies, mouse slices were boiled in citrate buffer (citric acid 1M in distillate H_2O) pH 5.9 for 5 min, washed three times in PBS 1x for 10 minutes, blocked for 1 h at room temperature (RT) with blocking solution and then incubated at 37°C for 1 h or overnight at 4°C with primary antibodies (listed in **Table 6**). Subsequently, brain sections were washed with PBS buffer and incubated with secondary antibodies (listed in **Table 7**) and 4′,6-diamidino-2-phenylindole (DAPI) staining (1:1000). After that, brain sections were washed in PBS and mounted.

For immunohistochemical analysis, human sections (5 µm of thickness) were pre-incubated at 55°C ON and then sequentially washed for 10 min in Xylene (catalog 131769.1611, Panreac), ethanol 100%, ethanol 96%, ethanol 70% and finally distilled H_2O, in order to remove paraffin and rehydrated them. Later, the sections were treated for 45 min at RT with 1% H_2O_2 in PBS to inactivate endogenous peroxidase and then boiled in citrate buffer (citric acid 1M in distillate H_2O) pH 5.9 for 5 min. Next, the sections were washed in PBS 1x for 10 minutes, blocked for 1 h with

block solution and finally incubated over night with rabbit anti-P2X7R antibody (listed in **Table 6**). On the second day, sections were incubated with avidin-biotin complex using the Elite Vectastain kit and staining reactions were performed with diaminobenzidine and 0.003% H_2O_2 for 10 min. Finally, brain sections were washed with PBS and mounted in FluorSave.

For immunofluorescence studies, human sections were pre-treated to remove paraffin, as previously described. Next, the sections were boiled in citrate buffer, washed in PBS 1x for 10 minutes, blocked for 1 h at room temperature (RT) with blocking solution and then incubated overnight at 4°C with rabbit anti-P2X7R antibody (listed in **Table 6**). Subsequently, brain sections were washed with PBS buffer, incubated 1 h at RT with avidin-biotin complex using the Elite Vectastain kit, then washed again with PBS buffer and incubated with Streptavidin (**Table 7**). Sections were later incubated with rabbit anti-Iba1 primary antibody (**Table 6**) and, washed in PBS buffer and finally incubated with secondary antibody (listed in **Table 7**) and 4′,6-diamidino-2-phenylindole (DAPI) staining (1:1000). After that, brain sections were washed in PBS and mounted.

2.10. Image Acquisition

Confocal images were acquired with a TCS SPE microscope from Leica Microsystems equipped with a Plan Fluor 10× dry objective lens NA=0.30, 40× Apochromat NA=1.15 oil objective lens and 63× Apochromat NA=1.3 oil objective lens (Leica Microsystems GmbH) and 4 different lasers lines (405, 488, 565 and 647nm). Pictures were acquired using the Leica software LAS AF v2.2.1 software as a z projection of focal planes (1.5 µm of thickness), and later converted in TIFF images using Z Project from ImageJ software on a range of selected planes.

Transmitted light images were acquired using DM 1000 microscope with DFC450 CCD camera using Leica Application Suite (v4.1). Sections were photographed with Plan 4× dry objective lens (NA = 0.1) and insets with Plan S-Fluor 20× or 40× dry objective lens.

2.11. Analysis of microglial morphology

Brain sections were stained with a rabbit polyclonal anti-Iba1 (Wako 1:200) and revealed with goat anti-rabbit IgG labelled with Alexa 488 (1:400). For each slice, 4 random pictures were taken, using the TCS SPE confocal microscope (Leica Microsystems, Wetzlar, Germany). Images were analysed using FIJI software (US National Institutes of Health, Bethesda, MD, United States).

Microglia cells morphology was evaluated following the protocol previously described by Young and Morrison, 2018. The protocol is a summary of steps and ImageJ plugins recommended to convert fluorescence and bright-field photomicrographs into representative binary and skeletonized

images, that then can be analysed using software plugins AnalyzeSkeleton (2D/3D) and FracLac for morphology data collection. The outputs of these plugins summarize cell morphology in terms of process endpoints, junctions, and length as well as complexity, cell shape, and size descriptors.

Skeleton analysis binary images were obtained from z-stack acquisition using a 40× objective. Binary images were then skeletonized and analysed through FIJI AnalyzeSkeleton (2D/3D) plugin, as previously described (Young and Morrison, 2018). The number of cell ramifications and the branch length were calculated for each experiment and treatment (at least 4 animals for experimental condition, each dot in the graphs represents the average of a minimum of 12 microglia cells).

For fractal analysis at least 18 random microglia cells from each experimental condition were analysed using FracLAc FIJI plugin, as described (Young and Morrison, 2018). The area covered by cells was calculated for each experiment and treatment.

2.12. Statistics

Data are shown as mean values ± SEM. The numbers of mice per group used in each experiment are annotated as "n" in the corresponding figure legends. Figures and statistical analyses were generated using GraphPad Prism (v6.00, www.graphpad.com). To assess whether the data met the normal distribution, the Shapiro-Wilk or Kolmogorov-Smirnov tests were used. For two-group comparison, data were analysed with two-tailed unpaired Student's t test. For multiple comparisons, data were analysed using a one-way ANOVA followed by Dunnett's post hoc tests when all groups were compared against a control group or one-way ANOVA followed by Tukey´s post hoc tests when all groups were compared among them. When required, a two-way ANOVA followed by Tukey´s post hoc tests were used. The statistical test used, and p-values are indicated in each figure legend. Significance was considered at *P≦0.05, **P≦0.01, ***P≦0.001 or ****P≦0.0001 throughout the study.

RESULTS

1. P2X7R IS UPREGULATED IN TAUOPATHY PATIENTS.

To evaluate whether P2X7R contributes to Tau-induced pathology, we initially analysed the expression levels of the receptor in *post mortem* hippocampal samples from patients of two different tauopathies, AD and PiD.

Human protein extracts were obtained from fresh samples of hippocampus and processed as described in section 2.8 of Materials and Methods. Western blot results revealed an increase of P2X7R protein levels in both PiD (227.5±40.1%) and AD patients (190.2±19.6%), **Figure 22**.

Further analysis showed an increase as well of *P2RX7* transcript levels in PiD and AD *post mortem* brains (52.0±8.7% in PiD and 53.4±1.3% in AD), **Figure 22**.

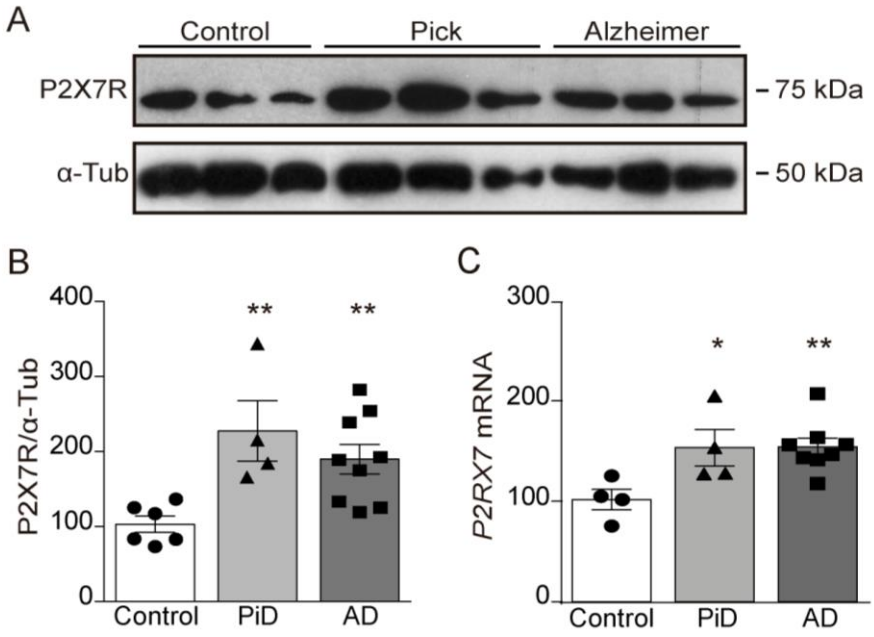

Figure 22. Analysis of P2X7R levels in Tauopathy patients. *A) Representative immunoblot of P2X7R using hippocampal homogenates from non-affected individuals (Control) and Pick´s disease (PiD) or Alzheimer´s disease (AD) patients. B) Quantification of P2X7 receptor protein levels in hippocampal homogenates from PiD (n = 4) and AD patients (n = 9) and non-affected individuals (n = 6). Levels of α-Tubulin (α-Tub) were used as loading control for normalization. C) Quantification of P2RX7 mRNA in the hippocampus from human controls (n=4), AD patients (n=8) and PiD patients (n=4). In all cases, the 100% value corresponds to the averaged amount of protein or messenger of P2X7R detected in the hippocampi of non-affected individuals. * P ≦ 0.05; ** P ≦ 0.01 using a One-way ANOVA followed by Dunnett's post hoc test considering non-affected individuals as the control group.*

2. THE P2X7R UPREGULATION FOUND IN TAUOPHATIES MAINLY OCCURS IN GLIAL LINEAGE.

After confirming that P2X7R is upregulated in Tauopathies, we wondered in which cell linage this upregulation mainly takes place. For this purpose, immunohistological studies were performed.

P2X7R immunohistochemistry (described in section 2.9 of Materials and Methods) was carried out on human hippocampal sections of both healthy (control) and AD and PiD brains (5 µm of thickness). In the healthy control brains, results revealed that P2X7R positive cells mainly present a neuronal-like morphology, but this morphology was not detected in brains from AD and PiD patients, **Figure 23**. Considering that previous studies had reported an enrichment of microglial cells expressing P2X7R in AD patients (Martin *et al.*, 2019; Martinez-Frailes *et al.*, 2019; McLarnon *et al.*, 2006; Parvathenani *et al.*, 2003), we co-stained the hippocampal *post mortem* samples from Tauopathies patients with the specific antibodies anti-P2X7R and anti-Iba-1 (a microglial marker). Results showed that PiD and AD patients presented a higher incidence of hippocampal microglial cells expressing P2X7R than the healthy controls, **Figure 24.**

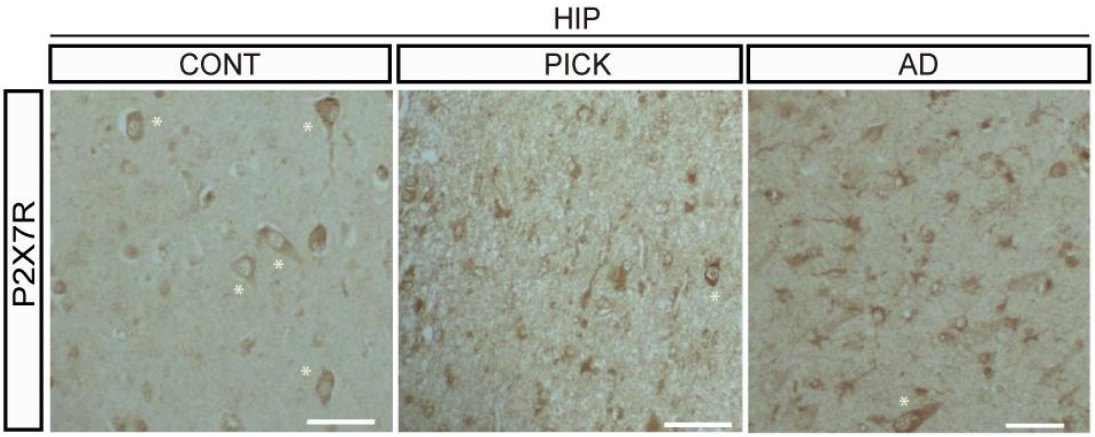

Figure 23. Immunohistochemical P2X7R expression in hippocampal sections from AD and PiD patients. *Representative images of immunohistochemical staining for P2X7R in hippocampi from human controls, AD and PiD patients. Asterisks to those with neuronal-like morphology. Scale bar = 50 µm.*

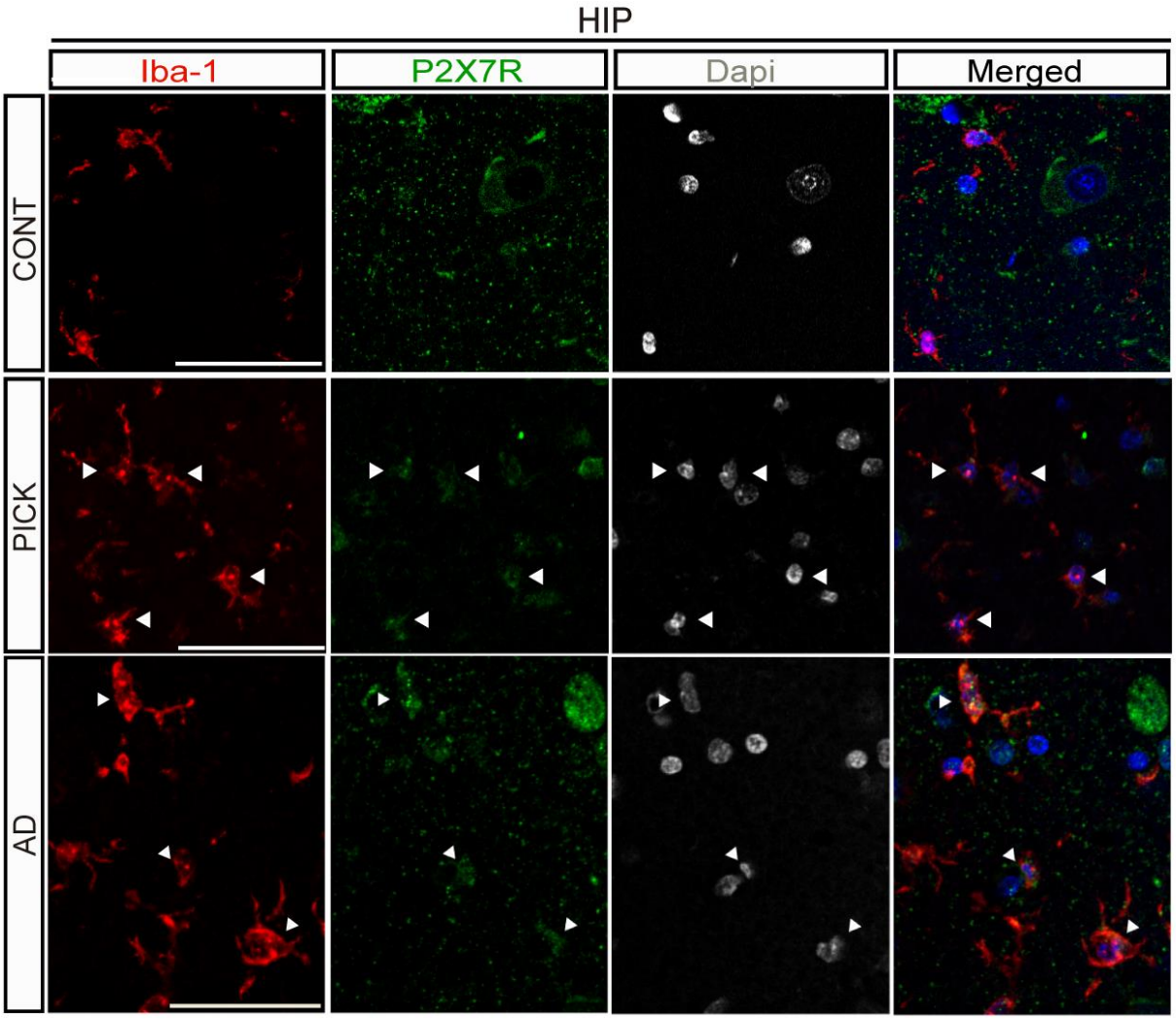

Figure 24. Upregulation of P2X7R expression in microglia cells from AD and PiD patients. *Hippocampal sections from human controls and PiD patients stained with specific microglial marker (Iba-1, red channel), P2X7R (green channel) and DAPI (grey channel). Merged channel in also showed. Arrowheads indicate microglial cells expressing P2X7R. Scale bar: 50 μm.*

Further studies using the specific astroglia marker GFAP revealed that AD and PiD patients also show an enrichment in hippocampal astrocytes expressing P2X7R, **Figure 25**.

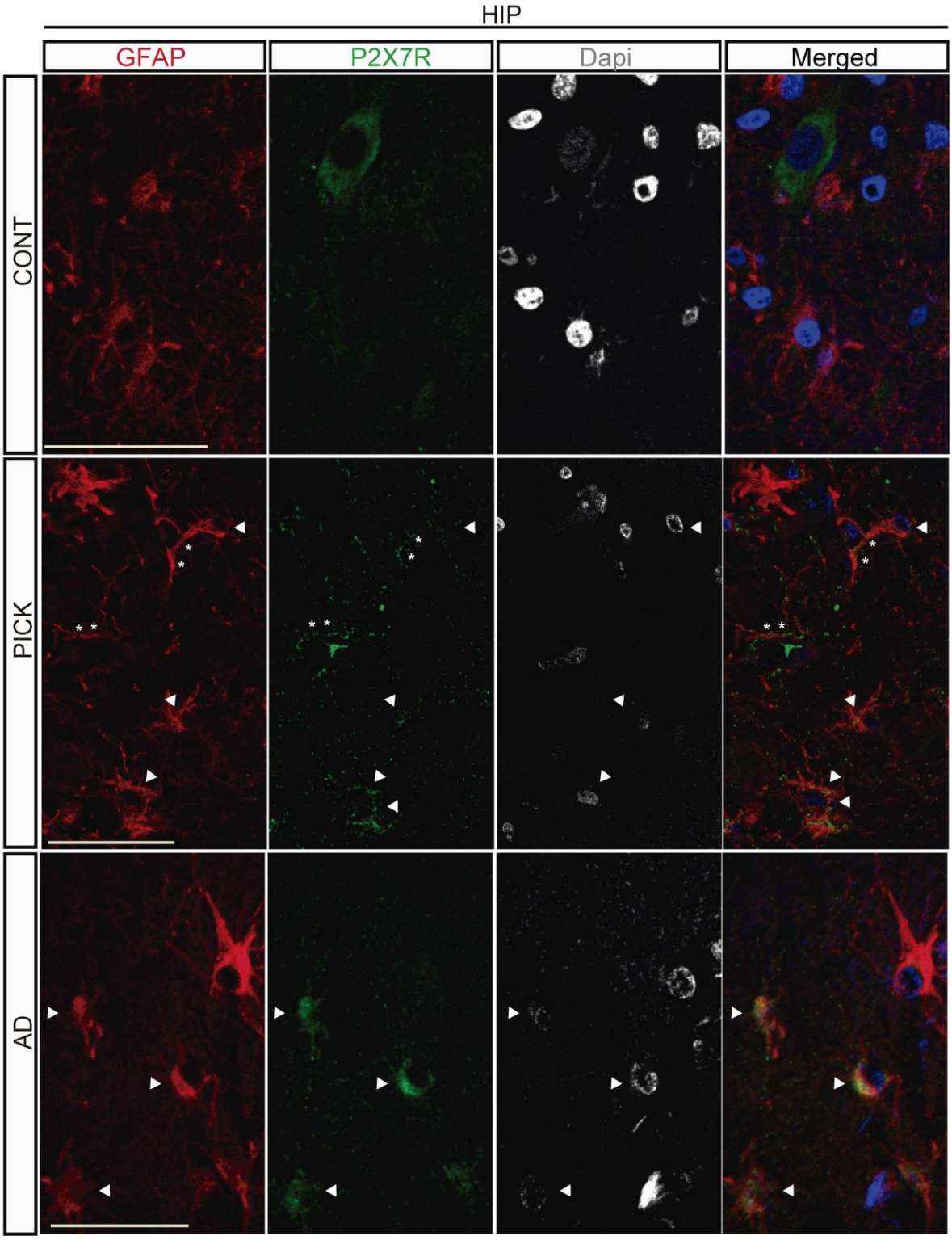

Figure 25. Upregulation of P2X7R expression in astrocytes from AD and PiD patients. *Hippocampal sections from human controls and PiD patients stained with specific astrocytes marker (GFAP, red channel), P2X7R (green channel) and DAPI (grey channel). Merged channel in also showed. Arrowheads indicate astrocytes expressing P2X7R. Asterisk indicate astrocytic processes expressing P2X7R. Scale bar: 50 µm.*

3. P301S MICE MIMICK THE P2X7R UPREGULATION FOUND IN TAUOPATHY PATIENTS.

Once confirmed P2X7R upregulation in human hippocampal microglial cells and astrocytes of tauopathies patients, the next step was to evaluate if this condition was phenocopied in the P301S mouse model. Western blot analysis on hippocampal homogenates revealed that 9-month-old heterozygous P301S mice, show higher levels of P2X7R protein (60.2±3.2%) and *P2rx7* mRNA (54.1±0.2%), compared with their WT littermates, **Figure 26**.

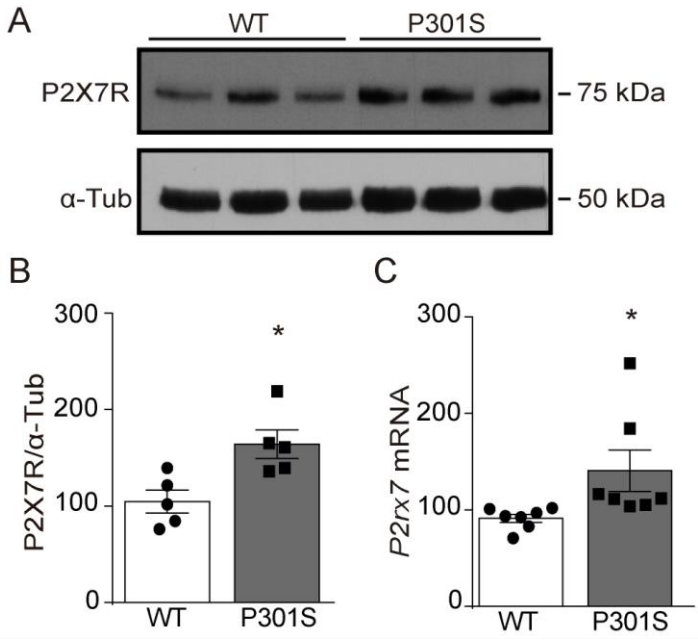

Figure 26. Evaluation of P2X7R levels in P301S mice. *A) Representative immunoblot of P2X7R protein levels in homogenates from hippocampi of 9-month-old P301S and wild-type (WT) mice of the same age. α-Tub was used as loading control. B) Graph shows P2X7R proteins levels in P301S and WT mice (n=5 mice per genotype). C) Quantification of P2rx7 mRNA in the hippocampus from P301S (n=7) and WT (n=7) mice. Data represent the mean ± standard error (SEM). * P ≦0.05 using unpaired two tailed Student's t-test.*

Later immunofluorescence studies on mouse hippocampal sections (20µm of thickness), confirmed that P301S mice, as well as Tauopathies patients, present a higher incidence of microglia cells and astrocytes expressing P2X7R than WT mice, **Figure 27-28**.

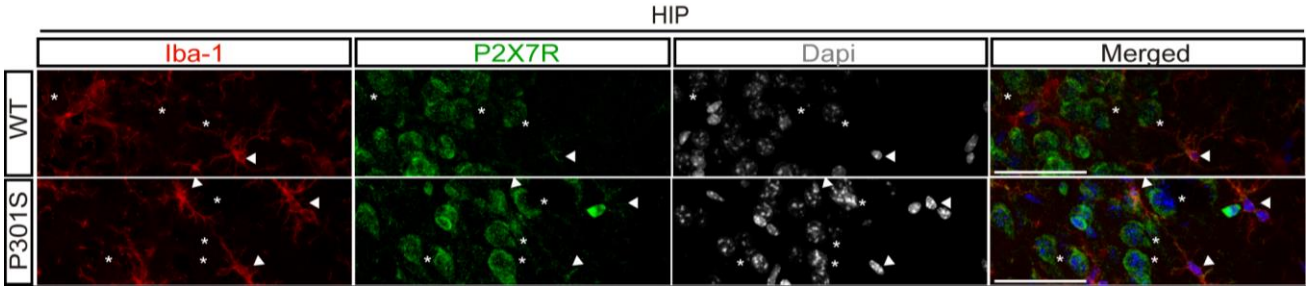

Figure 27. Upregulation of P2X7R expression in microglia cells from P301S mice. *Sagittal sections of hippocampus from P301S and WT mice stained with specific microglia marker (Iba-1, red channel), P2X7R (green channel) and DAPI (grey channel). Merged channel in also showed. Arrowheads indicate microglial cells expressing P2X7R and asterisks indicate P2X7R positive cells that are not microglia. Scale bar = 50 µm.*

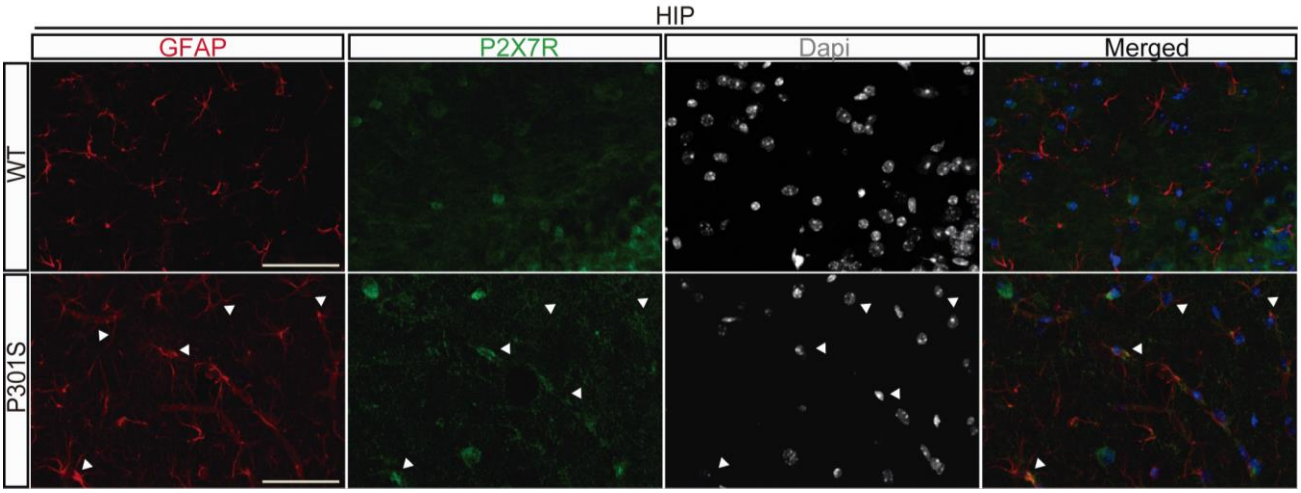

Figure 28. Upregulation of P2X7R expression in astrocytes from P301S mice. *Sagittal sections of hippocampus from P301S and WT mice stained with specific microglia marker (GFAP, red channel), P2X7R (green channel) and DAPI (grey channel). Merged channel in also showed. Arrowheads indicate astrocytes expressing P2X7R. Scale bar = 50 µm.*

4. P2X7R IS UPREGULATED IN ^{P2X7}EGFP;P301S MICE.

For the analysis of *P2rx7* gene transcription, we generated a double transgenic mice line (^{P2X7}EGFP;P301S) expressing the mutant form of MAPT and the EGFP immediately downstream of P2X7 receptor promoter. According to previous studies, increased P2X7R levels were found in the hippocampus of ^{P2X7}EGFP;P301S mice (109.0±43.97%) compared with their corresponding ^{P2X7}EGFP littermates, **Figure 29**.

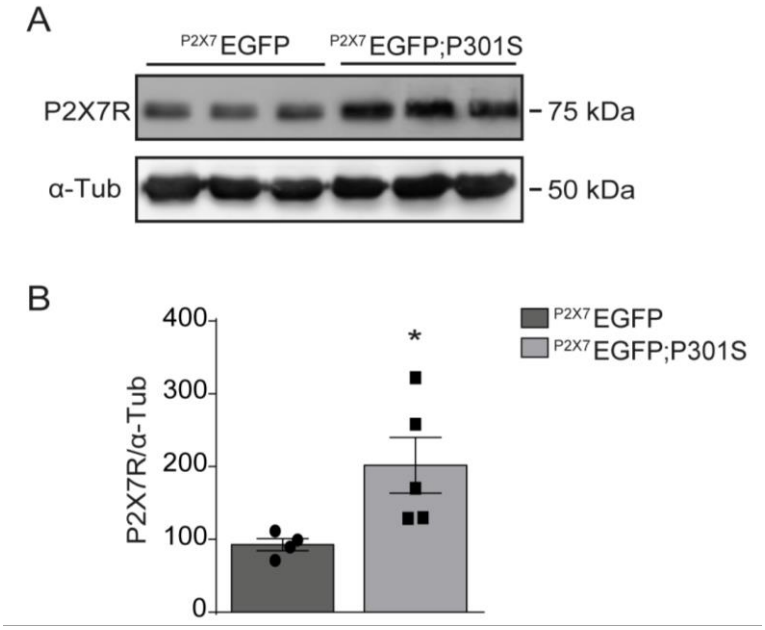

Figure 29. Analysis of P2X7R levels in ^{P2X7}EGFP;P301S mice. *A) Representative immunoblot of P2X7R protein levels in homogenates from hippocampi of 9-month-old ^{P2X7}EGFP;P301S and ^{P2X7}EGFP mice of the same age. α-Tub was used as loading control. B) Graph shows P2X7 receptor proteins levels in ^{P2X7}EGFP;P301S and ^{P2X7}EGFP mice (n≧4 mice per genotype). Data represent the mean ± standard error (SEM). * P ≦0.05 using unpaired two tailed Student's t-test.*

To confirm that P2X7R upregulation in glial lineage was the result of increased *P2rx7* gene transcription, a comparative analysis of cell-type specific expression was performed in ^{P2X7}EGFP;P301S mice by immunofluorescence. Hippocampal sagittal sections were stained using an antibody against the green fluorescent protein (GFP) and specific markers for microglia (Iba-1), for neurons (NeuN) and for astrocytes (GFAP). Results showed that ^{P2X7}EGFP;P301S mice, compared with their ^{P2X7}EGFP littermates, present higher transcription of *P2rx7* gene in glial lineage, thus confirming our hypothesis. In particular, higher number of Iba-1 and GFP positive cells (21.89±4.231, **Figure 30 A-B**) and GFAP and GFP positive cells (4.147±1.145, **Figure 30 C-D**) was found in ^{P2X7}EGFP;P301S mice. Interestingly, a significant reduction of *P2x7r* gene

transcription was found in neuronal cells; ^{P2X7}EGFP;P301S mice indeed presented lower number of Neun and GFP positive cells (-44.84±7.886, **Figure 30 E-F**).

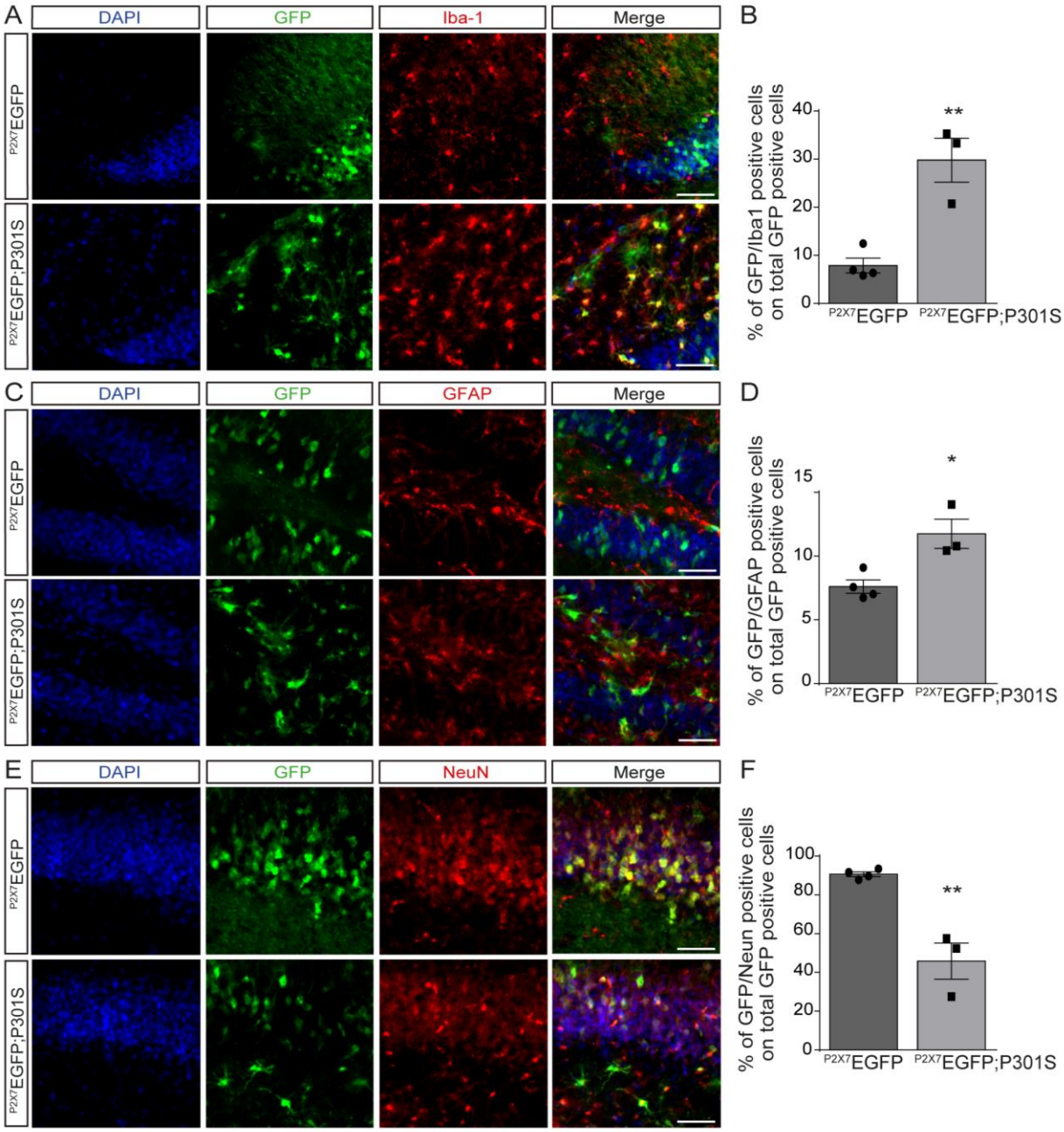

Figure 30. Tau induced toxicity promotes P2xr7 transcription in glial lineage. *(A, C, E) Representative confocal images of hippocampal sagittal sections from 9 month-old ^{P2X7}EGFP and ^{P2X7}EGFP;P301S mice stained with antibodies against microglial marker Iba-1 (A), astroglia marker GFAP (C), or neuronal marker NeuN (E), plus antibodies against EGFP protein. Merged images are also shown. Scale bar = 100 µm. (B, D, F) Graphs show quantification of hippocampal green microglia (B), green astrocytes (D) and green neurons (F) found in ^{P2X7}EGFP and ^{P2X7}EGFP;P301S mice (n ≧ 4 per genotype and n ≧ 4 sections per mouse). Data represent the mean ± standard error (SEM). *P ≦ 0.05 ** P ≦0.01 using unpaired Student's t-test.*

5. PHARMACOLOGICAL BLOCKADE OF P2X7R IMPROVES BEHAVIOURAL DEFICITS ASSOCIATED WITH P301S MICE.

To elucidate the role that P2X7R plays on Tau-induced toxicity, we analysed the effect of its *in vivo* pharmacological inhibition on behavioural associated deficits in P301S mice.

To this end, a set of 9 month-old P301S and WT mice were daily treated for three weeks with the specific P2X7R antagonist GSK 1482160A (GSK, 100 mg/kg, intraperitoneal injection i.p.) or the same volume of vehicle solution (Veh), **Figure 14**. After the treatment, the cognitive status of the four generated groups of mice was assessed with a battery of behavioural tests, **Figure 19**. As first step, we evaluated the anxiety-like behaviour of the mice with two different tests, the open field test (OF) and the elevated plus maze test (EPM).

The open field test is a common measure of exploratory behaviour and anxiety levels. OF setup and protocol followed for the test are described in section 2.3.1 of Materials and Methods. Mice anxiety levels are evaluated considering their tendency to avoid the open areas and the preference to stay close to the walls of the field. Our analysis revealed that P301S mice treated with vehicle solution (Veh-P301S), compared with WT mice treated with Veh (Veh-WT), spent more time in the central area, **Figure 31 A**, showing a decreased anxiety-like behaviour. Total distance travelled by mice during the test was also measured to confirm that this behaviour was not due to a deficit of general motor activity. In this case, the analysis showed that Veh-P301S did not present any difference in the total distance travelled, **Figure 31 A**.

The results obtained in OF were further confirmed in one more specific elevated plus maze test (section 2.3.2 of Material and Methods). Elevated plus maze test results revealed that Veh-P301S mice spent more time in the open arms of the apparatus compared with their Veh-WT littermates, **Figure 31 B**. Interestingly, this decreased anxiety-like behaviour was not observed when mice were treated with P2X7 receptor antagonist GSK, **Figure 31 A-B**.

After assessing the anxiety levels, motor coordination and locomotor functions of the mice were evaluated throughout the Rotarod test (section 2.3.3 of Material and Methods). Results obtained from this test revealed that Veh-P301S mice exhibited a locomotor deficit, **Figure 31 C**. On the contrary, these deficits were not found in P301S mice treated with GSK, which showed a motor coordination similar to the one observed in Veh- or GSK-WT mice, **Figure 31 C**.

We finally tested the learning ability and memory in our P301S mice and the effects of the pharmacological treatment on these skills. The the novel object recognition (NOR) test showed that P301S mice present deterioration in memory at the age tested. Remarkably, the pharmacological blockage of P2X7R not only prevented this deficit, but also significantly improved the memory capacity of the mice, **Figure 31 D**.

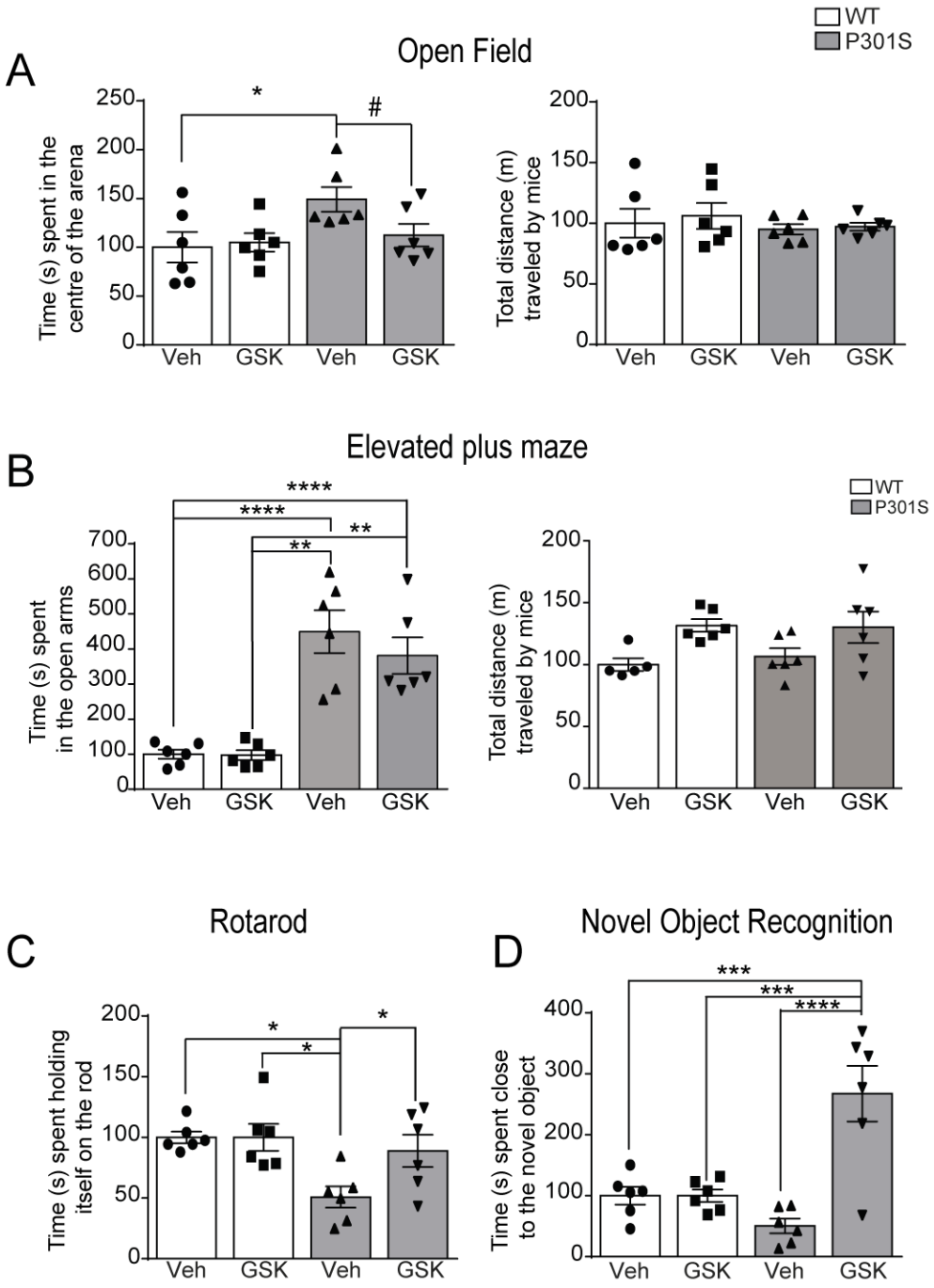

Figure 31. In vivo pharmacological blockage of P2X7R rescues some of the behavioural deficits associated with Tauopathy in P301S mice. *WT and P301S mice were intraperitoneally treated with either a vehicle solution or with the P2X7R antagonist GSK 1482160A for 3 weeks. At the end of the treatment all mice (Veh-WT n=6, GSK-WT n=6, Veh-P301S n=6, GSK-P301S n=6) underwent the open field test (OF), the elevated plus maze test (EPM), the rotarod test (RT), the novel object test (NOR) paradigms. (A) OF; graphs represent the time (s) spent by the mice in the center of the arena and the total distance travelled by mice in the apparatus. (B) EPM; graph represents the time (s) that mice spent in the open arms of the apparatus and the total distance travelled by mice in the apparatus. (C) RT; graph represents the time (s) spent by the mice holding on the rod before falling dawn. (D) NORT; graph represents the time (s) that the mice spent exploring the new object. Data represent the mean ± standard error (SEM). * P ≦0.05; ** P ≦0.01; *** P ≦0.001; **** P ≦0.0001 using a two-way ANOVA followed by Tukey´s post hoc test. # P ≦0.05 using unpaired two tailed Student's t-test.*

6. P2X7R BLOCKADE AFFECTS MICROGLIA PROLIFERATION AND MORPHOLOGY.

After behavioural assessment, mice were sacrificed and analysed to evaluate the impact of P2X7R on the pathological features of Tauopathy. Since we found that P2X7R upregulation mainly takes place in glial lineage, we decided to further investigate how the blockage of this receptor could affect this cell line. To this purpose, we initially focused on astrocytes and microglia proliferation capacity.

Astroglial proliferation was evaluated by counting the number of hippocampal astrocytes, identified by the marker GFAP. The analysis showed that pharmacological P2X7R blockage does not modify the increased astroglial proliferation rate found in P301S mice, **Figure 32**.

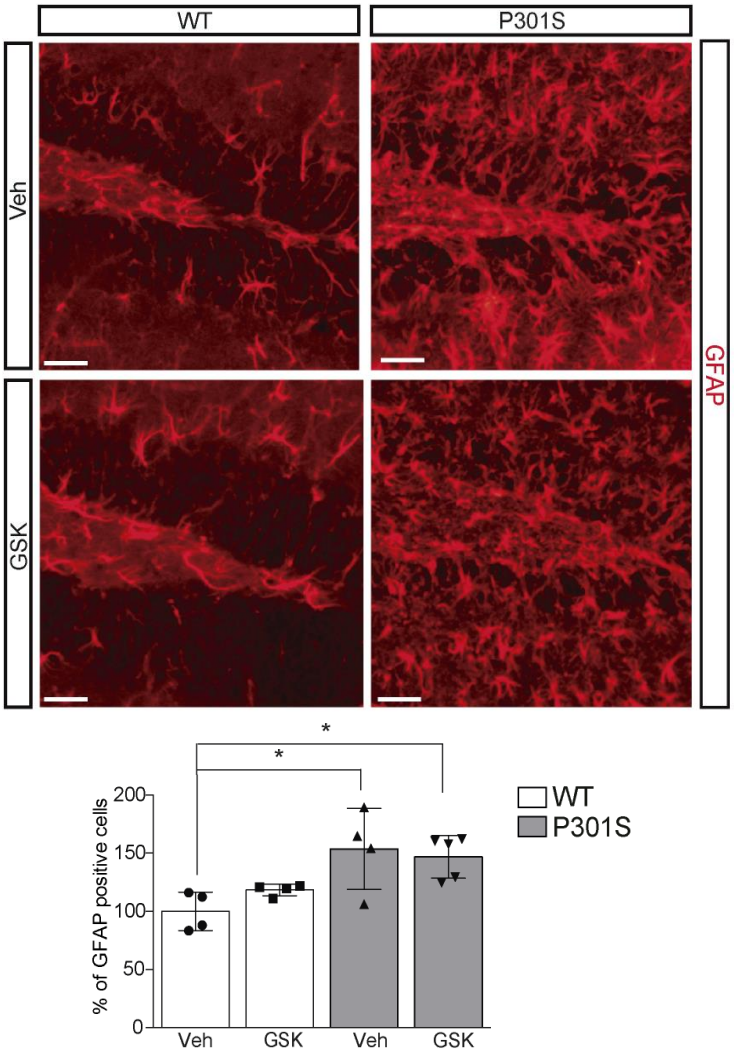

Figure 32. Pharmacological P2X7R blockade do not modify astrocytes proliferation. *Representative images of hippocampal sections from P301S and WT mice treated with vehicle solution or the P2X7R antagonist GSK stained with the astrocytes marker GFAP. Scale bar: 100 µm. The graph represents the quantification of GFAP positive cells in the hippocampus (n≧4 mice per genotype and treatment with n≧4 sections/mouse) * P ≦ 0.05; two-way ANOVA followed by Tukey´s post hoc test.*

In a similar way, microglial proliferation was evaluated by counting the number of hippocampal microglia cells, identified by the microglia marker Iba-1. The analysis showed that Veh-P301S mice present higher number of hippocampal microglia cells than the one observed in Veh-WT mice (475.5±38.8 microglia cells in Veh-P301S mice versus 290.8±22.0 in Veh-WT mice, **Figure 33**; interestingly this increase was not detected in GSK-P301S mice, **Figure 33**. The increase of microglia proliferation was later confirmed through immunofluorescence analysis using the specific proliferation marker Ki-67 (Veh-P301S mice showed 51.4±8.3 more Iba-1 and Ki-67 positive cells than Veh-WT mice), **Figure 34**.

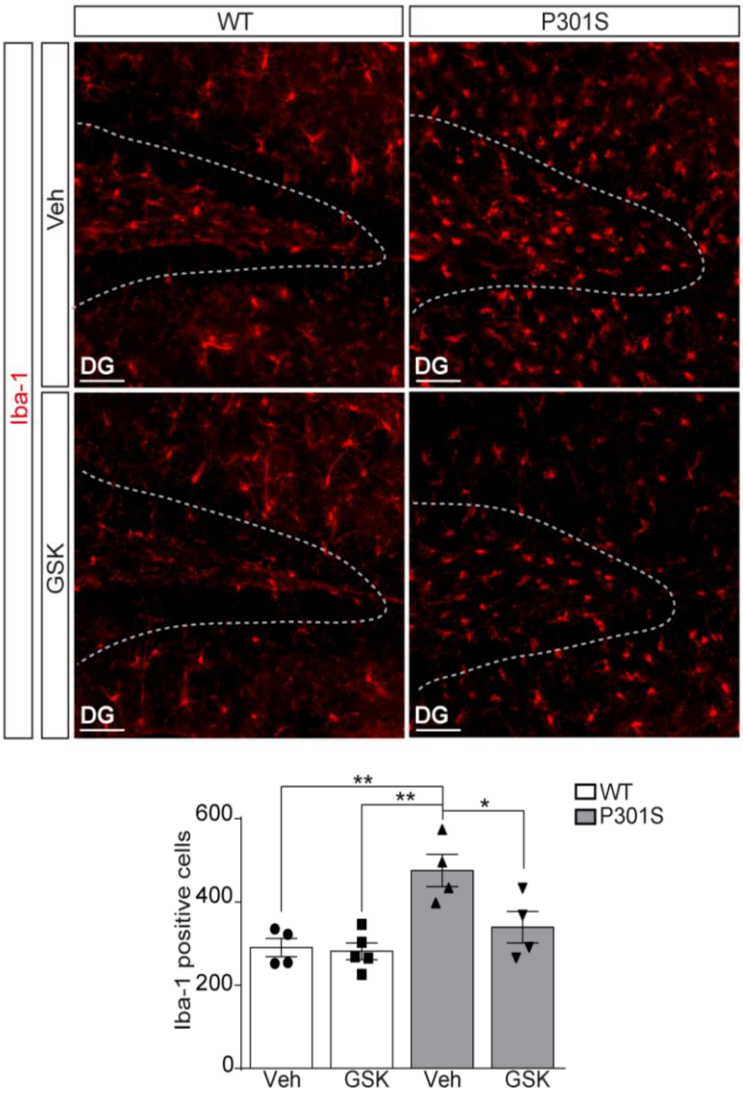

***Figure 33*. Pharmacological P2X7R blockade reverts microglial proliferation.** *Representative images of hippocampal sections from P301S and WT mice treated with vehicle solution or the P2X7R antagonist GSK stained with the microglial marker Iba-1. Dash lines indicate the granular layer of the dentate gyrus (DG). Scale bar: 100 µm. The graph represents the quantification of Iba1 positive cells in the hippocampus (n≧4 mice per genotype and treatment with n≧4 sections/mouse) * P ≦0.05; ** P ≦0.01 two-way ANOVA followed by Tukey´s post hoc test.*

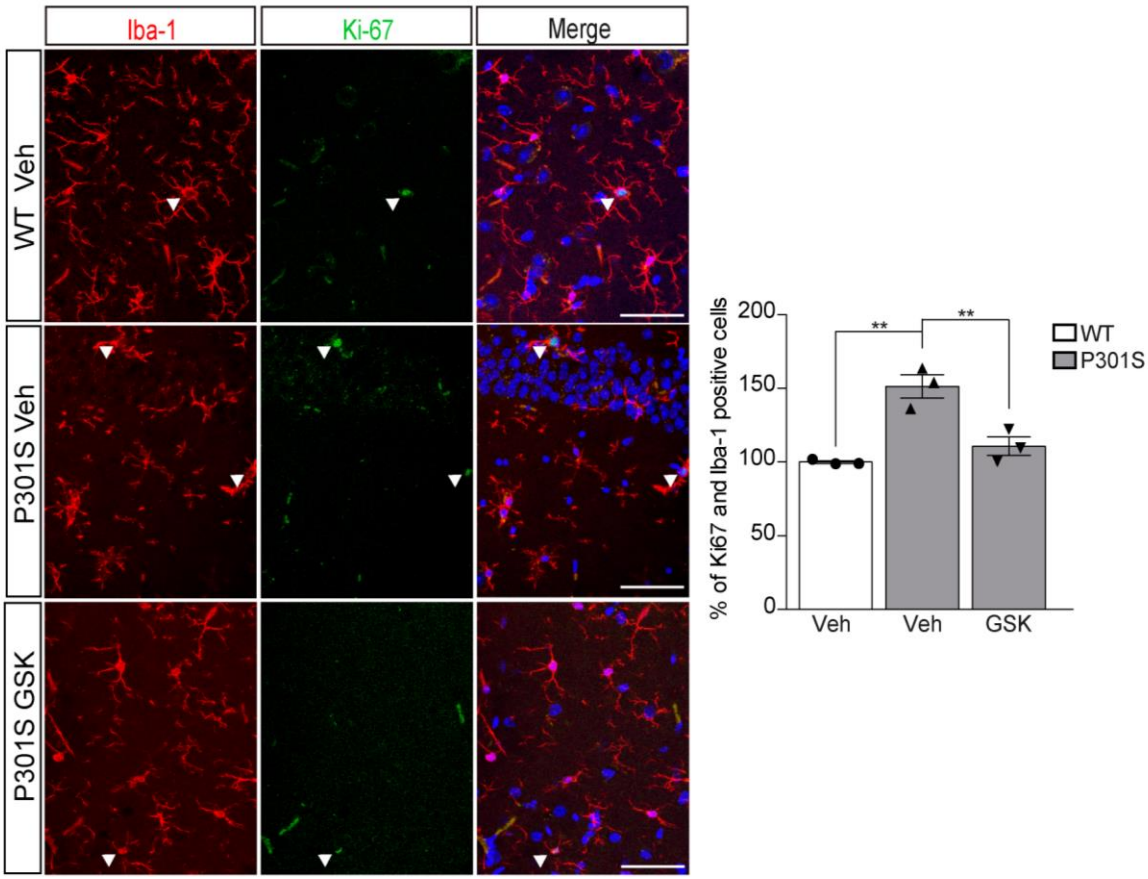

Figure 34*. *Pharmacological P2X7R blockade reverts microglial proliferation. *Representative images of hippocampal sections from P301S mice and wild-type treated with vehicle solution or GSK, stained with microglial marker Iba-1 (red channel) and proliferation marker Ki-67 (green channel). Merged images are also shown. Scale bar: 100 µm. The histogram represents the quantification of double Iba1 and Ki-67 positive cells in the hippocampus (n≧3 mice per genotype and treatment with n≧5 sections/mouse) ** P ≦ 0,01 using a two-way ANOVA followed by Tukey´s post hoc test*

Next, we decided to evaluate the impact of P2X7R blockade on microglia morphology as well. Microglia cells were examined following the protocol described in the section 2.11 of Material and Methods. The analysis showed that Veh-P301S mice present hippocampal microglia with less and shorter ramifications than the ones observed in Veh-WT mice, **Figure 35 B-C**. As a consequence of this different morphology, Veh-P301S microglia cells cover a smaller brain area than WT mice, **Figure 35 E**. This phenotype was not found in GSK-P301S mice. On the contrary, they showed similar microglia cells to the ones observed in Veh-WT mice, both for number and length of ramifications. Accordingly, GSK-P301S mice microglia can cover wider brain areas than Veh-P301S mice microglia, **Figure 35.**

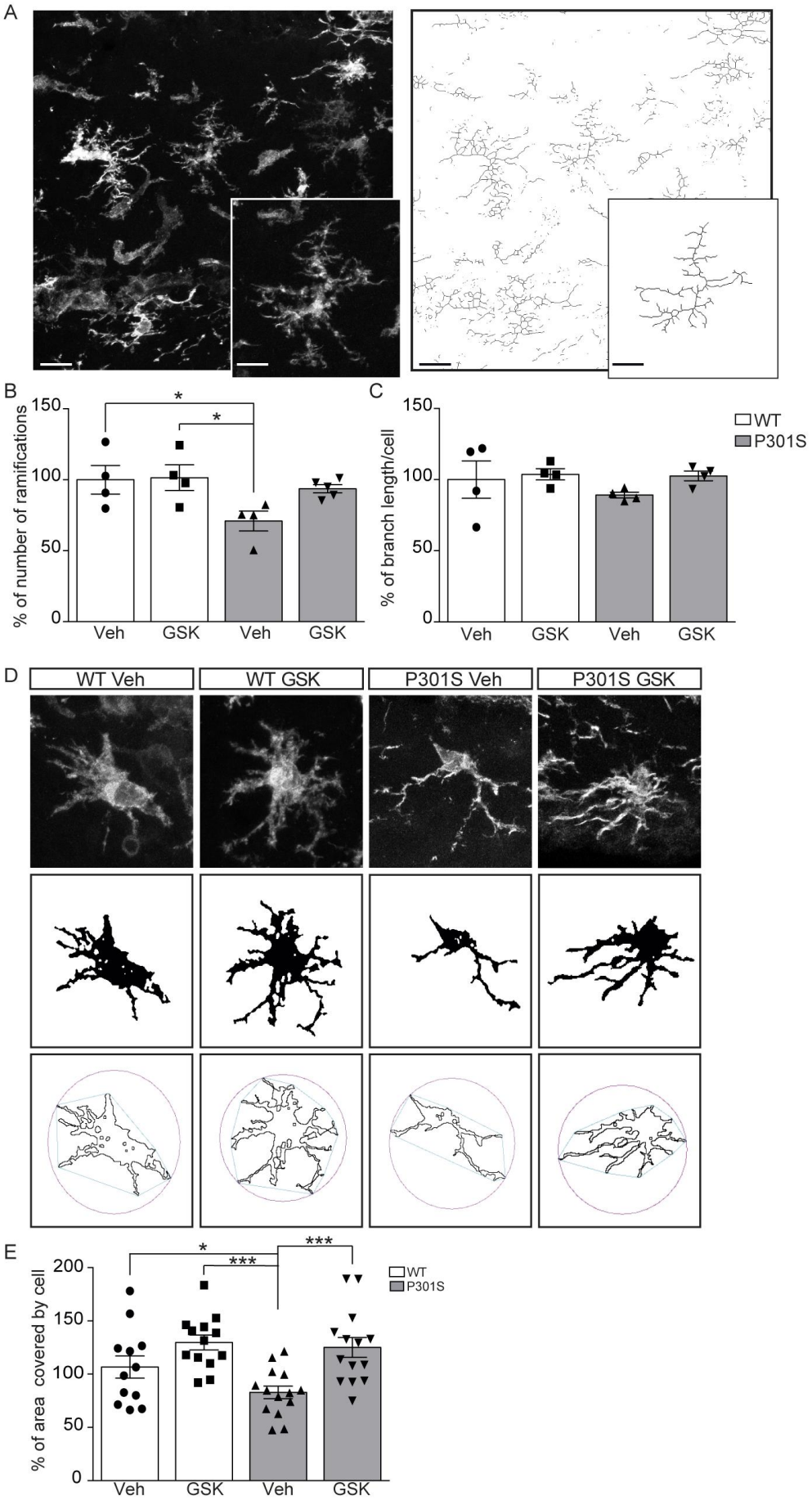
A
B
% of number of ramifications
150
100
50
0
*
*
Veh
GSK
Veh
GSK
C
% of branch length/cell
150
100
50
0
WT
P301S
Veh
GSK
Veh
GSK
D
WT Veh
WT GSK
P301S Veh
P301S GSK
E
% of area covered by cell
200
150
100
50
0
*
***
***
WT
P301S
Veh
GSK
Veh
GSK

Figure 35. Analysis of microglia morphology. *(A) Representative images of hippocampal microglia cells stained with the microglial marker Iba-1; insert represents a 2x magnification of a selected microglia cell; skeletonized binary representation of the same image. Scale bar =20 µm. Scale bar of insert image=10 µm. Graphs show the quantification of cell ramifications (B), and of branch lengths (C) using similar images as shown in A. The 100% value corresponds to the number of ramifications and total branch lengths detected in hippocampal microglia cell from WT mice (n≧4 mice per genotype and treatment and, n ≧4 sections per mouse, being analysed a minimum of 12 microglia cells per section). * P ≦0.05 using a two-way ANOVA followed by Tukey´s post hoc test. (D) Representative images showing a selected microglia cell (upper panels), with its corresponding binary image (middle panels) and outline shape with the associated convex hull (blue) and enclosing circle (pink, bottom panels). (E), Graph shows the percentage of brain area covered by microglia cells for each condition. The 100% value corresponds to the brain area covered by microglia cells in WT mice (n=10 random microglia cells per genotype and experimental condition). Data represent the mean ± standard error (SEM). * P ≦0.05; *** P ≦0.001 using a two-way ANOVA followed by Tukey´s post hoc test.*

To further confirm that P2X7 receptor plays a critical role on the microglia cell lineage, we decided to evaluate the effect of its overexpression. To this end, we analysed the morphology of microglia cells from a BAC transgenic mouse line overexpressing P2X7 receptor fused to EGFP ($P2X7^{451P}$-EGFP). Interestingly, microglia cells from $P2X7^{451P}$-EGFP mice had shorter ramifications, smaller cell size and smaller nuclei area, compared to WT mice, resulting in smaller brain area coverage, **Figure 36**.

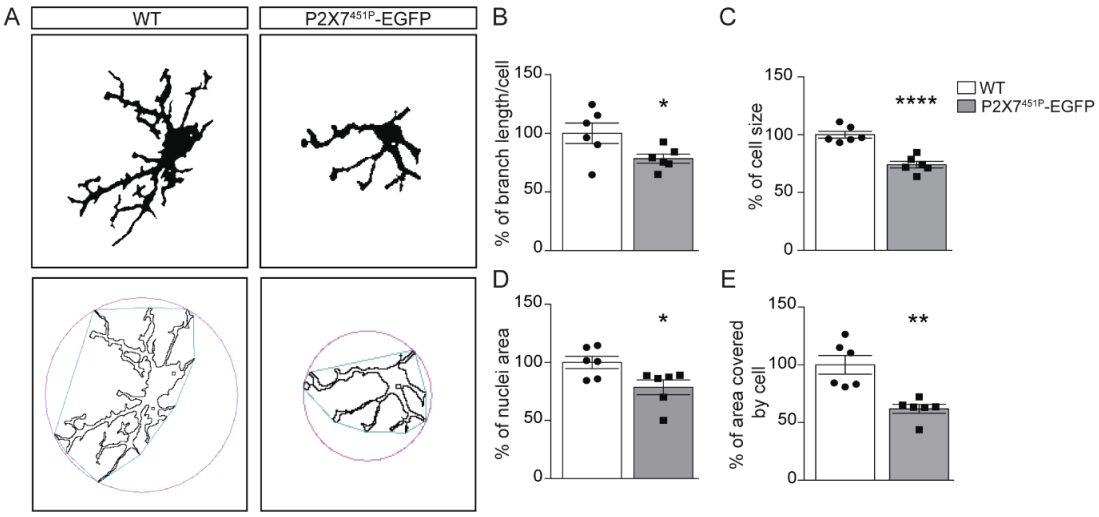

Figure 36. Analysis of microglia morphology in P2X7^{451P}-EGFP mice. *(A) Representative binary image of microglia cells with their corresponding associated convex hull (blue) and enclosing circle (pink) for corresponding outline shapes from microglia cells stained with specific microglial marker Iba-1. (B-E). Graphs show branch length quantification (B), microglial body size (C), nuclei area (D), and the percentage of brain area covered by microglia cells for each condition (E). The 100% value corresponds to the total branch length, the cell size, the nuclei size, and the brain area covered by microglia cells in WT mice (n≧ 4 mice per genotype and treatment and, n ≧4 sections per mouse, being analysed a minimum of 12 microglia cells per section). Data represent the mean ± standard error (SEM). * P≦0.05; ** P≦0.01; **** P ≦0.0001 using unpaired two tailed Student's t-test.*

7. *IN VIVO* P2X7R BLOCKADE AFFECTS MICROGLIA FUNCTIONALITY.

Once evaluated the effect of P2X7 receptor blockade on microglia proliferation and morphology, we decided to analyse microglia phagocytic and migratory capacity as well.

To this purpose, five micron-diameter fluorescent microspheres were intrahippocampally (i.h.) administered to a set of WT and P301S mice treated with GSK 1482160A or vehicle solution every 24 hours for 8 days before the injection. Three days after microsphere injection, the mice were sacrificed, and hippocampal sections were stained with anti-Iba-1 antibody to identify microglia cells. The analysis showed that P301S mice treated with vehicle, present a higher number of phagocytic microglia cells than Veh-WT mice, **Figure 37 A-B**. Interestingly, although *in vivo* P2X7 blockade did not modify the number of phagocytic microglia in both genotypes, it caused an increase in their phagocytic capacity both in WT and P301S mice (1.4 ± 0.2 and 1.6 ± 0.3 beads per microglia in Veh-WT and Veh-P301S mice respectively versus 2.5 ± 0.4 and 3.0 ± 0.6 beads per microglia in GSK-WT and GSK-P301S mice respectively).

We also evaluated the migration capacity of microglia cells, analysing their recruitment to the injury site caused by beads injection. Results revealed that the Veh-P301S mice tend to present more microglia cells next to the injection site than the WT mice treated with vehicle. *In vivo* P2X7R inhibition significantly reduced the number of microglia at the injection site in P301S mice. A similar tendency was detected in WT mice, **Figure 37 D-E**.

Since it is widely described in literature that P2X7R plays a critical role in the inflammasome activation and release of inflammatory cytokines, we analysed the levels of some of these proteins. Western blot analysis revealed that Veh-P301S mice, as expected, present higher levels of IL-1β (49.6 ± 11.7% more, **Figure 38 A-B**) and IL-6 (158.6 ± 35.3% more, **Figure 38 A-C**) than Veh-WT mice. Moreover, we measured the levels of the Tumor necrosis factor (TNF-α), but in this case no significant differences were found, **Figure 38 A-D**. Surprisingly, GSK treatment only reverted the increase of IL-1β levels detected in P301S mice, **Figure 38 A-B**.

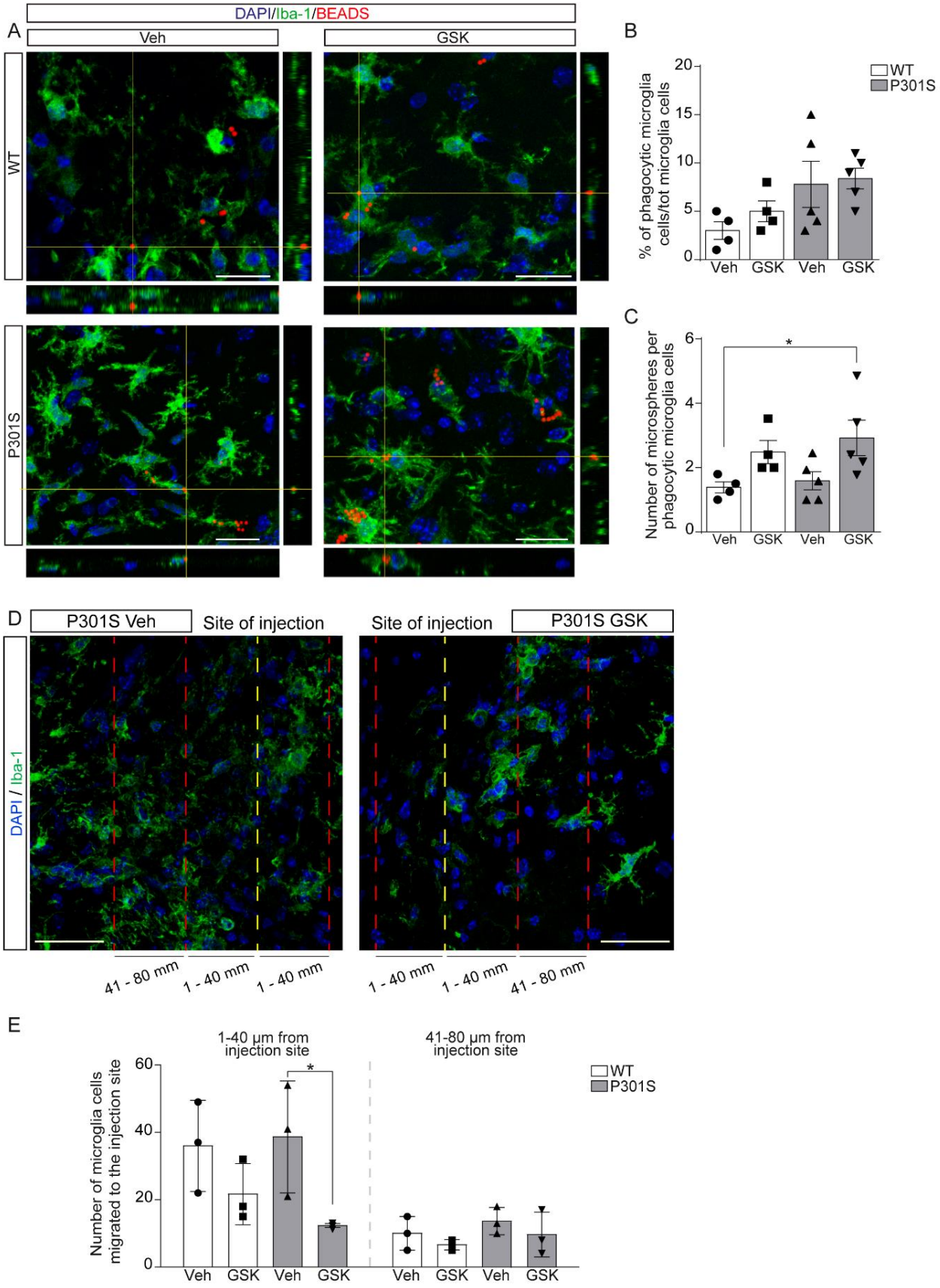

Figure 37. In vivo P2X7R blockade affects microglia functionality. *(A) Representative confocal images and its corresponding orthogonal views of hippocampal sections from 9 months-old WT and P301S mice intraperitoneally*

*treated with either vehicle solution or GSK for 3 weeks before intracranial administration of fluorescent microspheres to the hippocampus. Yellow lines represent the location where an orthogonal view was obtained. Sections were stained with antibodies against microglial marker Iba-1 (green) and nuclear marker DAPI (blue). Fluorescent microspheres are visualized in red. Scale bar: 25 µm. Graphs represent the number of microglial cells phagocyting microspheres (B) and the number of incorporated fluorescent microspheres per microglia (C) (n≧4 mice per genotype and treatment and, n ≧4 sections per mouse) * P ≦ 0.05 using a two-way ANOVA followed by Tukey´s post hoc test. (D) Representative immunofluorescence images of hippocampal sections stained with microglial marker Iba-1 used to evaluate the microglial migration toward the site of injection (yellow line). Distances of 40 and 80 µm from the injured site are identified with dash red lines. (E) The graph represents the number of hippocampal microglial cells found in every delimitated area (n≧3 mice per genotype and treatment and, n≧4 sections per mouse) * P ≦ 0.05 using a Two-way ANOVA followed by Tukey´s post hoc test.*

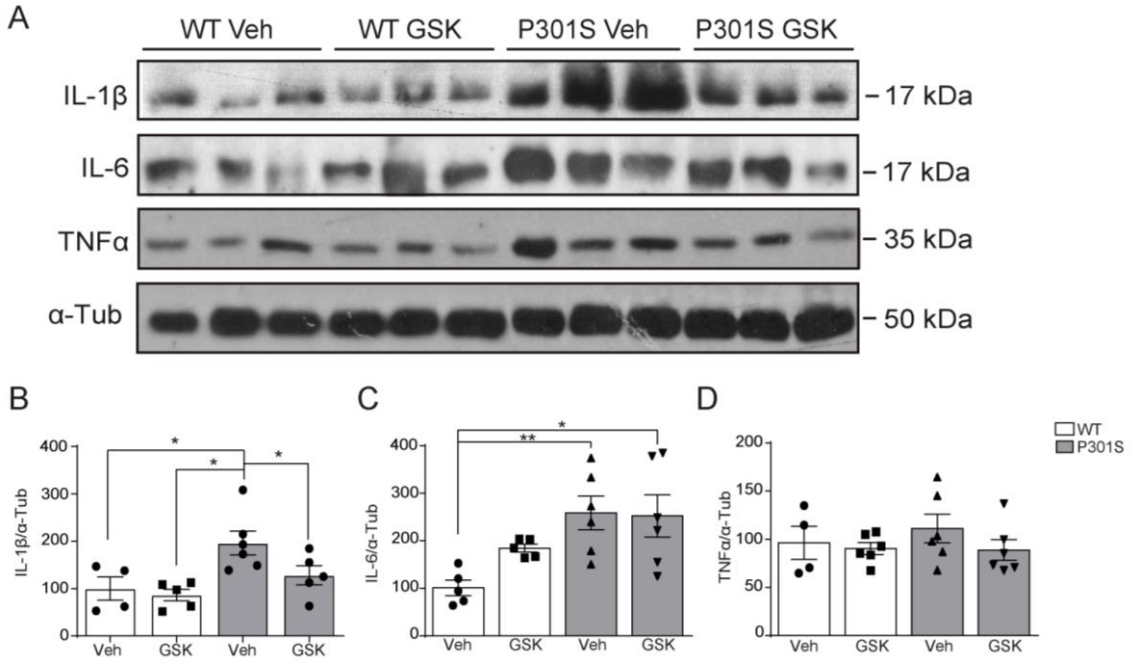

Figure 38. In vivo P2X7R inhibition reduces the high levels of IL-1β secretion detected in P301S mice. *(A) Representative Western blot detection of IL-1β, IL-6 and TNF-α in the hippocampus from WT and P301S mice treated with vehicle solution or GSK. Graphs show quantification of IL-1β (B), IL-6 (C), and TNF-α (D) levels detected in hippocampal homogenates from WT and P301S mice treated with vehicle or GSK (n≧4 mice per genotype and treatment). Data represent the mean ± standard error (SEM). * P ≦ 0.05; ** P ≦ 0.01 using a two-way ANOVA followed by Tukey´s post hoc test.*

8. P2X7R PHARMACOLOGICAL INHIBITION REDUCES INTRACELLULAR TAU PHOSPHORYLATION.

Tau phosphorylation state is controlled by many serine/threonine or tyrosine kinases as well as phosphatases; this homeostasis is disrupted in tauopathies favouring Tau hyper-phosphorylation (Buée, 2000; Hasegawa, 2006). Considering that it was previously demonstrated that pharmacological inhibition of P2X7 receptor induces a significant decrease in the number of hippocampal amyloid plaques, through inhibition of GSK3 activity in cultured hippocampal neurons (Díaz-Hernández, 2012), we next evaluated if this effect is also detectable in P301S model. Western blot analysis revealed that P2X7R blockade reduces the phosphorylated tau levels in Ser202/Thr305 and Ser396/404 sites, identified by AT8 and PHF1 antibodies respectively (50.1±1.7% and 27.2±12.3% lower than in Veh-P301S mice, **Figure 39 A-B-C**. In line with these results, a significant increase in tau dephosphorylation was detected in Ser 195/198/199/202 with TAU1 antibody (72.2±20.4% higher than in Veh-P301S mice, **Figure 39 A-D**). Noteworthy, later immunohistochemical analysis showed that P2X7 inhibition causes a significant reduction in the number of positive AT8 positive neurons, **Figure 39 E-F**.

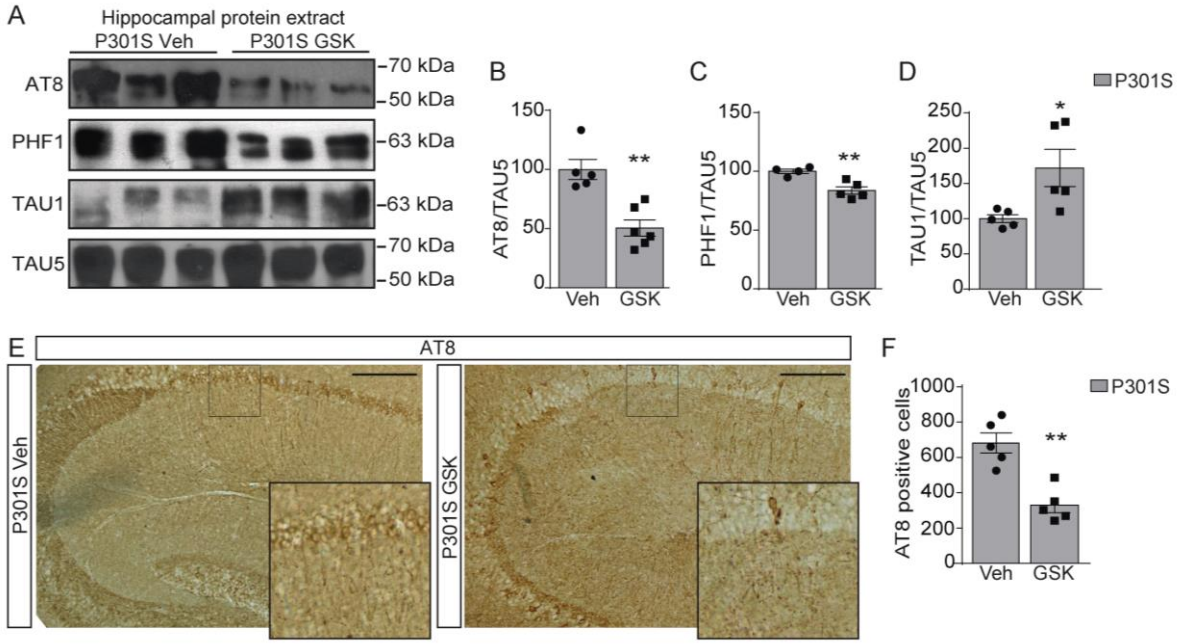

Figure 39. In vivo P2X7R inhibition reduces intracellular Tau phosphorylation. *(A) Western blot detection of the different Tau phosphorylation sites and GAPDH levels in hippocampal protein extract. (B, C, D) Graphs show the quantification of phosphorylated Tau protein levels identified by the selective antibodies AT8 (A), PHF-1 (B), TAU1 (C) in homogenates of hippocampus from P301S mice treated with vehicle solution (n≧4 mice) or GSK (n≧5 mice). Total Tau protein levels were identified using the antibody Tau5 and were used as a loading control for normalization purposes. The 100% value corresponds to the amount of phosphorylated Tau levels detected in the hippocampi of vehicle treated P301S mice. Data represent the mean ± standard error (SEM). * P≦ 0.05 **; P ≦ 0.01 using an*

*unpaired two tailed Student's t-test. (E) AT8 immunostaining in hippocampus from P301S mice treated with vehicle solution or GSK. Insert represents a 2x magnification of the indicated area. Scale bar = 100 µm. (F) Graph represents the quantification of AT8 positive cells both in Veh-P301S and GSK-P301S mice (n≧4 mice per genotype and treatment and n≧4 sections per mouse). ** P ≦0.01 using an unpaired two tailed Student's t-test.*

Once observed that the pharmacological blockage of P2X7R reduces the higher levels of phosphorylated Ser202 and Thr305 sites in P301S mice, we decided to check the status of a serine/threonine protein kinase that mediates the addition of phosphate molecules onto serine and threonine amino acid residues, the GSK3 enzyme. The analysis showed that P301S mice present lower levels of phosphorylated-GSK3β, **Figure 40 A-B**. Interestingly, P2X7R pharmacological blockage determined a significant increase of phosphorylated-GSK3β, **Figure 40 C-D.** Since the phosphorylation of Ser 9/21 sites in GSK3 has been related to a decrease of GSK3 enzyme activity (Díaz-Hernández, 2012; Hernandez *et al*., 2013), we hypothesized that P2X7R-blockage promotes Tau dephosphorylation by favouring the GSK3 inhibition.

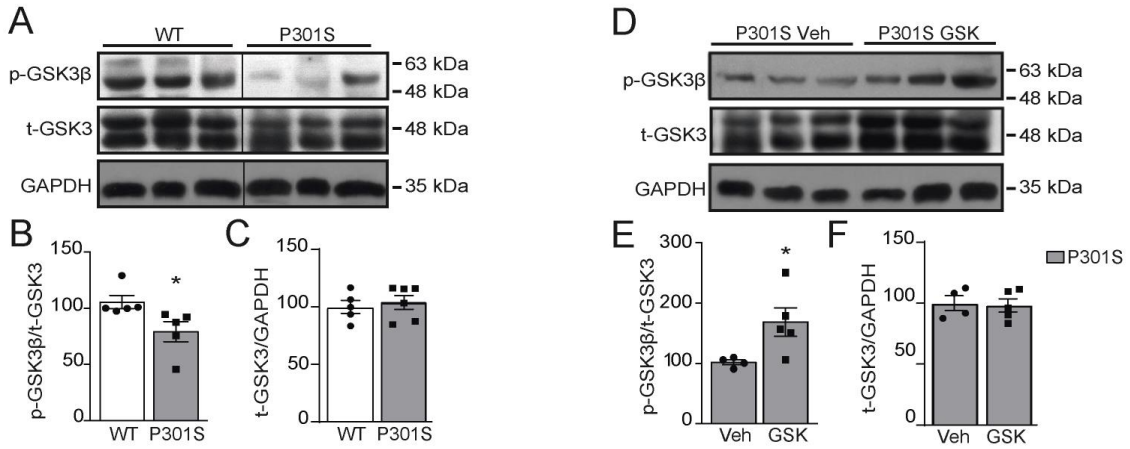

Figure 40. In vivo P2X7R inhibition increases the levels of phosphorylated-GSK3β enzyme. *(A-D) Western blot detection of p-GSK3β and total GSK3 levels in hippocampal protein extract. (B, E) Graphs show the quantification of p-GSK3β levels in the hippocampus from WT and P301S mice (n=5 mice per genotype) (B), or P301S mice treated with vehicle or GSK (n=5 mice per treatment) (E). Levels of total-GSK3 were used as loading control for normalization purposes. The 100% value corresponds to p-GSK3/t-GSK3 levels detected in hippocampi of WT mice (B) or vehicle treated P301S mice (E) respectively. Data represent the mean ± standard error (SEM). * P≦0.05 using an unpaired two tailed Student's t-test. (C, F) Graphs show the quantification of total-GSK3 using the housekeeping GAPDH for normalization purposes.*

To support the hypothesis that P2X7R plays an important role in the regulation of intraneuronal Tau protein phosphorylation, we analysed the levels of phosphorylated Ser202 and Thr305 sites in

P2X7^{451P}EGFP mice. Remarkably, we found that mice overexpressing P2X7R present a significant increase in AT8 levels, **Figure 41**.

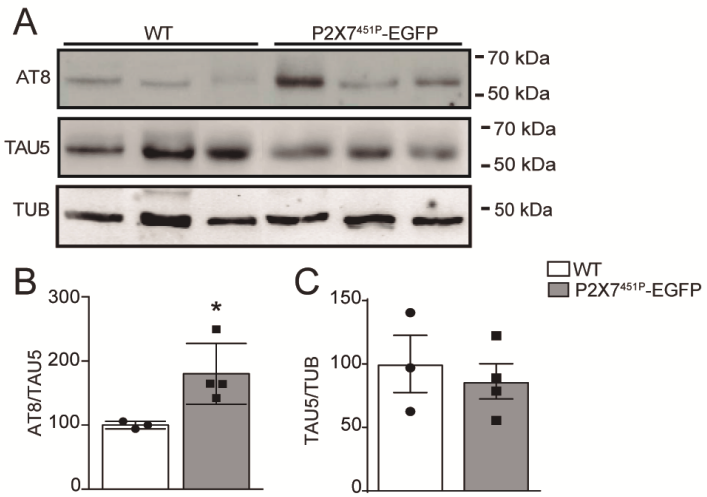

Figure 41. P2X7R overexpressing determines an increase of Tau phosphorylation. *Representative immunoblot (A) and quantification (B) of phospho-Tau protein levels in hippocampal extracts from WT mice, and P2X7$_{451P}$-EGFP mice (n≧3 mice per genotype). The 100% value corresponds to phospho-Tau protein levels detected in WT mice. Data represent the mean ± standard error (SEM). * P≦0,05; using unpaired two tailed Student's t-test. (C) Graph shows the quantification of TAU5 using the housekeeping TUB for normalization purposes.*

9. P2X7R INHIBITION REVERTS CELLULAR DEATH.

P2X7 receptor is known to be involved in the regulation of various cell death pathways, including apoptosis, necrosis, and autophagy (Miras-Portugal *et al*., 2017; Zhao, 2018). The involvement of this receptor in regulating cell death has been widely demonstrated in immune cells (Di Virgilio, 2015) and in neurons as well (Sugiyama 2010; Ohishi 2016; Miras-Portugal *et al*., 2017). Similarly, studies from our lab proved that P2X7R inhibition reduces neuronal death associated with different neurodegenerative diseases, including Huntington disease (HD) and AD (Díaz-Hernández, 2009; Díaz-Hernández, 2012). It was previously reported that P301S mice present a reduction in the number of hippocampal neurons (Yoshiyama *et al*., 2007). For this reason, we decided to elucidate if P2X7R inhibition generally improves neuronal survival in Tauopathies. To this aim, we used the neuronal marker Neun to identify and quantify the number of neurons in the hippocampus of WT and P301S mice treated with either vehicle or GSK solution. Our analysis showed that Veh-P301S mice, compared to Veh-WT mice, present a significant reduction in the number of hippocampal neurons (38.3±2.2% less than Veh-WT mice, **Figure 42 A**. Accordingly, Veh-P301S showed a higher number of hippocampal cleaved-Caspase-3 positive apoptotic cells than Veh-WT mice (5,4±2,4 times more than Veh-WT mice, **Figure 42 B**. Interestingly, P301S mice treated with GSK

showed neither the reduction in hippocampal neurons, nor the increase in apoptotic cells detected in Veh-P301S mice, **Figure 42 A-B**.

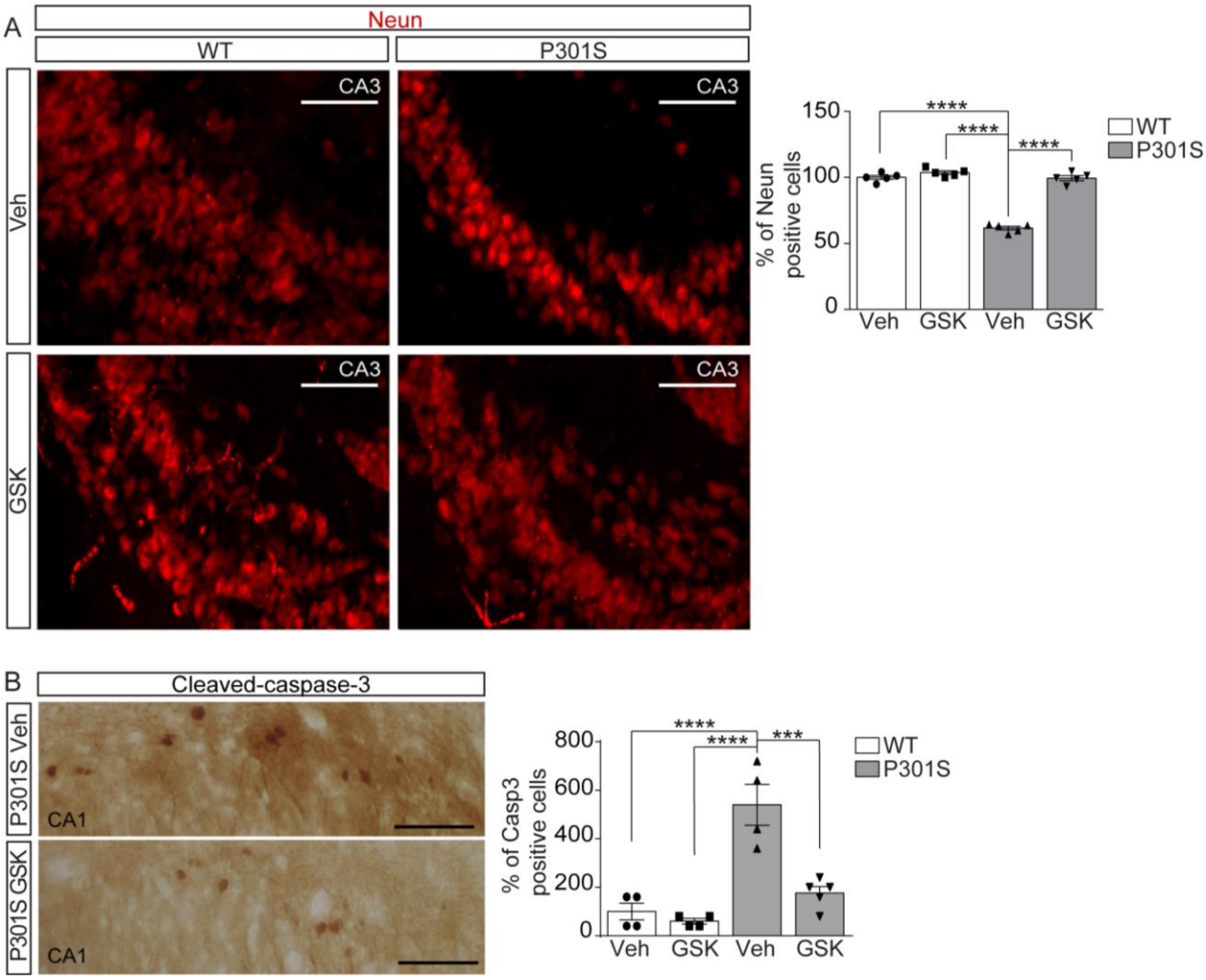

Figure 42. In vivo P2X7R inhibition enhances neuronal survival. *(A) Representative immunofluorescence images of hippocampal CA3 area stained with NeuN from WT and P301S mice treated with vehicle solution or the P2X7 inhibitor GSK 1482160A. Scale bar = 100 μm. Graph represents the quantification of neuronal hippocampal cells identified as NeuN positive (n≧4 mice per genotype and treatment and n≧4 sections per mouse). (B) Cleaved Caspase-3 immunostaining in hippocampus from WT and P301S mice treated with vehicle solution or GSK. Scale bar =100 μm. Graph represents the quantification of hippocampal cleaved Caspase-3 positive cells (n≧4 mice per genotype and treatment and n≧4 sections per mouse). *** P ≦0.001; **** P ≦0.0001 using a two-way ANOVA followed by Tukey´s post hoc test.*

10. P2X7R EXPRESSION LEVELS IN P301S;P2X7$^{-/-}$ AND P301S;P2X7^{451P}-EGFP MICE.

To confirm the potential therapeutic role of P2X7R in Taupathies, we evaluated how the genetic depletion or overexpression of P2X7R affect Tau-induced toxicity. To this end we generated P2X7 null mice expressing a mutant form of MAPT (P301S;P2X7-/- mice), and a double transgenic mice line expressing a mutant form of MAPT and overexpressing EGFP-tagged P2X7 receptor mice (P301S;P2X7^{451P}-EGFP).

P2X7R levels were evaluated in the newly generated transgenic lines. Western blot analysis on hippocampal homogenates allowed us to confirm both the absence of hippocampal P2X7R in P301S;P2X7$^{-/-}$ mice and P2X7R overexpression in P301S;P2X7^{451P}-EGFP, **Figure 43**.

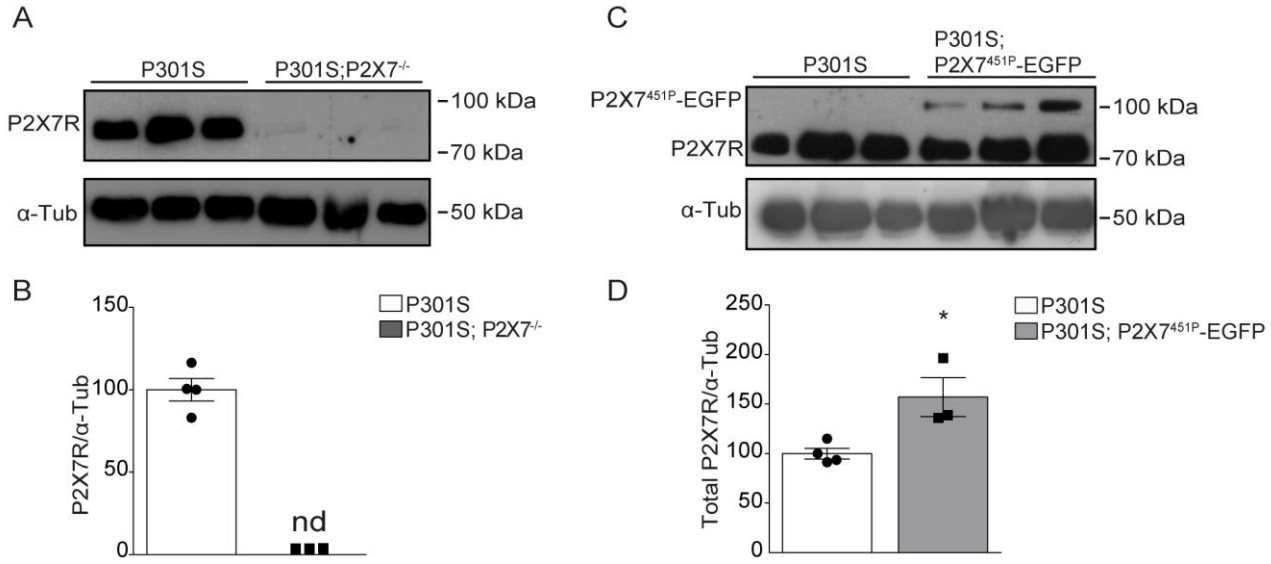

Figure 43. Genetic P2X7R knockout and overexpression in P301S mice. *(A) Representative immunoblot of P2X7R protein levels in hippocampal homogenates from P301S mice and P301S;P2X7$^{-/-}$. (B) Graph shows P2X7R protein levels in P301S mice and P301S;P2X7$^{-/-}$ mice (n≧3 mice per genotype). Levels of α-Tub protein were used as loading control for normalization purposes. The 100% value corresponds to P2X7R/α-Tub levels detected in the hippocampi of P301S mice. nd = not detected. (C) Representative immunoblot of P2X7R native and P2X7^{451P}-EGFP proteins levels in hippocampal homogenates from P301S mice and P301S;P2X7^{451P}-EGFP mice. (D) Graph shows P2X7R protein levels in P301S mice and P301S;P2X7^{451P}-EGFP mice (n≧3 mice per genotype). Levels of α-Tub protein were used as loading control for normalization purposes. The 100% value corresponds to total P2X7R/α-Tub (P2X7R plus P2X7^{451P}-EGFP) levels detected in the hippocampi of P301S mice. * P ≦0.05 using unpaired two tailed Student's t-test.*

11. P2X7R GENETIC KNOCKOUT IMPROVES BEHAVIOURAL DEFICITS ASSOCIATED WITH P301S MICE.

Next P301S;P2X7$^{-/-}$ and P301S;P2X7^{451P}-EGFP mice underwent a battery of behavioural tests similar to the one designed for the pharmacological approach. The results obtained with the EPM test revealed that P301S;P2X7$^{-/-}$ mice spent less time in the open arms compared with P301S mice, whereas P301S;P2X7^{451P}-EGFP mice exhibited opposite scores, **Figure 44 A-B**.

The beneficial effects of P2X7R pharmacological blockage where further corroborated by the results of the rotarod and NOR test. P301S;P2X7$^{-/-}$ mice, indeed, spent more time holding on the rotarod apparatus; in contrast P301S;P2X7^{451P}-EGFP mice spent less time on the apparatus compared with P301S mice, **Figure 44 C-D**. Finally, P301S;P2X7$^{-/-}$ mice, compared with P301S mice, exhibited an increase in memory capacity in the NOR test, spending more time exploring the novel object than the P301S mice. Even in this last test P301S;P2X7^{451P}-EGFP mice obtained opposite results, **Figure 44 E-F**.

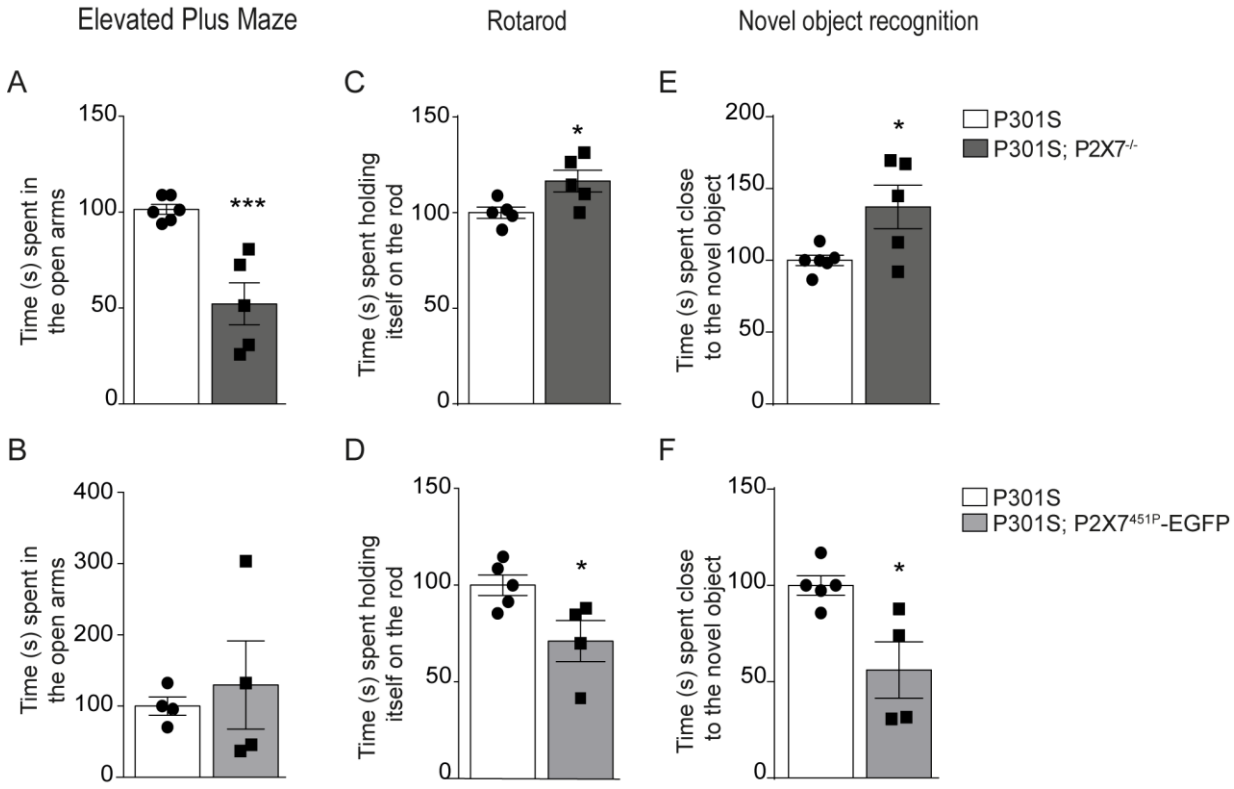

Figure 44. Genetic P2X7R knockdown improves behavioral deficits associated with Tau-toxicity. *6 months-old P301S, P301S;P2X7$^{-/-}$, and P301S;P2X7^{451P}-EGFP mice underwent the elevated plus maze test (EPMT), the rotarod test (RT), the novel object test (NORT). (A-B) EPMT; graph represents the time(s) that mice spent in the open arms. (C-D) RT; graph represents the time(s) spent by the mice holding on the rod before falling dawn. (E-F) NORT; graph represents the time(s) that mice spent exploring the new object. Data represent the mean ± standard error (SEM) (n=4 P301S;P2X7^{451P}-EGFP mice, n=6 P301S;P2X7$^{-/-}$ mice and n≧4 P301S mice). * P≦ 0.05; *** P ≦ 0.001 using unpaired two tailed Student's t-test.*

12. P2X7R GENETIC KNOCKOUT REDUCES INTRACELLULAR TAU PHOSPHORYLATION.

Finally, we further validated the effect of GSK treatment on tau phosphorylation by evaluating the levels of phosphorylated-GSK3β and phosphorylated Ser202/Thr305 sites in P301S;P2X7$^{-/-}$ and P301S^{451P}EGFP mice. The analysis showed that the absence of P2X7R determines a significant rise of phosphorylated-GSK3β (66.4±0.5% higher than P301S mice), as well as a reduction of intracellular Tau phosphorylation levels (60.1±15.2% lower than P301S mice), **Figure 45 A-B**. Contrarily, P2X7R overexpression caused a reduction in phosphorylation of GSK3β enzyme (20,0±2,7% lower than in P301S mice), and a rise in intracellular phosphorylated Tau protein (37,4±7,0% higher than in P301S mice), **Figure 45 A-B**. Accordingly, a significant reduction in the number of AT8 positive stained cells was observed in P301S;P2X7$^{-/-}$ mice, **Figure 45 C-D**. Noteworthy, P301S;P2X7^{451P}EGFP mice didn't present an increase in positive AT8 neurons, **Figure 45 C-D**.

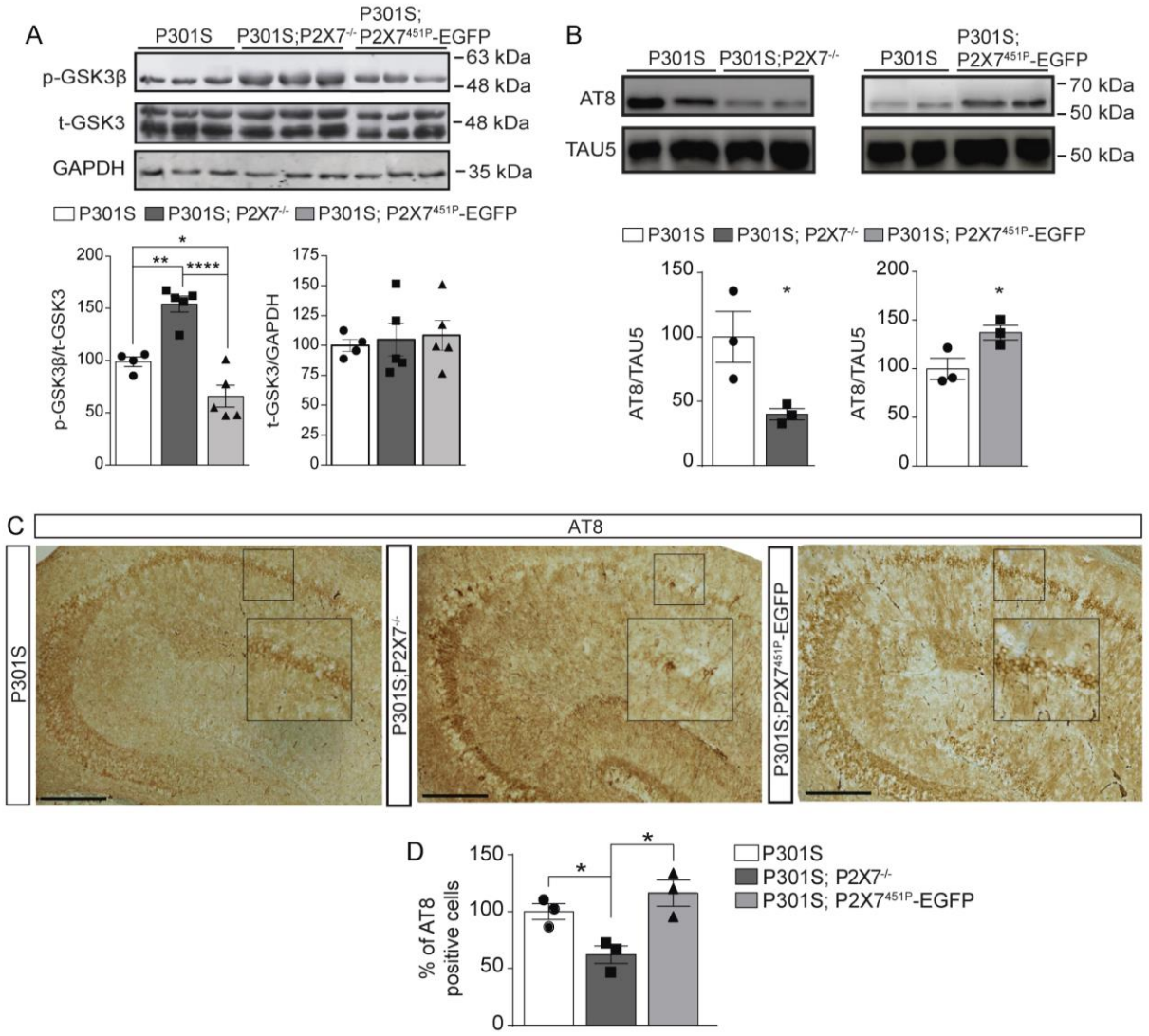

Figure 45. Genetic P2X7R knockdown reduces intracelular Tau-phosphorylation. *(A) Representative immunoblot and quantification of p-GSK3 protein levels in hippocampal homogenates from P301S, P301S;P2X7$^{-/-}$, and P301S;P2X7^{451P}-EGFP mice (n≧5 mice per genotype). Levels of total GSK3 were used as loading control for normalization purposes. The 100% value corresponds to p-GSK3/t-GSK3 levels detected in the hippocampi of P301S mice. Total-GSK3 was quantified using the housekeeping GAPDH for normalization purposes. * P≦0.05 ** P ≦0.01 **** P ≦0.0001 using a One-way ANOVA followed by Tukey post hoc test considering P301S mice as the control group. (B) Representative immunoblot and quantification of phosphorylated Tau protein levels in hippocampal homogenates from P301S, P301S;P2X7$^{-/-}$, and P301S;P2X7^{451P}-EGFP mice (n=3 mice per genotype). Levels of total Tau proteins were used as loading control for normalization. The 100% value corresponds to AT8/TAU5 levels detected in the hippocampi of P301S mice. * P≦0.05 using an unpaired two tailed Student's t-test. (C) Representative images of hippocampal slices from P301S, P301S;P2X7$^{-/-}$, and P301S;P2X7^{451P}EGFP mice stained with antibodies anti phospho-Tau (AT8, n=3 mice per genotype and n≧4 sections per mouse). Scale bar=100 µm. Insert represents a 2x magnification of the indicated area. Scale bar=100 µm. (D) Graph represents the quantification of AT8 positive cells. * P ≦0.05 using a One-way ANOVA followed by Tukey post hoc test considering P301S mice as the control group.*

13. P2X7R KNOCKOUT REVERTS CELLULAR DEATH.

The effect of P2X7R blockade on neuronal survival was later confirmed in P301S;P2X7$^{-/-}$ mice, which presented a significant increase in the number hippocampal neurons (38.42±6.5% more than P301S mice, **Figure 46 A-B**. Unexpectedly, P301S;P2X^{7451P}-EGFP mice didn't show any reduction in the number of neurons compared with P301S mice, **Figure 46 A-B.**

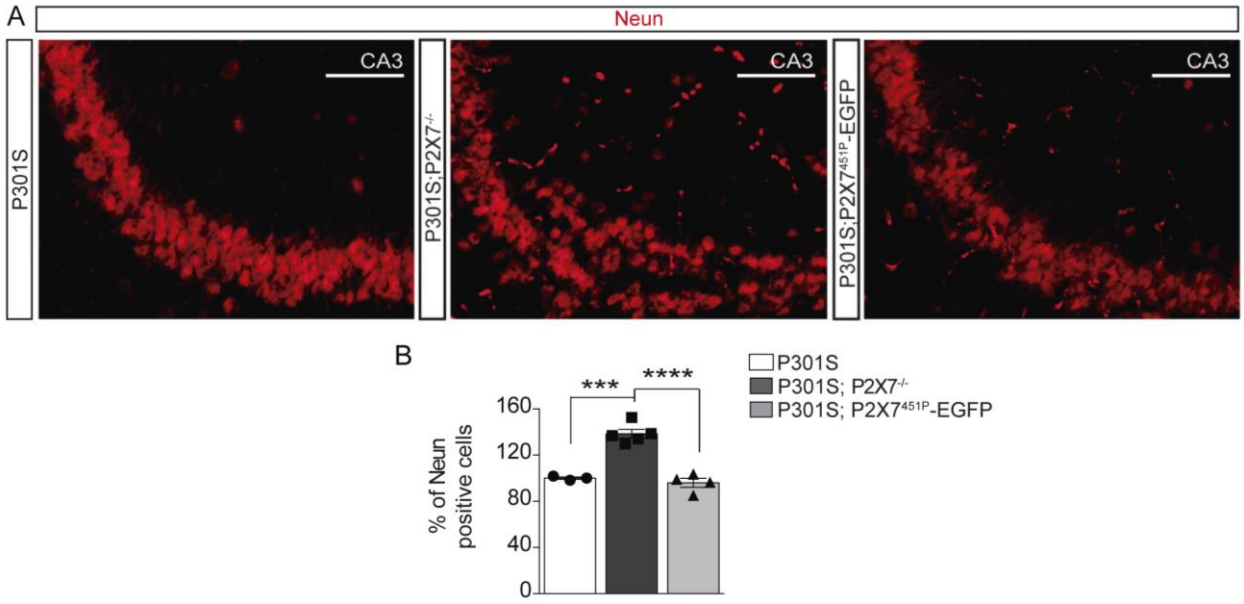

Figure 46. P2X7R knockout increases the number of hippocampal neurons. *(A) Representative images of hippocampal CA3 area slices from P301S, P301S;P2X7$^{-/-}$and P301S;P2X^{7451P}-EGFP mice stained with NeuN (n≧3 mice per genotype and n≧4 sections per mouse). Scale bar: 100 µm. (B) Graph represents the quantification of NeuN positive cells. *** P ≦0.001; **** P ≦0.0001 using a One-way ANOVA followed by Tukey post hoc test considering P301S mice as the control group.*

14. P2X7R GENETIC KNOCKOUT AFFECTS MICROGLIA PROLIFERATION AND MORPHOLOGY.

In a next step, we evaluated the effect that P2X7R depletion or overexpression has on the astrocytes and microglia proliferation.

Analysis of the number of hippocampal astrocytes showed that both the absence and the overexpression of P2X7 receptor do not affect the increase in astroglia proliferation associated with tau toxicity, **Figure 47**.

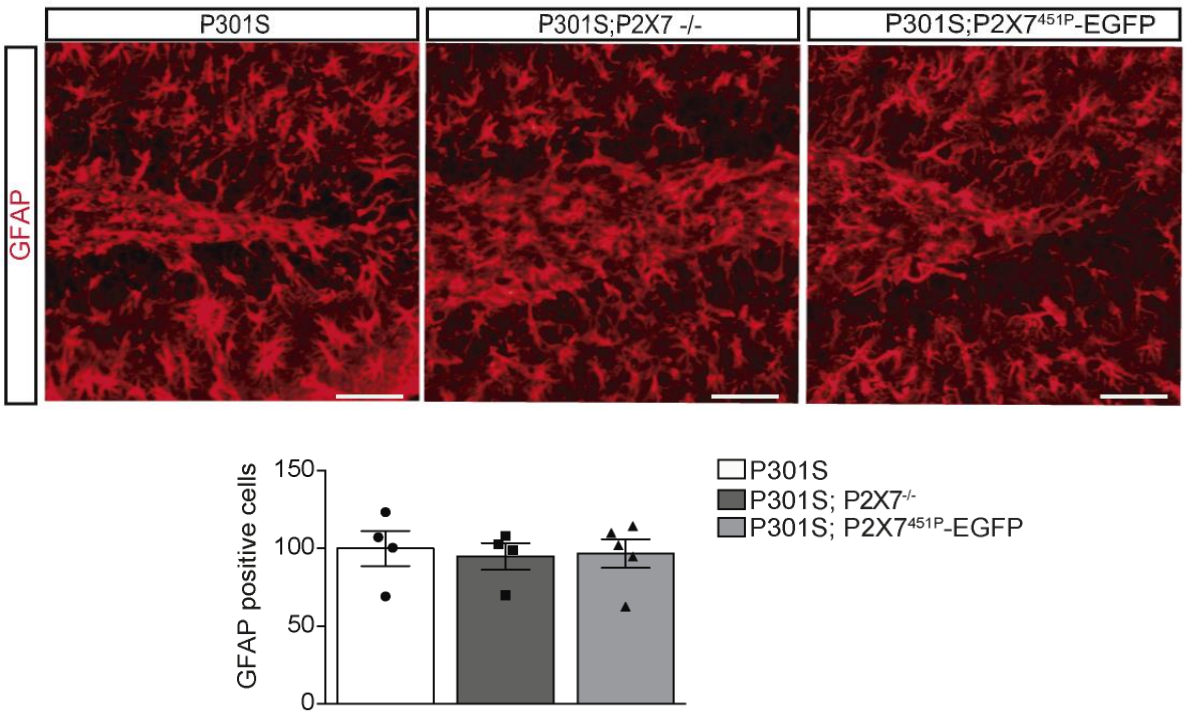

Figure 47. Genetic deletion or overexpression of P2X7R do not modify astrocytes proliferation. *Representative images of hippocampal sections from P301S, P301S;P2X7$^{-/-}$ and P301S;P2X7^{451P}-EGFP mice stained with the astrocytes marker GFAP. Scale bar: 100 µm. The graph represents the quantification of GFAP positive cells in the hippocampus (n≧4 mice per genotype and treatment with n≧4 sections/mouse). One-way ANOVA followed by Tukey post hoc test.*

In line with the results obtained in the pharmacological approach, P301S;P2X7$^{-/-}$ mice presented a lower number of hippocampal microglia cells than their P301S littermates (100±8.25 in P301S mice versus 72.95±4.42 in P301S;P2X7$^{-/-}$ mice), **Figure 48 A-B**. Moreover, P301S;P2X7$^{-/-}$ mice showed microglia cells with a higher number and longer ramifications, consequently covering more brain area, **Figure 49 B-C-D-E**.

Surprisingly, no changes were detected in P301S;P2X7^{451P}-EGFP mice, which showed microglia cells similar for number and morphology to the ones observed in P301S mice, **Figure 48-49**.

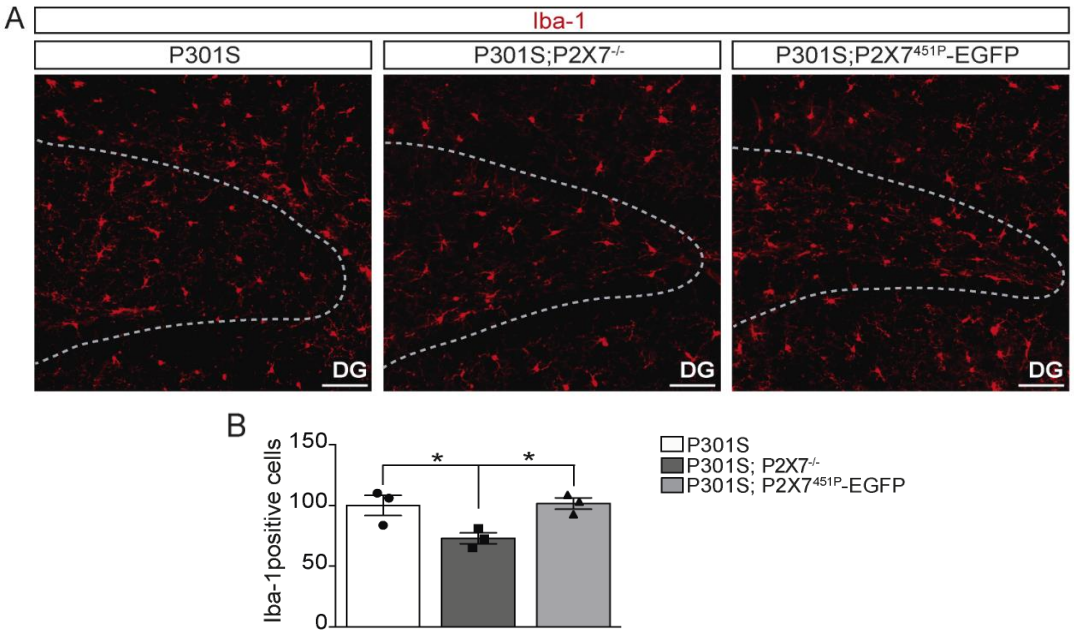

Figure 48. P2X7R genetic knockdown reverts microglia proliferation. *(A) Representative images of hippocampal sections from P301S, P301S;P2X7$^{-/-}$ and P301S;P2X7^{451P}-EGFP mice, stained with the microglial marker Iba-1. Dash lines indicate the granular layer of the dentate gyrus (DG). Scale bar: 100 μm. (B) The graph represents the quantification of Iba1 positive cells in the hippocampus (n≧3 mice per genotype with n≧4 sections/mouse) * P ≦0.05; using a One-way ANOVA followed by Tukey post hoc test.*

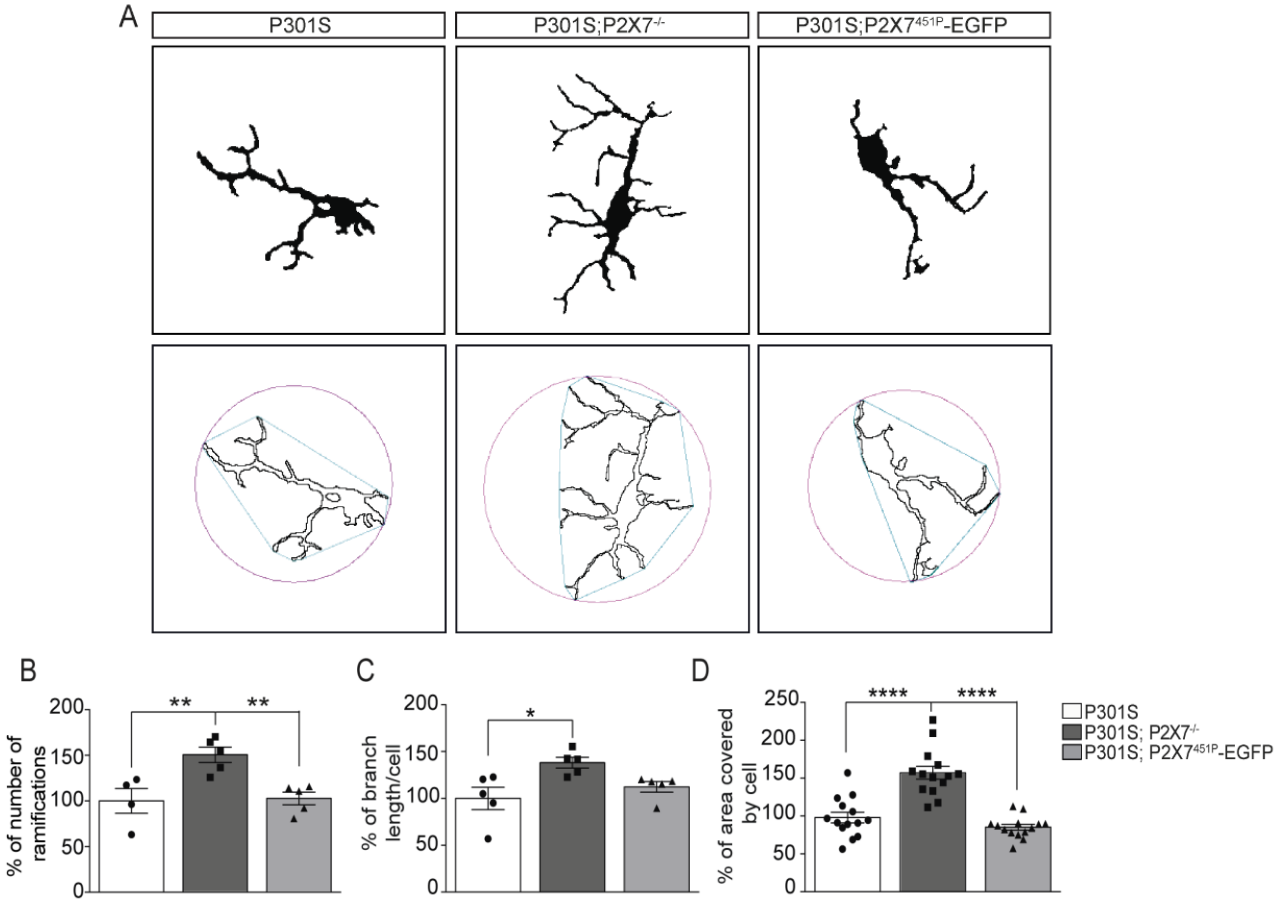

Figure 49. P2X7R genetic knockdown determines microglia morphological changes. *(A) Representative images showing the binary image of microglia cells (upper panels) with their corresponding outline and associated convex hull (blue) and enclosing circle (pink) for corresponding outline shapes (bottom panels). (B, C, D) Graphs show the quantification of cell ramifications (B), of branch lengths (C), and the percentage of brain area covered by microglia cells (D). The 100% value corresponds to the number of ramifications, total branch lengths and brain area covered by microglia cells in P301S mice (n≧4 mice per genotype and treatment and, n ≧4 sections per mouse, being analyzed a minimum of 12 microglia cells per section). * p ≦0.05 ** p ≦0.01 **** p ≦0.0001 using a One-way ANOVA followed by Tukey post hoc test considering P301S mice as the control group.*

We also analysed the levels of IL-1β in our transgenic mice. The analysis showed that the absence of P2X7R determines a reduction of IL-1β levels (46.15±8.54% lower than P301S mice), but again no changes were detected in P301S;P2X7^{451P}-EGFP mice, **Figure 50.**

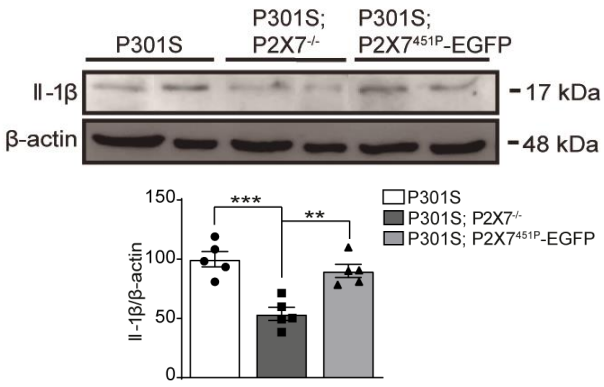

Figure 50. Representative Western blot detection of IL-1β *in hippocampal homogenates from P301S, P301S;P2X7$^{-/-}$, and P301S;P2X7$^{451P\text{-}EGFP}$. Graph shows quantification of IL-1β in hippocampal homogenates from P301S, P301S;P2X7$^{-/-}$, and P301S;P2X7$^{451P\text{-}EGFP}$ mice (n=5 mice per genotype). Data represent the mean ± standard error. ** P ≦0.01; *** P ≦0.001 using a One-way ANOVA followed by Tukey post hoc test.*

15. P2X7R BLOCKADE INCREASES EXTRACELLULAR TAU PHOSPHORYLATION.

Finally, since TNAP enzyme dephosphorylate eTau and P2X7R can modulate its expression, we decided to measure the levels of phosphorylated extracellular Tau in CSF collected from P301S mice treated or not with GSK solution. Our analysis showed that P2X7R inhibition induces an increase in the phosphorylated rate of eTau protein in Ser202/Thr205 sites, **Figure 51 A**. Once observed the increase of phosphorylated eTau in CSF, we further analysed the levels of TNAP enzyme in our mice to confirm that it is involved in this process. The results revealed that P301S mice treated with GSK presented lower protein levels of TNAP enzyme than Veh-P301S mice, **Figure 51 B**.

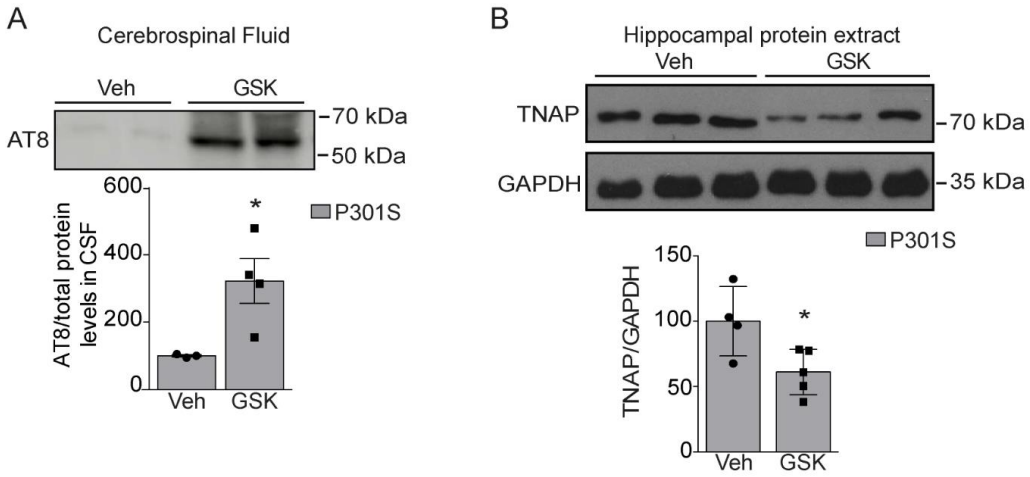

Figure 51. P2X7R pharmacological inhibition increases extracellular Tau phosphorylation. *(A) Representative immunoblot and quantification of phospho-Tau (Ser202/Thr205) protein levels in CSF samples from P301S mice treated with vehicle or GSK (n=3 mice per genotype and treatment). Total protein levels detected by ponceau staining were used as loading control for normalization purposes. The 100% value corresponds to phospho-Tau protein levels detected in CSF from vehicle treated P301S mice. * P ≦ 0.05 using an unpaired two tailed Student's t-test. (B) Western blot detection of TNAP levels in hippocampal protein extract. Graph shows the quantification of TNAP levels detected both in Veh-P301S and GSK-P301S mice. Total GAPDH protein levels were used as a loading control for normalization purposes. The 100% value corresponds to TNAP levels detected in Veh-treated P301S mice. Data represent the mean ± standard error (SEM). * p≦0.05 using an unpaired two tailed Student's t-test.*

The results obtained with the pharmacological approach were later confirmed in P301S;P2X7$^{-/-}$ and P301S^{451P}-EGFP mice. The analysis showed that P301S;P2X7$^{-/-}$ present higher levels of phosphorylated eTau and lower levels of TNAP, **Figure 52 A-B**, whereas P301S^{451P}-EGFP exhibit opposite results, **Figure 52 A-B**.

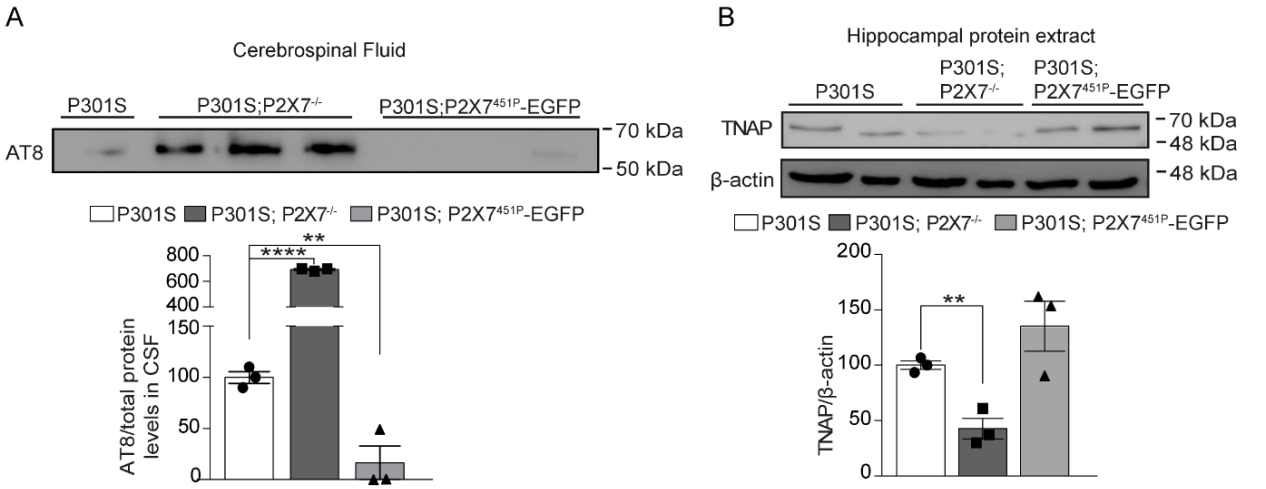

Figure 52. Genetic P2X7R knockdown increases extracellular Tau phosphorylation. *Representative immunoblot and quantification of phospho-Tau (Ser202/Thr205) protein levels in CSF samples from P301S, P301S;P2X7$^{-/-}$, and P301S;P2X7^{451P}-EGFP mice (n=3 mice per genotype). Total protein levels detected by ponceau staining were used as loading control for normalization purposes. The 100% value corresponds to phospho-Tau protein levels detected in CSF from P301S mice. ** P ≦ 0.01; **** P ≦ 0.0001 using a One-way ANOVA followed by Dunnett´s post hoc test considering P301S mice as the control group. (K) Western blot detection of TNAP levels in hippocampal protein extract from P301S, P301S;P2X7$^{-/-}$, and P301S;P2X7^{451P}-EGFP mice (n=3 mice per genotype). Graphs show the quantification of TNAP levels in homogenates of hippocampus from P301S, P301S;P2X7$^{-/-}$, and P301S;P2X7^{451P}-EGFP mice (n=3 mice per genotype). Total β-actin protein levels were used as a loading control for normalization purposes. The 100% value corresponds to the amount of TNAP levels detected in the hippocampi of P301S mice. ** P ≦ 0,01 using a One-way ANOVA followed by Dunnett´s post hoc test considering P301S mice as the control group.*

DISCUSSION

P2X7R upregulation in microglia cells is involved in the chronic microglia activation and proliferation associated with Tauopathies.

It is widely known that accumulation of Aβ in senile plaques initiates the inflammatory process on AD (McGeer *et al.*, 2000) and promotes the activation of the microglial cells around them (Selkoe, 2002). A first evidence suggesting the involvement of P2X7 receptor in AD was provided by P2X7R upregulation in microglial cells surrounding amyloid plaques. This upregulation was observed in both AD patients and different AD mouse models (Parvathenani *et al.*, 2003; McLarnon *et al*., 2006; Ryu and McLarnon, 2008). Therefore, these findings suggested that P2X7 upregulation was somehow linked to Aβ accumulation and the consequent neuroinflammatory response.

Several evidences support the role played by P2X7R in Aβ toxicity associated with AD (Francistiová *et al.*, 2020). However, little is known about its possible role in tau-induced toxicity. A recent work, using a specific radiotracer binding P2X7R, showed that 9-months-old P301S mice present significantly higher levels of this radiotracer in the brain than their corresponding WT control mice (Jin *et al*., 2018). Further analysis revealed that P2X7R was mainly found in hippocampal astrocytes in P301S mice (Jin *et al*., 2018). However, no robust data about the molecular mechanism causing the glial P2X7R upregulation were provided in these studies.

In this project, our aim was to further investigate the role of P2X7R on tau-induced toxicity in AD. Our study confirmed P2X7R upregulation in AD patients, and it also detected a significant increase in the receptor expression levels in both PiD patients and P301S mice. This upregulation was mainly observed in glial lineage: an increase of P2X7R transcription was found in astrocytes and microglia cells. Our data not only confirmed that P2X7 receptor is increased in microglia cells on AD, as previously reported (Parvathenani *et al*., 2003; McLarnon *et al*., 2006; Lee *et al.*, 2011; Martínez-Frailes *et al.*, 2019), but we also demonstrated that this upregulation occurs in astrocytes and in the absence of a significant Aβ accumulation.

Over the recent years, the presence of P2X7 receptor in neurons has been the subject of a long-stating debate (Illes *et al.*, 2017; Miras-Portugal *et al.*, 2017); some groups indeed found P2X7R in neurons (Miras-Portugal *et al.*, 2017), whereas others detected it mainly in glial cells, especially microglia cells, but not in neurons (Illes *et al.*, 2017). In the present work, we used two mouse lines mimicking the tau-induced toxicity (P301S and ^{P2X7}EGFP;P301S mice) and we detected that there is a change in the P2X7 receptor distribution pattern under these pathological conditions. We showed that under physiological conditions, P2X7R is mainly transcribed in neurons at hippocampal level. On the other hand, in a pathological condition, where neuroinflammation causes microglia proliferation and activation, there is a decrease in P2X7R transcription in neurons and an increase in microglia cells. These results are in line with the ones previously obtained in our group

using a mouse line mimicking the Aβ-induced toxicity (Martínez-Frailes *et al.*, 2019), and they suggest that neuroinflammation regulates the expression of P2X7 receptor both in neurons and in glial cells. Former studies support this idea. It has been reported that P2X7R pharmacological blockade or downregulation through small RNA interference attenuated LPS-induced neuroinflammation (Bianco *et al.*, 2006; Lu *et al.*, 2013), by avoiding microglia activation (Lu *et al.*, 2013) and decreasing microglia proliferation (Bianco *et al.*, 2006). Since proinflammatory cytokines released by P2X7R may cause the upregulation of P2X7R itself, this positive feedback loop might promote and maintain, over time, an exacerbating microglial response contributing in this way to the adverse effects associated with neuroinflammation (Mosher and Wyss-Coray, 2014).

During neuroinflammation, ramified microglia can switch from a "resting state" to an "activated state", characterized by shorter and thicker processes. Alternatively, microglia can adopt a "reactive state", with a typical small and spherical shape (Davis *et al.*, 1994). In line with these data, our analysis of microglia morphology revealed that P301S mice present hippocampal microglia with fewer and shorter ramifications than the ones observed in WT mice; this phenotype was not observed when P2X7 receptor was pharmacologically inhibited or genetically knocked out. As pharmacological or genetical blockade of P2X7 receptor in P301S mice re-established the resting state in activated microglia, we postulated that increased expression of P2X7R in microglia cells plays a critical role in the activation of this cell lineage in Tauopathies.

A more recent work showed that blockage of microglia proliferation leads to an attenuation of tau-induced neurodegeneration and results in functional improvement in P301S mice (Mancuso *et al.*, 2019). In line with these studies, the *in vivo* P2X7R blockade not only determined a reduction in microglia activation, but it also induced a decrease in microglia proliferation and improved the associated behavioural deficits observed in P301S mice.

Additionally, it is important to highlight that in P301S mice a prominent microglial activation precedes tangle formation (Yoshiyama *et al.*, 2007). Moreover, recent studies showed that NLRP3 activation may induce tau hyperphosphorylation and aggregation in an IL-1β-dependent manner (Ising *et al.*, 2019).

Therefore, considering all the previous studies and the results obtained in the present work, it is reasonable to think that P2X7R upregulation in microglia is one of the molecular mechanisms causing the chronic microglia activation and proliferation associated with Tauopathies. Nevertheless, P2X7R overexpression in P301S mice neither exacerbated morphological changes associated with microglial activation nor their proliferation. To elucidate these results, we analysed the impact of P2X7 receptor overexpression on microglia cells morphology. Interestingly, microglia cells from P2X7^{451P}-EGFP mice, compared with the ones from WT mice, were in an activated state,

characterized not only by shorter ramifications, but also by smaller cellular size and nuclei area, resulting in smaller brain area covered by microglia. Further corroboration of our assumption was also provided by previous *in vitro* studies, in which it was reported that overexpression of P2X7 receptor is sufficient to drive the activation and proliferation of microglia in absence of pathological insults (Monif *et al.*, 2009).

These data suggest that P2X7R overexpression is sufficient to drive a basal activation of microglia lineage, even in the absence of a pathological insult. This hypothesis could explain why we did not observe a stronger microglial activation in P301S;P2X7^{451P}-EGFP mice.

P2X7R upregulation in microglia cells affects microglia migration and phagocytic capacity.

During neuroinflammation, extracellular ATP induces morphological changes in microglia cells favouring their rapid migration towards local brain injury and acting on their phagocytic capacity (Davalos *et al.*, 2005; Di Virgilio *et al.*, 2009). Initial studies indicated that extracellular purines modulate the microglial migration and phagocytosis through their specific metabotropic receptors P2Y12, P2Y1, or P2Y6 (Inoue, 2008; De Simone *et al.*, 2010; Bernier *et al.*, 2013; Langfelder *et al.*, 2015). However, later works have provided additional data indicating that other purinergic receptors may be involved in this phenomenon. It has been reported that cytoskeleton changes in microglial cells caused by ATP-induced P2X7R activation reduce their phagocytic capacity (Fang *et al.*, 2009). Moreover, *in vitro* studies using mouse primary microglial cells demonstrated that both P2X7R genetic depletion using specific RNA interference and its pharmacological inhibition by BBG favours microglial phagocytosis of fibrillar A$\beta_{1\text{-}42}$ and decreases IL-1β secretion capacity (Ni *et al*., 2013). A recent work from our group, using *in vitro* and *in vivo* approaches, showed that inhibition of P2X7 receptor, significantly increased the phagocytic capacity of microglial cells and confirmed that ATP-induced P2X7R activation promotes microglial migration (Martínez-Frailes *et al.*, 2019).

In line with previous findings, our current results showed that *in vivo* P2X7R blockade leads to a reduction in microglia migration towards the injury site both in WT and P301S mice. In addition, we also demonstrated that P2X7R inhibition determines an increase of microglia phagocytic capacity. Supporting these results, we also observed that both pharmacological and genetic blockade of P2X7R led to a significant reduction in IL-1β secretion.

P2X7R blockade reduces intraneuronal Tau phosphorylation.

During the last years, studies using new pharmacological and biomolecular tools provided evidence supporting the presence of functional P2X7 receptor in neurons (Miras-Portugal *et al.*, 2017). In this

cell lineage, P2X7R has been shown to regulate critical functions, such as axonal growth and branching (Díaz-Hernández *et al*., 2008). Previous *in vitro* studies also demonstrated that inhibition of P2X7R induces a significant decrease in the number of hippocampal amyloid plaques through inhibition of GSK3β activity in cultured hippocampal neurons (Díaz-Hernández *et al*., 2012).

In line with these data, we observed that both pharmacological and genetic blockade of P2X7R determine a reduction in tau phosphorylation as well as an increase in phospho-GSK3β levels. The phosphorylation of GSK3 at Ser 9 and Ser 21 residues, for both α and β isoforms, can be taken as indicative of its inhibition level. Additionally, former studies showed that P2X7R is involved in GSK3 inhibition (Ortega *et al.*, 2009; Díaz-Hernández, 2012; Hernandez *et al*., 2013). Given these previous findings, we assumed that P2X7R plays a role not only in APP processing, but also in the regulation of tau phosphorylation *via* GSK3β signalling.

Although these results suggest an involvement of neuronal P2X7R in the reduction of tau phosphorylation, a contribution of microglia to the beneficial effects described before can not be excluded. It was recently reported that loss of NLRP3 inflammasome function reduced tau hyperphosphorylation and aggregation by regulating tau kinases and phosphates. This work placed NLRP3 activation upstream of tau pathology; indeed, it was showed that activation of NLRP3 induces tau hyperphosphorylation and aggregation, at least partially through tau kinases in an IL-1β-dependent manner (Ising *et al.*, 2019). Moreover, this study provided evidence that tau oligomers and monomers have direct effects on microglia by activating NLRP3; as non-fibrillar tau can actively be released by neurons, it could thereby contribute to chronic microglial activation in tauopathies (Ising *et al.*, 2019). Likewise, another study reported that IL-1β overexpression promotes tau phosphorylation in a GSKβ dependent way (Gosh *et al.*, 2013). In this work it was observed that sustained IL-1β expression determines a decrease in the phospho-Ser 9 epitope of GSK3β, which is indicative of increased GSK3β activity (Gosh *et al.*, 2013). Considering these findings, it is reasonable to think that the decrease in intraneuronal tau phosphorylation associated with the pharmacological or genetic P2X7R blockade might be caused by the reduction in IL-1β secretion from microglia. Supporting this idea, we observed that P2X7R overexpression is sufficient to determine an increase in the intraneuronal phosphorylated tau levels, even in the absence of tau-induced toxicity.

Since the effects observed in our experimental model could not be explained considering the sole contribution of microglial P2X7R, we hypothesize that blockade of P2X7R can affect tau phosphorylation rate through mechanisms that take place in both neurons and microglia cells. According to this idea, P2X7R inhibition could lead to a decrease in intraneuronal tau

phosphorylation in two different ways: in neurons, through inhibition of the GSK3 enzyme, while in microglia cells through a reduction of IL-1β secretion.

P2X7R blockade determines a neuroprotective effect by maintaining high levels of phosphorylated extracellular tau.

During the last years, several studies reported the great potential of P2X7R as a drug target to ameliorate the symptomatology and neuropathology associate with AD. *In vivo* approaches demonstrated that P2X7R blockade leads to a significant reduction of APP-induced toxicity (Chen *et al.*, 2014; Díaz-Hernández *et al.*, 2012; Martin *et al.*, 2019; Ryu and McLarnon, 2008).

Despite the evidence supporting the idea of possible clinical trials with P2X7R antagonists (Calzaferri *et al.*, 2020), the efficiency of this therapeutic approach to treat Tauopathies has not been tested yet. In this work, for the first time, we suggest that the blockade of P2X7R is a potential therapeutic strategy to treat Tauopathies by showing the neuroprotective effect associated with its inhibition.

Interestingly, this neuroprotective effect is linked to an increase in the amount of phosphorylated extracellular tau. A recent work reported that the process of tau phosphorylation and release into the CSF is a dynamic mechanism with these features: 1) it begins decades before symptoms, and subsequently unfolds over a period of nearly two decades; 2) it occurs in a pattern such as that phosphorylation of different tau sites closely follows disease progression; 3) it decreases significantly in a site-dependent manner near the onset of cognitive decline and the rise in aggregated tau (Barthélemy *et al*., 2020). Therefore, in this study Barthélemy *et al.* suggest an inverse correlation between the presence of hyperphosphorylated tau in CSF and the onset of symptoms during the progression of the disease. In early stages of the disease, when clinical symptoms are not yet evident, levels of extracellular phosphorylated tau are higher than those observed in healthy controls. On the opposite, during late stages of the pathology, these levels decrease in concomitance with the onset of cognitive decline (Barthélemy *et al*., 2020). Similarly, a previous work from our group reported that dephosphorylated extracellular tau, but not the hyperphosphorylated one, causes neuronal toxicity (Díaz-Hernández *et al.*, 2010). This study showed that dephosphorylated tau protein behaves as an agonist of muscarinic M1 and M3 receptors, provoking a robust and sustained intracellular calcium increase and finally triggering neuronal death (Díaz-Hernández *et al.*, 2010). Moreover, it was demonstrated that TNAP acts like an essential component in this process; the enzyme recognizes and dephosphorylates the hyperphosphorylated tau protein, enabling its interaction with M1 and M3 receptors (Díaz-Hernández *et al.*, 2010). In addition, another study from our group demonstrated that there is a

relationship between P2X7 receptor and TNAP at the transcriptional level: inhibition of P2X7R reduces TNAP expression while addition of exogenous TNAP enhances P2X7R expression (Díez-Zaera *et al.*, 2011).

In line with data previously described, we found that *in vivo* P2X7R inhibition induces an increase in extracellular phosphorylated tau in CSF, correlating with a decrease in the levels of TNAP enzyme. On the other hand, P2X7R overexpression increases TNAP expression, causing a reduction in the phosphorylated extracellular tau levels. Interestingly, we observed that P2X7R blockade also reduces neuronal death associated with tauopathy.

Considering these results, we propose that one of the molecular mechanisms by which P2X7R blockade determines beneficial effect might be by maintaining high levels of extracellular phosphorylated tau through regulation of TNAP.

However, even in this case we can't exclude a contribution from microglia cells. As described before, we observed that P2X7R blockade causes an increase in microglia phagocytic capacity. Since it was reported that extracellular tau can be internalized by microglia cells (Luo *et al.*, 2015), it is reasonable to think that tau induced P2X7R upregulation in microglia cells might contribute to Tauopathy progression by reducing the phagocytosis of extracellular tau.

In addition, the neuroprotective effect associated to the blockage of P2X7R could be due to the role that the receptor plays in the presynaptic terminals. One of the major hallmarks of AD is the extensive loss of synapses correlating with cognitive impairment. During the last years, evidence suggested a possible correlation between the synaptic dysfunction associated with AD and the dysregulation of P2X7 receptor mediated neurotransmission; this dysregulation may be triggered by the Aβ-induced eATP increase (Francistiová *et al.*, 2020). In line with this idea, a recent work showed that P2X7R deficiency rescued the synaptic alteration and the long-term potentiation deficits detected in APP/PS1 mice (Martin *et al.*, 2019). Moreover, our group also demonstrated that neuronal P2X7R transcription is reduced in J20 mice (a transgenic mouse line for human APP) both in early and advanced stages (Martínez-Frailes *et al.*, 2019). This phenomenon could be an adaptive physiological response to avoid or at least reduce the neuronal loss associated with AD (Martínez-Frailes *et al.*, 2019).

Considering the data we obtained, we hypothesize that P2X7R inhibition could determine beneficial effects on tau induced toxicity through three different mechanisms: 1) it reverts microglia activation leading to a reduction in the secretion of IL-1β, finally causing a reduction of tau phosphorylation in a GSK3β dependent way; 2) it reduces intraneuronal tau phosphorylation via GSK3β by direct inhibition of neuronal P2X7R; 3) it reduces the eTau induced-neurotoxicity by avoiding its extracellular dephosphorylation by TNAP, **Figure 53**.

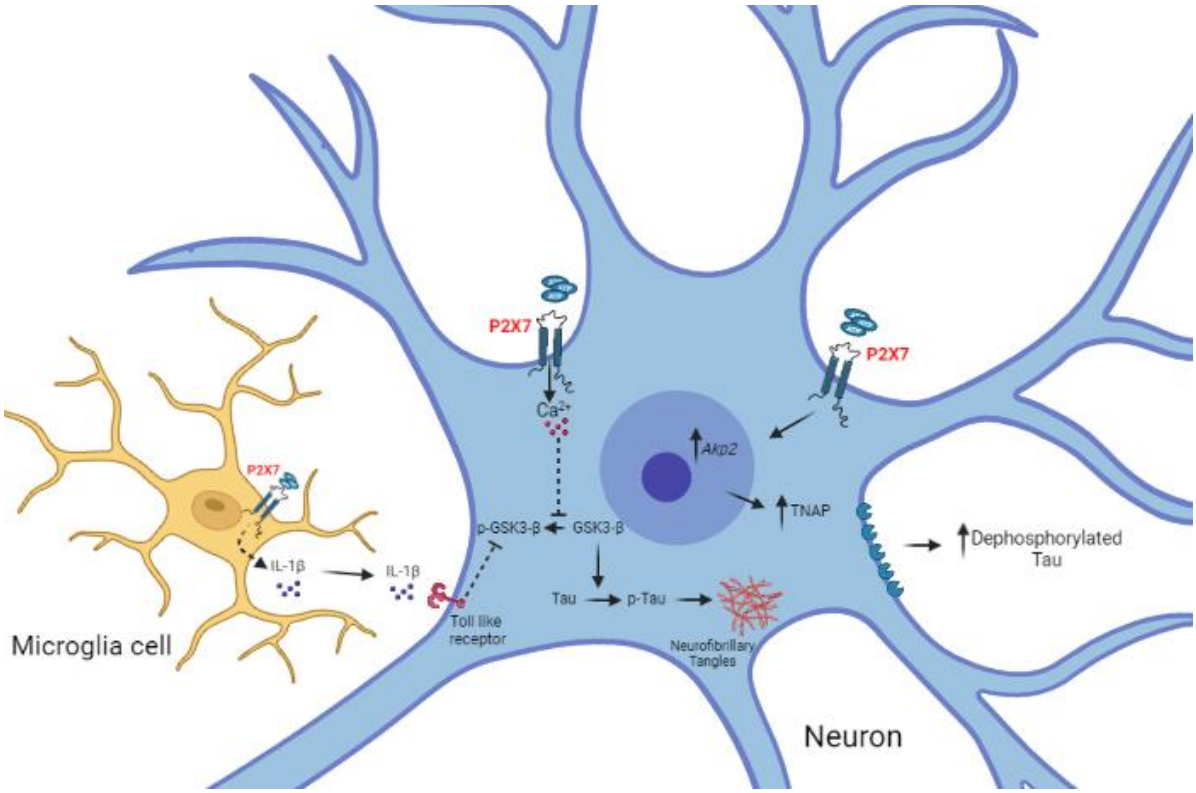

Figure 53. Possible mechanisms underlying the role played by P2X7 receptor in Tau-induced toxicity.

P2X7R blockade improves the cognitive impairment associated with tau-toxicity.

As a consequence of the beneficial effects of P2X7R inhibition described above, we also observed that the blockade of P2X7 receptor leads to a general improvement in the cognitive impairment associated with tau. We found that pharmacological blockage was able to improve not only the memory deficit in our symptomatic mice, but also their anxiety-like behaviour and their motor coordination. Our results indicate that P2X7 receptor plays a deleterious role in tauopathies and suggest that its blockade may be a promising approach to treat Tauopathies.

On the basis of the relevant role that extracellular tau protein has in the spreading of the pathology associated to Tauopathies, during the last years a new set of therapeutic approaches have been evaluated. These clinical trials focused on different strategies: 1) reducing the intracellular

phosphorylated Tau rate (Dominguez *et al.*, 2012), 2) avoiding Tau aggregation (Wisniewski and Goni, 2015), or 3) promoting tau removal through administration of anti-tau antibodies (Yanamandra *et al*., 2013). Although antibodies that recognize and remove extracellular tau have been successfully used in mouse models (Yanamandra *et al*., 2013), active immunotherapy may have harmful effects (Rozenstein-Tsalkovich *et al.*, 2013). It was indeed reported that repeated immunization with anti-tau antibodies in a proinflammatory environment may cause encephalitis (Rozenstein-Tsalkovich *et al.*, 2013). Passive immunotherapy approach also has been considered but failed to increase the life expectancy in Tauopathy mouse models (d'Abramo *et al.*, 2013; Wisniewski and Goni, 2015).

Furthermore, it's under debate which could be the most affective therapeutic approach between active and passive immunization. In line with the above-mentioned information, we believe that our data provide new evidences supporting the role of P2X7R inhibition as a promising therapeutic strategy to treat tauopathies.

Very recently, on the 7th of June 2021, the U.S. Food and Drug Administration (FDA) approved a new Alzheimer's treatment, based on passive immunization strategy, after nearly two decades without any new medication for this disease (https://www.fda.gov/news-events/press-announcements/fda-grants-accelerated-approval-alzheimers-drug). The drug, aducanumab, which will go by the brand name Aduhelm, is a fully human immunoglobulin G 1 (IgG1) antibody that binds a specific conformational epitope of Aβ. The antibody was developed by Biogen and Eisai and it was demonstrated to actively engage and clear amyloid plaques both in transgenic APP models and in human participants in early stage of the disease or with mild dementia (Sevigny *et al*., 2016). Further, after one year of monthly infusions, participants receiving aducanumab had slower decline in the Clinical Dementia Rating Scale (CDR) and in Mini-Mental State Examination (MMSE) in a phase 1 trial (Sevigny *et al*., 2016). However, two phase 3 trials in mild AD were stopped early for futility in March 2019 after interim analysis suggested no change in cognitive decline (Selkoe, 2019). Later, in October 2019, Biogen announced that the interim futility analysis was wrong, and subsequent analysis of a larger data set instead showed that one of the trials had met its primary endpoint, a significant reduction in decline. On July 2020 Biogen submitted a biologics license application to the FAD, but the approval only arrived in June 2021, after a first denial in November 2020. Reactions among Alzheimer's researchers are split between enthusiasm and scepticism. The main reason behind the scepticism of different researchers is that the treatment, for now, only has a demonstrated effect on a surrogate endpoint, in this case amyloid plaque reduction, that is expected to lead to a subsequent clinical benefit. This pathway requires post-approval trials to demonstrate such a benefit and FDA approval could be later revoked if the

treatment does not pan out. A lot of researchers are questioning whether a putative functional benefit of a treatment exceeds its risk of brain oedema and microhaemorrhages, the most severe side effects associated with this drug (Sevigny *et al*., 2016). The diverse opinions and the FDA's accelerated approval program reflect the great need to find an efficient treatment for the cause of the disease, and not a treatment that only targets its symptoms.

In this work we show that the blockade of P2X7R could be considered a promising treatment for AD, and in general for Tauopathies, since it reduces neuroinflammation, improves neuronal survival and ameliorates the behavioural deficits associated with tau-toxicity. Furthermore, since we used symptomatic mice, our results indicate that this strategy could be effective to revert the pathophysiological hallmarks and behavioural alterations associated with Tauopathies even in symptomatic patients in the advanced stages of the disease.

CONCLUSIONS

Based on the results of this PhD dissertation, the following conclusions can be drawn:

- P2X7 receptor plays a critical role in tau-induced toxicity by regulating microglia activation and functionality.

- P2X7R also regulates tau phosphorylation rate in intra- and extracellular compartments through modulation of GSK3 signalling pathway and TNAP expression, respectively.

- P2X7R blockade improves the cognitive impairment associated with tau-toxicity.

- Our results indicate that P2X7R blockade might be considered a promising treatment for Tauopathies, since it reduces neuroinflammation, improves neuronal survival, and ameliorates behavioural deficits associated with these diseases.

BIBLIOGRAPHY

Abberley L., Bebius A., Beswick P.J., Billinton A., Collis K.L., Dean D.K., Fonfria E., Gleave R.J., Medhurst S.J., Michel A.D., Moses A.P., Patel S., Roman S.A., Scoccitti T., Smith B., Steadman J.G., Walter D.S. 2010. Identification of 2-oxo-N-(phenylmethyl)-4-imidazolidinecarboxamide antagonists of the P2X(7) receptor. *Bioorg Med Chem Lett.* 20(22):6370-4. PMID: 20934331.

Abbracchio M.P., Burnstock G. 1994. Purinoceptors: are there families of P_{2X} and P_{2Y} purinoceptors? *Pharmacol Ther* 64:445–475. PMID: 7724657.

Abbracchio M.P., Boeynaems J.M., Barnard E.A., Boyer J.L., Kennedy C., Miras-Portugal M.T., King B.F., Gachet C., Jacobson K.A., Weisman G.A., Burnstock G., 2003. Characterization of the UDP-glucose receptor (re-named here the P2Y14 receptor) adds diversity to the P2Y receptor family. *Trends Pharmacol Sci* 24, 52–5. PMID: 12559763.

Ahmed Z.; Cooper J.; Murray T.K.; Garn K.; McNaughton E.; Clarke H.; Parhizkar S.; Ward M.A.; Cavallini A.; Jackson S.; et al. 2014. A novel in vivo model of tau propagation with rapid and progressive neurofibrillary tangle pathology: The pattern of spread is determined by connectivity, not proximity. *Acta Neuropathol.*, 127, 667–683 PMID: 24531916.

Aisen P. S., Davis K. L., Berg J. D., Schafer K., Campbell K., Thomas R. G., et al. 2000. A randomized controlled trial of prednisone in Alzheimer's disease. Alzheimer's disease cooperative study. *Neurology* 54, 588–593. PMID: 10680787.

Akira S., Takeda K. 2004. Toll-like receptor signalling. *Nat Rev Immunol*. (7):499-511. PMID: 15229469.

Ali Z., Laurijssens B., Ostenfeld T., McHugh S., Stylianou A., Scott-Stevens P., Hosking L., Dewit O., Richardson J.C., Chen C. 2013. Pharmacokinetic and pharmacodynamic profiling of a P2X7 receptor allosteric modulator GSK1482160 in healthy human subjects. *Br J Clin Pharmacol*. 75(1):197-207. PMID: 22568863.

Allgaier C., Reinhardt R., Scha¨dlich H., Rubini P., Bauer S., Reichenbach A., Illes P. 2004. Somatic and axonal effects of ATP via P2X2 but not P2X7 receptors in rat thoracolumbar sympathetic neurones. *J Neurochem* 90:359–367. PMID: 15228593.

Alloisio S., Cervetto C., Passalacqua M., Barbieri R., Maura G., Nobile M., Marcoli M. 2008. Functional evidence for presynaptic P2X7 receptors in adult rat cerebrocortical nerve terminals. *FEBS Lett* 582:3948 –3953. PMID: 18977353.

Alquezar C., Arya S., Kao A.W. 2021. Tau Post-translational Modifications: Dynamic Transformers of Tau Function, Degradation, and Aggregation. *Front Neurol*. 7;11:595532. PMID: 33488497.

Alzheimer A., Stelzmann R.A., Schnitzlein H.N., Murtagh F.R. 1995. An English translation of Alzheimer's 1907 paper, "Uber eine eigenartige Erkankung der Hirnrinde". *Clin Anat.* 8(6):429-31. PMID: 8713166.

Alzheimer's-Association. 2020. Alzheimer's disease facts and figures. *Alzheimers Dement*. 15, 321–387. PMID: 32157811.

Amadio S., Parisi C., Montilli C., Carrubba A.S., Apolloni S., Volonté C. 2014. P2Y12 Receptor on the Verge of a Neuroinflammatory Breakdown [WWW Document]. *Mediators Inflamm.* 2014:975849. PMID: 25180027

Amadio S., Parisi C., Piras E., Fabbrizio P., Apolloni S.,Montilli C., et al. 2017. Modulation of P2X7 receptor during inflammation in multiple sclerosis. *Front. Immunol.* 8:1529. PMID: 29187851.

Andorfer C., Acker C.M., Kress Y., Hof P.R., Duff K., Davies P. 2005. Cell-cycle reentry and cell death in transgenic mice expressing nonmutant human tau isoforms. *J. Neurosci.* 25, 5446–5454. PMID: 15930395.

Andreadis A. 2006. Misregulation of tau alternative splicing in neurodegeneration and dementia. *Prog. Mol. Subcell. Biol.* 44, 89–107. PMID: 17076266.

Apolloni S., Amadio S., Parisi C., Matteucci A., Potenza R. L., Armida M., et al. 2014. Spinal cord pathology is ameliorated by P2X7 antagonism in a SOD1-mutant mouse model of amyotrophic lateral sclerosis. *Dis.Model.Mech*. 7, 1101–1109. PMID: 25038061.

Armstrong J.N., Brust T.B., Lewis R.G., MacVicar B.A. 2002. Activation of presynaptic P2X7-like receptors depresses mossy fiber-CA3 synaptic transmission through p38 mitogen-activated protein kinase. *J Neurosci* 22: 5938–5945. PMID: 12122056.

Atkinson L., Batten T.F., Moores T.S., Varoqui H., Erickson J.D., Deuchars J. 2004. Differential co-localisation of the P2X7 receptor subunit with vesicular glutamate transporters VGLUT1 and VGLUT2 in rat CNS. *Neuroscience* 123:761–768. PMID: 14706788.

Avila J., Jiménez J.S., Sayas C.L., et al. 2016. Tau Structures. *Front Aging Neurosci*. 8:262. PMID: 27877124.

Avila J. 2006. Tau protein, the main component of paired helical filaments. *J. Alzheimers. Dis.* 171–175. PMID: 16914856.

Barden J.A., Bennett M.R. 2000. Distribution of P2X purinoceptor clusters on individual rat dorsal root ganglion cells. *Neurosci Lett* 287(3):183–186. PMID: 10863025.

Barden N., Harvey M., Gagné B., Shink E., Tremblay M., Raymond C., et al. 2006. Analysis of single nucleotide polymorphisms in genes in the chromosome 12Q24.31 region points to P2RX7 as a susceptibility gene to bipolar affective disorder. *Am. J. Med. Genet. Part B Neuropsychiatr. Genet*. 141, 374–382. PMID: 16673375.

Barthélemy N.R., Li Y., Joseph-Mathurin N., Gordon B.A., Hassenstab J., Benzinger T.L.S., Buckles V., Fagan A.M., *et al.* 2020. Dominantly Inherited Alzheimer Network. A soluble phosphorylated tau signature links tau, amyloid and the evolution of stages of dominantly inherited Alzheimer's disease. *Nat Med.* 26(3):398-407. PMID: 32161412.

Bartlett R., Stokes L., Sluyter R. 2014. The P2X7 receptor channel: recent developments and the use of P2X7 antagonists in models of disease. *Pharmacol Rev.* 66(3):638-75. PMID: 24928329.

Bartlett R., Yerbury J.J., Sluyter R. 2013. P2X7 receptor activation induces reactive oxygen species formation and cell death in murine EOC13 microglia. *Mediators Inflamm.* 2013:271813. PMID: 23431238.

Bartlett R., Sluyter V., Watson D., Sluyter R., Yerbury J.J. 2017. P2X7 antagonism using Brilliant Blue G reduces body weight loss and prolongs survival in female SOD1(G93A) amyotrophic lateral sclerosis mice. *PeerJ* 5:e3064. PMID: 28265522.

Bartlett R., Yerbury J. J. & Sluyter R. 2013. P2X7 receptor activation induces reactive oxygen species formation and cell death in murine EOC13 microglia. *Mediators Inflamm*. 271813. PMID: 23431238.

Beamer E., Gölöncsér F., Horváth G., Bekő K., Otrokocsi L., Koványi B., Sperlágh B. 2016. Purinergic mechanisms in neuroinflammation: An update from molecules to behavior. *Neuropharmacology, Special Issue: Purines in Neurodegeneration and Neuroregeneration* 104, 94–104. PMID: 26384652.

Bernier L. P., Ase A. R., Boué-Grabot É., and Séguéla P. 2013. Inhibition of P2X4 function by P2Y6 UDP receptors in microglia. *Glia* 61, 2038–2049. PMID: 24123515.

Beurel E., Grieco S.F., Jope R.S. 2015. Glycogen synthase kinase-3 (GSK3): regulation, actions, and diseases. *Pharmacol Ther*. 148:114-31. PMID: 25435019.

Bhat R. V., Shanley J., Correll M. P., Fieles W. E., Keith R. A., Scott C. W. and Lee C. M. 2000. Regulation and localization of tyrosine216 phosphorylation of glycogen synthase kinase-3beta in cellular and animal models of neuronal degeneration. Proc. *Natl. Acad. Sci USA* 97, 11074–11079. PMID: 10995469.

Bianco F., Ceruti S., Colombo A., Fumagalli M., Ferrari D., Pizzirani C., et al. 2006. A role for P2X7 in microglial proliferation. *J. Neurochem*. 99, 745–758. PMID: 16836656.

Bidula, S., Dhuna, K., Helliwell, R. et al. 2019. Positive allosteric modulation of P2X7 promotes apoptotic cell death over lytic cell death responses in macrophages. *Cell Death Dis* 10, 882 PMID: 31767863.

Bijur G. N. and Jope R. S. 2001. Proapoptotic stimuli induce nuclear accumulation of glycogen synthase kinase-3 beta. *J. Biol. Chem*. 276, 37436–37442. PMID: 11495916.

Bo X., Kim M., Nori S.L., Schoepfer R., Burnstock G., North R.A. 2003. Tissue distribution of P2X4 receptors studied with an ectodomain antibody. *Cell Tissue Res* 313(2):159–165 PMID: 12845522.

Boche D., Perry V. H., and Nicoll J. A. R. 2013. Activation patterns of microglia and their identification in the human brain. *Neuropathol. Appl. Neurobiol.* 39, 3–18. PMID: 23252647.

Bodin P., Burnstock G. 2001. Purinergic signalling: ATP release. *Neurochemical research* 26: 959-69 PMID: 11699948.

Braak H., Alafuzoff I., Arzberger T., Kretzschmar H., and Del Tredici K. 2006. Staging of Alzheimer disease-associated neurofibrillary pathology using paraffin sections and immunocytochemistry. *Acta Neuropathol.* 112, 389–404. PMID: 16906426

Braak H., and Braak E. 1991. Neuropathological stageing of Alzheimer-related changes. *Acta Neuropathol.* 82, 239–259. PMID: 1759558.

Braak H., Thal D.R., Ghebremedhin E., and Del Tredici K. 2011. Stages of the pathologic process in Alzheimer disease: age categories from 1 to 100 years. *J. Neuropathol. Exp. Neurol.* 70, 960–969. PMID: 22002422.

Bradbury E.J., Burnstock G., McMahon S.B. 1998. The expression of P2X3 purinoreceptors in sensory neurons: effects of axotomy and glial-derived neurotrophic factor. *Mol Cell Neurosci* 12(4-5):256-68 PMID: 9828090.

Braithwaite S.P., Stock J.B., Lombroso P.J., Nairn A.C. 2012. Protein phosphatases and Alzheimer's disease. *Prog Mol Biol Transl Sci.* 106:343-79. PMID: 22340724

Brake A.J., Wagenbach M.J., Julius D. 1994. New structural motif for ligand-gated ion channels defined by an ionotropic ATP receptor. *Nature.* 371:519–523. PMID: 7523952.

Bramblett G.T., Goedert M., Jakes R., Merrick S.E., Trojanowski J.Q., Lee V.M. 1993. Abnormal tau phosphorylation at Ser396 in Alzheimer's disease recapitulates development and contributes to reduced microtubule binding. *Neuron* 1089–1099. PMID: 8318230.

Broom D.C., Matson D.J., Bradshaw E., Buck M.E., Meade R., Coombs S., Matchett M., Ford K.K., Yu W., Yuan J., Sun S.H., Ochoa R., Krause J.E., Wustrow D.J., Cortright D.N. 2008. Characterization of N-(adamantan-1-ylmethyl)-5-[(3R-amino-pyrrolidin-1-yl)methyl]-2-chloro-benzamide, a P2X7 antagonist in animal models of pain and inflammation. *J Pharmacol Exp Ther.* 327(3):620-33. PMID: 18772321.

Browne L. E. 2012. Structure of P2X receptors. *WIREs Membr Transp Signal* 1:56–69. PMID: 27377721

Buée L., Bussière T., Buée-Scherrer V., Delacourte A., Hof P.R. 2000. Tau protein isoforms, phosphorylation and role in neurodegenerative disorders. *Brain Res Brain Res Rev.* 33(1):95-130. PMID: 10967355.

Buell G.N., Talabot F., Gos A., Lorenz J., Lai E., Morris M.A., Antonarakis S.E. 1998. Gene structure and chromosomal localization of the human P2X7 receptor. *Recept Channels.* 5(6):347-54. PMID: 9826911.

Burnstock G. 1972. Purinergic nerves. *Pharmacol Rev* 24:509–581. PMID: 4404211.

Burnstock G. 2009. Purinergic regulation of vascular tone and remodelling. *Auton Autacoid Pharmacol* 29(3):63–72. PMID: 19566746.

Burnstock G. 2014. Purinergic signalling in endocrine organs. *Purinergic Signal* 10(1):189–231. PMID: 24265070.

Burnstock G., Arnett T.R., Orriss I.R. 2013. Purinergic signalling in the musculoskeletal system. *Purinergic Signal* 9(4):541–72. PMID: 23943493

Burnstock G., Boeynaems J. 2014. Purinergic signalling and immune cells. *Purinergic Signal* 10(4):529–564. PMID: 25352330

Burnstock G., Kennedy C. 1985. Is there a basis for distinguishing two types of P2-purinoceptor? *Gen Pharmacol*.;16(5):433-40. PMID: 2996968.

Burnstock G., Knight G.E. 2004. Cellular distribution and functions of P2 receptor subtypes in different systems. *Int Rev Cytol* 240: 31–304. PMID: 15548415.

Burnstock G. 2007b. Purine and pyrimidine receptors. *Cellular and molecular life sciences: CMLS* 64: 1471-83. PMID: 17375261.

Burnstock G. 1978. A basis for distinguishing two types of purinergic receptor. *In: Straub RW, editor. Cell membrane receptors for drugs and hormones: a multidisciplinary approach. New York: Raven Press; pp.* 107–118.

Burnstock G. 2012. Discovery of purinergic signalling, the initial resistance and current explosion of interest. *Br J Pharmacol*. 167(2):238-55. PMID: 22537142

Burnstock G. 1976. Do some nerve cells release more than one transmitter? *Neuroscience.* 1:239–248. PMID: 11370511.

Burnstock G. 2006. Pathophysiology and therapeutic potential of purinergic signaling. *Pharmacol Rev*. 58(1):58-86. PMID: 16507883.

Burnstock G. 2007. Physiology and pathophysiology of purinergic neurotransmission. *Physiol Rev.* 87(2):659-797. PMID: 17429044.

Burnstock G. 2016. Purinergic Mechanisms and Pain. *Adv Pharmacol*. 75:91-137. PMID: 26920010.

Burnstock G. 2008. Purinergic signalling and disorders of the central nervous system. *Nat Rev Drug Discov*. 7(7):575-90. PMID: 18591979.

Burnstock G. 2017. Purinergic Signalling: Therapeutic Developments. *Front Pharmacol*. 25;8:661. PMID: 28993732

Burnstock G. 1997. The past, present and future of purine nucleotides as signalling molecules. *Neuropharmacology.* 36(9):1127-39. PMID: 9364468.

Butt A.M. 2011. ATP: a ubiquitous gliotransmitter integrating neuron-glial networks. *Semin Cell Dev Biol.* 22(2):205-13. PMID: 21376829.

Caceres A. 1990. Kosik, K.S. Inhibition of neurite polarity by tau antisense oligonucleotides in primary cerebellar neurons. *Nature* 343, 461–463. PMID: 2105469.

Cai Z., Zhao Y., Zhao B. 2012. Roles of glycogen synthase kinase 3 in Alzheimer's disease. Curr Alzheimer Res. 9(7):864-79. PMID: 22272620.

Calzaferri F., Ruiz-Ruiz C., de Diego A.M.G., de Pascual R., Méndez-López I., Cano-Abad M.F., Maneu V., de los Ríos C., Gandía L. & García A.G. 2020. The purinergic P2X7 receptor as a potential drug target to combat neuroinflammation in neurodegenerative diseases. *Med Res Rev*. 40 (6):2427-2465. PMID: 32677086.

Carmo M. R., Menezes A. P., Nunes A. C., Pliassova A., Rolo A. P., Palmeira C. M., et al. 2014. The P2X7 receptor antagonist Brilliant Blue G attenuates contralateral rotations in a rat model of Parkinsonism through a combined control of synaptotoxicity, neurotoxicity and gliosis. *Neuropharmacology* 81, 142–152. PMID: 24508709.

Carter R.L., Fricks I.P., Barrett M.O., Burianek L.E., Zhou Y., Ko H., Das A., Jacobson K.A., Lazarowski E.R., Harden T.K. 2009. Quantification of Gi-mediated inhibition of adenylyl cyclase activity reveals that UDP is a potent agonist of the human P2Y14 receptor. *Mol. Pharmacol*. 76, 1341–1348. PMID: 19759354.

Cavaliere F., Amadio S., Dinkel K., Reymann K.G., Volonte C. 2007. P2 receptor antagonist trinitrophenyl-adenosine-triphosphate protects hippocampus from oxygen and glucose deprivation cell death. *J Pharmacol Exp Ther* 323(1):70–77. PMID: 17620457.

Cervetto C., Mazzotta M.C., Frattaroli D., Alloisio S, Nobile M., Maura G., Marcoli M. 2012. Calmidazolium selectively inhibits exocytotic glutamate release evoked by P2X7 receptor activation. *Neurochem Int* 60:768 –772. PMID: 22417724.

Chai X., Dage J.L., Citron M. 2012. Constitutive secretion of tau protein by an unconventional mechanism. *Neurobiol Dis.* 48(3):356-66. PMID: 22668776.

Chan C.M., Unwin R.J., Bardini M., Oglesby I.B., Ford A.P., Townsend-Nicholson A., Burnstock G. 1998. Localization of P2X1 purinoceptors by autoradiography and immunohistochemistry in rat kidneys. *Am J Physiol* 274(4 Pt 2):F799–804. PMID: 9575906.

Chataigneau T., Lemoine D., Grutter T. 2013. Exploring the ATP-binding site of P2X receptors. *Front Cell Neurosci.* 30;7:273. PMID: 24415999.

Cheewatrakoolpong B., Gilchrest H., Anthes J.C., Greenfeder S. 2005. Identification and characterization of splice variants of the human P2X7 ATP channel. *Biochem. Biophys. Res. Commun*. 332, 17–27. PMID: 15896293.

Chen X., Hu J., Jiang L., Xu S., Zheng B., Wang C., Zhang J., Wei X., Chang L., Wang Q. 2014. Brilliant Blue G improves cognition in an animal model of Alzheimer's disease and inhibits amyloid-beta-induced loss of filopodia and dendrite spines in hippocampal neurons. *Neuroscience* 279, 94–101. PMID: 25193238.

Cheung K.K., Chan W.Y., Burnstock G. 2005. Expression of P2X purinoceptors during rat brain development and their inhibitory role on motor axon outgrowth in neural tube explant cultures. *Neuroscience* 133:937–945. PMID: 15964486.

Chiozzi P., Sarti A. C., Sanz J. M., Giuliani A. L., Adinolfi E., Vultaggio-Poma V., et al. 2019. Amyloid beta-dependent mitochondrial toxicity in mouse microglia requires P2X7 receptor expression and is prevented by nimodipine. *Sci. Rep*. 9:6475. PMID: 31019207.

Clavaguera F., Bolmont T., Crowther R.A., Abramowski D., Frank S., Probst A., Fraser G., Stalder A.K., Beibel M., Staufenbiel M., et al. 2009. Transmission and spreading of tauopathy in transgenic mouse brain. *Nat. Cell Biol.* 11, 909–913. PMID: 19503072.

Cockayne D.A., Dunn P.M., Zhong Y., Rong W., Hamilton S.G., Knight G.E., Ruan H-Z., Ma B., Yip P., Nunn P., McMahon S.B., Burnstock G., Ford A.P.D.W. 2005. P2X2 knockout mice and P2X2/P2X3 double knockout mice reveal a role for the P2X2 receptor subunit in mediating multiple sensory effects of ATP. *J Physiol* 567(2):621–639 66. PMID: 15961431.

Coddou C., Yan Z., Obsil T., Huidobro-Toro J.P., Stojilkovic S.S. 2011. Activation and Regulation of Purinergic P2X Receptor Channels. *Pharmacol. Rev*. PMID: 21737531.

Coleman P.D., Yao P.J. 2003. Synaptic slaughter in Alzheimer's disease. *Neurobiol. Aging* 1023–1027. PMID: 14643374.

Collo G., Neidhart S., Kawashima E., Kosco-Vilbois M., North R.A., Buell G. 1997. Tissue distribution of the P2X7 receptor. *Neuropharmacology* 36:1277–1283. PMID: 9364482

Cox J.A., Barmina O., Voigt M.M. 2001. Gene structure, chromosomal localization, cDNA cloning and expression of the mouse ATP-gated ionotropic receptor P2X5 subunit. *Gene* 270(1– 2):145–152. PMID: 11404011.

Cuadra A.E., Custer E.E., Bosworth E.L., Lemos J.R. 2014. P2X7 receptors in neurohypophysial terminals: evidence for their role in arginine-vasopressin secretion. *J Cell Physiol* 229:333–342. PMID: 24037803

Czeh M., Gressens P., and Kaindl A. M. 2011. The yin and yang of microglia. Dev. Neurosci. 33, 199–209. PMID: 21757877.

D'ambrosi N., Finocchi P., Apolloni S., Cozzolino M., Ferri A., Padovano V., et al. 2009. The proinflammatory action of microglial P2 receptors is enhanced in SOD1 models for amyotrophic lateral sclerosis. *J. Immunol*. 183, 4648–4656. PMID: 19734218.

d'Abramo C., Acker C.M., Jimenez H.T., Davies P. 2013. Tau passive immunotherapy in mutant P301L mice: antibody affinity versus specificity. *PLoS One* 8**,** e62402. PMID: 23638068.

Dahl R., Sergienko E.A., Su Y., Mostofi Y.S., Yang L., Simao A.M., Narisawa S., Brown B., Mangravita-Novo A., Vicchiarelli M., Smith L.H., O'Neill W.C., Millán J.L., Cosford N.D. 2009. Discovery and validation of a series of aryl sulfonamides as selective inhibitors of tissue-nonspecific alkaline phosphatase (TNAP). *J Med Chem*. 52(21):6919-25. PMID: 19821572

Davalos D., Grutzendler J., Yang G., Kim J. V., Zuo Y., Jung S., et al. 2005. ATP mediates rapid microglial response to local brain injury in vivo. *Nat. Neurosci*. 8, 752–758. PMID: 15895084.

Davis E.J., Foster T.D., Thomas W.E. Cellular forms and functions of brain microglia. *Brain Res Bull.* 1994;34(1):73-8. PMID: 8193937.

de Diego-Garcia L., Ramirez-Escudero M., Sebastian-Serrano A., Diaz-Hernandez J.I., Pintor J., Lucas J.J., Diaz-Hernandez M. 2017. Regulation of proteasome activity by P2Y2 receptor underlies the neuroprotective effects of extracellular nucleotides. Biochim. *Biophys. Acta 1863* (1), 43–51. PMID: 27768902.

de Jong D., Jansen R., Hoefnagels W., Jellesma-Eggenkamp M., Verbeek M., Borm G., et al. 2008. No effect of one-year treatment with indomethacin on Alzheimer's disease progression: a randomized controlled trial. *PLoS One* 3:e1475. PMID: 18213383.

De Simone R., Niturad C. E., De Nuccio C., Ajmone-Cat M. A., Visentin S., and Minghetti L. 2010. TGF-b and LPS modulate ADP-induced migration of microglial cells through P2Y1 and P2Y12 receptor expression. *J. Neurochem*. 115, 450–459. PMID: 20681951.

Delarasse C., Auger R., Gonnord P., Fontaine B., and Kanellopoulos J. M. 2011. The purinergic receptor P2X7 triggers alpha-secretase-dependent processing of the amyloid precursor protein. *J. Biol. Chem*. 286, 2596–2606. PMID: 21081501.

Deuchars S.A., Atkinson L., Brooke R.E., Musa H., Milligan C.J., Batten T.F. *et al*. 2001. Neuronal P2X7 receptors are targeted to presynaptic terminals in the central and peripheral nervous systems. *J Neurosci* 21:7143–7152. PMID: 11549725.

Dhulipala P.D., Wang Y.X., Kotlikoff M.I. 1998. The human P2X4 receptor gene is alternatively spliced. *Gene* 207(2):259–266. PMID: 9511769.

Di Virgilio F., Dal Ben D. Sarti A.C., Giuliani A.L., Falzoni S. 2017. The P2X7 Receptor in Infection and Inflammation. *Immunity*. 47(1):15-31 PMID: 28723547.

Di Virgilio F., 2015. P2X receptors and inflammation. Curr Med Chem 22, 866–77. PMID: 25524252.

Di Virgilio F., Ceruti S., Bramanti P., and Abbracchio M. P. 2009. Purinergic signalling in inflammation of the central nervous system. *Trends Neurosci*. 32,79–87. PMID: 19135728.

Di Virgilio F., Schmalzing G., and Markwardt F. 2018b. The elusive P2X7 macropore. *Trends Cell Biol.* 28, 392–404. PMID: 29439897.

Díaz-Hernández J.I., Gomez-Villafuertes R., León-Otegui M., Hontecillas-Prieto L., Del Puerto A., Trejo J.L., Lucas J.J., Garrido J.J., Gualix J., Miras-Portugal M.T., Diaz-Hernandez M. 2012. In vivo P2X7 inhibition reduces amyloid plaques in Alzheimer's disease through GSK3β and secretases. *Neurobiol Aging*. 33(8):1816-28. PMID: 22048123.

Díaz-Hernández J.I., Sebastián-Serrano Á., Gómez-Villafuertes R., Díaz-Hernández M., Miras-Portugal M.T. 2015. Age-related nuclear translocation of P2X6 subunit modifies splicing activity interacting with splicing factor 3A1. *PLoS One.* 10(4):e0123121. PMID: 25874565.

Díaz-Hernández M., Cox J.A., Migita K., Haines W., Egan T.M., 2002. Voigt M.M. Cloning and characterization of two novel zebrafish P2X receptor subunits. *Biochem Biophys Res Commun*. 295(4):849-53. PMID: 12127972.

Díaz-Hernández M., del Puerto A., Diaz-Hernandez J.I., Diez-Zaera M., Lucas J.J., Garrido J.J., Miras-Portugal M.T. 2008. Inhibition of the ATP-gated P2X7 receptor promotes axonal growth and branching in cultured hippocampal neurons. *J Cell Sci* 121, 3717–3728. PMID: 18987356.

Díaz-Hernández M., Gómez-Ramos A., Rubio A., Gómez-Villafuertes R., Naranjo J.R., Miras-Portugal M.T., Avila J. 2010. Tissue-nonspecific alkaline phosphatase promotes the neurotoxicity effect of extracellular tau. J Biol Chem. 285(42):32539-48. PMID: 20634292.

Díaz-Hernández M., Pereira M.F., Pintor J., Cunha R.A.., Ribeiro J.A, Miras- Portugal M.T. 2002b. Modulation of the rat hippocampal dinucleotide receptor by adenosine receptor activation. *J Pharmacol Exp Ther* 301:441-450. PMID: 11961042.

Díaz-Hernández M., Pintor J., Castro E., Miras-Portugal M.T. 2002. Co-localisation of functional nicotinic and ionotropic nucleotide receptors in isolated cholinergic synaptic terminals. Neuropharmacology. 42(1):20-33. PMID: 11750913.

Díaz-Hernández M., Pintor J., Castro E., Miras-Portugal M.T. 2001. Independent receptors for diadenosine pentaphosphate and ATP in rat midbrain single synaptic terminals. Eur J Neurosci. 14(6):918-26. PMID: 11595030.

Díaz-Hernández M., Pintor J., Miras-Portugal M.T. 2000. Modulation of the dinucleotide receptor present in rat midbrain synaptosomes by adenosine and ATP. *Br J Pharmacol* 130:434-440. PMID: 10807683.

Díaz-Hernández M., Diez-Zaera M., Sanchez-Nogueiro J., Gomez-Villafuertes R., Canals J. M., Alberch J., et al. 2009. Altered P2X7-receptor level and function in mouse models of Huntington's disease and therapeutic efficacy of antagonist administration. *FASEB J* 23, 1893–1906. PMID: 19171786.

Díez -Zaera M., Diaz-Hernandez J.I., Hernandez-Alvarez E., Zimmermann H., Diaz-Hernandez M., Miras-Portugal M.T. 2011. Tissue-nonspecific alkaline phosphatase promotes axonal growth of hippocampal neurons. *Mol Biol Cell* 22(7):1014–1024. PMID: 21289095.

Ding S., and Sachs F. 1999. Single channel properties of P2X2 purinoceptors. *J. Gen.Physiol.* 113, 695–720. PMID: 10228183.

DiSabato D.J., Quan N., Godbout J.P. 2016. Neuroinflammation: the devil is in the details. *J Neurochem*. 139 Suppl 2(Suppl 2):136-153. PMID: 26990767.

DiTella M., Feiguin F., Morfini G., Caceres, A. 1994. Microfilament-associated growth cone component depends upon tau for its intracellular localization. *Cell Motil. Cytoskelet.* 29, 117–130. PMID: 7820862.

Domínguez J. M., Fuertes A., Orozco L., Monte-Millán M. D., Delgado E., and Medina M. 2012. Evidence for irreversible inhibition of glycogen synthase kinase-3b by tideglusib. *J. Biol. Chem*. 287, 893–904. PMID: 22102280.

Doody R. S., Raman R., Farlow M., Iwatsubo T., Vellas B., Joffe S., et al. 2013. A phase 3 trial of semagacestat for treatment of Alzheimer's disease. *N. Engl. J. Med*. 369, 341–350. PMID: 23883379.

Dos Santos-Rodrigues A., Grañé-Boladeras N., Bicket A., Coe I.R. 2014. Nucleoside transporters in the purinome. *Neurochem Int.* 73:229-37. PMID: 24704797.

Drury A.N., Szent-Györgyi A. 1929. The physiological activity of adenine compounds with especial reference to their action upon the mammalian heart. *J Physiol.* 68(3):213-37. PMID: 16994064.

Dujardin S., Lécolle K., Caillierez R., Bégard S., Zommer N., Lachaud C., Carrier S., Dufour N., Aurégan G., Winderickx J., Hantraye P., Déglon N., Colin M., Buée L. 2014. Neuron-to-neuron wild-type Tau protein transfer through a trans-synaptic mechanism: relevance to sporadic tauopathies. *Acta Neuropathol Commun.* 2:14. PMID: 24479894.

Egan M. F., Kost J., Tariot P. N., Aisen P. S., Cummings J. L., Vellas B., et al. 2018. Randomized trial of Verubecestat for mild-to-moderate Alzheimer's disease. *N. Engl. J. Med*. 378, 1691–1703. PMID: 29719179.

Engel T., Goni-Oliver P., Lucas J. J., Avila J. and Hernandez F. 2006. Chronic lithium administration to FTDP-17 tau and GSK-3beta overexpressing mice prevents tau hyperphosphorylation and neurofibrillary tangle formation, but pre-formed neurofibrillary tangles do not revert. *J. Neurochem*. 99, 1445–1455. PMID: 17059563.

Engel T., Gomez-Villafuertes R., Tanaka K., Mesuret G., Sanz-Rodriguez A., Garcia-Huerta P., et al. 2012. Seizure suppression and neuroprotection by targeting the purinergic P2X7 receptor during status epilepticus in mice. *FASEB J*. 26, 1616–1628. PMID: 22198387.

Erb L., Weisman G.A., 2012. Coupling of P2Y receptors to G proteins and other signaling pathways. *Wiley Interdiscip Rev Membr Transp Signal* 1, 789–803. PMID: 25774333.

Ercan E., Eid S., Weber C., Kowalski A., Bichmann M., Behrendt A., Matthes F., Krauss S., Reinhardt P., Fulle S., Ehrnhoefer D.E. 2017. A validated antibody panel for the characterization of tau post-translational modifications. *Mol Neurodegener*. 12(1):87. PMID: 29157277.

Fa M., Puzzo D., Piacentini R., Staniszewski A., Zhang H., Baltrons M.A., Li Puma D.D., Chatterjee I., Li J., Saeed F., et al. 2016. Extracellular tau oligomers produce an immediate impairment of LTP and memory. *Sci. Rep*. 6, 19393 PMID: 26786552.

Fabbrizio P., Amadio S., Apolloni S., and Volonte C. 2017. P2X7 receptor activation modulates autophagy in SOD1-G93A mouse microglia. *Front. Cell. Neurosci*. 11:249. PMID: 28871219.

Fang K. M., Yang C. S., Sun S. H., and Tzeng S. F. 2009. Microglial phagocytosis attenuated by short-term exposure to exogenous ATP through P2X receptor action. *J. Neurochem*. 111, 1225–1237. PMID: 19860838.

Fedde K.N., Whyte M.P., 1990. Alkaline phosphatase (tissue-nonspecific isoenzyme) is a phosphoethanolamine and pyridoxal-5'-phosphate ectophosphatase: normal and hypophosphatasia fibroblast study. *Am. J. Hum. Genet*. 47 (5), 767–775. PMID: 2220817.

Ferrer I., Gomez-Isla T., Puig B., Freixes M., Ribé E., Dalfó E., Avila J. 2005. Current advances on different kinases involved in tau phosphorylation, and implications in Alzheimer's disease and tauopathies. *Curr Alzheimer Res.* 2(1):3-18. PMID: 15977985.

Fitz J.G. 2007. Regulation of cellular ATP release. *Trans Am Clin Climatol Assoc*. 118:199-208. PMID: 18528503.

Franceschini A., Capece M., Chiozzi P., Falzoni S., Sanz J.M., Sarti A.C., Bonora M., Pinton P., Di Virgilio F. 2015. The P2X7 receptor directly interacts with the NLRP3 inflammasome scaffold protein. *FASEB J*, 29(6):2450-2461. PMID: 25690658.

Francistiová L., Bianchi C., Di Lauro C., et al. 2020. The Role of P2X7 Receptor in Alzheimer's Disease. *Front Mol Neurosci*. 13:94. PMID: 32581707.

Fruman D.A., Rommel C. 2014. PI3K and cancer: lessons, challenges and opportunities. *Nat Rev Drug Discov.* 13(2):140-156. PMID: 24481312.

Fujita T., Tozaki-Saitoh H., Inoue K. 2009. P2Y1 receptor signaling enhances neuroprotection by astrocytes against oxidative stress via IL-6 release in hippocampal cultures. *Glia* 57, 244–257. PMID: 18756525.

Gachet C. 2008. P2 receptors, platelet function and pharmacological implications. *Thromb Haemost* 99(3):466–472. PMID: 18327393.

Gandelman M., Peluffo H., Beckman J. S., Cassina P., and Barbeito L. 2010. Extracellular ATP and the P2X7 receptor in astrocyte-mediated motor neuron death: implications for amyotrophic lateral sclerosis. *J. Neuroinflammation* 7:33. PMID: 20534165.

Gao M., Wang M., Green M.A., Hutchins G.D., Zheng Q.H. 2015. Synthesis of [(11)C] GSK1482160 as a new PET agent for targeting P2X(7) receptor. *Bioorg Med Chem Lett*. 25(9):1965-70. PMID: 25819093.

Garcia-Guzman M., Stuhmer W., Soto F. 1997. Molecular characterization and pharmacological properties of the human P2X3 purinoceptor. *Brain Res Mol Brain Res* 47(1–2):59–66. PMID: 9221902.

Ghosh S., Wu M.D., Shaftel S.S., Kyrkanides S., LaFerla F.M., Olschowka J.A., O'Banion M.K. 2013. Sustained interleukin-1β overexpression exacerbates tau pathology despite reduced amyloid burden in an Alzheimer's mouse model. *J Neurosci*. 33(11):5053-64. PMID: 23486975.

Goding J.W., Grobben B., Slegers H. 2003. Physiological and pathophysiological functions of the ecto-nucleotide pyrophosphatase/phosphodiesterase family. *Biochim Biophys Acta*. 1638(1):1-19. PMID: 12757929.

Gómez-Ramos A., Díaz-Hernández M., Rubio A., Díaz-Hernández J.I., Miras-Portugal M.T., Avila J. 2009. Characteristics and consequences of muscarinic receptor activation by tau protein. *Eur Neuropsychopharmacol*. 19(10):708-17. PMID: 19423301.

Gómez-Ramos A., Díaz-Hernández M., Rubio A., Miras-Portugal M.T., Avila J. 2008. Extracellular tau promotes intracellular calcium increase through M1 and M3 muscarinic receptors in neuronal cells. *Mol Cell Neurosci.* 37(4):673-81. PMID: 18272392.

Gomez-Ramos A., Diaz-Hernandez M., Cuadros R., Hernandez F., Avila J. 2006. Extracellular tau is toxic to neuronal cells. *FEBS Lett*. 580, 4842–4850. PMID: 16914144.

Gómez-Villafuertes R., del Puerto A., Diaz-Hernandez M., Bustillo D., Diaz-Hernandez J.I., Huerta P.G., Artalejo A.R., Garrido J.J., Miras-Portugal M.T. 2009. Ca2+/calmodulin-dependent kinase II signaling cascade mediates P2X7 receptor-dependent inhibition of neuritogenesis in neuroblastoma cells. *FEBS J* 276, 5307–5325. PMID: 19682070.

Gómez-Villafuertes R., Gualix J., Miras-Portugal M.T. 2001. Single GABAergic synaptic terminals from rat midbrain exhibit functional P2X and dinucleotide receptors, able to induce GABA secretion. *J Neurochem*. 77(1):84-93. PMID: 11279264.

Gomez-Villafuertes R., Garcia-Huerta P., Diaz-Hernandez J.I., Miras-Portugal M.T., 2015. PI3K/Akt signaling pathway triggers P2X7 receptor expression as a pro-survival factor of neuroblastoma cells under limiting growth conditions. *Sci Rep*, 5:18417. PMID: 26687764.

Goncalves F. Q., Lopes J. P., Silva H. B., Lemos C., Silva A. C., Goncalves N., et al. 2019. Synaptic and memory dysfunction in a beta-amyloid model of early Alzheimer's disease depends on increased formation of ATP-derived extracellular adenosine. *Neurobiol. Dis*. 132:104570. PMID: 31394204.

Gong C.X., Singh T.J., Grundke-Iqbal I., Iqbal K. 1993. Phosphoprotein phosphatase activities in Alzheimer disease brain. *J Neurochem*. 61(3):921-7. PMID: 8395566.

Gong S., Zheng C., Doughty M.L., Losos K., Didkovsky N., Schambra U.B., Nowak N.J., Joyner A., Leblanc G., Hatten M.E., Heintz N. 2003. A gene expression atlas of the central nervous system based on bacterial artificial chromosomes. *Nature*. 425(6961):917-25. PMID: 14586460.

Grygorowicz T., Welniak-Kaminska M., and Struzynska L. 2016. Early P2X7Rrelated astrogliosis in autoimmune encephalomyelitis. *Mol. Cell. Neurosci*. 74, 1–9. PMID: 26921791.

GSK. 4-benzoyl-1-substituted-piperazin-2-one derivatives as P2X7 modulators. US20100311749 (2010)

GSK. 5,6,7,8-tetrahydro [1,2,4] triazolo [4,3-A] pyrazine derivatives as P2X7 modulators. US20120157436 (2012)

GSK. Imidazolidine carboxamide derivatives as P2X7 modulators. US20100075968 (2010)

GSK. Pyrazole derivatives as P2X7 modulators. US20110046137 (2011)

GSK. Thiadiazolidinedioxide P2X7 receptor antagonists. WO2011054947 (2011)

Gu B.J., Sluyter R., Skarratt K.K. et al. 2004. An Arg307 to Gln polymorphism within the ATP-binding site causes loss of function of the human P2X7 receptor. *J Biol Chem* 279: 31287–95. PMID: 15123679.

Gu B.J., Zhang W.Y., Bendall L.J., Chessell I.P., Buell G.N., Wiley J.S. 2000. Expression of P2X7 purinoceptors on human lymphocytes and monocytes: evidence for nonfunctional P2X7 receptors. Am J *Physiol Cell Physiol*. 279(4):C1189-97. PMID: 11003599.

Gualix J., Gómez-Villafuertes R., Díaz-Hernández M., Miras-Portugal M.T. 2003. Presence of functional ATP and dinucleotide receptors in glutamatergic synaptic terminals from rat midbrain. *J Neurochem*. 87(1):160-71. PMID: 12969263.

Guo W., Xu X., Gao X., Burnstock G., He C., Xiang Z. 2008. Expression of P2X5 receptors in the mouse CNS. *Neuroscience* 156(3):673–692. PMID: 18773945.

Guo T., Zhang D., Zeng Y., Huang T.Y., Xu H., and Zhao Y. 2020. Molecular and cellular mechanisms underlying the pathogenesis of Alzheimer's disease. *Mol. Neurodegener*. 15, 40 PMID: 32677986.

Gustin A., Kirchmeyer M., Koncina E., Felten P., Losciuto S., Heurtaux T., et al. 2015. NLRP3 inflammasome is expressed and functional in mouse brain microglia but not in astrocytes. *PLoS One* 10:e0130624. PMID: 26091541.

Gutiérrez-Martín Y., Bustillo D., Gómez-Villafuertes R., Sánchez-Nogueiro J., Torregrosa-Hetland C., Binz T., Gutiérrez L.M., Miras-Portugal M.T., Artalejo A.R. 2011. P2X7 receptors trigger ATP exocytosis and modify secretory vesicle dynamics in neuroblastoma cells. *J Biol Chem.* 286(13):11370-81. PMID: 21292765.

Hanger D.P., Anderton B.H., Noble W. 2009. Tau phosphorylation: the therapeutic challenge for neurodegenerative disease. *Trends Mol Med.* 15:112– 9. PMID: 19246243.

Hasegawa M. 2006. Biochemistry and molecular biology of tauopathies. *Neuropathology*. 2006 Oct;26(5):484-90. PMID: 17080729.

Hattori M., and Gouaux E. 2012. Molecular mechanism of ATP binding and ion channel activation in P2X receptors. *Nature* 485, 207–212. PMID: 22535247.

He Y., Zeng M. Y., Yang D., Motro B., and Nunez G. 2016. NEK7 is an essential mediator of NLRP3 activation downstream of potassium efflux. *Nature* 530, 354–357. PMID: 26814970.

Heneka M.T., Carson M.J., El Khoury J., Landreth G.E., Brosseron F., Feinstein D.L., Jacobs A.H., Wyss-Coray T., Vitorica J., Ransohoff R.M., *et al.* 2015. Neuroinflammation in Alzheimer's disease. *The Lancet Neurology* 14, 388–405. PMID: 25792098.

Henley D., Raghavan N., Sperling R., Aisen P., Raman R., and Romano G. 2019. Preliminary results of a trial of Atabecestat in preclinical Alzheimer's disease. *N. Engl. J. Med*. 380, 1483–1485. PMID: 30970197.

Hernandez F., Lucas J.J., Avila J. 2013. GSK3 and tau: two convergence points in Alzheimer's disease. *J Alzheimers Dis.* 33 Suppl 1:S141-4. PMID: 22710914.

Hirokawa N., Funakoshi T., Sato-Harada R., Kanai Y. 1996. Selective stabilization of tau in axons and microtubule-associated protein 2C in cell bodies and dendrites contributes to polarized localization of cytoskeletal proteins in mature neurons. *J Cell Biol*. 132(4):667-79. PMID: 8647897.

Hogarty M.D. Maris J.M. 2012. PI3King on MYCN to improve neuroblastoma therapeutics. *Cancer Cell*, 21:(2), 145-147. PMID: 22340587.

Holmes B.B., Furman J.L., Mahan T.E., et al. 2014. Proteopathic tau seeding predicts tauopathy in vivo. *Proc Natl Acad Sci U S A*. 111(41):E4376-E4385. PMID: 25261551.

Honore P., Donnelly-Roberts D., Namovic M.T., Hsieh G., Zhu C.Z., Mikusa J.P., Hernandez G., Zhong C., Gauvin D.M., Chandran P., Harris R., Medrano A.P., Carroll W., Marsh K., Sullivan J.P., Faltynek C.R., Jarvis M.F. 2006. A-740003 [N-(1-{[(Cyanoimino)(5-quinolinylamino) methyl]amino}-2,2-dimethylpropyl)-2-(3,4-dimethoxyphenyl)acetamide], a Novel and Selective P2X7 Receptor Antagonist, Dose-Dependently Reduces Neuropathic Pain in the Rat. *J. Pharmacol. Exp. Ther*. 319, 1376–1385. PMID: 16982702.

Hooper C., Killick R., Lovestone S. 2008. The GSK3 hypothesis of Alzheimer's disease. *J Neurochem.*;104(6):1433-1439. PMID: 18088381.

Hracsko Z., Baranyi M., Csolle C., Goloncser F., Madarasz E., Kittel A., et al. 2011. Lack of neuroprotection in the absence of P2X7 receptors in toxin-induced animal models of Parkinson's disease. *Mol. Neurodegener*. 6:28. PMID: 21542899.

Idzko M., Ferrari D., Eltzschig H.K. 2014. Nucleotide signalling during inflammation. *Nature* 509(7500):310–317. PMID: 24828189.

Illes P., Khan T. M., and Rubini P. 2017. Neuronal P2X7 receptors revisited: do they really exist? *J. Neurosci*. 37:7049–7062. PMID: 28747388.

Illes P., Rubini P., Ulrich H., Zhao Y., Tang Y. 2020. Regulation of Microglial Functions by Purinergic Mechanisms in the Healthy and Diseased CNS. *Cells.* 9(5):1108. PMID: 32365642.

Inoue K. 2008. Purinergic systems in microglia. *Cell. Mol. Life Sci*. 19, 3074–3080. PMID: 18563292.

Ising C., Venegas C., Zhang S., Scheiblich H., Schmidt S. V., Vieira-Saecker A., et al. 2019. NLRP3 inflammasome activation drives tau pathology. *Nature* 575, 669–673. PMID: 31748742.

Ittner L.M., Ke Y.D., Delerue F., Bi M., Gladbach A., van Eersel J., et al. 2010. Dendritic function of tau mediates amyloid-beta toxicity in Alzheimer's disease mouse models. *Cell* 142:387e97. PMID: 20655099.

Jacobson K.A., Jarvis M.F., and Williams M. 2002. Purine and pyrimidine (P2) receptors as drug targets. *J Med Chem* 45:4057–4093. PMID: 12213051.

Jacobson K.A. 2010. P2X and P2Y Receptors Scientific Review. *Tocris Biosci.* https://www.tocris.com/literature/scientific-reviews/p2x-and-p2y-receptors.

Jankowsky J. L., Fadale D. J., Anderson J., Xu G. M., Gonzales V., Jenkins N. A., et al. 2004. Mutant presenilins specifically elevate the levels of the 42 residue beta-amyloid peptide in vivo: evidence for augmentation of a 42- specific gamma secretase. *Hum. Mol. Genet.* 13:159–170. PMID: 14645205.

Janks L., Sharma C. V. R., and Egan T. M. 2018. A central role for P2X7 receptors in human microglia. *J. Neuroinflammation* 15:325. PMID: 30463629.

Jiang L.H., Baldwin J., Roger S., Baldwin S. 2013. Insights into the Molecular Mechanisms Underlying Mammalian P2X7 Receptor Functions and Contributions in Diseases, Revealed by Structural Modeling and Single Nucleotide Polymorphisms. *Frontiers in Pharmacology* 10.3389/fphar.2013.00055 PMID: 23675347.

Jiang L.H., Mackenzie A.B., North R.A., and Surprenant A. 2000. Brilliant blue G selectively blocks ATP-gated rat P2X(7) receptors. *Mol Pharmacol* 58:82–88. PMID: 10860929.

Jimenez-Mateos E.M., Smith J., Nicke A., Engel T. 2019. Regulation of P2X7 receptor expression and function in the brain. *Brain Res. Bull.* 151:153-163. PMID: 30593878.

Jimenez-Pacheco A., Diaz-Hernandez M., Arribas-Blazquez M., Sanz- Rodriguez A., Olivos-Ore L. A., Artalejo A. R., et al. 2016. Transient P2X7 receptor antagonism produces lasting reductions in spontaneous seizures and gliosis in experimental temporal lobe epilepsy. *J. Neurosci.* 36, 5920–5932. PMID: 27251615.

Jimenez-Pacheco A., Mesuret G., Sanz-Rodriguez A., Tanaka K., Mooney C., Conroy R., et al. 2013. Increased neocortical expression of the P2X7 receptor after status epilepticus and anticonvulsant effect of P2X7 receptor antagonist A-438079. *Epilepsia* 54, 1551–1561. PMID: 23808395.

Jin H., Han J., Resing D., Liu H., Yue X., Miller R. L., et al. 2018. Synthesis and in vitro characterization of a P2X7 radioligand [123I]TZ6019 and its response to neuroinflammation in a mouse model of Alzheimer disease. *Eur. J. Pharmacol.* 820, 8–17. PMID: 29225193.

Kaczmarek-Hájek K., Lörinczi E., Hausmann R., Nicke A. 2012. Molecular and functional properties of P2X receptors--recent progress and persisting challenges. *Purinergic Signal.* 8(3):375-417. PMID: 22547202.

Kaczmarek-Hajek K., Zhang J., Kopp R., Grosche A., Rissiek B., Saul A., Bruzzone S., Engel T., Jooss T., Krautloher A., Schuster S., Magnus T., Stadelmann C., Sirko S., Koch-Nolte F., Eulenburg V., Nicke A. 2018. Re-evaluation of neuronal P2X7 expression using novel mouse models and a P2X7-specific nanobody. *Elife.* 7:e36217. PMID: 30074479.

Kaidanovich-Beilin O., Woodgett J.R. 2011. GSK-3: Functional Insights from Cell Biology and Animal Models. *Front Mol Neurosci.* 4:40. PMID: 22110425.

Kanemaru K., Takio K., Miura R., Titani K. & Ihara Y. 1992. Fetal-type phosphorylation of the tau in paired helical filaments. *J. Neurochem.* 58:1667–1675. PMID: 1560225.

Kaniyappan S., Chandupatla R.R., Mandelkow E.M., Mandelkow E. 2017. Extracellular low-n oligomers of tau cause selective synaptotoxicity without affecting cell viability. *Alzheimers Dement*. 13:1270–1291. PMID: 28528849.

Karasawa A., Kawate T., 2016. Structural basis for subtype-specific inhibition of the P2X7 receptor. Elife. 5:e22153. PMID: 27935479.

Karch C.M., Jeng A.T., Goate A.M. 2012. Extracellular tau levels are influenced by variability in tau that is associated with tauopathies. *J. Biol. Chem.* 287:42751–42762. PMID: 23105105.

Kasuya G., Fujiwara Y., Tsukamoto H. *et al*. 2017. Structural insights into the nucleotide base specificity of P2X receptors. *Sci Rep* **7,** 45208. PMID: 28332633.

Kawate T., Michel J.C., Birdsong W.T., Gouaux E. 2009. Crystal structure of the ATP-gated P2X(4) ion channel in the closed state. Nature. 460(7255):592-8. PMID: 19641588.

Keystone E.C., Wang M.M., Layton M., Hollis S., McInnes IB; D1520C00001 Study Team. 2012. Clinical evaluation of the efficacy of the P2X7 purinergic receptor antagonist AZD9056 on the signs and symptoms of rheumatoid arthritis in patients with active disease despite treatment with methotrexate or sulphasalazine. *Ann Rheum Dis*. 71(10):1630-5. PMID: 22966146.

Kim S. Y., Moon J. H., Lee H. G., Kim S. U., and Lee Y. B. 2007. ATP released from beta-amyloid-stimulated microglia induces reactive oxygen species production in an autocrine fashion. *Exp. Mol. Med.* 39, 820–827. PMID: 18160853.

Kittner H., Franke H., Fischer W., Schultheis N., Krügel U., Illes P. 2003. Stimulation of P2Y1 receptors causes anxiolytic-like effects in the rat elevated plus-maze: implications for the involvement of P2Y1 receptor-mediated nitric oxide production. *Neuropsychopharmacol. Off. Publ. Am. Coll. Neuropsychopharmacol.* 28, 435–444. PMID: 12629523.

Kopp R., Krautloher A., Ramírez-Fernández A., Nicke A., 2019. P2X7 Interactions and Signaling – Making Head or Tail of It. *Front. Mol. Neurosci*. 12:183. PMID: 31440138.

Kornum B.R., Kawashima M., Faraco J., Lin L., Rico T.J., Hesselson S., Axtell R.C., Kuipers H., Weiner K., Hamacher A., Kassack M.U., Han F., Knudsen S., Li J., Dong X., Winkelmann J., Plazzi G., Nevsimalova S., Hong S.-C., Honda Y., Honda M., Högl B., Ton T.G.N., Montplaisir J., Bourgin P., Kemlink D., Huang Y.-S., Warby S., Einen M., Eshragh J.L., Miyagawa T., Desautels A., Ruppert E., Hesla P.E., Poli F., Pizza F., Frauscher B., Jeong J.-H., Lee S.-P., Strohl K.P., Longstreth W.T., Kvale M., Dobrovolna M., Ohayon M.M., Nepom G.T., Wichmann H.-E., Rouleau G.A., Gieger C., Levinson D.F., Gejman P.V., Meitinger T., Peppard P., Young T., Jennum P., Steinman L., Tokunaga K., Kwok P.-Y., Risch N., Hallmayer J., Mignot E. 2011. Common variants in P2RY11 are associated with narcolepsy. Nat. Genet. 43:66–71. PMID: 21170044.

Koshimizu T.A., Tsujimoto G. 2006. Functional role of spliced cytoplasmic tails in P2X2-receptor-mediated cellular signaling. *J Pharmacol Sci*. 101(4):261-6. PMID: 16891773.

Kozlenkov A., Le Du M.H., Cuniasse P., Ny T., Hoylaerts M.F., Millán J.L. 2004. Residues determining the binding specificity of uncompetitive inhibitors to tissue-nonspecific alkaline phosphatase. *J Bone Miner Res.* 19(11):1862-72. PMID: 15476587.

Kukley M., Barden J.A., Steinhauser C., Jabs R. 2001. Distribution of P2X receptors on astrocytes in juvenile rat hippocampus. *Glia* 36:11–21. PMID: 11571780.

Kukulski F., Levesque S.A., Lavoie E.G., Lecka J., Bigonnesse F., et al. 2005. Comparative hydrolysis of P2 receptor agonists by NTPDases 1, 2, 3 and 8. *Purinergic signalling* 1: 193-204. PMID: 18404504.

Kurz A., Riemenschneider M., Buch K., Willoch F., Bartenstein P., Muller U., Guder W. 1998. Tau protein in cerebrospinal fluid is significantly increased at the earliest clinical stage of Alzheimer disease. Alzheimer Dis. Assoc. Disord. 12:372–377. PMID: 9876968.

Laliberte R. E., Eggle J., and Gabel C. A. 1999. ATP treatment of human monocytes promotes caspase-1 maturation and externalization. *J. Biol. Chem*. 274, 36944–36951. PMID: 10601248.

Lalo U., Pankratov Y., Wichert S.P., Rossner M.J., North R.A., Kirchhoff F., Verkhratsky A. 2008. P2X1 and P2X5 subunits form the functional P2X receptor in mouse cortical astrocytes. *J Neurosci* 28(21):5473–5480. PMID: 18495881.

Lameh J., Philip M., Sharma Y.K., Moro O., Ramachandran J., Sadee W. 1992. Hm1 muscarinic cholinergic receptor internalization requires a domain in the third cytoplasmic loop. *J. Biol. Chem.* 267:13406–13412. PMID: 1618842.

Langfelder A., Okonji E., Deca D., Wei W. C., and Glitsch M. D. 2015. Extracellular acidosis impairs P2Y receptor-mediated Ca2C signalling and migration of microglia. *Cell Calcium* 57:247–256. PMID: 25623949.

Lazarowski E.R., Boucher R.C., Harden T.K. 2003. Mechanisms of release of nucleotides and integration of their action as P2X- and P2Y-receptor activating molecules. *Mol Pharmacol*. 64(4):785-95. PMID: 14500734.

Lazarowski E.R., Shea D.A., Boucher R.C., Harden T.K. 2003. Release of cellular UDP-glucose as a potential extracellular signaling molecule. *Molecular pharmacology* 63: 1190-7. PMID: 12695547.

Lazarowski E.R. 2012. Vesicular and conductive mechanisms of nucleotide release. *Purinergic signalling* 8: 359-73. PMID: 22528679.

Lee H. G., Won S. M., Gwag B. J., and Lee Y. B. 2011. Microglial P2X(7) receptor expression is accompanied by neuronal damage in the cerebral cortex of the APPswe/PS1dE9 mouse model of Alzheimer's disease. *Exp. Mol. Med*. 43, 7–14. PMID: 21088470.

Lee V.M., Goedert M., Trojanowski J.Q. 2001. Neurodegenerative tauopathies. *Annu. Rev. Neurosci*. 24, 1121–1159. PMID: 11520930.

Lenertz L.Y., Gavala M.L., Hill L.M., Bertics P.J. 2009. Cell signaling via the P2X(7) nucleotide receptor: linkage to ROS production, gene transcription, and receptor trafficking. *Purinergic Signal,* 2009, *5,* (2), 175-187. PMID: 19263245.

León D., Sánchez-Nogueiro J., Marín-García P., Miras-Portugal M.A. 2008. Glutamate release and synapsin-I phosphorylation induced by P2X7 receptor activation in cerebellar granule neurons. Neurochem Int 52:1148–1159. PMID: 18242779.

Levarska L., Zilka N., Jadhav S., Neradil P., Novak M. 2013. Of rodents and men: The mysterious interneuronal pilgrimage of misfolded protein tau in Alzheimer's disease. *J. Alzheimers Dis*. 37:569–577. PMID: 23948940.

Liang S.X., Jenkins N.A., Gilbert D.J., Copeland N.G., Phillips W.D. 2001. Structure and chromosome location of the mouse P2X(1) purinoceptor gene (P2rx1). *Cytogenet Cell Genet* 92(3–4):333– 336. PMID: 11435708.

Liedtke D., Hofmann C., Jakob F, Klopocki E., Graser S. 2020. Tissue-Nonspecific Alkaline Phosphatase-A Gatekeeper of Physiological Conditions in Health and a Modulator of Biological Environments in Disease. Biomolecules. 10(12):1648. PMID: 33302551.

Linden J., Koch-Nolte F., and Dahl G. 2019. Purine release, metabolism, and signaling in the inflammatory response. Ann. Rev. Immunol. 37, 325–347. PMID: 30676821.

Ling Y., Morgan K., and Kalsheker N. 2003. Amyloid precursor protein (APP) and the biology of proteolytic processing: relevance to Alzheimer's disease. *Int. J. Biochem. Cell Biol*. 35, 1505–1535. PMID: 12824062.

Liu Y., Pattamatta A., Zu T., Reid T., Bardhi O., Borchelt D.R., Yachnis A.T., Ranum L.P. 2016. C9orf72 BAC Mouse Model with Motor Deficits and Neurodegenerative Features of ALS/FTD. *Neuron.* 4;90(3):521-34. PMID: 27112499.

Llorens-Martín M., Jurado J., Hernández F., Avila J. GSK-3β, a pivotal kinase in Alzheimer disease. *Front Mol Neurosci.* 21;7:46. PMID: 24904272.

Londos C., Cooper D.M., Wolff J. 1980. Subclasses of external adenosine receptors. *Proc Natl Acad Sci USA* 77: 2551–2554. PMID: 6248853.

Long J. M., and Holtzman D. M. 2019. Alzheimer disease: an update on pathobiology and treatment strategies. Cell 179, 312–339. PMID: 31564456.

Longhurst P.A., Schwegel T., Folander K., Swanson R. 1996. The human P2x1 receptor: molecular cloning, tissue distribution, and localization to chromosome 17. *Biochim Biophys* Acta 1308 (3):185–188. PMID: 8809107.

Loomis P.A., Howard T.H., Castleberry R.P., Binder L.I. 1990. Identification of nuclear tau isoforms in human neuroblastoma cells. *Proc. Natl. Acad. Sci. USA* 87, 8422–8426. PMID: 1700432

Lopez Lopez C., Tariot P. N., Caputo A., Langbaum J. B., Liu F., Riviere M. E., et al. 2019. The Alzheimer's prevention initiative generation program: study design of two randomized controlled trials for individuals at risk for clinical onset of Alzheimer's disease. *Alzheimers Dement.* 5, 216–227. PMID: 31211217.

Lu K., Wang J., Hu B., Shi X., Zhou J., Tang Y., et al. 2013. Brilliant blue G attenuates lipopolysaccharide-mediated microglial activation and inflammation. *Neural Regen. Res*. 8, 599–608. PMID: 25206704.

Lucae S., Salyakina D., Barden N., Harvey M., Gagné B., Labbé M., *et al.* 2006. P2RX7, a gene coding for a purinergic ligand-gated ion channel, is associated with major depressive disorder. *Hum. Mol. Genet*. 15, 2438–2445. PMID: 16822851.

Lucas J. J., Hernandez F., P., Moran M. A., Hen R. and Avila J. 2001. Decreased nuclear beta-catenin, tau hyperphosphorylation and neurodegeneration in GSK-3beta conditional transgenic mice. *EMBO J*. 20, 27–39. PMID: 11226152.

Luo W., Liu W., Hu X., Hanna M., Caravaca A., Paul S.M. 2015. Microglial internalization and degradation of pathological tau is enhanced by an anti-tau monoclonal antibody. *Sci Rep* 5**,** 11161. PMID: 26057852.

Lustig K.D., Shiau A.K., Brake A.J., Julius D. 1993. Expression cloning of an ATP receptor from mouse neuroblastoma cells. *Proc Natl Acad Sci U S A.* 90:5113–5117. PMID: 7685114

Ly D., Dongol A., Cuthbertson P., Guy T. V., Geraghty N. J., Sophocleous R. A., *et al*. 2020. The P2X7 receptor antagonist JNJ-47965567 administered thrice weekly from disease onset does not alter progression of amyotrophic lateral sclerosis in SOD1(G93A) mice. *Purinergic Signal* 16, 109–122. PMID: 32170537.

Magnoni S., Esparza T.J., Conte V., Carbonara M., Carrabba G., Holtzman D.M., Zipfel G.J., Stocchetti N., Brody D.L. 2012. Tau elevations in the brain extracellular space correlate with reduced amyloid-beta levels and predict adverse clinical outcomes after severe traumatic brain injury. *Brain* 135, 1268–1280. PMID: 22116192.

Mairet-Coello G., Courchet J., Pieraut S., Courchet V., Maximov A., Polleux F. 2013. The CAMKK2-AMPK kinase pathway mediates the synaptotoxic effects of Abeta oligomers through Tau phosphorylation. *Neuron* 78, 94–108. PMID: 23583109.

Majerova P., Zilkova M., Kazmerova Z., Kovac A., Paholikova K., Kovacech B., Zilka N., Novak M. 2014. Microglia display modest phagocytic capacity for extracellular tau oligomers. *J. Neuroinflamm.* 11:161 PMID: 25217135.

Mancuso R., Fryatt G., Cleal M., Obst J., Pipi E., Monzon-Sandoval J., Ribe E., Winchester L., Webber C., Nevado A., Jacobs T., Austin N., Theunis C., Grauwen K., Daniela Ruiz E., Mudher A., Vicente-Rodriguez M., Parker C.A., Simmons C., Cash D., Richardson J., Consortium N., Jones D.N.C., Lovestone S., Gomez-Nicola D., Perry V.H. 2019. CSF1R inhibitor JNJ-40346527 attenuates microglial proliferation and neurodegeneration in P301S mice. *Brain* 142**,** 3243-3264. PMID: 31504240.

Marcellino D., Suarez-Boomgaard D., Sanchez-Reina M. D., Aguirre J. A., Yoshitake T., Yoshitake S., *et al.* 2010. On the role of P2X(7) receptors in dopamine nerve cell degeneration in a rat model of Parkinson's disease: studies with the P2X(7) receptor antagonist A-438079. *J. Neural. Transm.* 117, 681–687. PMID: 20387084.

Marcoli M., Cervetto C., Paluzzi P., Guarnieri S., Alloisio S., Thellung S., Nobile M., Maura G. 2008. P2X7 pre-synaptic receptors in adult rat cerebrocortical nerve terminals: a role in ATP-induced glutamate release. *J Neurochem* 105:2330 –2342. PMID: 18315565.

Martin D.L., Barke K.E. 1998. Are GAD65 and GAD67 associated with specific pools of GABA in brain? *Perspect Dev Neurobiol*. 5(2-3):119-29. PMID: 9777630.

Martin E., Amar M., Dalle C., Youssef I., Boucher C., Le Duigou C., *et al*. 2019. New role of P2X7 receptor in an Alzheimer's disease mouse model. *Mol. Psychiatry* 24, 108–125. PMID: 29934546.

Martínez-Frailes C., Di Lauro C., Bianchi C., de Diego-García L., Sebastián-Serrano Á., Boscá L., Díaz-Hernández M. 2019. Amyloid Peptide Induced Neuroinflammation Increases the P2X7 Receptor Expression in Microglial Cells, Impacting on Its Functionality. *Front Cell Neurosci*. 12;13:143. PMID: 31031598.

Matsuura S., Kishi F., Kajii T. 1990. Characterization of a 5′-flanking region of the human liver/bone/kidney alkaline phosphatase gene: two kinds of mRNA from a single gene. *Biochem Biophys Res Commun* 168:993–1000. PMID: 2346496.

Matute C., Torre I., Perez-Cerda F., Perez-Samartin A., Alberdi E., Etxebarria E., *et al*. 2007. P2X(7) receptor blockade prevents ATP excitotoxicity in oligodendrocytes and ameliorates experimental autoimmune encephalomyelitis. *J. Neurosci*. 27, 9525–9533. PMID: 17728465.

McCarthy A.E., Yoshioka C., Mansoor S.E. 2019. Full-Length P2X7 Structures Reveal How Palmitoylation Prevents Channel Desensitization. *Cell* 179, 659-670.e13. PMID: 31587896.

McGeer P. L., McGeer E. G., and Yasojima K. 2000. Alzheimer disease and neuroinflammation. *J. Neural Transm*. Suppl. 59, 53–57. PMID: 10961418.

McKhann G. M., Knopman D. S., Chertkow H., Hyman B. T., Jack CR Jr, Kawas C. H., *et al*. 2011. The diagnosis of dementia due to Alzheimer's disease: recommendations from the National Institute on Aging-Alzheimer's Association workgroups on diagnostic guidelines for Alzheimer's disease. *Alzheimers Dement*. 7, 263–269. PMID: 21514250.

McLarnon J. G., Ryu J. K., Walker D. G., and Choi H. B. 2006. Upregulated expression of purinergic P2X(7) receptor in Alzheimer disease and amyloidbeta peptide-treated microglia and in peptide-injected rat hippocampus. *J. Neuropathol. Exp. Neurol*. 65, 1090–1097. PMID: 17086106.

Medina M., Avila J. 2014. The role of extracellular Tau in the spreading of neurofibrillary pathology. *Front Cell Neurosci*. 8:113. PMID: 24795568.

Merezhko M., Brunello C.A., Yan X., Vihinen H., Jokitalo E., Uronen R.L., Huttunen H.J. 2018. Secretion of Tau via an Unconventional Non-vesicular Mechanism. *Cell Rep*. 25(8):2027-2035.e4. PMID: 30463001.

Metcalfe M.J., Figueiredo-Pereira M.E. 2010. Relationship between tau pathology and neuroinflammation in Alzheimer's disease. *Mt Sinai J Med*. 77(1):50-58. PMID: 20101714.

Metzger M.W., Walser S.M., Aprile-Garcia F., Dedic N., Chen A., Holsboer F., Arzt E., Wurst W., Deussing J.M. 2017. Genetically dissecting P2rx7 expression within the central nervous system using conditional humanized mice. *Purinergic Signal* 13:153–170. PMID: 27858314.

Michel C.H., Kumar S., Pinotsi D., Tunnacliffe A., St George-Hyslop P., Mandelkow E., Mandelkow E.M., Kaminski C.F., Kaminski Schierle G.S. 2014. Extracellular monomeric tau protein is sufficient to initiate the spread of tau protein pathology. *J. Biol. Chem*. 289, 956–967. PMID: 24235150.

Millan J.L. 2006. Alkaline Phosphatases : Structure, substrate specificity and functional relatedness to other members of a large superfamily of enzymes. *Purinergic signalling* 2: 335-41. PMID: 18404473.

Minkiewicz J., de Rivero Vaccari J.P., Keane R.W. 2013. Human astrocytes express a novel NLRP2 inflammasome. *Glia*, 61:(7), 1113-1121. PMID: 23625868.

Miras-Portugal M.T., Díaz-Hernández M., Giráldez L., Hervás C., Gómez-Villafuertes R., Sen R.P., Gualix J., Pintor J. 2003. P2X7 receptors in rat brain: presence in synaptic terminals and granule cells. *Neurochem Res* 28:1597–1605. PMID: 14570406.

Miras-Portugal M.T., Gualix J., Pintor J. 1998. The neurotransmitter role of diadenosine polyphosphates. *FEBS Lett* 430:78–82. PMID: 9678598.

Miras-Portugal M.T., Sebastián-Serrano Á., de Diego García L., Díaz-Hernández M. 2017. Neuronal P2X7 Receptor: Involvement in Neuronal Physiology and Pathology. *J Neurosci*. 37(30):7063-7072. PMID: 28747389.

Monif M., Reid C.A., Powell K.L., Smart M.L., Williams D.A., 2009. The P2X7 receptor drives microglial activation and proliferation: a trophic role for P2X7R pore. *J Neurosci* 29**:**3781-3791. PMID: 19321774.

Morganti J. M., Riparip L.-K., and Rosi S. 2016. Call off the dog(ma): M1/M2 polarization is concurrent following traumatic brain injury. *PLoS One* 11:e0148001. PMID: 26808663.

Moore D., Chambers J., Waldvogel H., Faull R., Emson P., 2000. Regional and cellular distribution of the P2Y(1) purinergic receptor in the human brain: striking neuronal localisation. *J. Comp. Neurol*. 421, 374–384. PMID: 10813793.

Morgan J., Alves M., Conte G. *et al.* 2020. Characterization of the Expression of the ATP-Gated P2X7 Receptor Following Status Epilepticus and during Epilepsy Using a P2X7-EGFP Reporter Mouse. *Neurosci. Bull.* 36, 1242–1258. PMID: 32895896.

Mosher K. I., and Wyss-Coray T. 2014. Microglial dysfunction in brain aging and Alzheimer's disease. *Biochem. Pharmacol*. 88, 594–604. PMID: 24445162.

Mufti F., Jung Y.-H., Giancotti L.A., Yu J., Chen Z., Phung N.B., Jacobson K.A., Salvemini D. 2020. P2Y14 Receptor Antagonists Reverse Chronic Neuropathic Pain in a Mouse Model. *ACS Med. Chem. Lett.* 11:1281–1286. PMID: 32551012.

Mukai F., Ishiguro K., Sano Y. and Fujita S. C. 2002. Alternative splicing isoform of tau protein kinase I/glycogen synthase kinase 3beta. *J. Neurochem*. 81:1073–1083. PMID: 12065620.

Mulryan K., Gitterman D.P., Lewis C.J., Vial C., Leckie B.J., Cobb A.L., Brown J.E., Conley E.C., Buell G., Pritchard C.A., Evans R.J. 2000. Reduced vas deferens contraction and male infertility in mice lacking P2X1 receptors. *Nature* 403(6765):86–89. PMID: 10638758.

Nakatsuka T., Gu J.G. 2006. P2X purinoceptors and sensory transmission. *Pflugers Arch* 452(5):598–607. PMID: 16547751.

Narcisse L., Scemes E., Zhao Y., Lee S. C., and Brosnan C. F. 2005. The cytokine IL-1beta transiently enhances P2X7 receptor expression and function in human astrocytes. *Glia* 49, 245–258. PMID: 15472991.

Nawa G., Urano T., Tokino T., Ochi T., Miyoshi Y. 1998. Cloning and characterization of the murine P2XM receptor gene. *J Hum Genet* 43(4):262–267. PMID: 9852680.

Nelson D.W., Gregg R.J., Kort M.E., Perez-Medrano A., Voight E.A., Wang Y., Grayson G., Namovic M.T., Donnelly-Roberts D.L., Niforatos W., Honore P., Jarvis M.F., Faltynek C.R., Carroll W.A. 2006. Structure−Activity Relationship Studies on a Series of Novel, Substituted 1-Benzyl-5-phenyltetrazole P2X7 Antagonists. *J. Med. Chem*. 49:3659–3666. PMID: 16759108.

Newton K., Dixit V.M. 2012. Signaling in innate immunity and inflammation. *Cold Spring Harb Perspect Biol*. 4(3):a006049. PMID: 22296764.

Ni J., Wang P., Zhang J., Chen W., and Gu L. 2013. Silencing of the P2X(7) receptor enhances amyloid-beta phagocytosis by microglia. *Biochem. Biophys. Res. Commun*. 434, 363–369. PMID: 23562658.

Nicke A., Kuan Y.-H., Masin M., Rettinger J., Marquez-Klaka B., Bender O., Górecki D.C., Murrell-Lagnado R.D., Soto F., 2009. A Functional P2X7 Splice Variant with an Alternative Transmembrane Domain 1 Escapes Gene Inactivation in P2X7 Knock-out Mice. *J. Biol. Chem*. 284, 25813–25822. PMID: 19546214.

Nishida K. *et al*. 2012. Mitochondrial dysfunction is involved in P2X7 receptor-mediated neuronal cell death. *J. Neurochem*. 122, 1118–1128 PMID: 22774935.

Nörenberg W., Illes P. 2000. Neuronal P2X receptors: localisation and functional properties. *Naunyn-Schmied Arch Pharmacol* 362, 324–339. PMID: 11111827.

North R.A. 2002. Molecular physiology of P2X receptors. *Physiol Rev*. 82(4):1013-67. PMID: 12270951.

Nubling G., Levin J., Bader B., Israel L., Botzel K., Lorenzl S., Giese A. 2012. Limited cleavage of tau with matrix-metalloproteinase MMP-9, but not MMP-3, enhances tau oligomer formation. *Exp. Neurol*. 237, 470–476. PMID: 22890115.

Nykänen N.P., Kysenius K., Sakha P., Tammela P., Huttunen H.J. 2012. γ-Aminobutyric acid type A (GABAA) receptor activation modulates tau phosphorylation. *J Biol Chem.* 287(9):6743-52. PMID: 22235112.

Ohishi A., Keno Y., Marumiya A., Sudo Y., Uda Y., Matsuda K., Morita Y., Furuta T., Nishida K., Nagasawa K. 2016. Expression level of P2X7 receptor is a determinant of ATP-induced death of mouse cultured neurons. *Neuroscience* 319:35– 45. PMID: 26812038.

Olla I., Santos-Galindo M., Elorza A., and Lucas J. J. 2020. P2X7 receptor upregulation in Huntington's Disease Brains. *Front. Mol. Neurosci* 13, 567430. PMID: 33122998.

Orioli E., De Marchi E., Giuliani A.L., Adinolfi E. 2017. P2X7 receptor orchestrates multiple signalling pathways triggering inflammation, autophagy and metabolic/trophic responses. *Curr Med Chem* 24(21):2261 –2275. PMID: 28266268.

Ortega F., Pérez-Sen R., Delicado E.G. *et al.* 2009. $P2X_7$ Nucleotide Receptor is Coupled to GSK-3 Inhibition and Neuroprotection in Cerebellar Granule Neurons. *Neurotox Res* 15, 193–204. PMID: 19384592.

Palygin O., Lalo U., Verkhratsky A., Pankratov Y. 2010. Ionotropic NMDA and P2X1/5 receptors mediate synaptically induced Ca2+ signalling in cortical astrocytes. *Cell Calcium* 48 (4):225–231. PMID: 20926134.

Park J.H., Kim Y.C. 2017. P2X7 receptor antagonists: a patent review (2010-2015). *Expert Opin Ther Pat*. 27(3):257-267. PMID: 27724045.

Parvathenani L. K., Tertyshnikova S., Greco C. R., Roberts S. B., Robertson B., and Posmantur R. 2003. P2X7 mediates superoxide production in primary microglia and is up-regulated in a transgenic mouse model of Alzheimer's disease. *J. Biol. Chem.* 278, 13309–13317. PMID: 12551918.

Peeraer E., Bottelbergs A., Van Kolen K., Stancu I.C., Vasconcelos B., Mahieu M., Duytschaever H., Ver Donck L., Torremans A., Sluydts E., *et al*. 2015. Intracerebral injection of preformed synthetic tau fibrils initiates widespread tauopathy and neuronal loss in the brains of tau transgenic mice. *Neurobiol. Dis*. 73, 83–95. PMID: 25220759.

Pelegrin P., Surprenant A. 2006. Pannexin-1 mediates large pore formation and interleukin-1beta release by the ATP-gated P2X7 receptor. *EMBO J.* 25(21):5071-82. PMID: 17036048.

Perea J.R., Llorens-Martín M., Ávila J., Bolós M. 2018. The Role of Microglia in the Spread of Tau: Relevance for Tauopathies. *Front Cell Neurosci*. 12:172. PMID: 30042659.

Pérez-Sen R., Queipo M.J., Morente V., Ortega F., Delicado E., Miras-Portugal M.T. 2015. Neuroprotection Mediated by P2Y13 Nucleotide Receptors in Neurons. *Comput. Struct. Biotechnol. J.* 13, 160–168. PMID: 25750704.

Perregaux D. G., McNiff P., Laliberte R., Conklyn M., and Gabel C. A. 2000. ATP acts as an agonist to promote stimulus-induced secretion of IL-1 beta and IL-18 in human blood. *J. Immunol*. 165, 4615–4623. PMID: 11035104.

Pétrilli V., Papin S., Dostert C., Mayor A., Martinon F., Tschopp J. 2007. Activation of the NALP3 inflammasome is triggered by low intracellular potassium concentration. *Cell Death Differ*. 14(9):1583-9. PMID: 17599094.

Pooler A.M., Phillips E.C., Lau D.H., Noble W., Hanger D.P. 2013. Physiological release of endogenous tau is stimulated by neuronal activity. *EMBO Rep*. 14:389–394. PMID: 23412472.

Price D. L., and Sisodia S. S. 1998. Mutant genes in familial Alzheimer's disease and transgenic models. *Annu. Rev. Neurosci*. 21, 479–505. PMID: 9530504.

Puzzo D., Piacentini R., Fa M., Gulisano W., Li Puma D.D., Staniszewski A., Zhang H., Tropea M.R., Cocco S., Palmeri A., *et al*. LTP and memory impairment caused by extracellular Abeta and tau oligomers is APP-dependent. *eLife* 6:e26991. PMID: 28696204.

Rafehi M., Malik E.M., Neumann A., Abdelrahman A., Hanck T., Namasivayam V., Müller C.E., Baqi Y. 2017. Development of Potent and Selective Antagonists for the UTP-Activated P2Y4 Receptor. *J. Med. Chem.* 60, 3020–3038. PMID: 28306255.

Ralevic V., Burnstock G. 1998. Receptors for purines and pyrimidines. *Pharmacol Rev.* 50(3):413-92. PMID: 9755289.

Ransohoff R. M. 2016. A polarizing question: do M1 and M2 microglia exist? *Nat. Neurosci*. 19:987–991. PMID: 27459405.

Rappold P. M., Lynd-Balta E., and Joseph S. A. 2006. P2X7 receptor immunoreactive profile confined to resting and activated microglia in the epileptic brain. *Brain Res.* 1089, 171–178. PMID: 16635480.

Rathmann K.L., Conner C.S. 1984. Alzheimer's disease: Clinical features, pathogenesis, and treatment. *Drug Intell. Clin. Pharm*. 18:684–691. PMID: 6383752.

Reynolds C.H., Garwood C.J., Wray S., Price C., Kellie S., Perera T., Zvelebil M., Yang A., Sheppard P.W., Varndell, I.M., et al. 2008. Phosphorylation regulates tau interactionswith Src homology 3 domains of phosphatidylinositol 3-kinase, phospholipase Cgamma1, Grb2, and Src family kinases. *J. Biol. Chem*. 283:18177–18186. PMID: 18467332.

Rodriguez-Martin T., Cuchillo-Ibanez I., Noble W., Nyenya F., Anderton B.H., Hanger D.P. 2013. Tau phosphorylation affects its axonal transport and degradation. *Neurobiol. Aging* 34, 2146–2157. PMID: 23601672.

Roger S., Pelegrin P., Surprenant A. 2008. Facilitation of P2X7 Receptor Currents and Membrane Blebbing via Constitutive and Dynamic Calmodulin Binding. *J. Neurosci.* 28, 6393–6401. PMID: 18562610.

Rozenstein-Tsalkovich L., Grigoriadis N., Lourbopoulos A., Nousiopoulou E., Kassis, I., Abramsky O., Karussis D., Rosenmann H. 2013. Repeated immunization of mice with phosphorylated-tau peptides causes neuroinflammation. *Exp Neurol* 248**,** 451-456. PMID: 23876516.

Ruan H.Z., Burnstock G. 2005. The distribution of P2X5 purinergic receptors in the enteric nervous system of mouse. *Cell Tissue Res* 319(2):191–200. PMID: 23876516.

Rubio M.E., Soto F. 2001. Distinct localization of P2X receptors at excitatory postsynaptic specializations. *J Neurosci* 21(2):641–653. PMID: 11160443.

Ruiz-Ruiz C., Calzaferri F., and Garcia A. G. 2020. P2X7 receptor antagonismas a potential therapy in amyotrophic lateral sclerosis. *Front.Mol. Neurosci*. 13:93. PMID: 32595451.

Rumney R.M.H., Wang N., Agrawal A. *et al*. 2012. Purinergic signalling in bone. *Front Endocrinol* 3:116. PMID: 23049524.

Ryu J.K., McLarnon J.G. 2008. Block of purinergic P2X(7) receptor is neuroprotective in an animal model of Alzheimer's disease. *Neuroreport* 19**,** 1715-1719. PMID: 18852683.

Saez-Orellana F., Fuentes-Fuentes M. C., Godoy P. A., Silva-Grecchi T., Panes J. D., Guzman L., *et al*. 2018. P2X receptor overexpression induced by soluble oligomers of amyloid beta peptide potentiates synaptic failure and neuronal dyshomeostasis in cellular models of Alzheimer's disease. *Neuropharmacology* 128, 366–378. PMID: 29079292.

Salloway S., Sperling R., Fox N. C., Blennow K., Klunk W., Raskind M., *et al*. 2014. Two phase 3 trials of bapineuzumab in mild-to-moderate Alzheimer's disease. *N. Engl. J. Med.* 370, 322–333. PMID: 24450891.

Saltiel A. R. and Kahn C. R. 2001. Insulin signalling and the regulation of glucose and lipid metabolism. Nature 414, 799–806. PMID: 11742412.

Saman S., Kim W., Raya M., Visnick Y., Miro S., Saman S., Jackson B., McKee A.C., Alvarez V.E., Lee N.C., Hall G.F. 2012. Exosome-associated tau is secreted in tauopathy models and is selectively phosphorylated in cerebrospinal fluid in early Alzheimer disease. *J Biol Chem.* 287(6):3842-9. PMID: 22057275.

Sánchez-Nogueiro J., Marín-García P., Miras-Portugal M.T. 2005. Characterization of a functional P2X(7)-like receptor in cerebellar granule neurons from P2X(7) knockout mice. *FEBS Lett* 579:3783–3788. PMID: 15978588.

Sanz J. M., Chiozzi P., Ferrari D., Colaianna M., Idzko M., Falzoni S., *et al*. 2009. Activation of microglia by amyloid {beta} requires P2X7 receptor expression. *J. Immunol*. 182, 4378–4385. PMID: 19299738.

Savio L.E.B., de Andrade Mello P., da Silva C.G., Coutinho-Silva R. 2018. The P2X7 Receptor in Inflammatory Diseases: Angel or Demon? Front Pharmacol 9:52. PMID: 29467654.

Sawada K., Echigo N., Juge N., Miyaji T., Otsuka M., Omote H., Yamamoto A., Moriyama Y. 2008. Identification of a vesicular nucleotide transporter. *Proc Natl Acad Sci USA.* 2105(15):5683-6. PMID: 18375752.

Schaffer B., Wiedau-Pazos M. and Geschwind D. H. 2003. Gene structure and alternative splicing of glycogen synthase kinase 3 beta (GSK-3beta) in neural and non-neural tissues. *Gene* 302, 73–81. PMID: 12527198.

Scheller J., Chalaris A., Schmidt-Arras D., Rose-John S. 2011. The pro- and anti-inflammatory properties of the cytokine interleukin-6. *Biochim Biophys Acta*. 1813(5):878-88. PMID: 21296109.

Sebastián-Serrano Á., de Diego-García L., di Lauro C., Bianchi C., Díaz-Hernández M. 2019. Nucleotides regulate the common molecular mechanisms that underlie neurodegenerative diseases; Therapeutic implications. *Brain Res Bull*. 151:84-91. PMID: 30721769.

Sebastián-Serrano Á., de Diego-García L., Díaz-Hernández M. 2018. The Neurotoxic Role of Extracellular Tau Protein. *Int J Mol Sci*. 19(4):998. PMID: 29584657.

Sebastián-Serrano Á., de Diego-García L., Martínez-Frailes C., Ávila J., Zimmermann H., Millán J.L., Miras-Portugal M.T., Díaz-Hernández M. 2014. Tissue-nonspecific Alkaline Phosphatase Regulates Purinergic Transmission in the Central Nervous System During Development and Disease. *Comput Struct Biotechnol J.* 13:95-100. PMID: 25709758.

Sebastián-Serrano Á., Engel T., de Diego-García L., Olivos-Oré L.A., Arribas-Blázquez M., Martínez-Frailes C., Pérez-Díaz C., Millán J.L., Artalejo A.R., Miras-Portugal M.T., Henshall D.C., Díaz-Hernández M. 2016. Neurodevelopmental alterations and seizures developed by mouse model of

infantile hypophosphatasia are associated with purinergic signalling deregulation. *Hum Mol Genet*. 25(19):4143-4156. PMID: 27466191.

Selkoe D. J. 2002. Alzheimer's disease is a synaptic failure. *Science* 298, 789–791. PMID: 12399581.

Selkoe D.J. 2019. Alzheimer disease and aducanumab: adjusting our approach. *Nat Rev Neurol.* 15(7):365-366. PMID: 31138932.

Serrano-Pozo A., Frosch M.P., Masliah E., Hyman B.T. 2011. Neuropathological alterations in Alzheimer disease. *Cold Spring Harb. Perspect*. Med. 1, a006189. PMID: 22229116.

Sevigny J., Chiao P., Bussière T., Weinreb P.H., Williams L., Maier M., Dunstan R., Salloway S., Chen T., Ling Y., *et al*. 2016. The antibody aducanumab reduces Aβ plaques in Alzheimer's disease. *Nature* 537, 50–56. PMID: 27582220.

Shi H., Wang Y., Li X., Zhan X., Tang M., Fina M., Su L., Pratt D., Bu C.H., Hildebrand S., Lyon S., Scott L., Quan J., Sun Q., Russell J., Arnett S., Jurek P., Chen D., Kravchenko V.V., Mathison J.C., Moresco E.M., Monson N.L., Ulevitch R.J., Beutler B. 2016. NLRP3 activation and mitosis are mutually exclusive events coordinated by NEK7, a new inflammasome component. *Nat Immunol*, 17, (3), 250-258. PMID: 26642356.

Sidique S., Ardecky R., Su Y., Narisawa S., Brown B., Millán J.L., Sergienko E., Cosford N.D. 2009. Design and synthesis of pyrazole derivatives as potent and selective inhibitors of tissue-nonspecific alkaline phosphatase (TNAP). *Bioorg Med Chem Lett*. 19(1):222-5. PMID: 19038545.

Sim J.A., Young M.T., Sung H.Y., North R.A., Surprenant A. 2004. Reanalysis of P2X7 receptor expression in rodent brain. *J Neurosci* 24:6307– 6314. PMID: 15254086.

Simon D., Garcia-Garcia E., Royo F., Falcon-Perez J.M., Avila J. 2012. Proteostasis of tau. Tau overexpression results in its secretion via membrane vesicles. *FEBS Lett*. 586, 47–54. **PMID: 22138183.**

Singh S.K., Srivastav S., Yadav A.K., Srikrishna S., Perry G. 2016. Overview of Alzheimer's disease and some therapeutic approaches targeting abeta by using several synthetic and herbal compounds. *Oxidative Med. Cell. Longev*. 7361613. PMID: 27034741.

Smith M., Weiss M.J., Griffin C.A., Murray J.C., Buetow K.H., Emanuel B.S., Henthorn P.S., Harris H. 1988. Regional assignment of the gene for human liver/bone/kidney alkaline phosphatase to chromosome 1p36.1-p34. *Genomics.* 2(2):139-43 PMID: 3410475.

Sokolow S., Henkins K.M., Bilousova T., Gonzalez B., Vinters H.V., Miller C.A., Cornwell L., Poon W.W., Gylys K.H. 2015. Pre-synaptic c-terminal truncated tau is released from cortical synapses in Alzheimer's disease. *J. Neurochem*. 133, 368–379. PMID: 25393609.

Solle M., Labasi J., Perregaux D.G., Stam E., Petrushova N., Koller B.H., Griffiths R.J., Gabel C.A. 2001. Altered cytokine production in mice lacking P2X(7) receptors. *J Biol Chem* 276:125–132. PMID: 11016935.

Souslova V., Ravenall S., Fox M., Wells D., Wood J.N., Akopian A.N. 1997. Structure and chromosomal mapping of the mouse P2X3 gene. *Gene* 195(1):101–111. PMID: 9300827.

Souter S., Lee G. 2010. Tubulin-independent tau in Alzheimer's disease and cancer: Implications for disease pathogenesis and treatment. *Curr. Alzheimer Res.* 7:697–707. PMID: 20678073.

Sperlágh B., Köfalvi A., Deuchars J., Atkinson L., Milligan C.J., Buckley N.J., Vizi E.S. 2002. Involvement of P2X7 receptors in the regulation of neurotransmitter release in the rat hippocampus. *J Neurochem* 81:1196–1211. PMID: 12068068.

Sperlágh B., and Illes P. 2014. P2X7 receptor: an emerging target in central nervous system diseases. *Trends Pharmacol. Sci*. 35, 537–547. PMID: 25223574.

Spires-Jones T.L., Hyman B.T. 2014. The intersection of amyloid beta and tau at synapses in Alzheimer's disease. *Neuron* 82, 756–771. PMID: 24853936.

Stelmashenko O., Lalo U., Yang Y., Bragg L., North R.A., Compan V. 2012. Activation of trimeric P2X2 receptors by fewer than three ATP molecules. *Mol Pharmacol.* 82(4):760-6. PMID: 22828800.

Stokes L., Jiang L.H., Alcaraz L., et al. 2006. Characterization of a selective and potent antagonist of human P2X(7) receptors, AZ11645373. *Br J Pharmacol*. 149(7):880-887. PMID: 17031385.

Stokes L., Bidula S.M., Bibič L., Allum E. 2020. To Inhibit or Enhance? Is There a Benefit to Positive Allosteric Modulation of P2X Receptors? *Front. Pharmacol*. 11:627 PMID: 32477120.

Studer M., Terao M., Gianni M., Garattini E. 1991. Characterization of a second promoter for the mouse liver/bone/kidney-type alkaline phosphatase gene: cell and tissue specific expression. *Biochem Biophys Res Commun* 179:1352–60. PMID: 1930180.

Sugiyama T., Oku H., Shibata M., Fukuhara M., Yoshida H., Ikeda T. 2010. Involvement of P2X7 receptors in the hypoxia-induced death of rat retinal neurons. *Invest Ophthalmol Vis Sci.* 51(6):3236-43. PMID: 20071682.

Sultan A., Nesslany F., Violet M., Begard S., Loyens A., Talahari S., Mansuroglu Z., Marzin D., Sergeant N., Humez S., *et al*. 2011. Nuclear tau, a key player in neuronal DNA protection. *J. Biol. Chem*. 286, 4566–4575. PMID: 21131359.

Sun B., Li J., Okahara K., Kambayashi J. 1998. P2X1 purinoceptor in human platelets. Molecular cloning and functional characterization after heterologous expression. *J Biol Chem* 273 (19):11544–11547. PMID: 9565569.

Surprenant A., Rassendren F., Kawashima E., North R.A., Buell G. 1996. The cytolytic P2Z receptor for extracellular ATP identified as a P2X receptor (P2X7). *Science*. 3;272(5262):735-8. PMID: 8614837.

Takamori S., Holt M., Stenius K., Lemke E. A., Grønborg M., Riedel D., *et al.* 2006. Molecular anatomy of a trafficking organelle. *Cell* 127, 831–846. PMID: 17110340.

Takeuchi H., Iba M., Inoue H., Higuchi M., Takao K., Tsukita K., Karatsu Y., Iwamoto Y., Miyakawa T., Suhara T., Trojanowski J.Q., Lee V.M., Takahashi R. 2011. P301S mutant human tau transgenic mice manifest early symptoms of human tauopathies with dementia and altered sensorimotor gating. *PLoS One*. 6(6):e21050. PMID: 21698260.

Terao M., Pravtcheva D., Ruddle F.H., Mintz B. 1988. Mapping of gene encoding mouse placental alkaline phosphatase to chromosome 4. *Somat Cell Mol Genet.* 14(2):211-5. PMID: 3162338.

Terao M., Studer M., Gianní M., Garattini E. 1990. Isolation and characterization of the mouse liver/bone/kidney-type alkaline phosphatase gene. *Biochem J.* 268(3):641-8. PMID: 2363702.

Territo P.R., Meyer J.A., Peters J.S., Riley A.A., McCarthy B.P., Gao M., Wang M., Green M.A., Zheng Q.H., Hutchins G.D. 2017. Characterization of ^{11}C-GSK1482160 for Targeting the P2X7 Receptor as a Biomarker for Neuroinflammation. *J Nucl Med*. 58(3):458-465. PMID: 27765863.

Territo P.R., Zarrinmayeh H. 2021. $P2X_7$ Receptors in Neurodegeneration: Potential Therapeutic Applications From Basic to Clinical Approaches. *Front Cell Neurosci*. 15:617036. PMID: 33889073.

Terwel, D.; Dewachter, I.; Van Leuven, F. 2002. Axonal transport, tau protein, and neurodegeneration in Alzheimer's disease. *Neuromolecular Med*. 2(2):151-65. PMID: 12428809.

Thawkar B. S., and Kaur G. 2019. Inhibitors of NF-kappaB and P2X7/NLRP3/Caspase 1 pathway in microglia: Novel therapeutic opportunities in neuroinflammation induced early-stage Alzheimer's disease. *J. Neuroimmunol*. 326, 62–74. PMID: 30502599.

The Jackson Laboratory. 2019. *Mouse Strain Datasheet - 008169*. https://www.jax.org/strain/ 008169.

Toral-Rios D., Pichardo-Rojas P.S., Alonso-Vanegas M., Campos-Peña V. 2020. GSK3β and Tau Protein in Alzheimer's Disease and Epilepsy. *Front Cell Neurosci*. 14:19. PMID: 32256316.

Tsuda M., Tozaki-Saitoh H., Inoue K. 2010. Pain and purinergic signaling. *Brain Res Rev* 63(1–2):222–232. PMID: 19931560.

Turner C.M., Vonend O., Chan C., Burnstock G., Unwin R.J. 2003. The pattern of distribution of selected ATP-sensitive P2 receptor subtypes in normal rat kidney: an immunohistological study. *Cells Tissues Organs*. 175(2):105-17. PMID: 14605489.

Uemura K., Kuzuya A., Shimozono Y., Aoyagi N., Ando K., Shimohama S., Kinoshita A. 2007. GSK3beta activity modifies the localization and function of presenilin 1. *J Biol Chem*. 25;282(21):15823-32. PMID: 17389597.

Urano T., Nishimori H., Han H., Furuhata T., Kimura Y., Nakamura Y., Tokino T. 1997. Cloning of P2XM, a novel human P2X receptor gene regulated by p53. *Cancer Res*. 57(15):3281-7. PMID: 9242461.

Valera S., Hussy N., Evans R.J., Adani N., North R.A., Surprenant A., *et al.* 1994. A new class of ligand-gated ion channel defined by P_{2X} receptor for extra-cellular ATP. *Nature.* 371:516–519. PMID: 7523951.

Van Calker D., Müller M., Hamprecht B. 1979. Adenosine regulates via two different types of receptors, the accumulation of cyclic AMP in cultured brain cells. *J Neurochem* 33: 999–1005. PMID: 228008.

Vardy E.R., Kellett K.A., Cocklin S.L., Hooper N.M. 2012. Alkaline phosphatase is increased in both brain and plasma in Alzheimer's disease. *Neurodegener. Dis.* 9, 31–37. PMID: 22024719.

Venigalla M., Sonego S., Gyengesi E., Sharman M.J., Münch G. 2016. Novel promising therapeutics against chronic neuroinflammation and neurodegeneration in Alzheimer's disease. *Neurochem Int*. 95:63-74. PMID: 26529297.

Vial C., Evans R.J. 2002. P2X(1) receptor-deficient mice establish the native P2X receptor and a P2Y6-like receptor in arteries. Mol Pharmacol. 62(6):1438-45. PMID: 12435812.

Virginio C., Robertson G., Surprenant A., North R.A. 1998. Trinitrophenyl-substituted nucleotides are potent antagonists selective for P2X1, P2X3, and heteromeric P2X2/3 receptors. *Mol Pharmacol.* 53(6):969-73. PMID: 9614197.

Volonté C., D'Ambrosi N. 2009. Membrane compartments and purinergic signalling: the purinome, a complex interplay among ligands, degrading enzymes, receptors and transporters. *FEBS J*. 276(2):318-29. PMID: 19076212.

Walker D. G., and Lue L. F. 2015. Immune phenotypes of microglia in human neurodegenerative disease: challenges to detecting microglial polarization in human brains. *Alzheimers Res. Ther.* 7:56. PMID: 26286145.

Wang Y., Mandelkow E. 2016. Tau in physiology and pathology. *Nat Rev Neurosci*. 17(1):5-21. PMID: 26631930.

Wang S., Jing H., Yang H., Liu Z., Guo H., Chai L., *et al*. 2015. Tanshinone I selectively suppresses pro-inflammatory genes expression in activated microglia and prevents nigrostriatal dopaminergic neurodegeneration in a mouse model of Parkinson's disease. *J. Ethnopharmacol*. 164, 247–255. PMID: 25666429.

Wang W. Y., Tan M. S., Yu J. T., and Tan L. 2015. Role of pro-inflammatory cytokines released from microglia in Alzheimer's disease. *Ann. Transl. Med*. 3:136. PMID: 26207229.

Waxham M. Neal, CHAPTER 11 - Neurotransmitter Receptors, Editor(s): JOHN H. BYRNE, JAMES L. ROBERTS, From Molecules to Networks, Academic Press, 2004, Pages 299-334, ISBN 9780121486600.

Webb T.E., Simon J., Krishek B.J., Bateson A.N., Smart T.G., King B.F., *et al.* 1993. Cloning and functional expression of a brain G-protein-coupled ATP receptor. *FEBS Lett.* 324:219–225. PMID: 8508924.

Weingarten M.D., Lockwood A.H., Hwo S.Y., Kirschner M.W. 1975. A protein factor essential for microtubule assembly. *Proc. Natl. Acad. Sci. USA* 72, 1858–1862. PMID: 1057175.

Whyte, M. 2016. Hypophosphatasia - aetiology, nosology, pathogenesis, diagnosis and treatment. *Nat Rev Endocrinol* 12**,** 233–246. PMID: 26893260.

Williams DR. 2006. Tauopathies: classification and clinical update on neurodegenerative diseases associated with microtubule-associated protein tau. *Intern Med J.* 36(10):652-60. PMID: 16958643.

Wirkner K., Köfalvi A., Fischer W., Günther A., Franke H., Gröger-Arndt H., Nórenberg W., Madarász E., Vizi E.S., Schneider D., Sperlágh B., Illes P. 2005. Supersensitivity of P2X receptors in cerebrocortical cell cultures after in vitro ischemia. *J Neurochem* 95:1421–1437. PMID: 16313518.

Wischik C. M., Edwards P. C., Lai R. Y. K., Roth M., and Harrington C. R. 1996. Selective inhibition of Alzheimer disease-like tau aggregation by phenothiazines. *Proc. Natl. Acad. Sci. U.S.A.* 93, 11213–11218. PMID: 8855335.

Wischik C. M., Staff R. T., Wischik D. J., Bentham P., Murray A. D., Storey J. M. D., *et al*. 2015. Tau aggregation inhibitor therapy: an exploratory phase 2 study in mild or moderate Alzheimer's disease. *J. Alzheimers Dis*. 44, 705–720. PMID: 25550228.

Wisniewski T., Goni F. 2015. Immunotherapeutic approaches for Alzheimer's disease. *Neuron* 85**,** 1162-1176. PMID: 25789753.

Woodgett J.R. 1990. Molecular cloning and expression of glycogen synthase kinase-3/factor A. *EMBO J.* 9(8):2431-8. PMID: 2164470.

Xiang Z., Bo X., Burnstock G. 1998. Localization of ATP-gated P2X receptor immunoreactivity in rat sensory and sympathetic ganglia. *Neurosci Lett* 256(2):105–108. PMID: 9853714.

Yaar R., Jones M.R., Chen J.F., Ravid K. 2005. Animal models for the study of adenosine receptor function. *Journal of cellular physiology* 202: 9-20. PMID: 15389588.

Yamada K., Patel T.K., Hochgräfe K., Mahan T.E., Jiang H., Stewart F.R., Mandelkow E.M., Holtzman D.M. 2015. Analysis of in vivo turnover of tau in a mouse model of tauopathy. *Mol Neurodegener*. 26;10:55. PMID: 26502977.

Yamada K., Cirrito J.R., Stewart F.R., Jiang H., Finn M.B., Holmes B.B., Binder L.I., Mandelkow E.M., Diamond M.I., Lee V.M., *et al*. 2011. In vivo microdialysis reveals age-dependent decrease of brain interstitial fluid tau levels in P301S human tau transgenic mice. *J. Neurosci.* 31, 13110–13117. PMID: 21917794.

Yamada K., Holth J.K., Liao F., Stewart F.R., Mahan T.E., Jiang H., Cirrito J.R., Patel T.K., Hochgrafe K., Mandelkow E.M., *et al*. Neuronal activity regulates extracellular tau in vivo. *J. Exp. Med*. 211, 387–393. PMID: 24534188.

Yan Z., Khadra A., Li S., Tomic M., Sherman A., Stojilkovic S.S. 2010. Experimental characterization and mathematical modeling of P2X7 receptor channel gating. *J Neurosci* 30:14213–14224. PMID: 20962242.

Yanamandra K., Jiang H., Mahan T. E., Maloney S. E., Wozniak D. F., Diamond M. I., *et al.* 2015. Anti-tau antibody reduces insoluble tau and decreases brain atrophy. *Ann. Clin. Transl. Neurol*. 2, 278–288. PMID: 25815354.

Yaron J.R., Gangaraju S., Rao M.Y., Kong X., Zhang L., Su F., Tian Y., Glenn H.L., Meldrum D.R. 2015. $K(^{+})$ regulates $Ca(^{2+})$ to drive inflammasome signaling: dynamic visualization of ion flux in live cells. *Cell Death Dis, 6,* e1954. PMID: 26512962.

Ye L., Muench M. O., Fusaki N., Beyer A. I., Wang J., Qi Z., *et al*. 2013. Blood cell-derived induced pluripotent stem cells free of reprogramming factors generated by Sendai viral vectors. *Stem Cells Transl. Med*. 2, 558–566. PMID: 23847002.

Yegutkin G.G. 2014. Enzymes involved in metabolism of extracellular nucleotides and nucleosides: functional implications and measurement of activities. *Crit Rev Biochem Mol Biol*. 49(6):473-97. PMID: 25418535.

Yegutkin G.G. 2008. Nucleotide- and nucleoside-converting ectoenzymes: Important modulators of purinergic signalling cascade. *Biochim Biophys Acta*. 1783(5):673-94. PMID: 18302942.

Yiangou Y., Facer P., Durrenberger P., Chessell I. P., Naylor A., Bountra C., *et al.* 2006. COX-2, CB2 and P2X7-immunoreactivities are increased in activated microglial cells/macrophages of multiple sclerosis and amyotrophic lateral sclerosis spinal cord. *BMC Neurol*. 6, 12. PMID: 16512913.

Yoshiyama Y., M. Higuchi B. Zhang S. M. Huang N. Iwata T. C. Saido J. Maeda T. Suhara J. Q. Trojanowski y V. M. Lee 2007. «Synapse loss and microglial activation precede tangles in a P301S tauopathy mouse model». En: *Neuron* 53(3):337-351. PMID: 17270732.

Young K., Morrison H. 2018. Quantifying Microglia Morphology from Photomicrographs of Immunohistochemistry Prepared Tissue Using ImageJ. J Vis Exp. (136):57648. PMID: 29939190.

Young C.N., Sinadinos A., Lefebvre A., Chan P., Arkle S., Vaudry D., Gorecki D.C., 2015. A novel mechanism of autophagic cell death in dystrophic muscle regulated by P2RX7 receptor large-pore formation and HSP90. *Autophagy,* 11:(1), 113-130. PMID: 25700737.

Yu Q., Zhao Z., Sun J., Guo W., Fu J., Burnstock G., He C., Xiang Z. 2010. Expression of P2X6 receptors in the enteric nervous system of the rat gastrointestinal tract. Histochem Cell Biol 133 (2):177–188. PMID: 19946698.

Yu Y., Ugawa S., Ueda T., Ishida Y., Inoue K., Kyaw Nyunt A., Umemura A., Mase M., Yamada K., Shimada S. 2008. Cellular localization of P2X7 receptor mRNA in the rat brain. Brain Res 1194:45–55. PMID: 18177631.

Zabala A., Vazquez-Villoldo N., Rissiek B., Gejo J., Martin A., Palomino A., Perez-Samartín A., Pulagam K.R., Lukowiak M., Capetillo-Zarate E., Llop J., Magnus T., Koch-Nolte F., Rassendren F., Matute C., Domercq M. 2018. P2X4 receptor controls microglia activation and favors remyelination in autoimmune encephalitis. *EMBO Mol Med*. 10(8):e8743. PMID: 29973381.

Zhao H., Chen Y., Feng H. 2018. P2X7 Receptor-Associated Programmed Cell Death in the Pathophysiology of Hemorrhagic Stroke. *Curr Neuropharmacol*. 16(9):1282-1295. PMID: 29766811.

Zhong X., Zhu F., Qiao J., Zhao K., Zhu S., Zeng L., Chen X., Xu K. 2016. The impact of P2X7 receptor antagonist, brilliant blue G on graft-versus-host disease in mice after allogeneic hematopoietic stem cell transplantation. *Cell Immunol*. 310:71-77. PMID: 27544305.

Zimmermann H., Zebisch M., Sträter N. 2012. Cellular function and molecular structure of ecto-nucleotidases. *Purinergic Signal*. 8(3):437-502. PMID: 22555564.

Zimmermann H. 2016. Extracellular ATP and other nucleotides-ubiquitous triggers of intercellular messenger release. *Purinergic Signal*. 12(1):25-57. PMID: 26545760.

Zimmermann H. 2011. Purinergic signaling in neural development. *Semin Cell Dev Biol.* 22(2):194-204. PMID: 21320621.